80
68572

COMPREHENSIVE TECHNICAL REPORT

UNCLASSIFIED

APEX-904

cy 1

DIRECT AIR CYCLE — AIRCRAFT NUCLEAR PROPULSION PROGRAM

~~L.B. Klingler 3-31-86~~
~~Thomas McCaskey 1-19-87~~
~~JUN 0 3 1993~~
~~Karl Robertson 11-7-94~~
~~Rusty Grant 2-6-95~~
~~R Dickson 3-17-03~~

G. Staymates 1-24-04

HEAT TRANSFER REACTOR EXPERIMENT NO. 1

FLIGHT PROPULSION LABORATORY DEPARTMENT

GENERAL ELECTRIC

UNCLASSIFIED

TAN-P081

This is one of twenty-one volumes summarizing the General Electric Company's direct-air-cycle aircraft nuclear propulsion program. Additional copies are available from the United States Atomic Energy Commission, Division of Technical Information Extension, Oak Ridge, Tennessee.

The APEX number and title of each volume in the series is shown in the following list.

APEX-901	Program Summary and References
APEX-902	P-1 Nuclear Turbojet
APEX-903	Reactor Core Test Facility
APEX-904	Heat Transfer Reactor Experiment No. 1
APEX-905	Heat Transfer Reactor Experiment No. 2
APEX-906	Heat Transfer Reactor Experiment No. 3
APEX-907	XMA-1 Nuclear Turbojet
APEX-908	XNJ140E Nuclear Turbojet
APEX-909	Aircraft Nuclear Propulsion Systems Studies
APEX-910	Aircraft Nuclear Propulsion Application Studies
APEX-911	Remote Handling Equipment
APEX-912	Controls and Instrumentation
APEX-913	Metallic Fuel Element Materials
APEX-914	Ceramic Reactor Materials
APEX-915	Shield Materials
APEX-916	Moderator Materials
APEX-917	Organic, Structural and Control Materials
APEX-918	Reactor and Shield Physics
APEX-919	Aerothermodynamics
APEX-920	Applied Mechanics
APEX-921	Nuclear Safety

COMPREHENSIVE TECHNICAL REPORT
GENERAL ELECTRIC DIRECT-AIR-CYCLE
AIRCRAFT NUCLEAR PROPULSION PROGRAM

HEAT TRANSFER REACTOR EXPERIMENT NO. 1

Authors: G. THORNTON
S. H. MINNICH
C. HEDDLESON
Editor: D. H. CULVER

February 28, 1962

United States Air Force — Contract No. AF33(600)—38062
United States Atomic Energy Commission — Contract No. AT(11-1)—171

GENERAL ELECTRIC
NUCLEAR MATERIALS AND PROPULSION OPERATION
(Formerly Aircraft Nuclear Propulsion Department)
FLIGHT PROPULSION LABORATORY DEPARTMENT
Cincinnati 15, Ohio

DISTRIBUTION

INTERNAL

C. L. Chase
D. Cochran
E. B. Delson
M. C. Leverett
W. H. Long
H. F. Matthiesen
A. J. Rothstein (6)
D. R. Shoults
G. Thornton
Library (6)

EXTERNAL DISTRIBUTION

Col. Ola P. Thorne
Pentagon, Washington 25, D. C.

Capt. Hendricks
Andrews AFB, Md.

Lt. Col. Stanley Valcik (2)
A. S. D.
Wright-Patterson AFB, Ohio

Dr. Frank Pittman (2)
AEC
Washington 25, D. C.

DTIE (14) plus reproducible master
Oak Ridge, Tennessee

ABSTRACT

This is one of twenty-one volumes summarizing the Aircraft Nuclear Propulsion Program of the General Electric Company. This portion describes Heat Transfer Reactor Experiment No. 1, believed to be the first successful operation of a turbojet engine on nuclear power. Design data are presented, including a general description of the test assembly, the nuclear characteristics of the reactor, fuel element thermodynamic characteristics, and the control system. The three series of test runs are also described and the test results summarized.

The general objectives of Heat Transfer Reactor Experiment No. 1 were to demonstrate the feasibility of the direct air cycle system by operating a turbojet engine on nuclear power, to demonstrate the adequacy of reactor design features, and to evaluate aerothermodynamic and nuclear characteristics of the reactor for use in the design of militarily useful aircraft power plants.

ACKNOWLEDGEMENT

Acknowledgement is made of the contributions of D. T. Barry and L. D. Jordan.

PREFACE

In mid-1951, the General Electric Company, under contract to the United States Atomic Energy Commission and the United States Air Force, undertook the early development of a militarily useful nuclear propulsion system for aircraft of unlimited range. This research and development challenge to meet the stringent requirements of aircraft applications was unique. New reactor and power-plant designs, new materials, and new fabrication and testing techniques were required in fields of technology that were, and still are, advancing very rapidly. The scope of the program encompassed simultaneous advancement in reactor, shield, controls, turbomachinery, remote handling, and related nuclear and high-temperature technologies.

The power-plant design concept selected for development by the General Electric Company was the direct air cycle turbojet. Air is the only working fluid in this type of system. The reactor receives air from the jet engine compressor, heats it directly, and delivers it to the turbine. The high-temperature air then generates the forward thrust as it exhausts through the engine nozzle. The direct air cycle concept was selected on the basis of studies indicating that it would provide a relatively simple, dependable, and serviceable power plant with high-performance potential.

The decision to proceed with the nuclear-powered-flight program was based on the 1951 recommendations of the NEPA (Nuclear Energy for the Propulsion of Aircraft) project. Conducted by the Fairchild Engine and Airplane Corporation under contract to the USAF, the five-year NEPA project was a study and research effort culminating in the proposal for active development of nuclear propulsion for manned aircraft.

In the ensuing ten years, General Electric's Aircraft Nuclear Propulsion Department carried on the direct air cycle development until notification by the USAF and USAEC, early in 1961, of the cancellation of the national ANP program. The principal results of the ten-year effort are described in this and other volumes listed inside the front cover of the Comprehensive Technical Report of the General Electric Direct Air Cycle Aircraft Nuclear Propulsion Program.

Although the GE-ANPD effort was devoted primarily to achieving nuclear aircraft power-plant objectives (described mainly in APEX-902 through APEX-909), substantial contributions were made to all aspects of gas-cooled reactor technology and other promising nuclear propulsion systems (described mainly in APEX-910 through APEX-921). The Program Summary (APEX-901) presents a detailed description of the historical, programmatic, and technical background of the ten years covered by the program. A graphic summary of these events is shown on the next page.

Each portion of the Comprehensive Report, through extensive annotation and referencing of a large body of technical information, now makes accessible significant technical data, analyses, and descriptions generated by GE-ANPD. The references are grouped by subject and the complete reference list is contained in the Program Summary, APEX-901. This listing should facilitate rapid access by a researcher to specific interest areas or

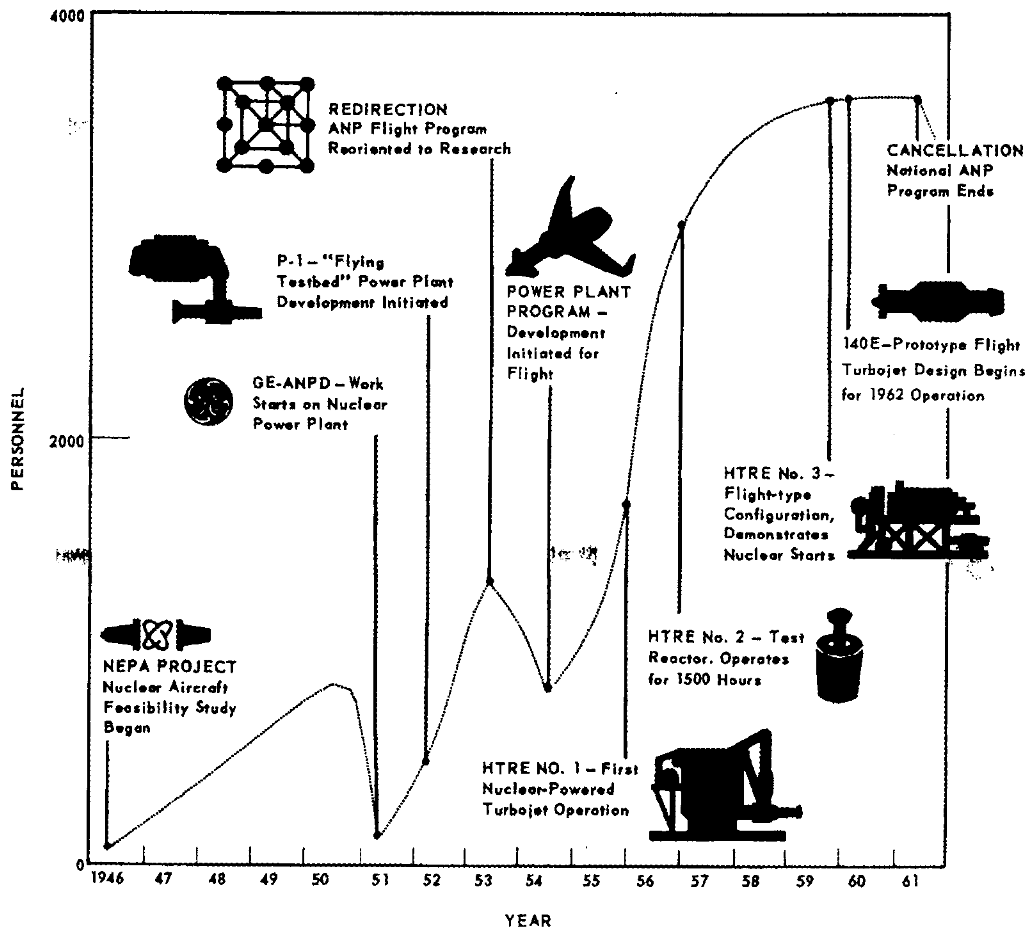

Summary of events – General Electric Aircraft Nuclear Propulsion Program*

*Detailed history and chronology is provided in Program Summary, APEX-901. Chronology information extracted from: Aircraft Nuclear Propulsion Program hearing before the Subcommittee on Research and Development of the Joint Committee on Atomic Energy, 86th Congress of The United States, First Session, July 23, 1959, United States Government Printing Office, Washington 1959.

sources of data. Each portion of the Comprehensive Report discusses an aspect of the Program not covered in other portions. Therefore, details of power plants can be found in the power-plant volumes and details of the technologies used in the power plants can be found in the other volumes. The referenced documents and reports, as well as other GE-ANPD technical information not covered by the Comprehensive Report, are available through the United States Atomic Energy Commission, Division of Technical Information Extension, Oak Ridge, Tennessee.

The Report is directed to Engineering Management and assumes that the reader is generally familiar with basic reactor and turbojet engine principles; has a technical understanding of the related disciplines and technologies necessary for their development and design; and, particularly in APEX-910 through APEX-921, has an understanding of the related computer and computative techniques.

The achievements of General Electric's Aircraft Nuclear Propulsion Program were the result of the efforts of many officers, managers, scientists, technicians, and administrative personnel in both government and industry. Most of them must remain anonymous, but particular mention should be made of Generals Donald J. Keirn and Irving L. Branch of the Joint USAF-USAEC Aircraft Nuclear Propulsion Office (ANPO) and their staffs; Messrs. Edmund M. Velten, Harry H. Gorman, and John L. Wilson of the USAF-USAEC Operations Office and their staffs; and Messrs. D. Roy Shoults, Samuel J. Levine, and David F. Shaw, GE-ANPD Managers and their staffs.

This Comprehensive Technical Report represents the efforts of the USAEC, USAF, and GE-ANPD managers, writers, authors, reviewers, and editors working within the Nuclear Materials and Propulsion Operation (formerly the Aircraft Nuclear Propulsion Department). The local representatives of the AEC-USAF team, the Lockland Aircraft Reactors Operations Office (LAROO), gave valuable guidance during manuscript preparation, and special appreciation is accorded J. L. Wilson, Manager, LAROO, and members of his staff. In addition to the authors listed in each volume, some of those in the General Electric Company who made significant contributions were: W. H. Long, Manager, Nuclear Materials and Propulsion Operation; V. P. Calkins, E. B. Delson, J. P. Kearns, M. C. Leverett, L. Lomen, H. F. Matthiesen, J. D. Selby, and G. Thornton, managers and reviewers; and C. L. Chase, D. W. Patrick, and J. W. Stephenson and their editorial, art, and production staffs. Their time and energy are gratefully acknowledged.

THE EDITORIAL BOARD:

Paul E. Lowe
Arnold J. Rothstein
James I. Trussell

November 8, 1961

CONTENTS

Reactor Dimensions 36

FIGURES

TABLES

1. INTRODUCTION AND SUMMARY

1.1 INTRODUCTION

In a series of tests during the year 1956, a direct air cycle reactor with metallic fuel elements and a water moderator was used as a heat source to power a modified General Electric J47 turbojet engine. This test series was designated Heat Transfer Reactor Experiment No. 1 (HTRE No. 1). The tests were performed at the National Reactor Testing Station in Idaho by the Aircraft Nuclear Propulsion Department of the General Electric Company (GE-ANPD) under contracts with the United States Air Force and Atomic Energy Commission.

A cutaway drawing of the HTRE No. 1 reactor is illustrated in Figure 1.1; a schematic drawing of the test assembly is shown in Figure 1.2.

The first operation of the HTRE No. 1 system on full nuclear power took place in January 1956. A total of 5004 megawatt hours operation was completed during the test program, at power levels up to 20.2 megawatts. HTRE No. 1 operated above 200 kilowatts for 485.6 hours and for 150.8 hours at full nuclear power without chemical assistance. During the first six hours of full power operation, fuel element damage occurred in three cartridges, because of a defect in the insulation liner. After correction of the liner defect and replacement of the damaged elements, power operation was resumed. The test operation was concluded after an endurance run of 100 hours at a reactor-discharge air temperature of 1280°F, and 44 hours at a reactor-discharge air temperature of 1380°F, thus exceeding the original test objective of 100 hours operation. Post-operation examination revealed that the fuel elements used in the endurance run incurred no gross oxidation or damage. As far as could be determined, the reactor could have been operated for considerably longer than the objective life at the design conditions.

This volume describes the HTRE No. 1 reactor and test assembly, the nuclear and aerothermodynamic characteristics of the reactor, the characteristics of the control system, and the results of the test operations. Most of the technical data presented in this volume is reproduced verbatim from an earlier document,[1*] although certain sections have been revised in their entirety.

Objectives of the HTRE No. 1 Program

The over-all objectives of the HTRE No. 1 Program were:

1. To demonstrate the feasibility of the direct cycle system by operating a turbojet engine on nuclear power.
2. To demonstrate the adequacy of the reactor design features and to evaluate aerothermodynamic and nuclear characteristics of the reactor for use in the design of militarily useful aircraft power plants.

*Superscripts refer to the reference lists that appear at the end of each section.

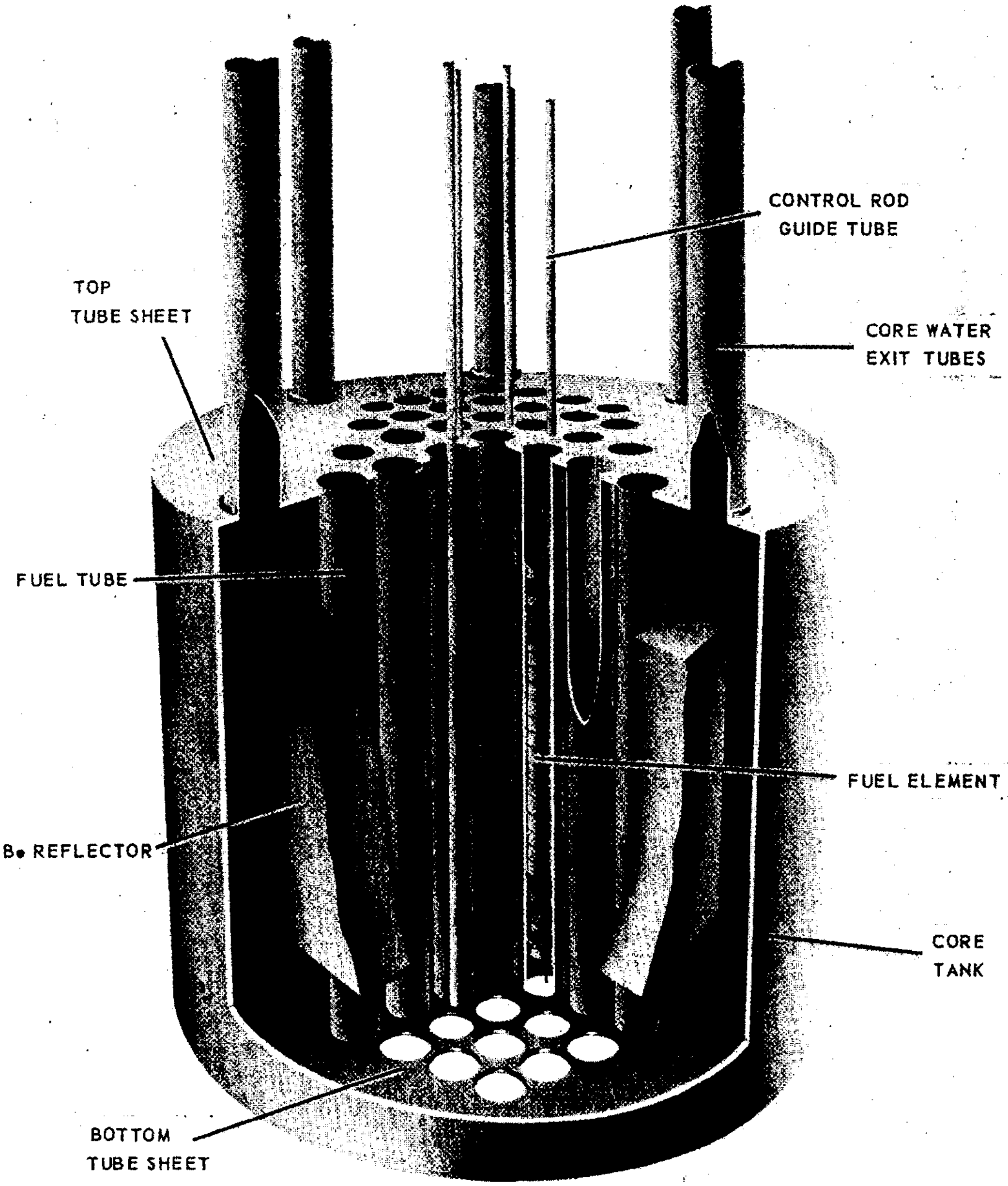

Fig. 1.1 – Drawing of D101A2 reactor core assembly

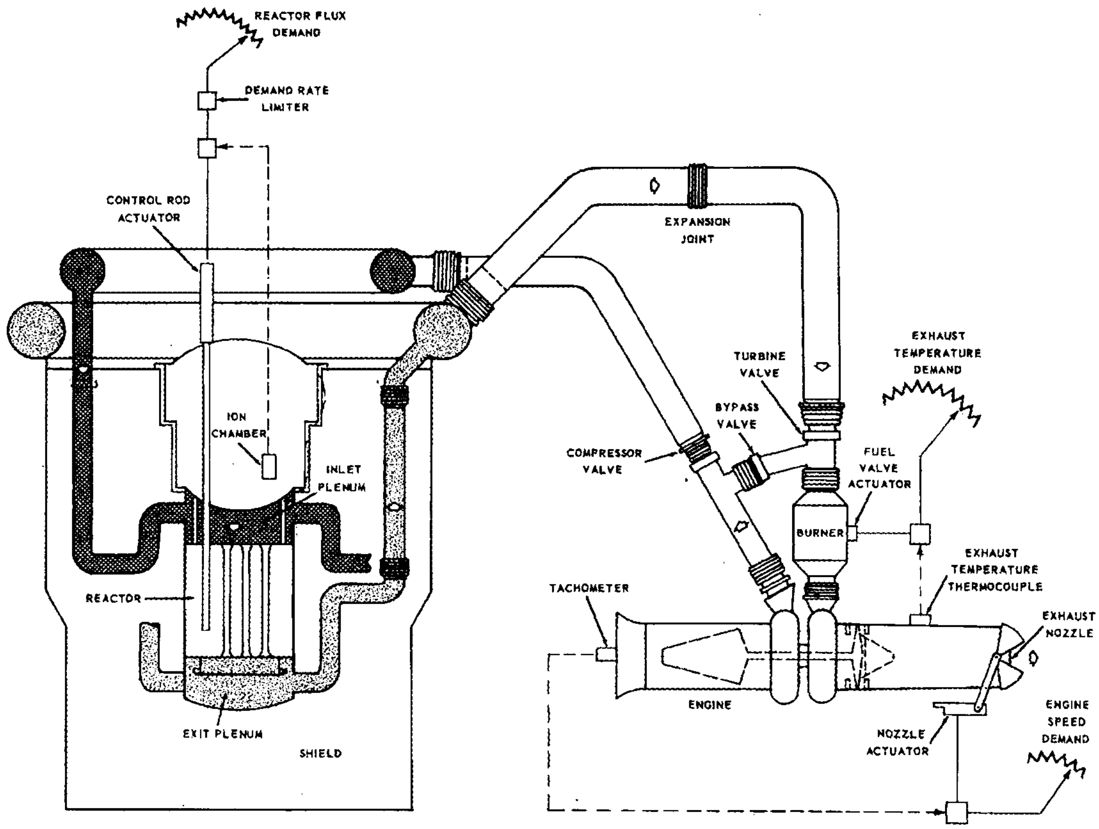

Fig. 1.2—Schematic drawing of HTRE No. 1 test assembly

More specifically, the technical objectives were:

1. To verify the nuclear characteristics of the reactor such as critical mass, power distribution, and time-dependent effects of a heterogeneous, air-cooled, water-moderated reactor of potential use for aircraft propulsion.
2. To determine aerodynamic flow distributions and thermodynamic characteristics such as heat transfer and temperatue variations of the fuel elements, structure, and coolant at high temperatures and high power levels.
3. To verify the methods of control of a direct air cycle reactor powering a turbojet engine.
4. To develop, fabricate, and test reactor components, primarily fuel elements, of potential use in aircraft nuclear power plants.
5. To develop handling methods that would make it possible to remotely assemble, disassemble, and repair nuclear aircraft reactors and power plants.
6. To verify over-all performance predictions of a direct air cycle nuclear turbojet system.
7. To develop personnel and equipment capabilities that could be readily used for the development and operation of a prototype nuclear aircraft propulsion system.

All of these program objectives were realized.

Backgound of the HTRE No. 1 Program

Prior to the initiation of the HTRE No. 1 program, the efforts of GE-ANPD had been directed primarily toward the design and development of the P-1 nuclear power plant, which was intended to propel a modified B-36 aircraft in a flight demonstration program. The P-1 power plant is summarized in APEX-902, "P-1 Nuclear Turbojet," of this Report. The P-1 program was cancelled in the spring of 1953 by the Department of Defense because the power plant did not fit a specific military requirement and because flight demonstration per se was not considered adequate justification for continuation of the program. Upon termination of the P-1 program, GE-ANPD activities were redirected toward a broad component-development program leading to militarily useful power plants without, however, the inclusion of a specific power plant objective.

During the summer of 1953, a General Electric Program Task Force was formed for the purpose of establishing a method to give direction for the component development program in the absence of a specific power plant objective. The Task Force recommended the construction of a Core Test Facility (CTF) which could serve as a test vehicle for a variety of reactor types of potential interest in actual propulsion systems. The CTF is described in APEX-903, "Reactor Core Test Facility" of this Report. After consideration of air supply requirements for the CTF, a turbojet engine was selected rather than a system utilizing a compressor driven by electric motors, diesel engines, or other power sources. The selection of the turbojet engine as an air supply permitted the incorporation of all the principal elements of a nuclear propulsion system, such as reactor, shield, engine, and controls, even though prototype components would not be utilized throughout. After review by government agencies, this proposal was adopted and constituted the primary activity of the GE-ANP program during the calendar years 1954 and 1955. HTRE No. 1 was the first reactor operated in the CTF; full power operation occurred in 1956.

Major Events in the HTRE No. 1 Program

September 1953	- Issuance of program recommendations for the HTRE No. 1 program[2]
November 1953	- Final design work initiated on the CTF
February 1954	- Preliminary design report for HTRE No. 1 reactor issued[3]
February 1954	- Approval received to proceed with CTF manufacture
March 1954	- AEC-AF approval received to proceed with manufacture of HTRE No. 1 reactor and control system
August 1954	- Criticality achieved on critical mockup of HTRE No. 1 reactor
September 1954	- Initial drawings released for reactor manufacture
April 1955	- Full scale mechanical mockup of reactor, controls and instrumentation, and moderator loop operated at GE-ANPD facilities in Evendale, Ohio, using simulated reactor signals
April 1955	- Production of fuel elements initiated
August 1955	- Reactor fabrication completed at Evendale and shipped to Idaho Test Station (ITS)
November 1955	- Initial criticality achieved at ITS using actual reactor and fuel elements
January 1956	- Full nuclear power operation of HTRE No. 1 system achieved at ITS
January 1957	- HTRE No. 1 test series completed.

Application of HTRE No. 1 Program Results

After the HTRE No. 1 program was initiated, specific military direction was provided to the GE-ANP program in the form of an objective power plant for the 125A Weapons System. The 125A Weapons System required operation of the nuclear power plant under subsonic cruise conditions and also during a chemically augmented supersonic sprint. Because of the high ram-air temperatures during the supersonic operation, rejection of heat from the liquid moderator by use of an air cooled radiator would have been difficult. Both pressurized water and unpressurized organic liquid were considered as a moderator fluid. These approaches were rejected, however, in favor of a solid, metallic, hydrided moderator that could be cooled directly by compressor discharge air, thus eliminating the need for an external radiator for moderator cooling. Consequently, the liquid moderator design was not used after the HTRE No. 1 operation except to the extent that the modified version of HTRE No. 1 (HTRE No. 2) was used as a test vehicle for more advanced reactor components. However, metallic fuel elements similar to those used in HTRE No. 1 were utilized with the solid moderator in the subsequent HTRE No. 3 operation and in the XMA-1A power plant design, in accordance with the requirements of the 125A program. HTRE No. 2 is summarized in APEX-905, "Heat Transfer Reactor Experiment No. 2," HTRE No. 3 in APEX-906, "Heat Transfer Reactor Experiment No. 3," and the XMA-1A in APEX-907, "XMA-1 Nuclear Turbojet."

Although the direction of reactor development was changed after HTRE No. 1, most of the experience and data gained in that program was directly applicable to the follow-on programs. Some of the more significant contributions of the HTRE No. 1 program to HTRE No. 3 and subsequent systems were as follows:

1. Reactor Physics

   The HTRE No. 1 reactor was highly heterogeneous with relatively highly absorbent, air-cooled, metallic fuel elements separated from adjacent fuel elements by a water moderator. There was a pronounced flux depression in the fuel elements with a flux peak occurring in the water region. To obtain maximum utilization from the fuel element material, it was decided to operate the fuel elements at nearly isothermal conditions. To do this, the inner rings of the fuel cartridges were more heavily loaded with uranium to compensate for the low flux and provide uniform radial power production within the fuel cartridges. The theory of flux depression and peaking and the compensation by varying uranium loading were developed for the HTRE No. 1 and were verified in both critical experiments and during power operation. The HTRE No. 3 reactor utilized essentially the same nuclear techniques as HTRE No. 1 except for refinements in detail. This was possible because the solid, hydrogenous moderator had only a secondary effect on the reactor physics, as compared to the effect of a liquid hydrogen moderator (water). The fuel elements in HTRE No. 1 and HTRE No. 3 were essentially identical in concept.

2. Aerothermal Characteristics

   The thermal design of the reactors in HTRE No. 1 and HTRE No. 3 differed primarily in that the moderator for HTRE No. 3 was air cooled and operated at a high temperature, whereas the water moderator used in HTRE No. 1 operated at a temperature of 160°F and was cooled by heat ejection from a radiator. Therefore, the thermal data derived from the HTRE No. 1 tests were applicable principally to the fuel element design of later metallic-fueled reactors. Predictions of variations in HTRE No. 1 fuel element temperature had been made to reflect gross radial, longitudinal, and fine radial power distribution within the fuel element as well as perturbations produced by contol rods, airflow maldistributions, and manufacturing tolerances in dimensions and fuel loadings. The experimental results were in close agreement with predictions. Consequently, refinements of the methods used for predicting temperatures in HTRE No. 1 were utilized for subsequent metallic-reactor designs.

   Consideration was given to the possibility of unpredicted maldistributions in airflow, both radially across the face of the reactor and between air passages within individual fuel elements. Experimental results indicated excellent flow stability even under low airflow conditions. Air pressure drops, both in the reactor and in the rest of the air system, were verified and formed a firm basis for subsequent reactor and propulsion system design.

3. Control

   The general method of controlling an air-cooled reactor operating in series with a chemical burner and coupled to a conventional jet engine was worked out for HTRE

No. 1 in a manner that would allow full power operation either at full nuclear power, full chemical power, or any combination of the two. The system developed for HTRE No. 1 proved to be very satisfactory and provided a firm basis for future power plant and reactor control system design. There had been some concern that the reactor might be particularly subject to rapid and perhaps uncontrollable variations in fuel element temperature under transient operating conditions due to the low heat capacity of the fuel elements, the poor heat transfer characteristics of air as a coolant, and a slightly positive moderator temperature coefficient. Operating experience verified the analytical predictions that the control was very stable in operation with transient temperature control well within the capability of the control system response characteristics.

Generally speaking, HTRE No. 1 operation indicated the extremely fast response that was provided in the control system was unnecessary for fully developed nuclear turbojet operation. As a result, the design of future nuclear power plant control systems could proceed in the direction of simplification of the normal operating controls components and greater utilization of conventional techniques used in chemical turbojet engine control.

4. Component Development and Fabrication

The experience acquired from the HTRE No. 1 developed the capability for manufacturing metallic fuel elements and in other important fabrication areas, unique to gas-cooled systems, such as hot ducting, insulation, etc.

5. Remote Handling and Maintenance

The HTRE No. 1 reactor and over-all system, including controls, turbojet engine, and shield, were designed to be inspected and disassembled remotely in a hot shop, repaired as necessary, and placed back into operation. This reflected the practice that had been developed for conventional aircraft engines. Turbojet engines and aircraft components, in general, operate on a relatively short time cycle and under severe conditions. Furthermore, reliability is of greater importance in airborne systems than in terrestrial or marine systems. Consequently, provision must be made for critical inspection and, if necessary, replacement of components during normal aircraft and engine shutdowns. During the test program, the HTRE No. 1 was returned to the hot shop on several occasions, repairs or adjustments made, and system returned to operation. This experience proved the feasibility of routine maintenance of turbojet systems using a radioactive heat source.

Design improvements were identified that could be incorporated into subsequent power plants to facilitate maintenance work. Operator skills with remote handling devices were developed to perform inspection and maintenance operations rapidly and accurately. Standards were developed governing the extent to which maintenance must be performed remotely rather than manually from the standpoint of exposure to radiation, and the extent to which it is possible to work in and clean up contaminated areas and equipment. As a result of the remote handling and maintenance experience acquired during the HTRE No. 1 program, the problem of dealing safely with radioactive power plants was put into a proper perspective, a significant contribution to the problem of handling later nuclear power plants.

6. System Performance

The analytical predictions of over-all system temperatures, airflows, and pressure drops were verified during the operation of HTRE No. 1. This made it possible to predict with confidence the performance that could be expected from proposed nuclear turbojet power plants operating in military aircraft.

7. Personnel Capability

During the design and operation of HTRE No. 1, personnel capability was developed to such a degree that subsequent experimental and military nuclear systems could be designed, built, and operated with confidence and skill within a framework of practicability.

1.2 SUMMARY

1.2.1 GENERAL DESCRIPTION OF THE HTRE NO. 1 MODEL A TEST ASSEMBLY*

The Heat Transfer Reactor Experiment (HTRE) test assembly as conceived in the basic design consisted of an air-cooled reactor operating a single, modified J47 turbojet engine. The reactor used metallic fuel elements and water moderator. The turbojet engine and shield were part of a mobile facility called the Core Test Facility (CTF). A reactor core, shield plug, control actuators, source rod, startup fission chambers, and operating ion chambers were combined into an integral unit before insertion into the shield.

The reactor structure was aluminum and consisted of a cylindrical water vessel penetrated by air tubes, into which fuel cartridges were inserted for nuclear operation of the reactor. The air tubes were lined with a thin layer of stainless-steel-jacketed, mineral-wool, felt-type insulation to reduce escape of the fuel element heat into the water moderator. The dished-head transition section was an integral part of the reactor assembly in that it was connected to the reactor by control rod guide tubes and water tubes. The reactor and transition assembly were bolted to the bottom of the shield plug through a flange on the transition assembly. The transition section was made of aluminum and contained moderator water for neutron shielding.

The active core was a hexagonal bank of 37 aluminum tubes containing nickel-chromium fuel cartridges with sandwiched UO_2 fuel meat. A length of unfueled water-tube matrix extended on each end of the active core to serve as end reflector. The radial reflector consisted of beryllium slabs arranged in a hexagonal shell.

Fuel for the reactor was supplied by enriched UO_2 mixed with an 80 Ni - 20 Cr alloy in a weight ratio of 40 to 42 percent UO_2. The fuel mixture was clad with a modified nickel-chromium alloy and was fabricated in ribbon form. The fueled ribbon was formed into rings sealed at each end with braze-coated wire. Each fuel element consisted of a concentric arrangement of the fueled rings, joined and spaced at the leading edge by brazed channels, and spaced at the trailing edge by trapezoidal spacers. Eighteen elements, together with the forward ring assembly and the aft assembly, formed the fuel cartridge. The cartridge was divided into two sections on the basis of hydraulic diameter; the first eleven stages formed the first section, and the last seven formed the second section.

Control System

Engine controls were separate from the reactor controls. The only links between reactor and engine control systems were several safety interlocks that were operated by engine overspeed and loss of airflow when an engine was being shut down. Either of these conditions could scram the reactor.

The control system of the HTRE No. 1 reactor consisted of nuclear instrumentation, the dynamic control system, shim control system, safety system and interlocks, and sensory instruments.

Nuclear instrumentation consisted of three channels: the count-rate, log flux, and linear channels. The count-rate channel was used to determine the status of the reactor when the flux level was below 10^{-5} NF (full-power reactor flux level). Signals for the count-rate channel were produced by fission chambers. These signals were converted to log count rate and period signals. If the period became less than 5 seconds, the reactor was scrammed.

*The formal nomenclature of the HTRE No. 1 model A test assembly is "D101A." Three reactors were built for use in this test assembly. The A1 reactor was a mechanical mockup used for cold fitups and flow tests; the A2 and A3 were identical reactors built for power operation. With the A2 reactor inserted into the Core Test Facility the entire test assembly is designated D101A2.

The log-flux channel was supplied by compensated ion chambers located in the side ports of the Core Test Facility. The chamber signals were converted to log-flux and period signals. The period signal was used to control the reactor in the period range from 10^{-5} NF to full power.

In the linear-flux channel compensated ion chambers located in the top plugs were used as sensors in the power range. Each sensor supplied an input to the flux-regulation servo and a difference amplifier. The three flux-level signals were auctioned, and the highest signal was recorded. The high signal also supplied the input to the 1.1 NF trip circuit. If the flux level exceeded 1.1 NF, the reactor was scrammed.

The purpose of the flux-regulating servo was to maintain the reactor power level at the value selected by the operator. It was intended for operation between 1 percent and 100 percent NF. The shim rods moved to compensate for low-frequency changes to maintain the dynamic rods within a neutral position band.

Should the reactor tend to operate in unsafe regions, the power level could be quickly reduced by one of two methods:

1. Shutdown - The dynamic rods were driven into the reactor; this action called for insertion of all rods by sequence operation. After the trouble was corrected, a complete startup was necessary.
2. Scram - The shim-rod solenoid latches were released and all spring-loaded shim rods were completely inserted, together with the dynamic rods. Scram could be initiated manually or automatically. A reset was not possible until the trouble was corrected.

Thermodynamic sensors were located throughout the HTRE-CTF system. Two fuel cartridges were equipped with 18 thermocouples to obtain data on longitudinal and fine radial power distribution; all other cartridges were provided with two thermocouples.

Shield

The shield consisted of borated water, lead, and steel. It was designed to provide sufficient neutron and gamma shielding to reduce the combined effect of the induced activity of external components and the leakage of core decay gammas to 100 milliroentgens per hour 3 hours after 25 hours of operation at 40 megawatts. The primary purpose of the shield plug was to shield the area above the core insertion hole from nuclear radiation. The transition section added significantly to the shielding of the reactor. The plug had two steps to avoid straight-line passage for radiation streaming. It was made of stainless steel and contained moderator water for neutron shielding.

Aerodynamics and Thermodynamics

The practical limit on the power that could be extracted from the reactor was determined by the rate of heat transfer to the air. Heat transfer was limited by the maximum permissible fuel element temperature and the maximum amount of cooling air provided by the turbojet engine commensurate with system pressure loss.

It was necessary to regulate three nuclear power distributions in order to achieve the design performance. Longitudinal power distribution was controlled by placing the section having fuel elements with the smallest heat transfer area in the entrance region, since the temperature difference between fuel element and air could be large near the core inlet. This procedure allowed the highest heat transfer per unit area. The gross radial power was equalized from tube to tube by varying the spacing of the tubes. The beryllium reflector also helped maintain sufficiently high flux in the outer tubes. The fine radial power distribution within each tube was regulated by increasing the thickness of the fuel sheets near the center of the tube. This increase in fuel mass per unit heat transfer area compensated for the decrease in power per unit mass of fuel caused by self shielding at the center of the fuel element.

The air entered the turbojet engine and was compressed to five times the intake pressure. It was then collected in a scroll and ducted to a manifold on top of the shield tank. The air passed through the shield in parallel ducts and entered the air plenum chamber above the reactor. The air passed through the reactor, was heated, and entered a plenum chamber at the reactor exit. The air then returned to the turbine and was ducted into the exhaust-handling system.

The fuel element heat transfer area was designed for a nominal unperturbed maximum temperature of $1700^{\circ}F$ with a reactor air inlet temperature of $380^{\circ}F$ and a reactor air exit temperature of $1400^{\circ}F$ at an airflow rate of 60 pounds per second. The engine speed under these conditions was 7800 rpm.

The power plant was started on chemical fuel alone, with compressor air passing through the cold reactor. With the engine-speed and turbine-exhaust-temperature controls set at a predetermined level, the reactor was started and the power was increased. When the nuclear heat was detected by the turbine-exhaust thermocouples, the chemical fuel valve started to close. As the reactor power was increased, the chemical valve closed completely. Engine speed was held constant throughout.

Core Test Facility

The Core Test Facility consisted of the shielded reactor and engines together with several auxiliary systems. These comprised a self-contained unit mounted on a dolly. The reactor auxiliary systems were the in-transit aftercooling system, the auxiliary aftercooling blower, the auxiliary power unit, and the wiring leads between the shielded reactor and a coupling plug, which mated with a plug on the facility. The engine auxiliaries included the fuel system (except for tanks and booster pump), lubrication system, starter system, duct valve actuation system, and control and instrumentation wiring leads to the facility plug.

The auxiliary power system consisted of two diesel-electric systems rated at 20 kilowatts each. One system operated two 3-horsepower moderator aftercooling pumps, one 3-horsepower heat exchanger fan motor, and one 7.5-horsepower fan motor. One engine-alternator set carried the load through a low-voltage transfer switch. If trouble developed on the loaded set, the load was transferred to the other set. The aftercooling air blower supplied 4 pounds per second of air at 45 inches of water pressure at 5000 feet. The in-transit moderator cooling system had a circulating flow rate of 75 gpm with a heat-removal capacity of 74 Btu per second.

1.2.2 IET NO. 3

Three series of tests were performed during HTRE No. 1 operation. The first series covered the period from December 27, 1955, to February 25, 1956, and was designated Initial Engine Test (IET) No. 3. (Previous tests, designated IET No. 1 and IET No. 2, were not power operations.) The core used in this first test series was called the A2 core and was part of the first test assembly, the D101A2. In the second test series, IET No. 4, which was conducted during the period from April 17, 1956, to June 29, 1956, a slightly modified A2 core was used. After further modification based on test results and a series of shielding tests (IET No. 5), the third series of tests, designated IET No. 6, was performed during the period from September 24, 1956, to January 3, 1957. IET No. 6 employed a completely new reactor test assembly, the D101A3. A summary of these operations is given in reference 4.

Operation

The first series of operational tests using the A2 reactor was generally successful in that the system operated as intended without chemical assistance. The first test series consisted of the following operations: (1) making the reactor critical, (2) low-power tests in which the coolant air was supplied by auxiliary blowers, (3) tests in which the coolant air was supplied by the engine, which was operated both by the reactor and the auxiliary chemical source, and (4) operation of the engine system exclusively on reactor energy. Nuclear/power operating range was from ≅0 (critical) to 16.9 megawatts.

Experimental data showed reasonable agreement with expected values. The primary discrepancies involved somewhat high fuel element temperatures on the average and excessive temperature spreads. A few of these high local temperatures narrowed the region for matching of the reactor and engine power and hindered power transfers.

During the first all-nuclear run the engine system was successfully operated for a period of approximately 40 minutes, during which time the engine was both accelerated and decelerated by variation of reactor power. During this initial operation the exit air radioactivity monitors indicated possible fuel element rupture. Although the initial release rate was not sufficient to warrant immediate termination of testing, it did increase slightly with time and after 5-1/2 additional hours at full nuclear power it was decided to return the reactor to the hot shop. The reasons for this decision were twofold: (1) to investigate possible fuel element damage in the early phases, and (2) to preclude the occurrence of a hazardous radioactive situation involving either on- or off-site personnel.

When the reactor was disassembled and fuel cartridges were examined, it was discovered that two cartridges were damaged extensively with segments of the fuel elements melted or oxidized away. Analysis of the damage indicated that it resulted from differential air pressure across the insulation sleeve. The pressure differential caused the sleeve to collapse the steel liner against the fuel cartridge and restricted cooling air from the stages that were overheated. The insulation sleeve was redesigned and the power plant was equipped so that data could be gathered to evaluate this problem during future operations.

Experimental Data

The over-all system required more power and operated at higher temperature levels than had been anticipated in design, probably because of leakage in the CTF ducting. This condition limited both the range of system operation on full nuclear power and the maximum power levels that could be obtained.

The performance of system components generally gave good to excellent agreement with design predictions. Reactor and ducting pressure losses, system heat losses, structure heating rates, and moderator system behavior were in excellent agreement with predictions. The observed scatter of fuel element temperatures and maximum value of select fuel element temperatures were greater than anticipated.

Detailed analysis of reactor characteristics was restricted in some cases because instrumentation was limited and because some measurements appeared unreliable. Therefore, some analyses in this series interpreted data rather than presenting exact values based on recorded measurements.

Instrumentation limitations were particularly significant in the evaluation of fuel element temperatures. Most fuel element thermocouples were located in positions that were selected for special reasons, principally to evaluate temperature distributions. Therefore, a simple average of the thermocouple readings did not directly check design standards. The design list on average maximum fuel temperature was lower than the material capability to allow for known and statistical deviations between the as-built reactor and the ideal design. The average of observed temperatures at the eighteenth stage (expected location of the maximum temperature) fell about midway between the ideal average maximum design value and the expected maximum deviation. The inadequacy of instrumentation cast doubt on average thermocouple readings. Most thermocouples were located on outer rings, and dimensional deviations of insulation liner, from the same causes that led to collapse and damage to some cartridges, were believed to have contributed to temperature deviations. Later operation in IET No. 6 appeared to substantiate this conclusion.

Examination of fuel elements after remote disassembly of the reactor system indicated localized damage that may be attributed to a number of possible causes. During the operational phase, cocoon drainage measurements indicated considerable leakage of borated shield water into the environs of the core. Visual observation of the reactor core after its removal from the CTF showed encrustations of a boric acid residue on the top and bottom of the core tank and possibly in the fuel elements. Wrinkling and severe oxidation of several insulation liners were noted. Buckling of fuel element support rails and buckling of outermost rings of fuel elements were also observed after the insulation liners were stripped from fuel cartridges. Severe damage, melting or severe oxidation of fuel element material, was observed in two cartridges. A third cartridge showed some oxidation and exposure of fuel in several stages. The observed damage was believed to represent a progression of events caused by collapse of the insulation liner. It appeared that air leaked between the insulation liner and the aluminum fuel tube at the tube inlet. This air could not pass through bleed holes in the insulation liner in sufficient quantity to prevent a significant pressure differential across the liner. As a result, the liner buckled and the subsequent buckling of plates led to overtemperature and rapid oxidation.

The insulation liner collapse and resulting fuel element distortion have been demonstrated in cold-flow tests of cartridge assemblies in Evendale test facilities. Subsequent tests and data appraisals indicated no other explanation of how the damage started.

While it was not proved conclusively that insulation liner collapse was the only cause of the extensive damage observed, this hypothesis was adopted and corrective measures were based on it. It was also tentatively assumed that liner distortion could account for much of the temperature spread observed during operation. In addition to the program based on the hypothesis that insulation liner collapse was the cause of fuel element damage, certain redesigned engine and ducting components were incorporated into the system to lower required turbine temperatures and improve engine performance.

The A2 reactor core was reassembled using 24 original cartridges (some of these contained incipient distortions) and 13 virgin spare cartridges. A new set of insulation liners, which incorporated the changes indicated by damage inspection and by Evendale tests, was provided so that collapse of these liners was not expected in operation. In order to resume operation in a reasonable time, a complete redesign was not attempted. The remainder of the power plant test assembly was unchanged from the condition in which original operation took place. The system was expected to operate on part chemical power for a period of time in order to accomplish the objectives of IET No. 4.

1.2.3 IET NO. 4

Operation

The second series of operational tests was run at the Idaho Test Station during the period from April 17, 1956, through June 29, 1956. This test series was designated IET No. 4 and utilized the repaired and modified A2 core. The primary purpose of the tests was to determine whether modifications based on the results of the first test series had significantly improved the capabilities of the reactor. Additional objectives were (1) to make complete measurements of the power plant performance, (2) to measure xenon poisoning, and (3) to study and improve servo control of the reactor.

After the reactor was assembled for IET No. 4, the excess reactivity was measured and found to be 0.51 percent greater than during IET No. 3 operation. The chief cause of the higher reactivity was the use of thinner insulation liners. With the reactor critical, the airflow was brought up to its maximum value without any significant change in reactivity. Extensive engine performance data were obtained from the tests. The data covered the operation of both engines with reduced and ambient back pressure and with various settings of compressor and turbine valves to increase the pressure drop. The reactor was brought up to substantial power, and the performance map was made at gradually increasing nuclear power levels. The data were reproducible and showed no significant deviations from the results obtained in the early stages of IET No. 3.

A major effort was made to improve automatic control of the reactor. The main control-loop amplifier from the original servo system was discarded and replaced by a new and flexible circuit with an integrating network. The parameters of this circuit were adjusted empirically to give optimum performance, but no formal tests of its response were made. The final system, operating one dynamic rod only, gave satisfactory results from an operational standpoint, although reliability was not demonstrated and the system was susceptible to electronic noise. The reactor was controlled on neutron flux at power levels from 1 percent to full power and on fuel element temperatures at intermediate power levels. An attempt to control the reactor by controlling the temperature of the air leaving the hot torus was unsuccessful because of slow system response. Data were taken to permit the design of control componenets that would compensate for this slow response. Operation was routinely carried out on automatic control, although some long runs were made at high power with manual control.

In order to bring the temperature of the air leaving the hot torus to 1250°F, the reactor power was raised in steps. Four hours of operation were obtained in turn at 1100°F, 1150°F, and 1200°F. The system was then operated for 84 hours at a temperature of 1250°F. This temperature was chosen to duplicate essentially the reactor conditions that existed during the full nuclear power plant operation achieved during IET No. 3. The seasonally higher inlet air temperatures during IET No. 4 precluded full nuclear operation without an increase in power; chemical augmentation amounted to about 8 percent of the power required by the engine.

After several hours of operation at fuel flows of 300 pounds per hour, it was impossible to obtain ignition in the unit combustors in the usual manner. Examination of the fuel nozzles revealed extensive damage. To avoid continual replacement of these nozzles, a new technique was developed whereby the reactor was used to preheat the air to aid the ignition process.

From the start of power operation, radioactivity was observed on the stack monitor and rupture detector. Tests to pinpoint the cause of this release indicated that the measured particulate activity did not depend significantly upon fuel element plate temperature at low temperature levels but increased sharply at high plate temperatures. The activity showed a moderate dependency on fuel flow, since it decreased when the fuel flow was reduced. The effect of power on activity was not detectable at low powers, but showed a minor increase at the maximum power tested, 15.5 megawatts. It was therefore concluded that fuel element temperature level was the most significant parameter in determining release of radioactivity.

The release of radioactivity in stack gas was further investigated by the introduction of smoke into the base of the stack. The increase in measured particulate activity amounted to over 1000 curies per hour, the highest level observed during this test series. When the smoke had dissipated, the measured activity decreased to an average level of 135 curies per hour, a typical value for the conditions. It was believed that the smoke may have absorbed the radioactive gases in a manner that affected the efficiency of the detecting equipment.

The stack gas was sampled periodically by passing a small amount through a millipore filter and occasionally through a liquid scrubber to remove iodine. At high fractional nuclear powers, over 90 percent of the activity passed through the filters (99.99 percent efficiencies were achieved for particles 0.3 microns or over in diameter).

The filters that sample each fuel tube were removed and examined. Those connected to tubes 5, 26, 30, and 11 contained appreciable radioactivity. I^{131}, I^{132}, and I^{133} were detected in all of these filters, and uranium was detected in all but tube 5. Since cartridges in tubes 5, 26, and 30 were those that sustained extensive damage during IET No. 3, it was thought that the observed radioactivity in these filters resulted from contamination of the sampling system or from U^{235} plated in the tubes.

Attempts were made to localize the source of activity by inserting control rods, but results were not conclusive. The removing of rods in the vicinity of tube 11 appeared to have increased the activity slightly. The effect was not significant, however, in view of the temperature changes that this technique can accomplish.

The nature of the radioactivity release in this test series was different from that observed during IET No. 3. The radioactivity was emitted either as a gas or in the form of extremely small particles. The emission was relatively steady and continuous. There was no sudden onset of large-scale emission. However, conditions were similar for both tests in that the moving of control rods produced little effect, and there was no associated change in reactor performance.

On June 29th the D101A2 system was shut down for return to the hot shop for disassembly and inspection. The decision for shutdown was made to permit an examination of the reactor to determine whether any further modifications were necessary for tests with the A3 core. The reactor operation was entirely satisfactory (except for fission product evolution) at the time of the shutdown.

During this test series the reactor was operated for a total energy release to air of 1877 megawatt-hours and at a maximum sustained power level of 16.0 megawatts to air. The maximum sustained plate temperature recorded was 1991°F, with a maximum sustained average of 1701°F. The maximum core discharge temperature was 1394°F. The total operating time at a power to air of 16 megawatts was 84 hours.

Experimental Data

During IET No. 4 the system was operated under conditions that permitted extensive partial power-mapping of the system thermodynamic characteristics. Data were obtained over the range from full chemical power to reactor powers requiring as little as 300 pounds per hour of fuel flow. However, no data were obtained on full nuclear power.

Tests were conducted to determine the xenon poisoning both during operation and after shutdown. The results indicated that the apparent xenon poisoning was greater than predicted by a factor of 2.

The general day-to-day consistency of data was considerably better than during IET No. 3 operations, even though there were fewer thermocouples for air and fuel element temperature data. However, the exact correlation of reactor performance was limited by allowable reactor instrumentation. Thus certain analyses were restricted to the best interpretation of data rather than precise evaluation based on recorded measurements.

A substantial improvement in system operation was obtained during the IET No. 4 test series. The criteria for this improvement were:

1. The system operated 188 hours with a total system heat release of 2064.98 megawatt-hours as compared to 40 hours and 349 megawatt-hours for IET No. 3.
2. The reactor core damage was much less severe and occurred at a slower rate than during IET No. 3.
3. Since IET No. 4 utilized 24 cartridges from IET No. 3 operations and only two of these incurred moderate damage during operation, 22 cartridges operated undamaged for a total of 234 hours and generated 2414 total megawatt-hours to the system.
4. The control system components and the over-all system both showed improvement during their IET No. 4 operation in that the actuator trouble was reduced and the servo system responded better than during the first test series.

When the A2 core was removed from the CTF after IET No. 4 testing, the first view of the bottom tube sheet showed that three cartridges were unlatched and one had fallen out completely. Cartridges in tubes 4, 9, and 20 had dropped 4 inches, 8 inches, and 6 inches respectively. The fuel element and insulation sleeve from tube 33 remained in the CTF. After this cartridge was removed it was noted that the probe containing the exit air thermocouples and pitot tube for tube 33 exit was broken off. It was conjectured that the fuel cartridge in this tube was resting on the bottom of the cocoon, some 32 inches below its normal position.

During the latter stages of IET No. 4, an apparent loss of reactivity on the order of 1.8 percent $\Delta k/k$ was noted. It was thought that the fuel cartridge displacements could have caused such a loss of reactivity; subsequent tests confirmed this theory.

The tail assembly was missing from the cartridge in tube 9. Attempts to locate this tail assembly were unsuccessful at this time.

Inspection of the individual fuel cartridges indicated three burned cartridges, including one of the 13 replacements. Two of the burned cartridges exhibited only minor damage; the third had severely burned fuel plates in stages 11 through 18. Many of the other cartridges showed damage varying from dimpled fuel plates to broken and buckled rails. Most of the outer 2-mil cover foils of the insulation sleeve were either wrinkled or scorched.

Several explanations were advanced for the observed fuel cartridge damage:

1. Pressure differential may have caused collapse of the insulation liner against the fuel element.
2. Control rods adjacent to rails may have created thermal differentials that caused the cartridge to warp until contact was made with the insulation sleeve.
3. Inherent tolerance stackup or dimensions out of tolerance in the liner, cartridge, and core tube may have produced areas of low airflow that caused excessive oxidation.

1.2.4 IET NO. 6

Operation

The third series of heat transfer reactor experiments utilizing the A3 core and the CTF, and designated IET No. 6, was successfully conducted at predicted temperatures at the Idaho Test Station during the period from September 24, 1956, through January 3, 1957. The immediate objectives of IET No. 6 were as follows:

1. To evaluate the performance of the redesigned insulation liners.
2. To extend and supplement IET No. 3 low-flow and nuclear characteristics.
3. To verify the xenon characteristics determined during IET No. 4.
4. To continue basic controls investigations.
5. To conduct endurance testing with the engine on full nuclear power.

In the test program for IET No. 6, special emphasis was placed on tests to evaluate maximum no-air power dissipation and more extensive blower tests to obtain aftercooling data applicable to the HTRE No. 2 program and subsequent solid-moderated reactors. Upon completion of the engine-reactor mapping phase, the reactor was to be placed on high-power endurance test.

The reactor was first made critical on October 3, 1956, and exceeded 200 kilowatts or 1 percent power on October 12, 1956. During this period various low-power tests were conducted with no forced-air cooling and tests in which the coolant was supplied by aftercooling blowers. The results of these tests substantially checked and extended previous data obtained during IET No. 3. During this test it was possible to obtain a total temperature-rise ratio of 3:1 across the core with no indications of the flow maldistribution or instability that had been suspected for this type flow condition. With two blowers on high speed, it was possible to dissipate 2.35 megawatts with a maximum stage-18 plate temperature of 1860°F. During the heat dissipation test of the core with no forced-air cooling, 70 kilowatts of heat were dissipated with a maximum recorded plate temperature of 1150°F. Also during these tests, transient data were taken to determine the rate of fuel element temperature rise in order to ascertain core power distributions.

The initial transfer to full nuclear power occurred on November 7, 1956. After inspection of the data obtained during this operation, a two-phase endurance testing program was formulated. Phase A consisted of operating the reactor at as low a fuel element temperature as possible, consistent with stable engine operation without chemical addition, until 100 hours were accumulated. The purpose of this phase was to demonstrate 100 hours of engine operation on full nuclear power. In accordance with the initial transfer data, it was decided to control on $T_{3.65}$ for the first 100 hours with a temperature of 1150°F at $T_{3.65}$, corresponding to a core discharge temperature of 1280°F. For Phase B the reactor was taken to conditions similar to those during IET No. 4 operation. The $T_{3.65}$ exit-air temperature was raised to 1225°F, which corresponded to a maximum fuel element temperature of 1850°F and a core discharge temperature of 1380°F. The reactor was to operate at this condition until fission products were detected in the exhaust gases.

Because of unfavorable weather conditions, Phase A endurance testing was not resumed until November 15, 1956. On December 5th and 6th, the reactor was operated above 200 kilowatts for 28.35 consecutive hours. With the exception of a noise scram that occurred about four hours after startup, the reactor was on full nuclear power for 22 hours. Final shutdown was caused by unfavorable wind direction. Although the A2 reactor operated for 6 hours at full nuclear power, the initial fission fragments were detected after only half an hour of operation.

The Phase A, 100-hour endurance test, which began on November 15, 1956, was completed on December 11, 1956. This 100 hours of operation was accomplished on operational days with 23 transfers to full nuclear power. The first indication that changes were occurring within the A3 core was detected on the night of December 18, 1956, during Phase B operations. On the basis of information that indicated strong iodine peaks and other possible fission fragments, it was decided to terminate endurance testing in order to attempt to localize and determine the source of release. The next 2 weeks were utilized in determining which of the fuel cartridges were damaged. On January 3, 1957, the system was shut down for return to the hot shop for disassembly and fuel element inspection.

During the initial checkout of the A3 core in the CTF, a hot-spot reading of about 22 roentgens per hour was noted in a bend of riser 16. Attempts to identify the cause were unsuccessful, but it was conjectured that the hot spot was caused by the fuel element tail assembly that was missing when the fuel cartridges were removed from the A2 at the conclusion of IET No. 4. During a routine maintenance day late in December the tail assembly was found and removed from the butterfly valve of the bypass combustor. The tail assembly did not appear damaged except for slight flattening. The radiation reading of the tail assembly was 10 roentgens per hour at contact.

During IET No. 6 the reactor was transferred to full nuclear power 40 times and operated for a total energy release to air of 2811 megawatt-hours and a maximum sustained power level of 18.4 megawatts to air. The total operating time at condition A was 105.82 hours and at condition B, 38.95 hours.

Experimental Data

The testing of the D101A3 reactor core brought to a successful conclusion the HTRE No. 1 testing program with full realization of test objectives. The successful operation of the reactor in this test confirmed the hypothesis that the earlier failures were caused by mechanical difficulties with insulation liners and that the basic characteristics of the reactor were as predicted. Thus the gross, or average, thermodynamic performance of the reactor was the same as that observed during IET No. 4. The significant improvement was accomplished through the elimination of mechanically induced hot spots. The net result of the testing was that, although some minor difficulties remained to be resolved, the HTRE No. 1 system operated successfully as predicted in almost every respect. No basic unforeseen difficulties were encountered.

During the IET No. 6 test operations, many quantitative data were obtained concerning the nuclear and thermodynamic aspects of the system. These data essentially verify and extend data obtained during the two previous series of tests. A detailed analysis and comparison of these data is included in section 6. The significant data are summarized below.

1. The A3 core operated an X39-4 engine on nuclear power alone for 144.77 hours. Of this time, the core discharge air temperature averaged 1280°F for the first 106 hours and 1380°F for the remainder.
2. During this test series 3092 megawatt-hours of energy were developed during 40 transfers to full nuclear power as compared to 2409 megawatt-hours and three transfers on the two previous operations.
3. The X39-4 engine was operated for 22 consecutive hours on full nuclear power. This would have been 26 hours had not an instrumentation scram occurred 4 hours after startup.
4. Postoperation observation of the fuel elements indicated extensive plate blistering but no gross oxidation or melting as observed during previous operations. The condition of oxide layers examined indicated very low temperature-stress oxidation.
5. The no-flow and low-flow tests substantially extended and verified previous data. With aftercooling blowers on, it was possible to obtain a total temperature rise ratio of 3:1 across the core without observing any flow instability or maldistribution. With no flow, it was possible to dissipate 70 kilowatts with a maximum observed fuel element temperature of 1150°F.
6. An automatic reactor startup was achieved using the fission chambers and log-count-rate instrumentation. The reactor could be brought to any designated power in the power range by transferring to the dynamic servo system above 1 percent power and making interconnections appropriately in the shim withdraw bus.
7. The change in reactivity associated with a change in moderator temperature was considerably greater than measured during IET No. 2 (0.022 percent $\Delta k/k$ as compared to 0.017), and the rate of change of reactivity with temperature decreased considerably more at higher temperatures.

8. Measurements of rod-pattern effects substantiated the results of IET No. 3 tests, which indicated that the motion of a control rod affects the temperature in fuel cartridges remote from the rod as well as those immediately adjacent to it.
9. Results of the xenon poisoning tests were very similar to those obtained during IET No. 4.
10. The modifications to the X39-4 jet engines reduced the required fuel plate temperatures to the extent that transfer to and operation on full nuclear power presented no difficulties.

1.3 REFERENCES

1. "HTRE No. 1 Design and Operational Summary," GE-ANPD, APEX-398, 1958.
2. Trussell, J. I., "Core Tank Facility," GE-ANPD, DC 53-8-79, August 1953.
3. Long, W. H., "Preliminary Design Report for the First HTRE Core (AC-100A)," GE-ANPD, XDC 54-2-53, February 1954.
4. Heddleson, C. F., "HTRE-1 Operation Summary," GE-ANPD, XDCL 57-11-128, 1957.

2. DESIGN DATA

2.1 GENERAL DESCRIPTION OF THE HTRE NO.1 TEST ASSEMBLY

The HTRE No. 1 power plant test assembly[1] consisted of an air-cooled, metallic-fuel-element, water-moderator reactor operating a single, modified J47 turbojet engine. The entire test assembly included emergency cooling facilities and other IET equipment. The turbojet engine and shield were part of a mobile facility called the Core Test Facility (CTF). The CTF is shown in Figure 2.1. A reactor core and stepped shield plug were inserted in the shield. The core, shield plug, control actuators, source rod, startup fission chambers, and operating ion chambers were combined into an integral unit before insertion into the shield.

A simplified schematic drawing of the power plant and control system is shown in Figure 1.2. The air entered the turbojet engine and was compressed to approximately five times the intake pressure. From there it was collected in a scroll and ducted to a manifold on top of the shield tank. The air passed through the shield in a number of parallel ducts and entered the air plenum chamber above the reactor. The inlet plenum chamber is shown crosshatched in the drawing. The air passed through the reactor, was heated, and entered a plenum chamber at the reactor exit. The exit plenum chamber is shown shaded. From the plenum chamber the air returned to the engine, turned the turbine that drove the engine compressor, and was exhausted to the exhaust handling system.

The engine could be operated on nuclear or chemical fuel or a combination of both. The chemical fuel was burned in an external burner can, since the space normally occupied by burner cans in the engine was taken up by the air scrolls used in ducting the air to the reactor. When the engine was operating on chemical fuel, the compressor air could pass through either the reactor or a bypass duct.

The basic method of controlling the power plant is shown schematically in Figure 1.2.

When operating on chemical fuel only, the engine was controlled by regulation of the turbine exhaust temperature. A demand for increased temperature caused the chemical fuel valve to open and thus to supply more fuel to the burner can. When the designated temperature was reached, a thermocouple in the turbine exhaust fed back a signal to balance the temperature-demand signal. The engine speed could be changed by changing the area of the engine exhaust nozzle. Reducing the nozzle area increased the back pressure on the system and slowed down the engine. The engine speed was held constant by an automatic control system independent of variations in turbine exhaust temperature.

The reactor power was controlled by the insertion or withdrawal of poison rods. The neutron flux level in the top plug was used as a measure of reactor power.

The power plant was started on chemical fuel alone with compressor air passing through the cold reactor. Then with the engine speed and turbine exhaust temperature controls set at a predetermined level the reactor was started and the power increased. When the nuclear heat added to the air was detected by the turbine exhaust thermocouple, the chemi-

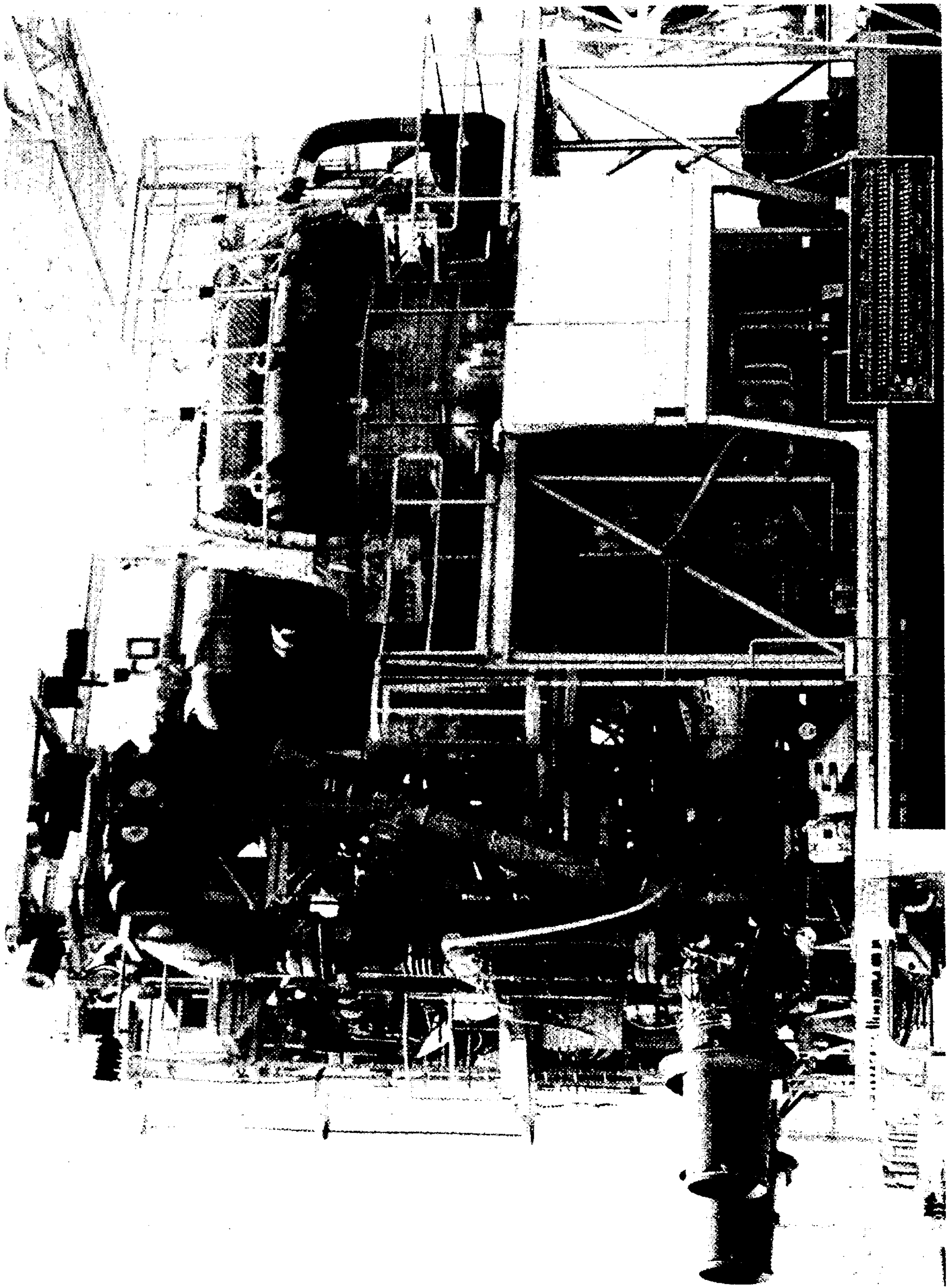

Fig. 2.1 – Core Test Facility

cal fuel valve would start to close in an attempt to maintain the exhaust temperature at the predetermined level. As the reactor power was increased, the chemical fuel valve closed completely. Engine speed was held constant throughout. Further increase in reactor power caused an increase in exhaust temperature. Temperature limiters caused automatic scram if the reactor operator allowed an excessive temperature increase while on nuclear power.

The reactor, fuel elements, and controls are described in the following sections.

2.1.1 REACTOR ASSEMBLY

The first reactor for the Heat Transfer Reactor Experiment was called the A2 reactor. An artist's conception of the reactor is shown in Figure 1.1. The reactor was air-cooled and had metallic fuel elements and a water moderator.

The reactor and shield plug assembly is shown in Figure 2.2. The dished head, which constituted the lower portion of the shield plug, was known as the transition section. It was an integral part of the reactor assembly in that it was connected by control rod guide tubes and water tubes to the reactor. The transition section was also made of aluminum.

A summary of the stress analysis for the A2 reactor is presented in reference 2.

The shield plug structure and the heavy gamma shielding were stainless steel. Moderator water was used for neutron shielding in the shield plug.

Reactor Components

Reactor components during assembly are shown in Figures 2.3 through 2.7. The core was a 37-tube bank of hexagonal pattern with radially varying tube spacings. The active portion of the lattice was a regular hexagonal prism 30.8 inches across flats, 35.5 inches across corners, and 29.125 inches long. The tubes extended 12.94 inches beyond each end of the active section. The tube bank was contained by tube sheets at each end and by a cylindrical shell that formed a tank 59 inches in diameter and 55 inches long. The core tank also contained the beryllium reflector, which was a 4-inch-thick hexagonal shell spaced 5/8 inch from the outside tubes and supported from brackets that were welded to the core tube sheets. The control rod guide tubes were welded into the top tube sheet and were located by small spacer plugs that were welded to the top face of the bottom tube sheet. These guide tubes not only guided the displacement-type control rods, which penetrated the core to the depth of the bottom of the active lattice, but also served as inlet tubes for moderator water. The water flow in the core was a two-pass system. The water flowed down the control rod guide tubes and diverged into two paths: part of the water traveled up along the fuel tubes and along the inside of the reflector; the remainder passed along the outside of the reflector.

The shield plug had two steps to avoid straight-line passage for radiation streaming. The top plate of the plug was bolted to the CTF shield. The control rod actuators were mounted on the top plate of the plug, as were the nuclear sensor supports, the neutron source actuators, the water inlet and outlet pipes, and the instrumentation leads for the reactor assembly.

2.1.2 THERMODYNAMIC CHARACTERISTICS

While a nuclear reactor can, in principle, deliver an unlimited amount of power, the practical limit on the power that can be extracted from a reactor of given size is imposed by the ability of the system to transfer the power to the coolant. Heat transfer is limited by the maximum temperature at which fuel elements can be operated, or, more specifically, by the maximum temperature difference that can be maintained between the fuel elements and the air coolant. Since, in the air cycle, pressure losses also impose a limitation on performance, it is desirable to keep the fuel element area to a mini-

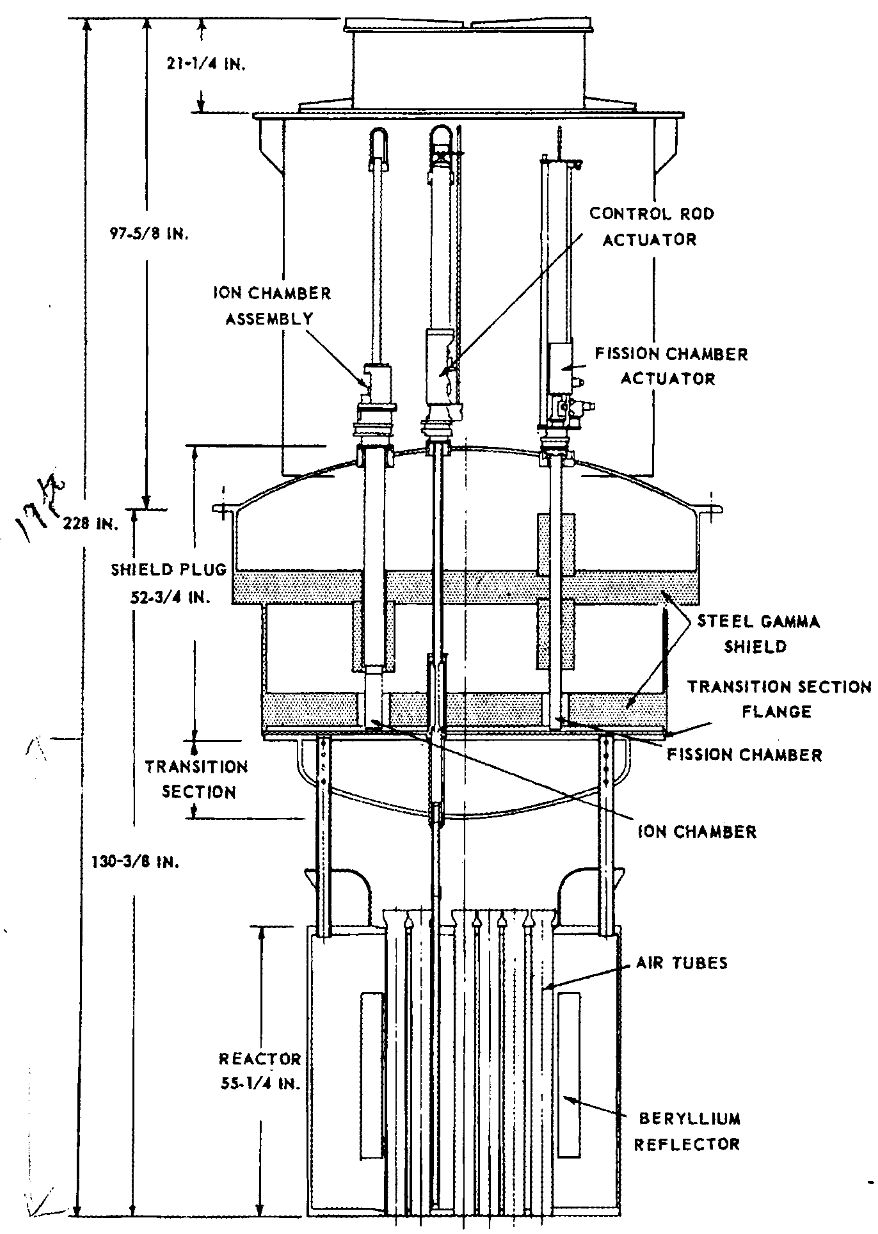

Fig. 2.2 – Schematic drawing of reactor assembly

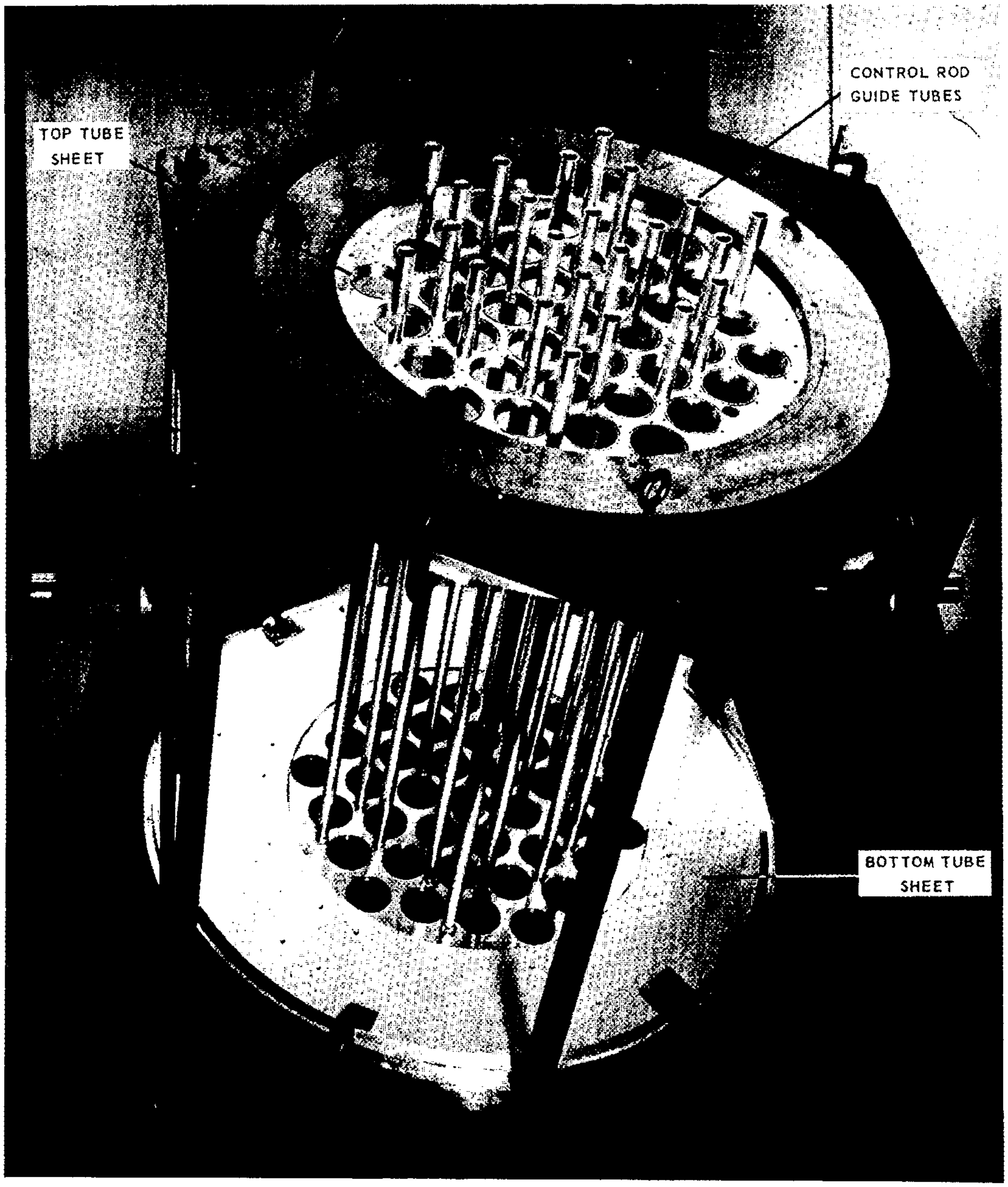

Fig. 2.3—Preliminary assembly of D101A2 core showing control rod guide tubes installed

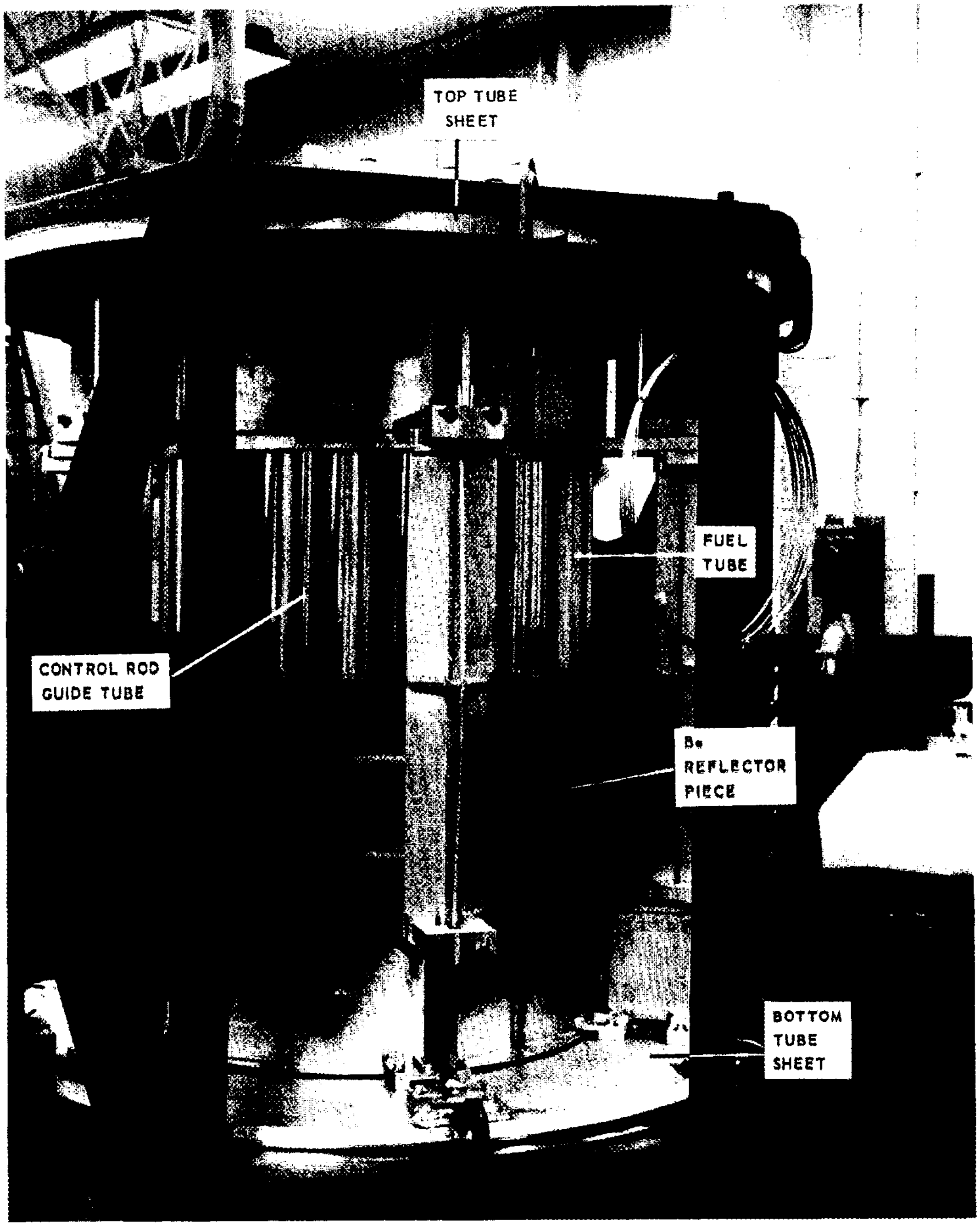

Fig. 2.4 – Assembly of D101A2 core with half of the beryllium reflector in place

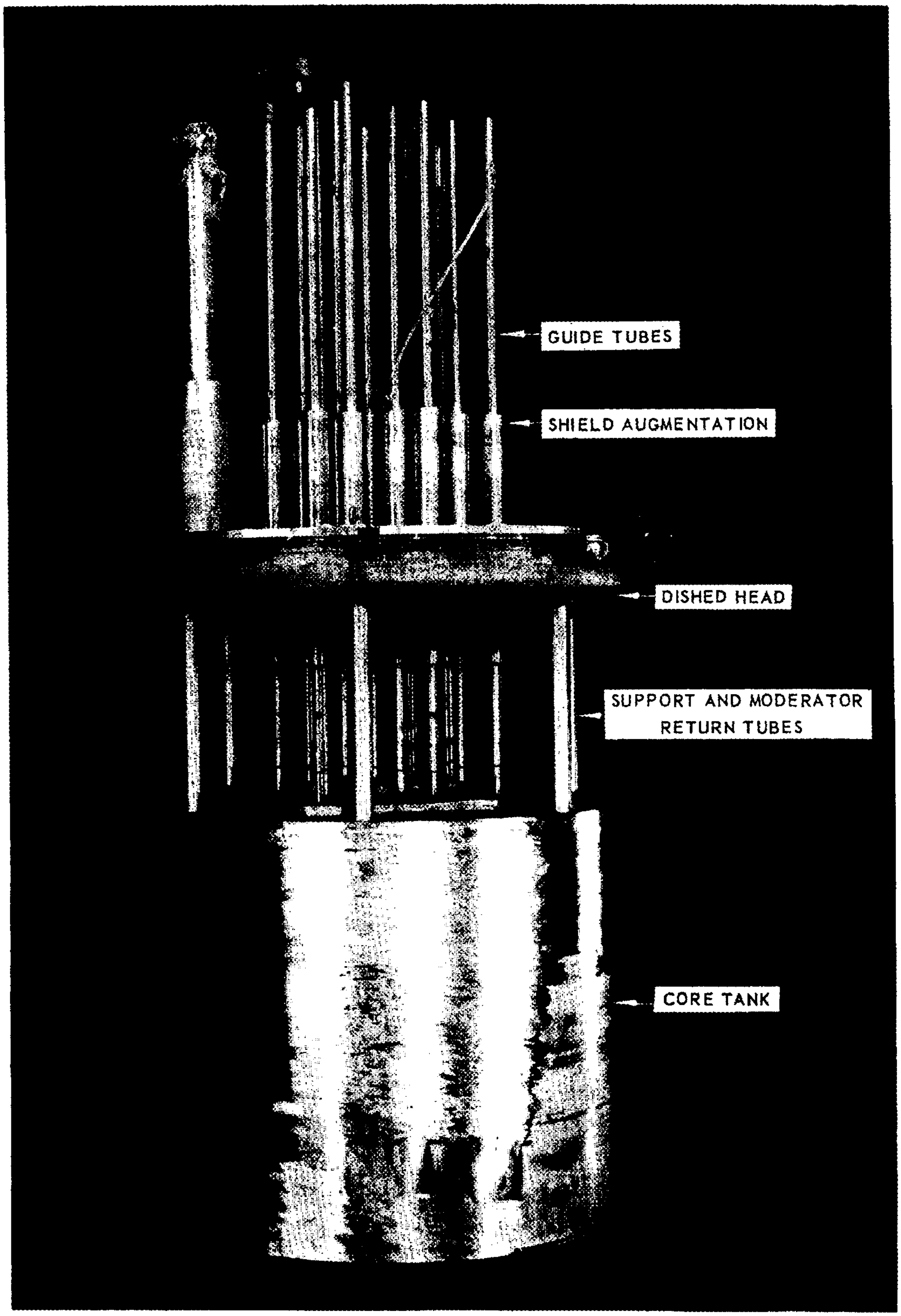

Fig. 2.5 – D101A2 core and transition section

UNCLASSIFIED

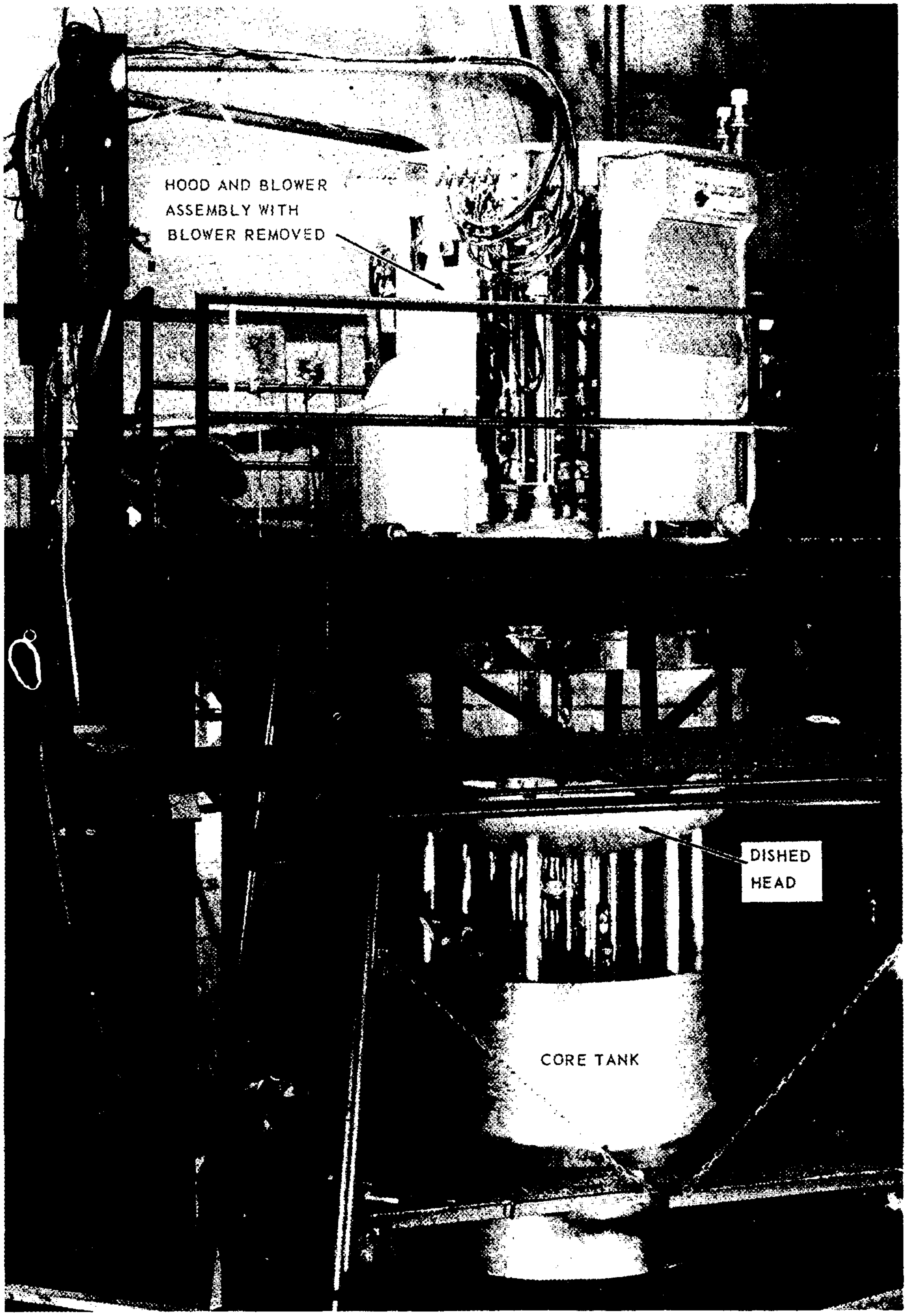

Fig. 2.6 – D101A2 core and shield plug in preliminary test stand

UNCLASSIFIED

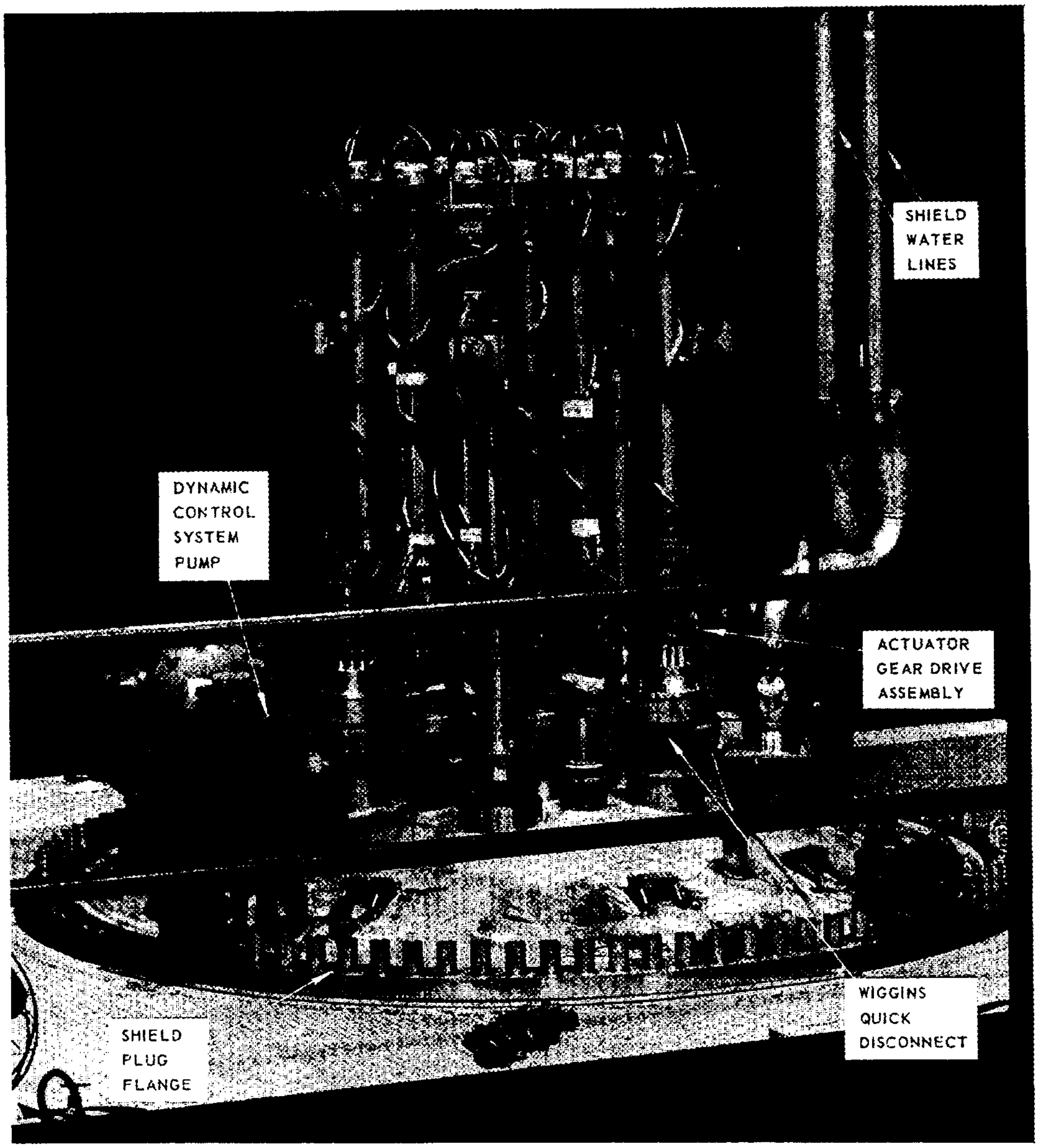

Fig. 2.7 – Top of D101A2 shield plug showing actuators (hood and blower removed)

mum. The optimum configuration is thus one in which the fuel elements are all operated at the maximum possible uniform temperature.

Three nuclear power distributions must be compensated for to achieve the design performance: (1) the longitudinal power distribution, (2) the gross radial power distribution, i. e., the variation of average power from tube to tube in the transverse plane, and (3) the fine radial power distribution, i. e., the variation of power per unit mass of fuel caused by self-shielding within a single fuel tube.

In the design of the D101A reactor, these three distributions are controlled in the following manner:

1. The fuel elements are divided into 18 stages for purposes of structural integrity; these 18 stages are in turn divided into two sections with 11 stages in the first and 7 in the second. Each section has a different total heat-transfer area per stage; the section in the entrance region has the smallest area, since the available temperature difference between fuel elements and air is high near the core inlet and allows high heat transfer per unit area.
2. The gross radial power is equalized from tube to tube by varying the spacing of the tubes. Near the outside of the reactor, where the power would normally be low, the tube spacing is increased. Thus more moderator is associated with each tube and the thermal flux between tubes is equalized. The beryllium reflector is also important in maintaining a sufficiently high flux in the outer tubes.
3. The fine radial power distribution within each tube is regulated by making the fuel sheets thicker near the center of the tube. Thus the fuel mass per unit heat-transfer area is increased in proportion to the decrease in power per unit mass of fuel caused by self shielding.

An important feature of these methods of power compensation is that all fuel cartridges may be designed to be identical, and fabrication is simplified.

The fuel-element heat-transfer area was designed for a nominal maximum fuel element temperature of 1700°F, with the assumption that the temperature of the discharge air is 1335°F. The term nominal means that if all the fuel elements were at the same temperature the designated combination of fuel element temperature and air temperature would be achieved. In operation, some departures from this condition occur because of power and flow maldistributions.

Experimental work on power distributions in the critical mockup indicated that the desired gross radial power distribution was effectively achieved. The ratio of peak to average power from tube to tube was estimated at 1. 05. The degree of power flattening achieved within the fuel tubes was limited by manufacturing tolerances to maldistributions of not over 10 percent. In operation, therefore, local temperatures could be in the neighborhood of 1900°F. Single-plate irradiation tests indicated that 80 Ni - 20 Cr has satisfactory oxidation resistance at this temperature. Since the temperature limitation is imposed by oxidation resistance over a long period of time, transient temperatures considerably higher could be tolerated.

2. 1. 3 FUEL ELEMENTS AND FUEL CARTRIDGES

A typical fuel cartridge is shown in Figure 2. 8. Its total weight was calculated at 18. 7 pounds. The cartridge was composed of 18 stages or elements, a forward ring assembly, and an aft assembly.

Each element consisted of a number of concentric rings joined and spaced at the leading edge by brazed channels and spaced at the trailing edge by trapezoidal spacers. Each ring was composed of fueled ribbon nominally 1-1/2 inches wide and sealed at each end with braze-coated wire equal in diameter to the thickness of the fueled ribbon. Fueled ribbon

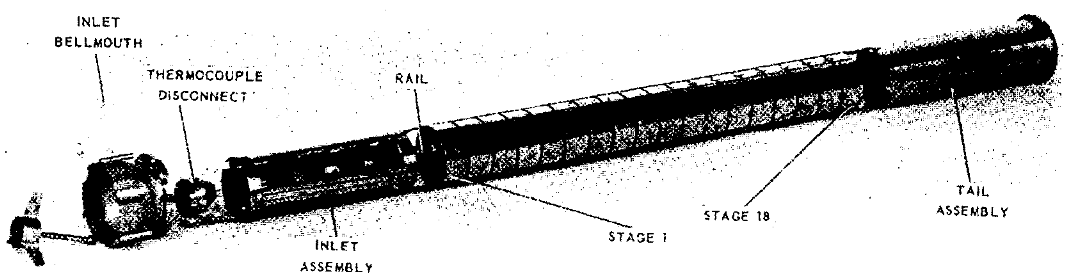

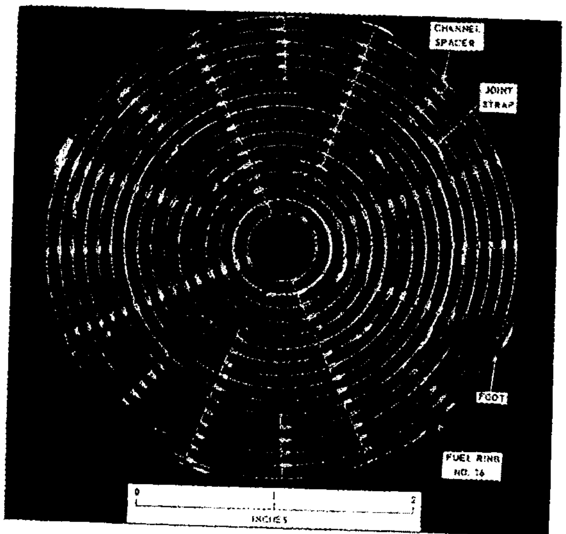

CORE A2 ELEMENT, FRONT VIEW

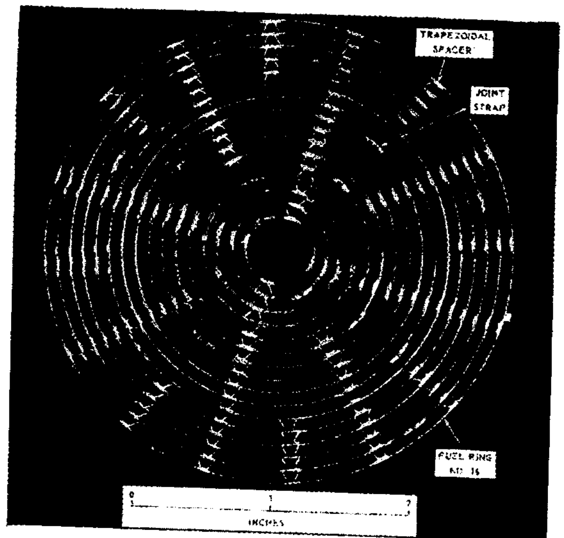

CORE A2 ELEMENT, REAR VIEW

Fig. 2.8 – D101A2 fuel element and cartridge assembly

was made up of the meat and 0.004-inch cladding on each surface. The meat was formed of a mixture of enriched UO_2 and special 80 Ni - 20 Cr material. The weight ratio of this mixture (UO_2/total) was 42 percent on all rings except for the innermost ring of all elements, for which the ratio was 40 percent. All the varying thicknesses of ribbon had nominally the same 0.004-inch cladding on each side. The cladding was a modified 80 Ni - 20 Cr.

The parts of the element were brazed together. The elements were spot-welded to four rails through non-fueled members. The forward ring assembly and the aft assembly were spot-welded to the four rails of the element assembly.

Connection and support of the cartridge in the core was automatic upon insertion. Disconnection for removal was accomplished by insertion of a disconnect rod, which opened the support fingers and allowed withdrawal of the cartridge. The disconnect rod did not remain in the core during operation.

2.1.4 SPECIFICATIONS AND DESIGN DATA

The general physical dimensions of the power plant and the basic design parameters are described in detail in reference 19. These design parameters are elaborated further in succeeding sections of this report.

2.2 NUCLEAR CHARACTERISTICS

2.2.1 ACTIVE CORE DIMENSIONS AND MATERIALS CONTENT

The active core of the HTRE No. 1 reactor was a hexagonal bank of 37, 4-inch OD (0.080-inch wall) aluminum tubes containing 80 Ni - 20 Cr fuel elements impregnated with UO_2. Each fuel element had a loaded length of 29.125 inches. The detailed nuclear design of the fuel elements is reported in reference 3. The tube layout with dimensions is shown in Figure 2.9.

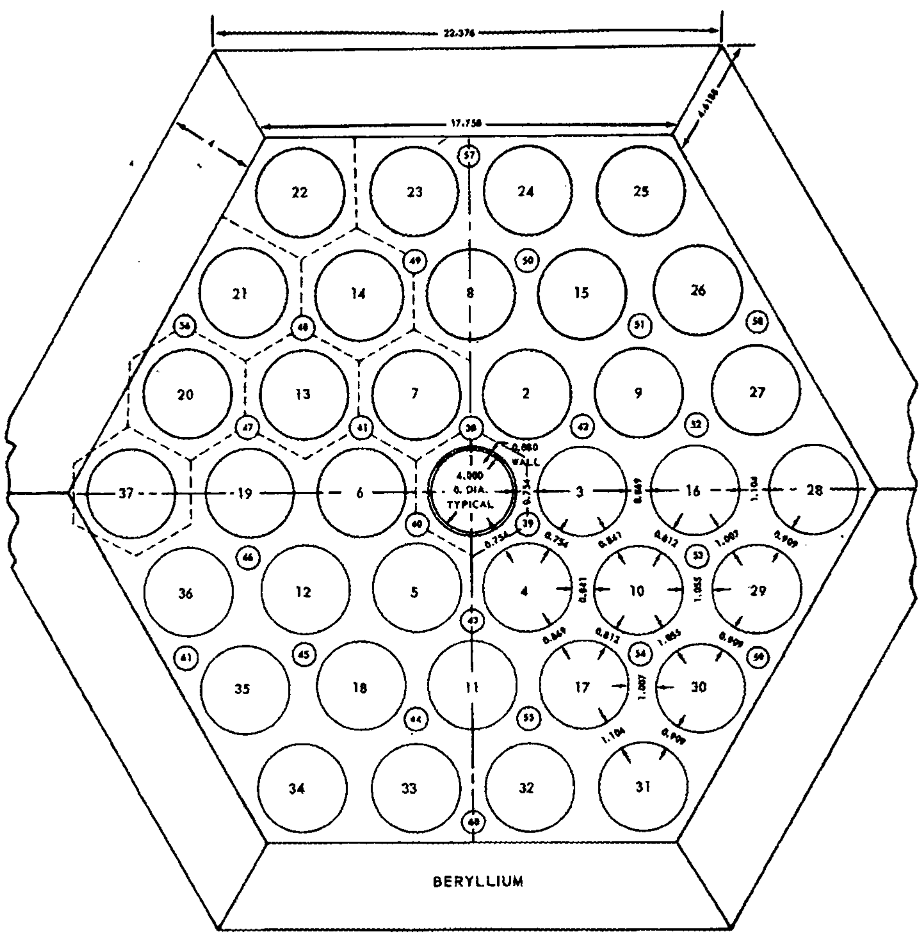

Fig. 2.9 – D101A2 active core dimensions and tube layout

Unloaded tube-water matrix extended on each end of the active core for 12-1/2 inches to serve as end reflector. Fuel element nose and tail assemblies occupied the void regions of the tubes (see Table 2.1). The radial reflector consisted of six 4-inch-thick, 32-inch-long beryllium slabs arranged in a hexagonal shell (see Figure 2.9).

Over-all dimensions, volume fractions, and weights of materials are shown in Table 2.2. In general, volumes were computed and weights derived. Specific gravities used are also shown.

The volume fractions given in Table 2.2 were computed from actual amounts of materials present based on a total core volume defined by the inside surface of the beryllium reflector. Macroscopic cross sections for the constituents of the fuel elements are given in reference 4.

Detailed Cell Dimensions of Active Core

As mentioned previously, gross radial power flattening was achieved by varying the spacing of tubes. The spacing between tubes is shown in Figure 2.9.

For purposes of analysis, it was convenient to divide the core into a series of fuel-moderator cells that defined the variation of moderator concentration over the core radius. Because the configuration was symmetrical, it could be assumed that the thermal flux had a zero derivative (maximum value) halfway between adjacent fuel tubes. The lines of symmetry were used to define the cells. Dotted lines on Figure 2.9 show typical cell boundaries. Most of the cells are irregular hexagons. It can be seen in Figure 2.9 that there were six unique cell configurations (e.g., tubes 1, 2, 9, 15, 25, 26) that defined the basic core geometry. Table 2.3 lists the parameters that were significant as the cell geometry varies.

Table 2.3 lists cell volumes and volume fractions. For tubes on the outer periphery of the core, cells were defined by the surface of the beryllium as shown in Figure 2.9. Since the peripheral tubes constituted nearly half the total number of tubes, the "average" core water volume fraction was more heavily weighted by these than by the central tubes.

To define a set of volume fractions for a homogeneous core model, it was thought preferable to include in the core only the water in symmetrical hexagonal cells surrounding the peripheral tubes. A set of such cells (20 and 37) is shown in Figure 2.9. The volume fractions defined by such a set of cells are given in Table 2.4.

For analyses, it was convenient to replace the hexagonal cell by a model consisting of the fuel tube surrounded by an annular moderator region, hence the tabulation "equivalent annulus thickness." The equivalence is based on equal water volume.

2.2.2 REACTIVITY

Table 2.5 shows calculated and measured reactivity changes due to various causes; Table 2.6 shows the energy distribution of neutron flux in the reactor normalized to a reactor power of 1 watt.

Reactivity Value of Materials

During measurements on the nuclear mockup made to establish the fuel loading requirement, the reactivity value of a number of materials was measured.[5,6] All measurements were made in single tubes, principally the central tube. Changes were essentially uniform with respect to length. The radial importance function with respect to the position of the tubes was essentially the same regardless of the nature of the change within the tube.

Experimental evidence showed that the changes in multiplication measured in single tubes were linearly superposable to determine the expected change in multiplication for 37 tubes. This was adopted as a working hypothesis. Division of the gross change in multiplication by multiplication observed in tube 1 produced the factor 24.8, which could be used used to relate tube-1 coefficients to gross changes in multiplication.

TABLE 2.1

COMPOSITION OF END REFLECTOR

Material	Volume Fraction	Weight, lb	Weight Fraction	Specific Gravity
Water	0.4280	158.284	0.5684 nose 0.5047 tail	1.00
Aluminum and insulation equivalent	0.0508	50.724	0.1821 nose 0.1618 tail	2.7
Stainless steel (0.010-in. + 0.002-in. insulation liners)	0.00627	18.040	0.0648 nose 0.0575 tail	7.78
Stainless steel (Fuel element structure)	0.01862 nose 0.03133 tail	51.430 nose 86.543 tail	0.1847 nose 0.2760 tail	7.78

TABLE 2.2

GROSS ACTIVE CORE PARAMETERS

Length:	29.125 in.
Diameter: across flats	30.758 in.
across corners	35.516 in.
Volume:	13.809 ft^3
Diameter of right circular cylinder of equivalent volume:	32.298 in.

Active core materials	Effective Volume Fraction		Weight, lb	Specific Gravity
Water	0.402		334.8	1.00
Aluminum and insulation equivalent[a]	0.0531		117.60	2.7
80 Ni - 20 Cr	0.0576	0.528	407.65	8.62
Uranium, 93.4% enriched	0.00588		90	18.68
Stainless steel	0.00942		60.16	7.78
Core volume			13.22 ft^3	

[a]Since the Thermoflex insulation consists of aluminum and magnesium oxides, it was lumped, for convenience, with the aluminum in fuel tubes and control rod guide tubes on a weight basis.

TABLE 2.3

HETEROGENEOUS CORE CELL PARAMETERS

Tube No.	Cell Volume, in.^{3}	Equivalent Annulus Thickness, in.	Volume Fractions[a]				
			Water	80Ni-20Cr	Uranium (Enriched)	Stainless Steel (Liners)	Stainless Steel (Feet and Rails)
1	568.853	0.4906	0.3544	0.06222	0.006343	0.007067	0.003106
2	581.400	0.5189	0.3690	0.06088	0.006206	0.006915	0.003039
9	606.437	0.5718	0.3944	0.05837	0.005951	0.006629	0.002913
15	616.638	0.5942	0.4051	0.05740	0.005852	0.006548	0.002864
25	699.047	0.7632	0.4758	0.05063	0.005162	0.005751	0.002527
26	689.372	0.7432	0.4679	0.05134	0.005235	0.005831	0.002563
Core		0.6513	0.4280	0.05519	0.005627	0.006273	0.002755

[a]Based on core volume of 13.809 ft^3

TABLE 2.4

HOMOGENEOUS CORE CELL PARAMETERS

Tube No.	Cell Volume, in.^{3}	Equivalent Annulus Thickness, in.	Volume Fractions[a]				
			Water	80Ni-20Cr	Uranium (Enriched)	Stainless Steel (Liners)	Stainless Steel (Feet and Rails)
1	568.852	0.4906	0.3544	0.06530	0.006656	0.007417	0.003260
2	581.399	0.5189	0.3690	0.06389	0.006513	0.007257	0.003189
9	606.438	0.5718	0.3944	0.06126	0.006245	0.006957	0.003057
15	616.637	0.5942	0.4051	0.06024	0.006142	0.006872	0.003006
25	639.559	0.6429	0.4271	0.05313	0.005417	0.006036	0.002652
26	625.311	0.6124	0.4134	0.05388	0.005494	0.006119	0.002690
Core		0.5894	0.4024	0.05792	0.005905	0.006583	0.002891

[a]Based on core volume of 13.158 ft^3

TABLE 2.5

CALCULATED REACTIVITY DATA

Excess Multiplication, Δ k	
Equilibrium xenon poisoning (20 mw)	-2.2%
Maximum xenon poisoning (20 mw)	-2.8%, 6-7 hr after shutdown
Water temperature change	(60° - 150°F) + 1.26%[a]
Expected cold, clean excess in HTRE	3.6%
Moderator temperature coefficient	at 60°F + 0.016%/°F[a] at 140°F + 0.012%/°F[a]
Percent thermal fissions	61
Leakage	29.0%
End reflector savings	2.7 in. per end
Radial reflector savings	8.4 in.

[a]Measured value

TABLE 2.6

CALCULATED NEUTRON FLUX

Group	Lethargy, u	Lower Energy Limit, Ev	$\int_0^u \phi(u)du$, neutrons/cm^2-sec-watt
	0	10^7	
1	0.50	6.065×10^6	0.1139×10^6
2	1.00	3.679×10^6	0.5515×10^6
3	1.50	2.231×10^6	1.2850×10^6
4	2.00	1.353×10^6	2.0642×10^6
5	2.50	8.208×10^5	2.7300×10^6
6	3.00	4.979×10^5	3.2568×10^6
7	3.50	3.020×10^5	3.6630×10^6
8	4.00	1.832×10^5	3.9762×10^6
9	6.00	2.479×10^4	4.8273×10^6
10	8.00	3.355×10^3	5.3992×10^6
11	10.00	454	5.9186×10^6
12	12.00	61.433	6.4066×10^6
13	14.00	8.314	6.8526×10^6
14	15.50	1.855	7.1570×10^6
15	16.50	0.6824	7.3458×10^6
16	17.50	0.2510	7.4928×10^6
17	18.50	0.9235	7.6029×10^6
18	19.554	0.03219	7.6869×10^6
Thermal			9.4971×10^6

$\bar{\phi}_{th}$ water $= 1.81 \times 10^6$ — V: volume fraction

$\bar{\phi}_{th}$ fuel $= 3.89 \times 10^5$ — W: water

$\bar{\phi}_{th} = \bar{\phi}_W V_W + \bar{\phi}_F V_F = 9.57 \times 10^5$ — F: fuel

The nuclear mockup contained two uniform fuel loadings: one with 60 pounds enriched uranium and one with 90 pounds. Both of these loadings have been used as base points for reactivity coefficients; their characteristics are summarized in Table 2.7.

Reflector experiments in the TRA-3 nuclear mockup are described in references 7 and 8.

Reactivity Versus Fuel Loading

A mass-versus-reactivity curve was established by varying the fuel loading in tube 1. For these measurements the 80 Ni - 20 Cr loading was also varied in a manner corresponding to the nickel-chromium alloy appearing in the fuel meat of the design fuel element. The design analysis is reported in reference 9.

Radial Importance Function

Figure 2.10 shows a composite of radial importance functions composed from the various types of measured reactivity coefficients.

Effect of Moderator Temperature

Figure 2.11 shows the change in multiplication constant for the reactor as a function of change in moderator temperature. The base point for this curve was the 90-pound-load nuclear mockup at 60.33°F. Since a very similar curve was obtained for the 60-pound loading, it was concluded that moderator temperature effects are essentially independent of the base multiplication constant (or fuel loading) of the reactor.

TABLE 2.7

CHARACTERISTICS OF CRITICAL MOCKUPS

	60-lb Loading		90-lb Loading[a]	
	lb per tube	lb total	lb per tube	lb total
Fuel (93.4% enriched U + TEFLON)	1.622	60	2.432	90
80 Ni - 20 Cr	9.19	340.03	11.18	413.66

[a]The 90-pound cartridge was insulated with 0.10-inch Thermoflex plus 0.010-inch inner and 0.002-inch outer stainless steel liners

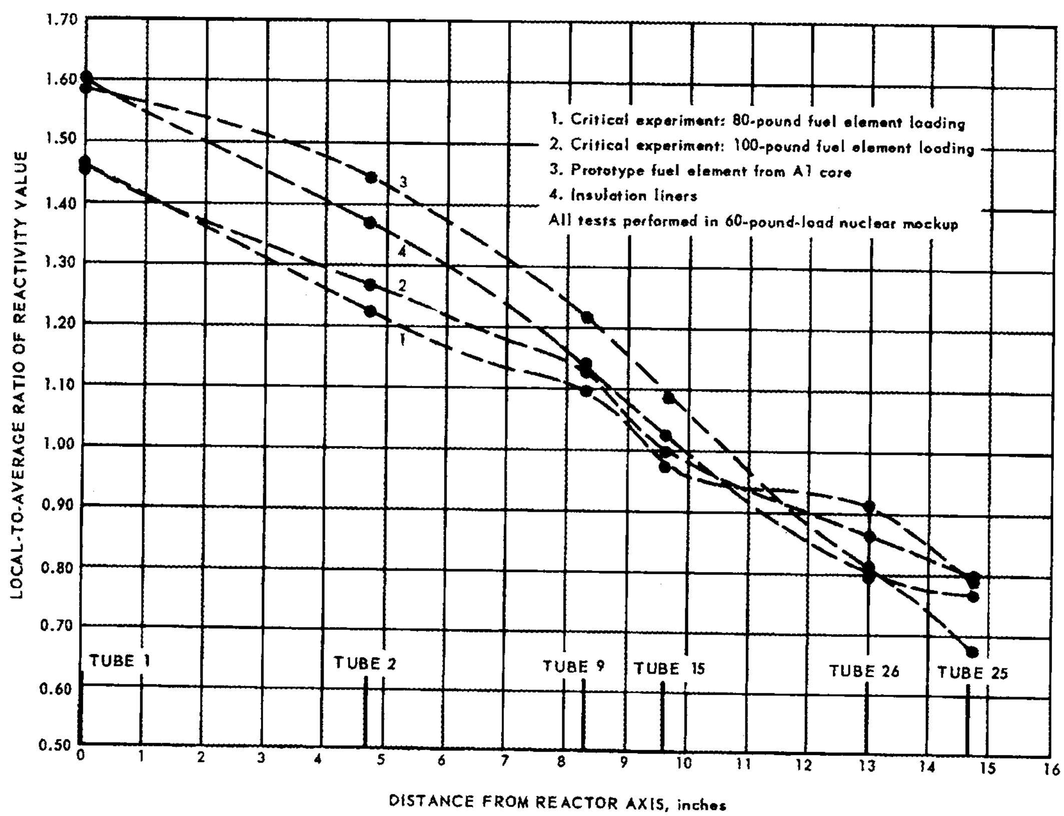

Fig. 2.10 – Comparison of radial importance functions for reactivity variations due to changes in single fuel elements

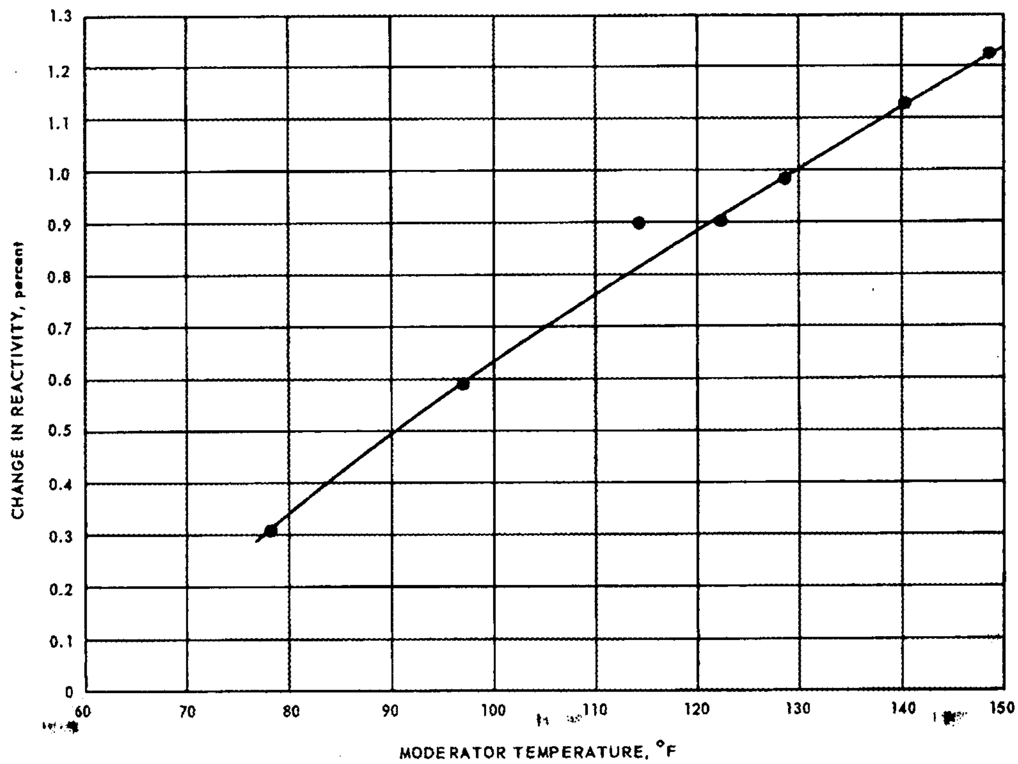

Fig. 2.11 – Change in reactivity versus change in moderator temperature, 90-pound mockup

Fission Product Poisoning

Table 2.8 summarizes the decrease in reactivity due to burnup and the poisoning effects of fission products. The calculations leading to this table were performed for a fuel inventory of 67 pounds enriched uranium so that they were not strictly applicable to core A, which had a 90-pound loading. The reactivity values would be slightly lower for the 90-pound loading. As the table shows, xenon poisoning is the only significant poisoning effect. Figure 5.3 in section 5 presents the xenon history determined from the IET No. 6 power operations. This history was computed using an equation for reactivity that accounted for the change in the thermal utilization factor caused by xenon. The experimental data points are included for comparison.

Control Data

Table 2.9 presents typical values of the control rod positions in the reactor. Since many of the positions were symmetrical, values are given only for typical positions as shown in the tube layout in Figure 2.9. As auxiliary data, the values determined in the 60-pound-load nuclear mockup are also given.

The tabulated values for the 90-pound loading were measured in a configuration in which almost all control rod positions were filled. There were three control rods around tube 1 (positions 38, 39, 40). Hence the variation between the tabulated rod values for the 60-pound and the 90-pound loadings may have been due more to rod shadowing than to intrinsic changes caused by the difference in loading. This hypothesis was supported by the fact that rods in the third and fourth rings, which were more widely separated, did not change in value.

TABLE 2.8

TOTAL POISONING AND DEPLETION REACTIVITY EFFECTS AFTER 100 HOURS AT 20 MEGAWATTS

	After 100 Hours Operation (20 mw)	One Hour After Shutdown	Ten Hours After Shutdown	One Hundred Hours After Shutdown
Xe^{135}	2.39%	2.65%	3.06%	0.01%
Sm^{149}	0.09%	0.10%	0.11%	0.18%
Fuel Depletion	0.03%	0.03%	0.03%	0.03%
Fission products exclusive of Xe^{135} and Sm^{149}	0.03%	0.03%	0.03%	0.03%
	2.54%	2.81%	3.23%	0.25%

TABLE 2.9

CONTROL ROD POSITION VALUES

Position Ring No.	Positions	Percent Δk Value per Position (60-lb loading)	Percent Δk Value per Position (90-lb loading)	No. Shim-Scram Positions	Percent Δk Total Value Shim-Scram Positions (90-lb loading)
1	38, 39, 40	0.55	0.58	2	1.16
2	41, 42, 43	0.49	0.51	3	1.53
3	44-56	0.37	0.37	10	3.70
4	57-62	0.23	0.23	6	1.38
			Totals	21	7.77

Although conclusive and detailed data on rod shadowing were not available, spot checks indicated that shadowing magnitudes were small.

Figure 2.12 shows an incremental calibration curve for control rods based on nuclear mockup data. The curve shows percentage of total rod values as a function of the length of rod inserted. Curves of this nature were obtained for three rods in the nuclear mockup. Variation in the shape of the three curves was negligible, so that the single curve presented here is considered representative.

Figures 2.13, 2.14, and 2.15 show the relation between reactivity and period as derived from reactor kinetics equations. The kinetics equations used were modified to account for the variation in leakage probability between fission-spectrum neutrons and delayed neutrons. The variation was accounted for by defining effective fractions of delayed neutrons. These fractions were larger than the actual fractions because the delayed neutrons were born at lower energies than those of the bulk of the fission spectrum and had smaller leakage probability. Effective values for delayed neutron fractions are shown in Table 2.10. The period reactivity relation shown is the one used for control rod calibrations in the critical mockup.

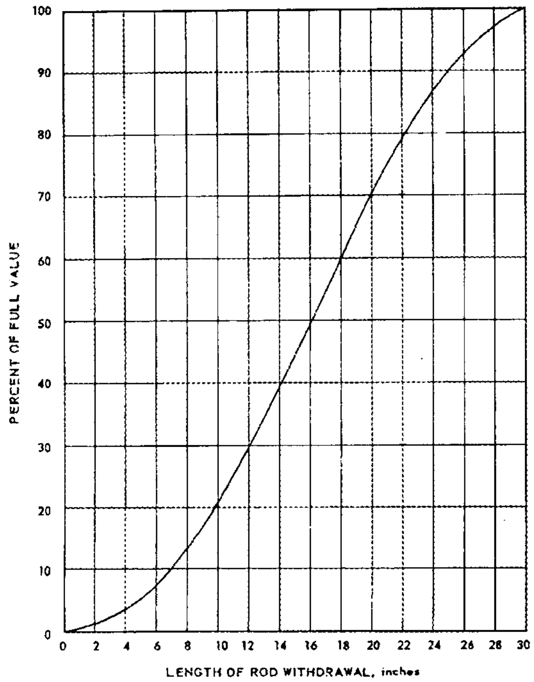

Fig. 2.12 – Incremental calibration curve for nuclear mockup control rod

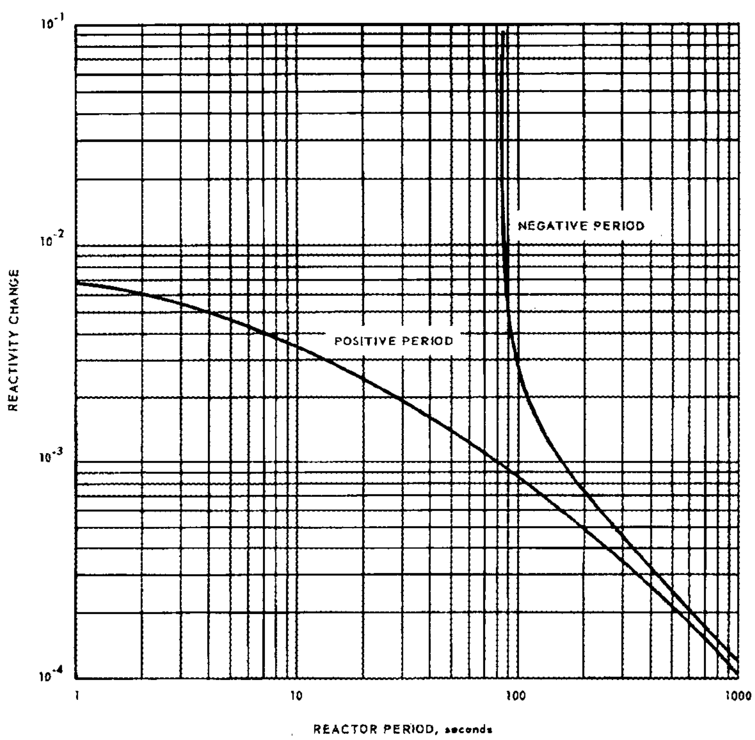

Fig. 2.13 – Stable period versus excess multiplication

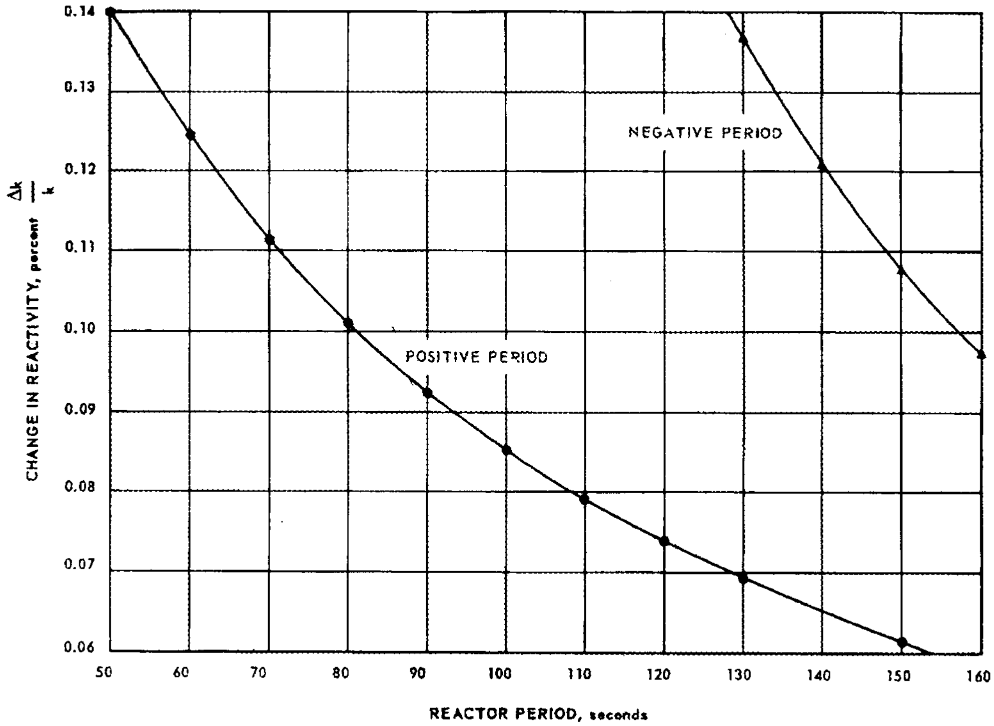

Fig. 2.14 – Stable period versus excess multiplication, reactor period 50–160 seconds

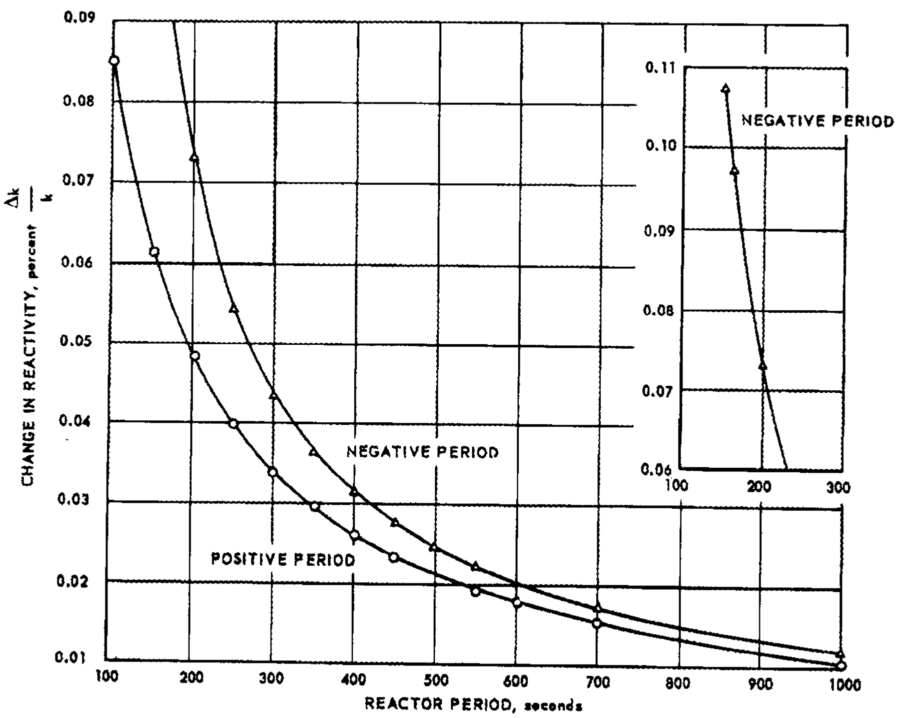

Fig. 2.15 – Stable period versus excess multiplication, reactor period 100–1000 seconds

TABLE 2.10

EFFECTIVE VALUES FOR DELAYED NEUTRON FRACTIONS

Delayed Neutron Group	Decay Constant λ_i sec^{-1}	Actual Fraction	Effective Fraction, β
1	14.3	0.00025	0.00029
2	1.61	0.00085	0.001011
3	0.456	0.00241	0.002821
4	0.151	0.00213	0.002521
5	0.0315	0.00166	0.002016
6	0.0124	0.00025	0.00032
Total		0.00755	0.008979

The equation used is:

$$k_{ex} = \frac{\iota}{T} \pm \sum_{1}^{6} \frac{\beta i}{1 + \lambda_i T}$$

where $\iota = 4 \times 10^{-5}$ seconds.

2.2.3 POWER DISTRIBUTIONS

A detailed discussion of the primary and secondary power distributions of the HTRE No. 1 is contained in APEX-398, pp. 59-82. Further elaborations are to be found in references 10 through 15.

2.3 FUEL ELEMENT THERMODYNAMIC DATA

2.3.1 GENERAL

Fuel element thermodynamic design work for the reactor consisted of defining a fuel element structure capable of dissipating a specified heat load within limitations of maximum allowable system pressure loss and maximum fuel element temperature. Checking of these various design criteria required the interrelation of engine variables, aerothermodynamic relations for the fuel element system, nuclear characteristics of the active core, and presssure-and heat-loss characteristics of the auxiliary systems connecting the engine to the reactor. The following paragraphs present pertinent data used for interrelation of these variables to check design and predict operating characteristics of the fuel element system.[15]

X39-4 Engine Characteristics

The engine characteristic data presented in Figures 2.16 through 2.19 were obtained from experimental tests of prototype engines. These data were required to establish reactor power to air, reactor airflow and temperature levels, and system pressure level. These values are expressed as a function of pressure loss from the compressor discharge scroll exit to the unit combustor inlet, a convenient frame of reference for both experimental and operational checkout (stations 3.1 and 3.8, Figure 2.20). Engine variables were a function of ambient conditions; performance data are included for one set of ambient conditions, the NACA standard day.

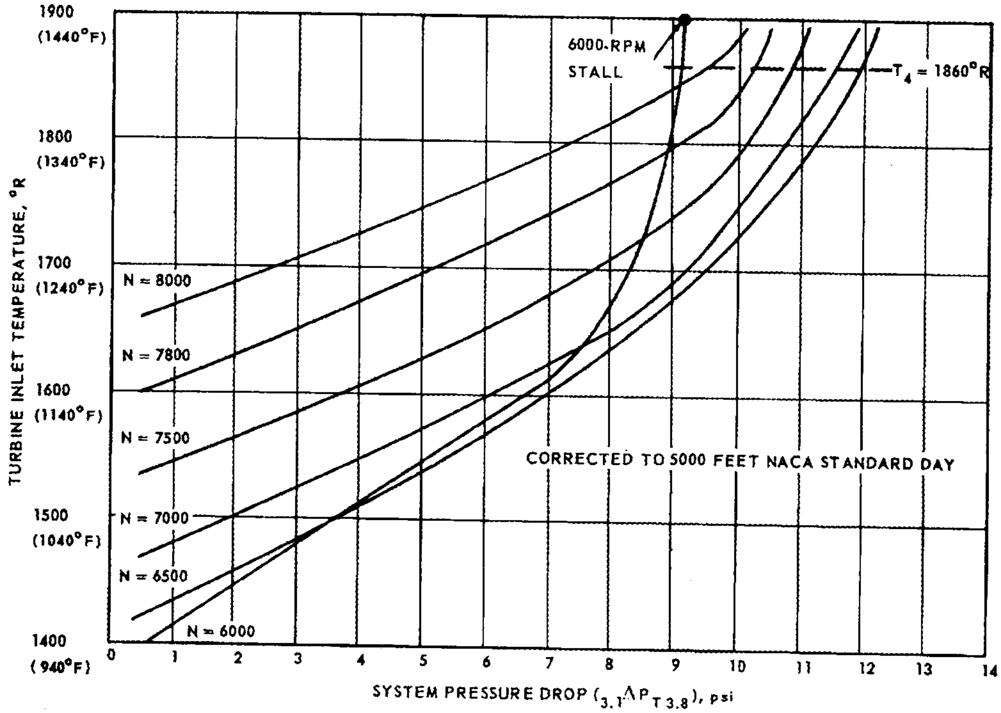

Fig. 2.16 – Turbine inlet temperature versus system pressure loss

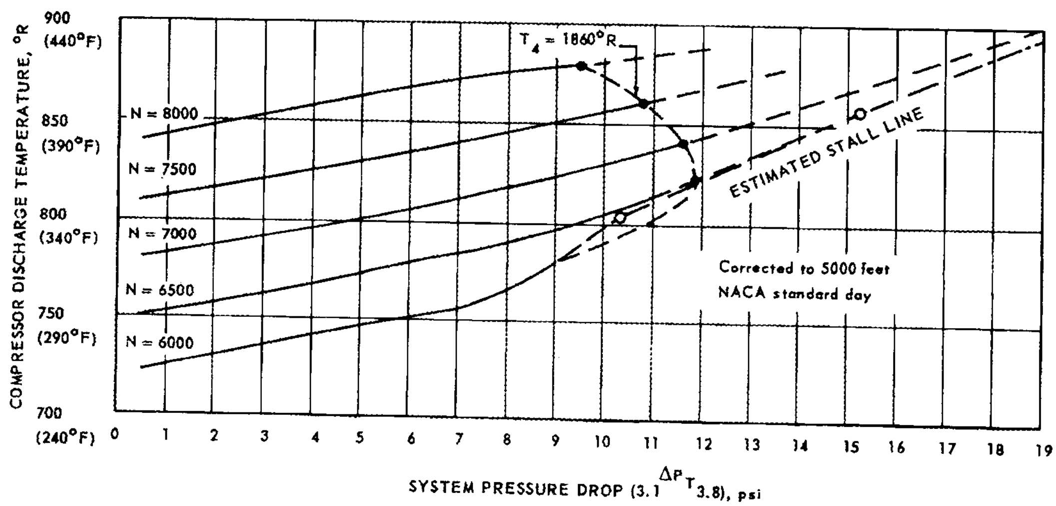

Fig. 2.17 – Compressor discharge temperature versus system pressure loss

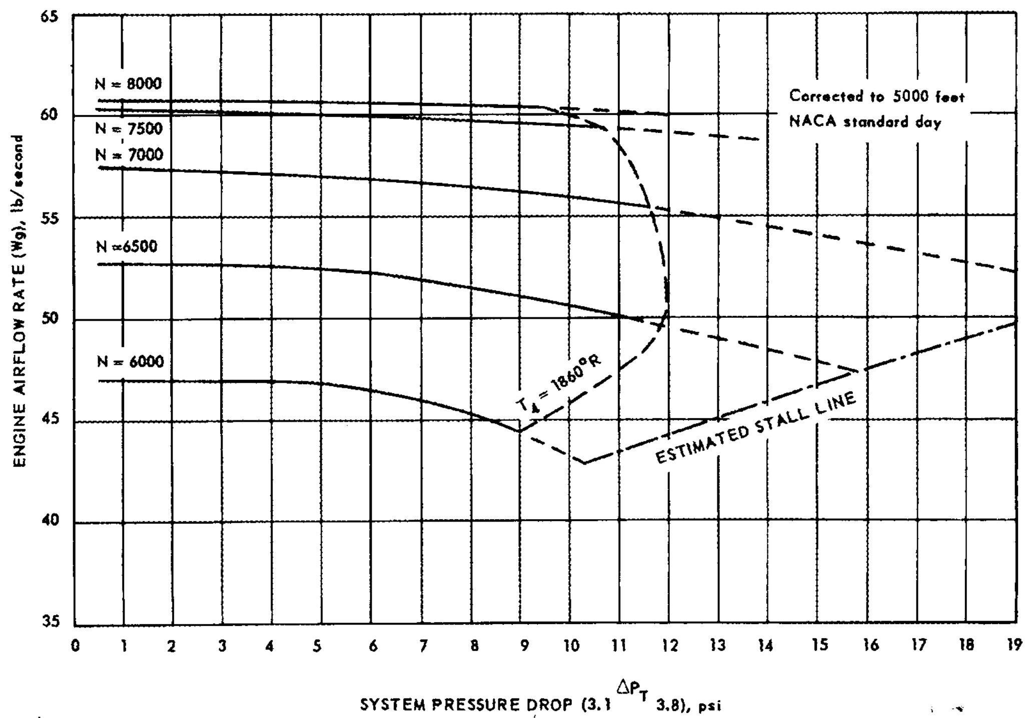

Fig. 2.18 – Airflow versus system pressure loss

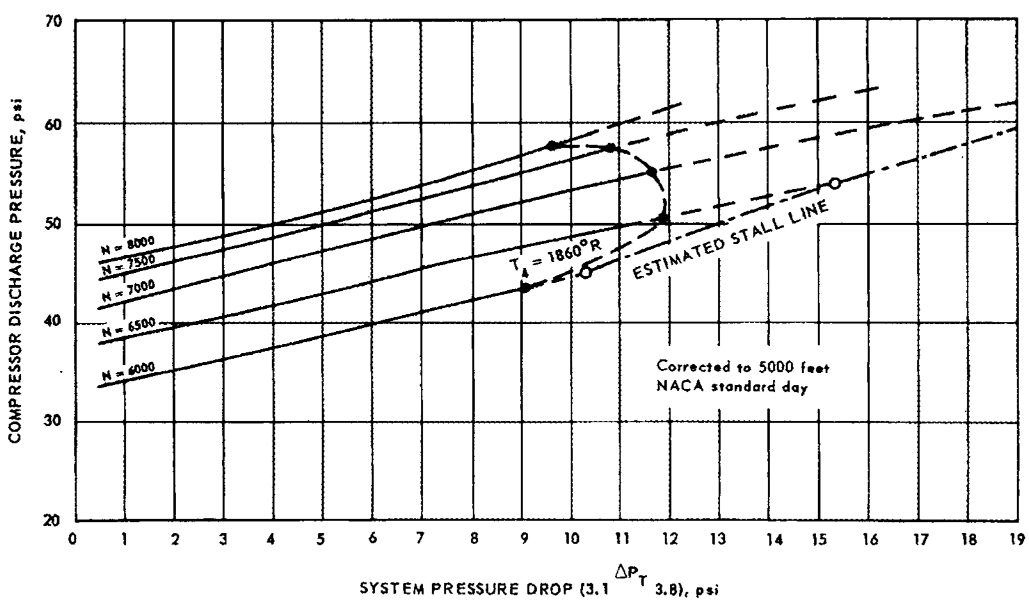

Fig. 2.19 – Compressor discharge pressure versus system pressure loss

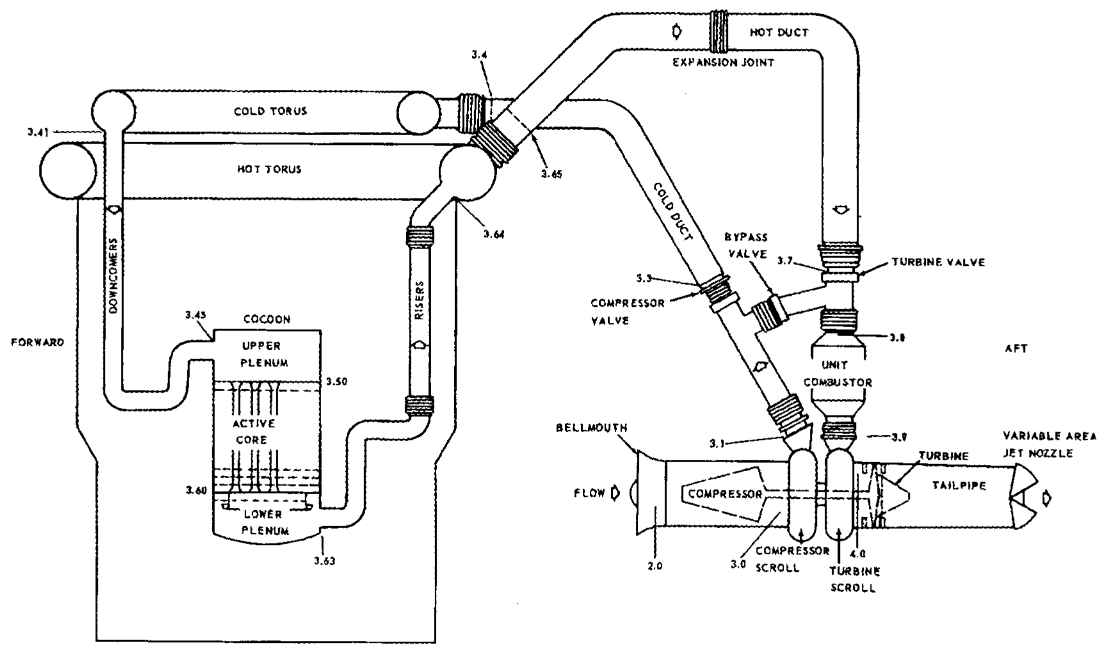

Fig. 2.20 – Schematic diagram of D101A engine airflow system showing station numbers

Auxiliary System Pressure and Heat Losses

The data presented in Figure 2.21 and in Table 2.11, obtained in part from quarter-scale-model flow tests and in part by analytical methods, were required to establish the additional reactor power necessary to overcome system heat losses and pressure loss of the system components.

Nuclear Power Distribution Curves

The nuclear power distribution curves for the system as derived from critical experiment data defined the spatial distribution of heat within the reactor. These data are shown in Figure 2.22 and in Tables 2.12 and 2.13. Since it is generally desirable to maintain a constant value of heat generation per unit of plate surface area, the individual plate fuel loadings were varied to compensate for flux decrease. Table 2.13 shows the degree of uniformity in fine radial power distribution that is possible in the reactor design. The deviations shown were largely caused by fabrication limitations on plate thickness, fuel concentration, and tolerances. An exception is the deviation noted in the outermost fuel plate, which was intentionally overloaded.

The following power curve definitions apply to Table 2.12:

P_{Fn} - fraction of total power generated in stage n
ϕAV_n - ratio of power generated in stage n to average power per stage, also = $P_F/0.05556$
ϕTE_n - ratio of power generation at trailing edge of stage n to average power in stage n
P/P_n - ratio of power generation in a tube to average power per tube.

The following nomenclature and definitions apply to Table 2.13:

t - plate or ring thickness
L - cut length of fueled section of ring
ΔA_H - surface area of fueled section of ring
ΣA_H - total fueled surface per element
P_P/P_{AV} - ratio of actual to average power dissipation per unit surface area

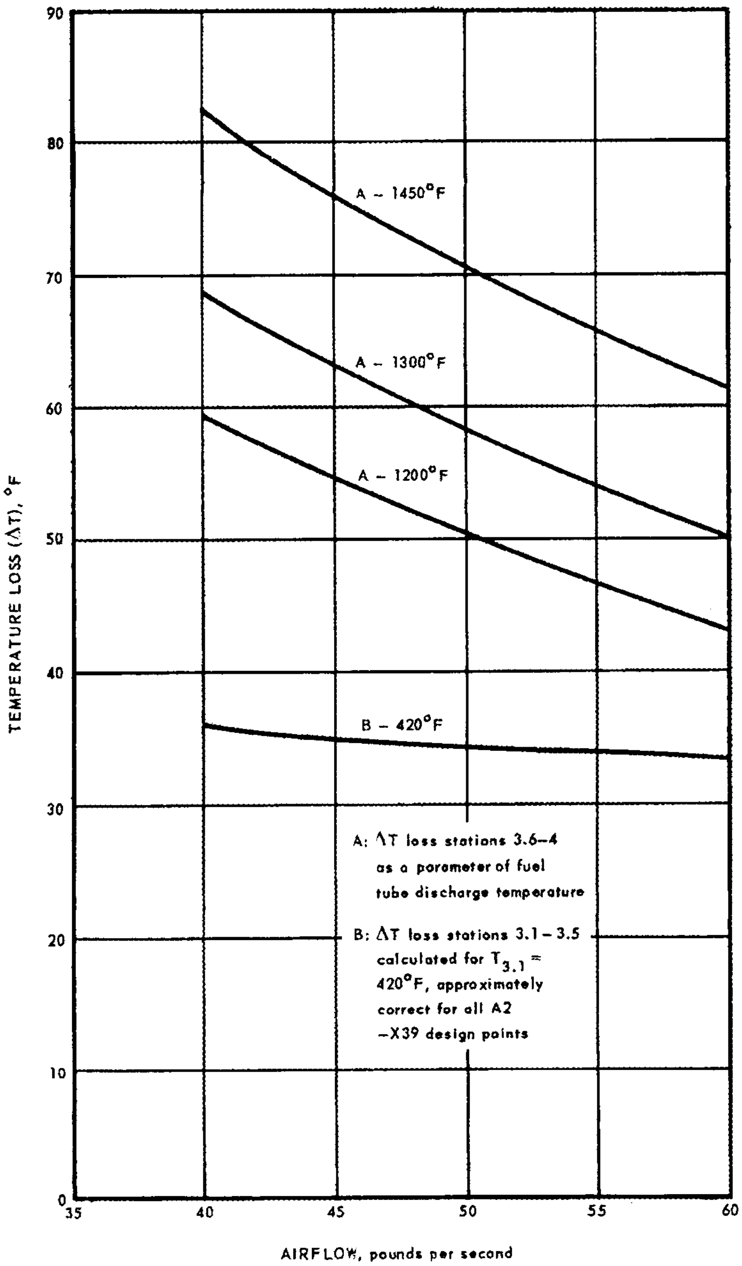

Fig. 2.21 – Temperature loss in CTF ducting system as a function of airflow and temperature

TABLE 2.11

CTF DUCTING LOSSES

	A_f, ft^2 [a]
Compressor Scroll Exit to Fuel Tube Inlet (3.1 - 3.5) [b]	
Compressor scroll exit - Compressor discharge valve exit (3.1 - 3.3)	
$\Delta P = 9.5 \times 10^{-6} W^2 T/P_s$	1.77
Compressor discharge valve - torus inlet (3.3 - 3.4)	
$\Delta P = 2.7 \times 10^{-6} W^2 T/P_s$	1.72
Torus inlet - torus exit (3.4 - 3.41)	
$\Delta P = 6.18 \times 10^{-6} W^2 T/P_s$	3.01
Torus exit - plenum exit (3.41 - 3.5)	
$\Delta P = 1.164 \times 10^{-6} W^2 T/P_s$	8.29
Fuel Tube Exit Plenum, Unit Combustor (3.6 - 3.8)	
Plenum inlet - torus inlet (3.6 - 3.64)	
$\Delta P = 2.39 \times 10^{-6} W^2 T/P_s$	7.52
Torus inlet - torus exit (3.64 - 3.65)	
$\Delta P = 0.848 \times 10^{-6} W^2 T/P_s$	7.52
Torus exit - turbine valve inlet (3.65 - 3.7)	
$\Delta P = 0.827 \times 10^{-6} W^2 T/P_s$	4.66
Turbine valve - unit combustor (3.7 - 3.8)	
$\Delta P = 6.5 \times 10^{-6} W^2 T/P_s$	2.18
W = Airflow, lb/sec	
T = Air temperature, $^{\circ}R$	
P_s = Static pressure, psia	
ΔP = Total pressure loss, psi	

[a] A_f value used to determine Mach number and associated static-to-total-pressure ratio

[b] Parentheses refer to station number

Element - refers to a single concentric ring unit of a fuel cartridge; the 18 elements were numbered in ascending sequence in a fuel cartridge.

Stage - refers to all (37) similarly numbered elements in the active core.

A_{ff} - the free flow area includes corrections for joint strips, spacers, channels, etc.

Fuel Element Specifications

The structural and aerothermodynamic characteristics of fuel elements in the core, shown in Tables 2.13, 2.14, and 2.15, were required for calculation of operational characteristics such as fuel element temperature and pressure loss. Two types of data are presented. Table 2.14 presents over-all average values of design characteristics used for gross performance calculations; Tables 2.13 and 2.15 contain tabulations of structural aerothermodynamic relations such as secondary local variations of fuel element hydraulic diameter and local heat flux, required for detailed analysis of operational characteristics.

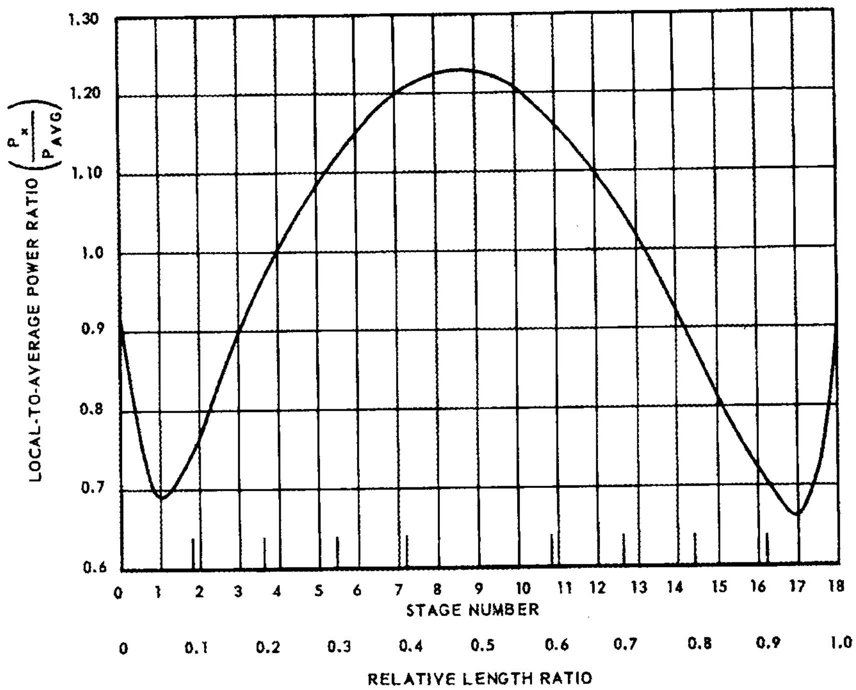

Fig. 2.22—Design longitudinal power curve, D101A2

TABLE 2.12

D101A2 CORE DESIGN POWER CURVES

Gross Longitudinal

Stage	ϕAV_n	ϕTE_n	P_{Fn}
1	0.7860	0.888	0.0437
2	0.7225	1.067	0.0402
3	0.8445	1.075	0.0469
4	0.9710	1.048	0.0539
5	1.071	1.035	0.0595
6	1.1475	1.028	0.0637
7	1.2115	1.018	0.0673
8	1.2505	1.005	0.0695
9	1.2620	1.001	0.0701
10	1.2515	0.987	0.0695
11	1.2115	0.98	0.0673
12	1.1525	0.971	0.0640
13	1.0735	0.962	0.0596
14	0.9825	0.952	0.0546
15	0.8740	0.943	0.0486
16	0.7655	0.951	0.0425
17	0.6860	0.968	0.0387
18	0.7365	1.274	0.0404

Gross Radial

Tube	P/P_{AV}
1	1.044
2-7	1.053
8-13	1.044
14-19 inclusive	1.009
20, 21, 23, 24, 26, 27	0.978
29, 30, 32, 33, 35, 36	0.978
22, 25, 28, 31, 34, 37	0.931

TABLE 2.13

FUEL ELEMENT PLATE SPECIFICATIONS FOR THE D101A2 REACTOR

Plate No.	t, in.	L, in.	tL, in.^{2}	ΔA_H, in.^{2}	$\Delta A_H / \Sigma A_H$	P_P/P_{AV}
Stages 1-11 inclusive						
1[a]	0.021	1.148	0.0241	3.352	0.0140	0.705
2	0.021	1.851	0.0389	5.404	0.0226	0.732
3	0.021	2.555	0.0537	7.460	0.0311	0.773
4	0.021	3.259	0.0684	9.516	0.0397	0.821
5	0.021	3.962	0.0832	11.568	0.0483	0.884
6	0.021	4.666	0.0980	13.624	0.0569	0.965
7	0.020	5.438	0.1088	15.878	0.0663	0.990
8	0.019	6.203	0.1179	18.112	0.0756	1.007
9	0.018	6.962	0.1253	20.328	0.0849	1.019
10	0.017	7.715	0.1312	22.528	0.0941	1.030
11	0.016	8.461	0.1354	24.706	0.1032	1.034
12	0.015	9.202	0.1380	26.870	0.1122	1.026
13	0.014	9.936	0.1391	29.012	0.1211	1.006
14	0.014	10.665	0.1493	31.142	0.1300	1.158
			1.4113	239.500		
Stages 12-18 inclusive						
1	0.021	1.493	0.0314	4.360	0.0152	0.838
2	0.021	2.128	0.0447	6.214	0.0216	0.877
3	0.021	2.762	0.0580	8.064	0.0280	0.920
4	0.021	3.397	0.0713	9.920	0.0345	0.974
5	0.020	4.030	0.0806	11.768	0.0409	0.962
6	0.019	4.658	0.0885	13.602	0.0473	0.948
7	0.019	5.280	0.1003	15.418	0.0536	1.029
8	0.017	5.899	0.1003	17.224	0.0599	0.927
9	0.017	6.509	0.1107	19.006	0.0661	1.012
10	0.016	7.117	0.1139	20.782	0.0723	0.983
11	0.015	7.719	0.1158	22.540	0.0784	0.944
12	0.015	8.316	0.1247	24.282	0.0844	1.043
13	0.014	8.912	0.1248	26.024	0.0905	0.998
14	0.013	9.501	0.1235	27.742	0.0965	0.927
15	0.013	10.086	0.1311	29.452	0.1024	1.039
16	0.013	10.670	0.1387	31.156	0.1083	1.180
			1.5583	287.554		

[a]Based on ID of 0.372 in.

The following definitions apply to Table 2.14:

D_H - hydraulic diameter for heat transfer
D_H' - hydraulic diameter for pressure loss
P_W - wetted perimeter, inches

TABLE 2.14

D101A2 REACTOR FUEL ELEMENT AEROTHERMODYNAMIC CHARACTERISTICS

Fuel Tube		
Tube outer radius, in.	2.00	
Tube wall thickness, in.	0.080	
Insulation thickness, in.	0.100	
Insulation liner thickness, in.	0.019	
Inner radius of airflow passage, in.	1.801	
Flow area for air and fuel elements per tube, in.^{2}	10.19	
Number of tubes	37	
Total area for air and fuel elements, in.^{2}	377.03	
Fuel Elements		
Stage	1-11	12-18
A_H fueled area per element, in.^{2}	239.50	287.554
A_H fueled area per element, ft^2	1.663	1.9969
A_H fueled area per stage, ft^2	61.53	73.885
A_{ff} free flow area per stage, in.^{2}	320.60	314.94
$D_H = 5.84\,(A_{ff}/A_H)$, in.	0.214	0.175
$D_H' = 4\,(A_{ff})/P_W$, in.	0.188	0.157

Fuel Tube Pressure Losses

Pressure losses through the fuel tube, presented in Figures 2.23 through 2.25, were caused primarily by friction and momentum changes occurring within the fuel elements and secondarily by comparable losses in fore and aft structures such as bellmouths, disconnects, and support rings. A diagrammatic sketch of the latter structure and tabulation of loss coefficients as determined from experimental tests[16] of dummy production cartridges for core A2 are shown in Figures 2.23 and 2.24. The friction factor relationship for the fuel element section, derived from similar tests, is shown in Figure 2.25.

The following are formulas for use with Figure 2.24.

$$q_{3.5} = \frac{5.83 \times 10^{-6}\,(W^2)\,T_{3.5}}{P_{s_{3.5}}}$$

$$q_{3.53} = \frac{5.83 \times 10^{-6}\,(W^2)\,T_{3.53}}{P_{s_{3.53}}}$$

where

q = dynamic head, psi
W = air weight flow, pounds per second
T = air temperature, $^{\circ}R$
P_s = air static pressure, psi

TABLE 2.15

MISCELLANEOUS D101A2 FUEL CARTRIDGE CHARACTERISTICS

Fuel Tube

For convenience the dynamic head (q) for structural components is always defined on the basis of the bare tube flow area equal to 377.03 in.^{2}.

Fuel Elements

Stage	1-11	12-18
Stage length, in.	1.5	1.5
Fueled length, in.	1.46	1.46
Total weight, lb/element	0.74445	0.81742
Total weight, lb/stage	27.54	30.25
Weight UO_2, lb/element	0.15248	0.15550
Weight UO_2, lb/stage	5.64	5.75
Weight 80Ni - 20Cr in plates, lb/element	0.53863	0.60475
Weight 80 Ni - 20 Cr in plates, lb/stage	19.93	22.38
Weight channels, spacers, etc., lb/element	0.05334	0.05717
Weight channels, spacers, etc., lb/stage	1.97	2.12
ID innermost ring 1, in.	0.372	0.482
Flow area inside innermost ring, in.^{2}/element	0.1087	0.1824
in.^{2}/stage	4.022	6.749
Annulus flow area, in.^{2}/element	0.8942	0.8942
in.^{2}/stage	33.09	33.09
Annulus hydraulic diameter for pressure loss, in.	0.12	0.12

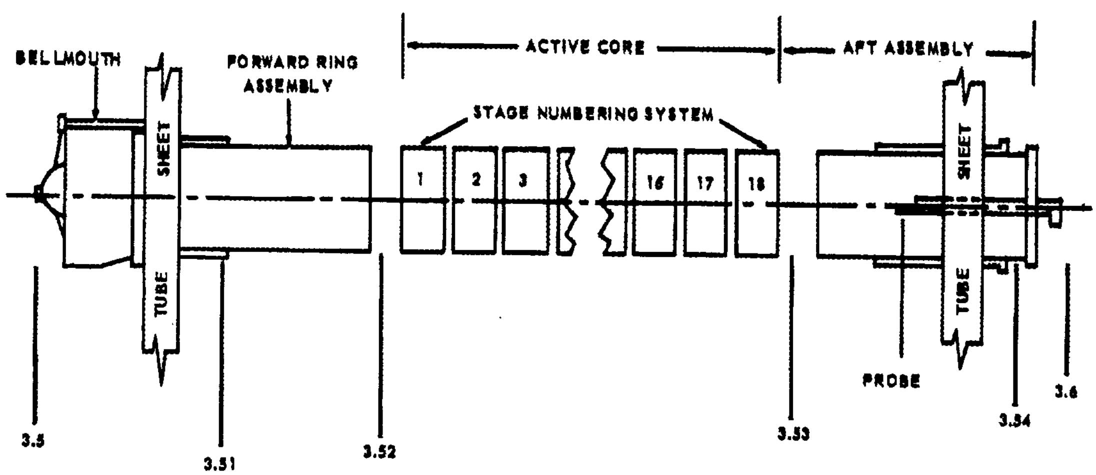

Fig. 2.23—Schematic drawing of fuel tube showing station numbers

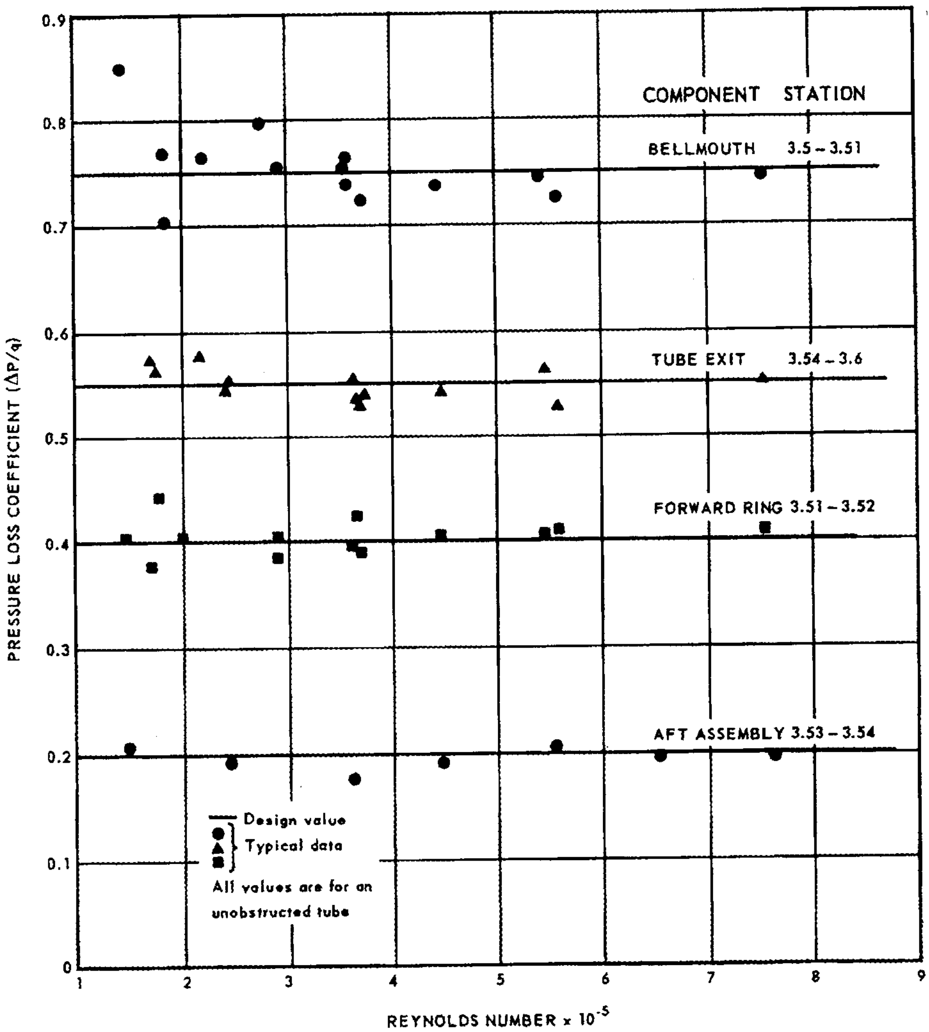

Fig. 2.24 – Pressure loss coefficient versus Reynolds number for cartridge structural components

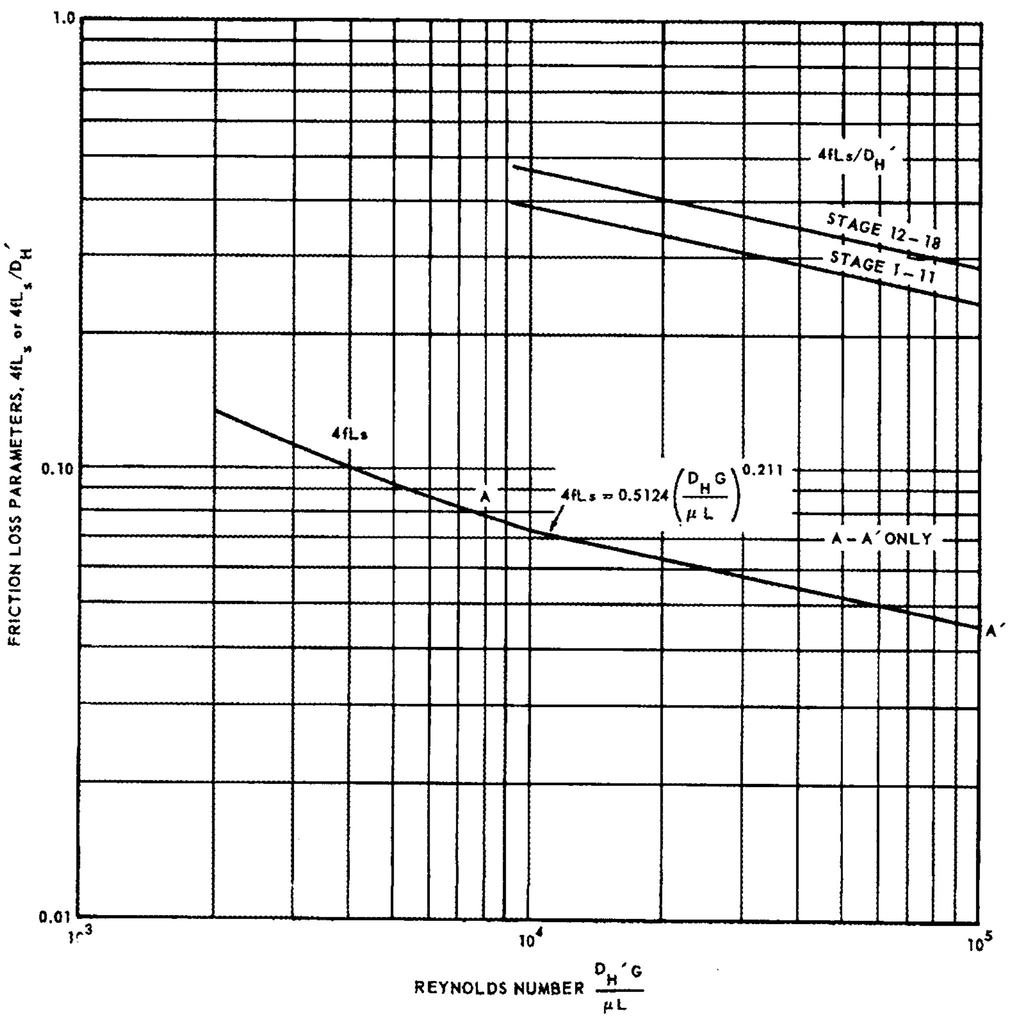

Fig. 2.25 – Plot of design friction factor relationship for A2 fuel elements

Heat Transfer Relationship

The design heat transfer relationship, as derived from tests of electrically heated fuel element prototypes and substantiated to some degree by tests of fueled specimens in the Materials Testing Reactor, is presented as a nomogram in Figure 2.26. These data were in general applicable to elements only at airflows in the range shown in Figure 2.18.

2.3.2 FUEL ELEMENT OPERATING CHARACTERISTICS

Determination of operating characteristics of fuel elements was usually required in four specific operational categories: (1) operation of system under partial nuclear power, (2) operation solely on nuclear power, (3) transfer from chemical to nuclear power, and (4) aftercooling operation. Operational characteristics during transfer are presented in subsequent paragraphs, and aftercooling is taken up in section 2.3.4. Treatment of the remaining two categories is essentially identical. Detailed analysis of these operations was usually limited, as will be the case in the following paragraphs in this report, to the full-nuclear-powered system, since it was the most important operation. Specifically, if fuel element behavior was satisfactory for an engine design point under full nuclear power, it was also satisfactory, almost without exception, for the same design point achieved with partial chemical power.

Determination of system operation points consistent with fuel element temperature limitations was an iterative process because fuel element and engine performance were interdependent. The operational analysis of the system entailed the matching of fuel element performance and engine variables to define a reactor operating line that could be superimposed on an engine performance map. The results of this work as applied to NACA Standard Day operation are shown in Figures 2.27 and 2.28. Figure 2.27 is a mating curve; i.e., the reactor operating line shown is the locus of all points mutually consistent with engine requirements and fuel element performance capabilities. Figure 2.28 indicates fuel element and air temperature profiles for typical match points.

Figure 2.29 illustrates engine-reactor mating lines for various types and fractions of system power inputs with unaugmented operation. Figures 2.30 and 2.31, derived from Figure 2.29 and associated engine-performance curves, illustrate the trends of fuel element temperature, average reactor-discharge-air temperature, and reactor power as the fractional nuclear power input is increased. The index parameter chosen for this work is "percent nuclear power," defined by the relation:

$$\text{Percent nuclear power} = 100 \frac{(h_{3.6} - h_{3.5})}{(h_{3.6} - h_{3.5}) + (h_4 - h_{3.8})}$$

where h_n is enthalpy of air corresponding to temperature at flow station, n.

Lines of constant fuel-flow rates are also included for operational reference; intermediate points may be determined by use of the preceding equation, Figure 2.31, and fuel heating value data.

Figure 2.32, derived from Figures 2.29, 2.30, and 2.31, illustrates open-nozzle transfer. The basic plot is reactor power to air versus engine speed for both 100 percent nuclear power and minimum chemical power. To transfer to nuclear power, the system was brought up to operation at some speed on the minimum chemical-operating line. At this point, the fuel flow was reduced to zero and the engine coasted to a lower speed whose power requirements correspond to the nuclear power component of the operating point on the minimum chemical line. Figure 2.32 permits evaluation of the speed change during transfer. Estimates of the increase in reactor air and fuel element temperatures due to decrease of airflow and decrease of speed as a result of the transfer can be obtained from Figures 2.30 and 2.31.

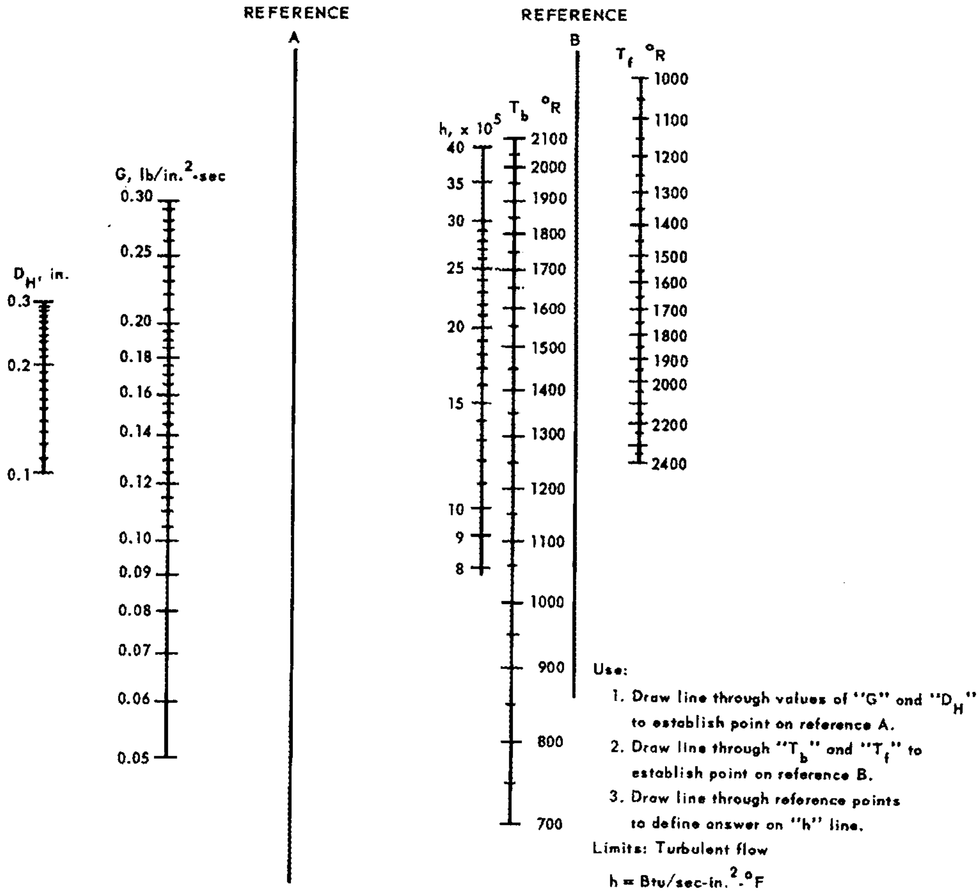

Fig. 2.26 – Nomogram for solution of design heat transfer relation,

$$h = 10.28 \times 10^{-5} \frac{G^{0.8}\, T_b^{0.8}}{D^{0.2}\, T_f^{0.56}}$$

In practice, the fuel element and reactor discharge air temperatures decreased slightly immediately after transfer because of fuel purge, which accelerated the engine somewhat before deceleration occurred.

Flow Distribution

All calculations assumed uniform airflow distribution in the fuel tubes. Factors that tended to negate this assumption include basic maldistribution caused by plenum configuration of the CTF, variations in fuel tube manufacture that led to differences in flow resistance, and variations in tube power due to gross radial power distribution and control rod position. (These variations caused variation of flow through the tubes.)

Fuel Element Flow Distribution

Because of manufacturing problems and design requirements for structural components in the fuel tube, certain variations of flow, which represented deviations from average conditions assumed in design, could be anticipated. Specific problems concerned flow through passages in contact with the innermost and outermost fuel rings, velocity profile variations caused by forward fuel tube structure, and flow variations caused by fabrication limitations on the degree of fine radial power flattening.

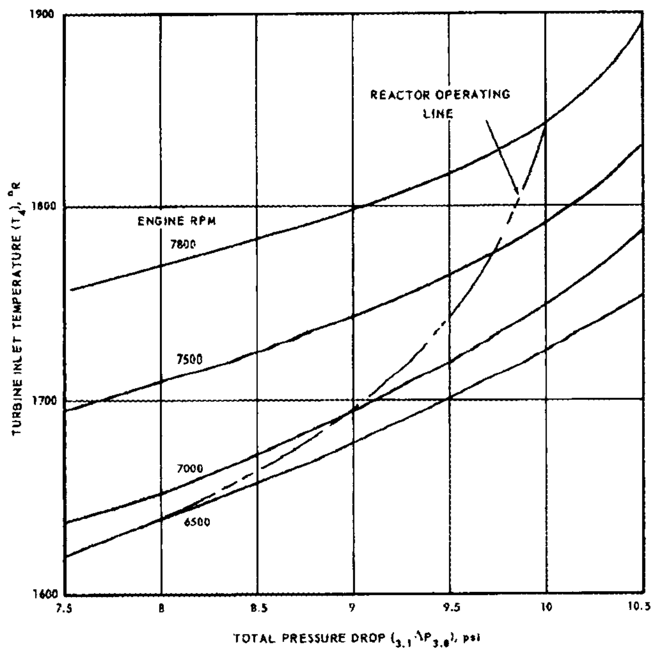

Fig. 2.27 – Plot of engine-reactor mating calculations for standard-day operation

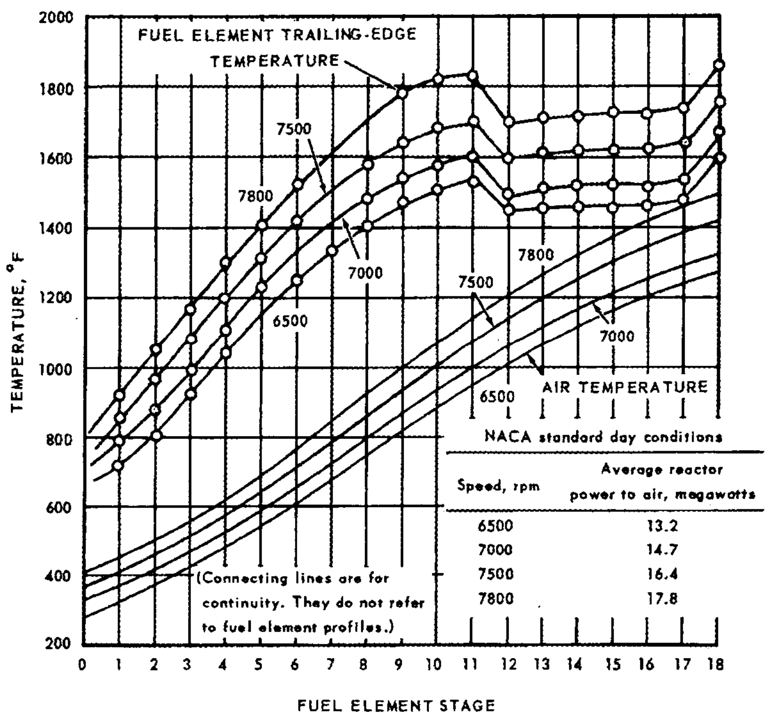

Speed, rpm	Average reactor power to air, megawatts
6500	13.2
7000	14.7
7500	16.4
7800	17.8

Fig. 2.28 – Fuel cartridge temperature profiles as a parameter of engine speed at various mating points

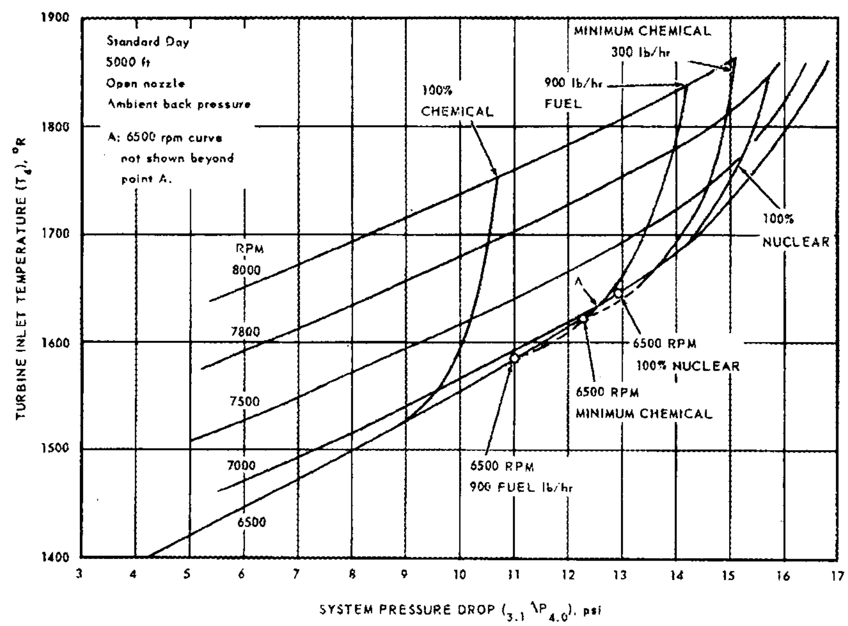

Fig. 2.29 – Engine-reactor mating points as a function of type and quantity of power source

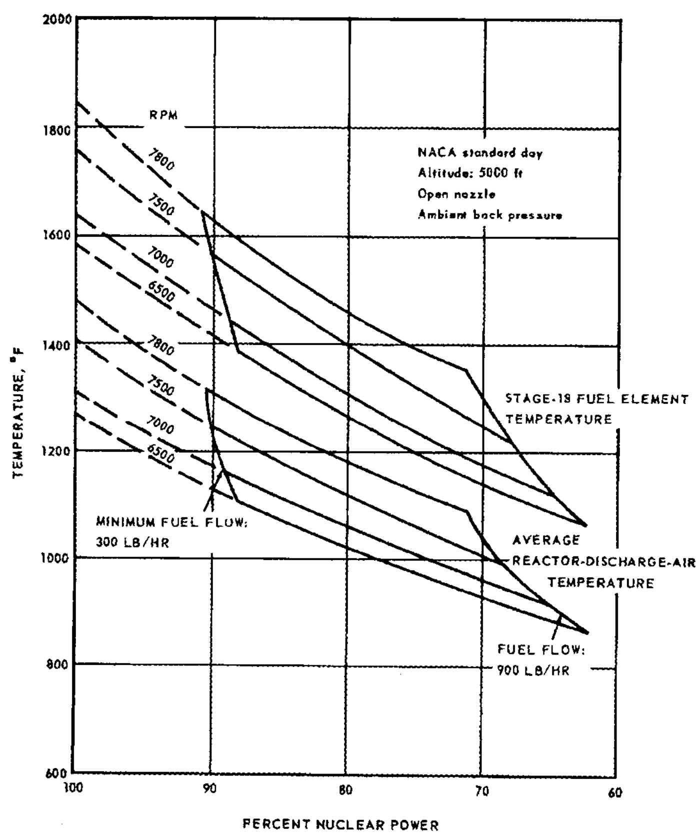

Fig. 2.30 – Fuel element and air temperatures as a function of percent nuclear power

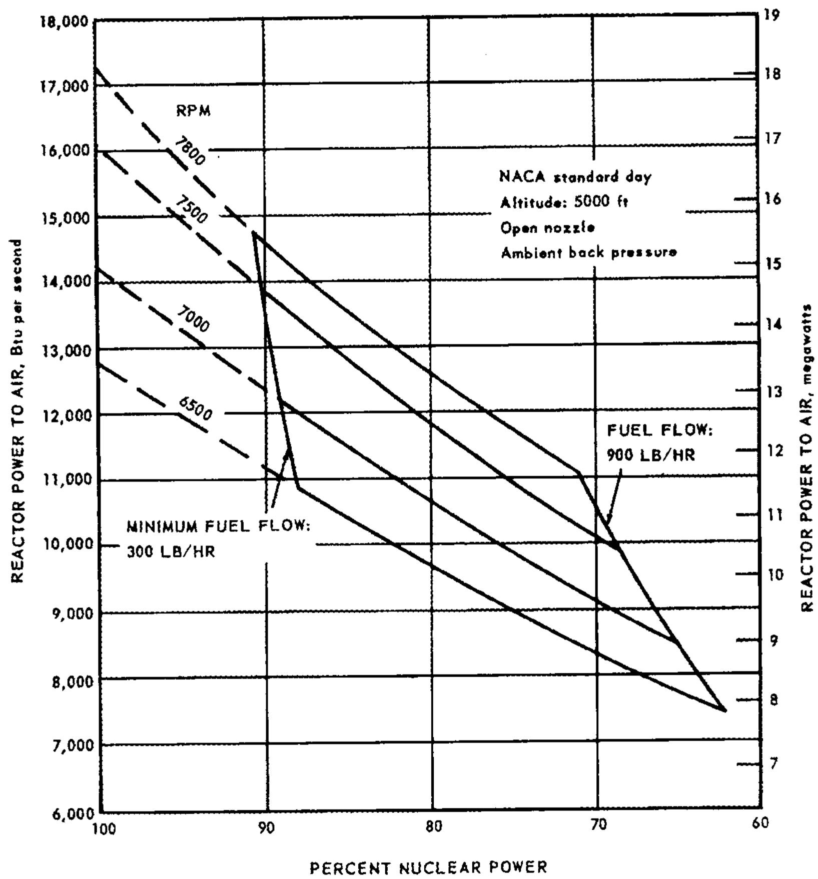

Fig. 2.31 – Reactor power to air as a function of percent nuclear power

Fuel Element Temperatures

Fuel element temperatures, which were a composite function of local air temperatures and velocities and of local power generation rates, were influenced by factors previously mentioned as well as by basic variations in the reactor longitudinal power curve, variation of heat transfer coefficient with geometry, and local power perturbations caused by control rod positioning or fabrication tolerances.

Heat transfer, pressure loss, and deviations within the engine system were the chief sources of error in the calculation of operating characteristics. (In the engine system, valve leakage was a principal problem.)

Many of these problems could be evaluated, and numerical values set, only by operational tests. However, prototype testing indicated that such problems as basic flow maldistribution and irregularity of power curves occurred within limits that presented no serious difficulty for fuel element operation. The core design provided a margin of safety for factors that could not be experimentally defined. The engine system could be varied so that operating requirements could be met with an even broader safety margin for the operation of fuel elements.

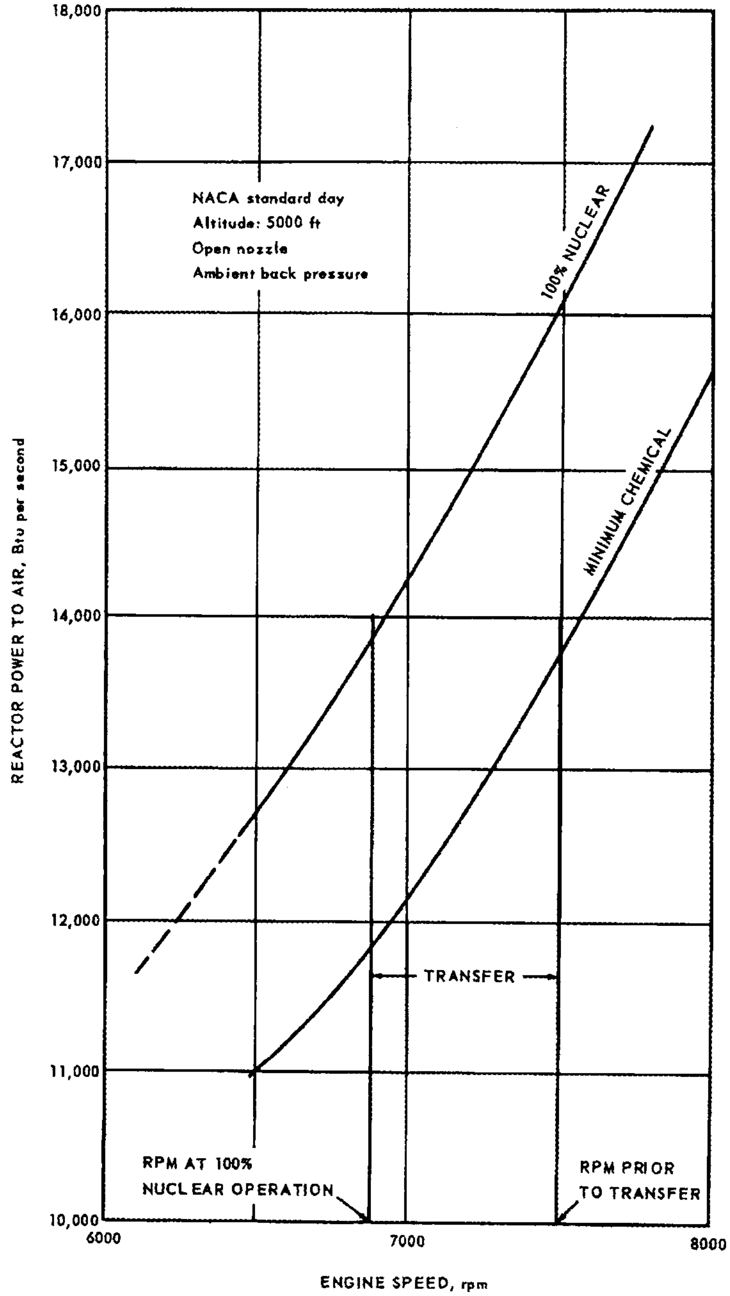

Fig. 2.32 – Reactor power at minimum chemical and 100 percent nuclear power illustrating open-nozzle transfer

Temperature Maldistributions

Figure 2.33 is a partial summary of temperature maldistribution problems. The lower portion of Figure 2.33 defines the average maximum overtemperature in air required primarily as a result of compensation for structural deviations in the fuel element and for gross radial power flattening effects. The upper set of curves in Figure 2.33 illustrates fuel element temperatures for various degrees of compensation and margin for error. Curve A illustrates temperature profiles for an ideal average fuel tube; curve B is the "hot tube" curve used in design. Curves C and D illustrate the effects of other error sources. Consideration of all possible sources of deviations, both beneficial and detrimental, indicated that the actual curve should be somewhere between curves B and C.

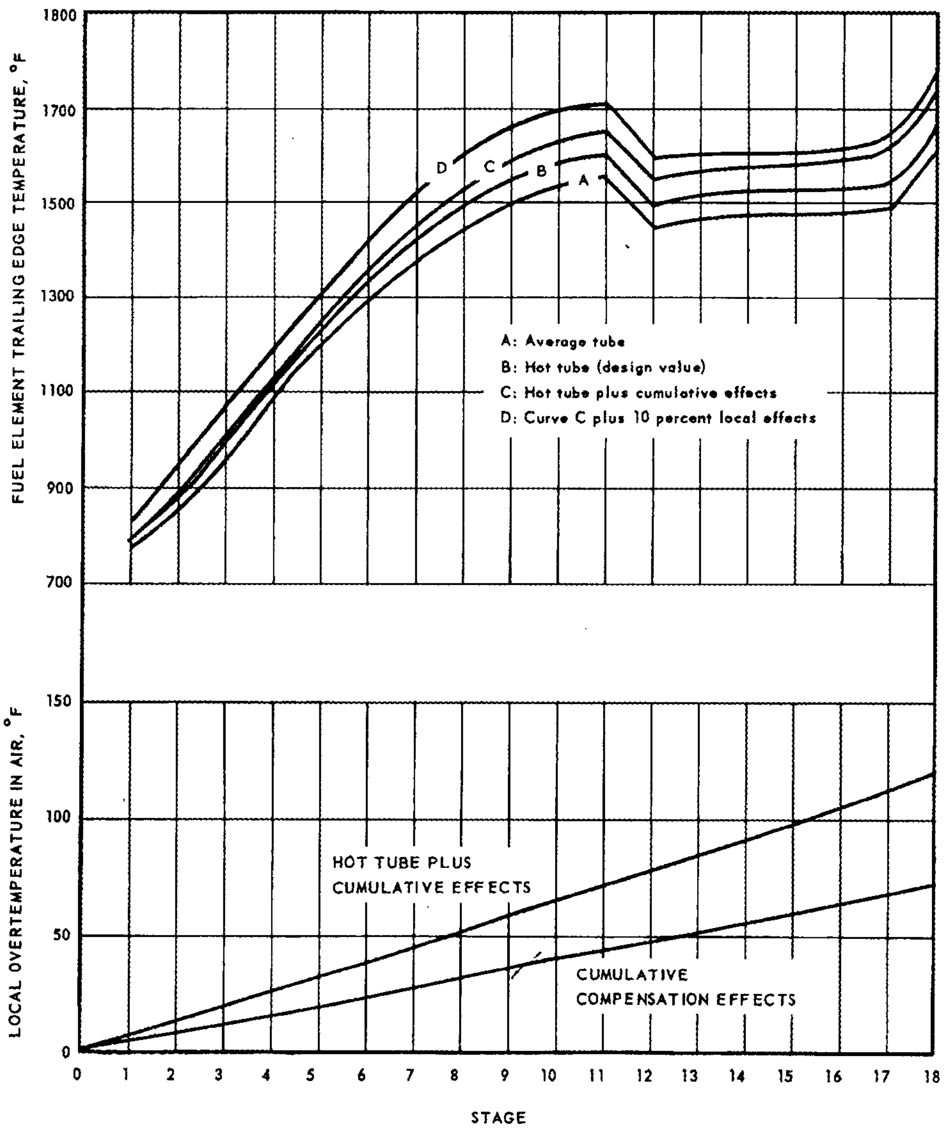

Fig. 2.33 – Fuel element temperatures and air temperature deviation for various operational possibilities at 7000-rpm standard-day mating point

However, this conclusion depended largely on mode of operation, even if all other design premises were exactly correct. As an example, the hot tube effect caused a maximum overtemperature of approximately 100^{o}F at high-temperature locations in the fuel cartridge. This overtemperature was caused by higher-than-average power and air temperature and by induced flow defects in the hot tube. However, it was possible that the hot tube effects could be alleviated by varying control rod position. If this were achieved, the actual temperature profiles would be expected to fall between curves A and B. Exact fuel element temperatures were difficult to define because of such variables as the effect of control rod position on hot tubes and the sensitivity of fuel element temperature to small-order deviations (example: the hot tube, which necessitated 100^{o}F deviation from average conditions, represented a 5 percent variation). Therefore, no attempt was made to define all possible engine-reactor mating points. The work discussed deals primarily with operation at 7000 rpm. This operating point was believed to represent a point at which safe operation could be insured even in the event of deviations in excess of those illustrated in Figure 2.33.

Compensation for Operational Problems

The surface area specification for the core design allowed margins for two anticipated sources of deviation: local errors and cumulative errors. These errors were defined with respect to their effect on fuel element temperature in the relation:

$$T_s = T_b + Q/A_H h$$

where

T_s = fuel element surface temperature
T_b = local air temperature
Q = heat generation rate
A_H = surface area
h = heat transfer coefficient

Local errors were generally those that affected the grouping ($Q/A_H h$); deviations in fuel-plate loading and local variation of heat transfer coefficient were typical of this category.

Cumulative errors were primarily those that caused deviations in local bulk temperature, the strongest effect usually occurring at the rear of the fuel tube.

Typical error sources and their anticipated magnitudes are shown in Table 2.16. These tabulations indicate that the early stages of the fuel element were sensitive to local effects and relatively insensitive to cumulative effects, whereas the reverse was true for the later stages. Because the early stages were overdesigned, the potential seriousness of local effects is considerably lessened (see Figure 2.28). Cumulative error effects were allowed for by overdesigning the rear stage group. Specifically, in terms of temperature profile in Figure 2.28, only the last stage operated near maximum design temperature; the rest of the stages were well below maximum. This upswing in temperature at the last stage was attributable to a sharp rise in power at the reactor ends (see Figure 2.22). In design calculations, this was considered the maximum temperature possible in such a situation. However, the upswing in temperature was considerably modified by conduction and fin effect of spacers and dead edge. This temperature effect could not be defined exactly either by experiment or analysis. The results of limiting-case studies, presented in Figure 2.34, indicated, however, that auxiliary surface effects could be expected to lower the peak value designated in design. All rear fuel elements would then operate below the maximum design temperature. In the design of the A2 core, it was decided to preserve the overdesign characteristics to provide for possible cumulative errors rather than to increase performance and temperature by removing surface area.

TABLE 2.16

ANTICIPATED DETRIMENTAL ERROR SOURCES IN D101A2 CORE DESIGN

Effect	Maximum Variation, percent	Resultant Maximum Over-temperature in Fuel Element, °F	
		Stages 1-11	Stages 12-18
Local Effects			
Inaccuracies in:			
Heat transfer relation	± 6	42	25
Longitudinal power curve	± 4 to 7	49	29
Gross radial power curve	± 1	7	4
Flux curve for fine radial loading	± 3	21	13
Manufacturing variations in:			
Fuel-area ratio	± 5	35	21
Operational variations:			
Control rod perturbations and/or circumferential scalloping	7	42	29
Cumulative Effects			
Basic flow perversity of system	+ 7 to - 2	44	72
Flow perversity induced by local effects	--	--	--
Leakage of engine air ahead of reactor	Undetermined		

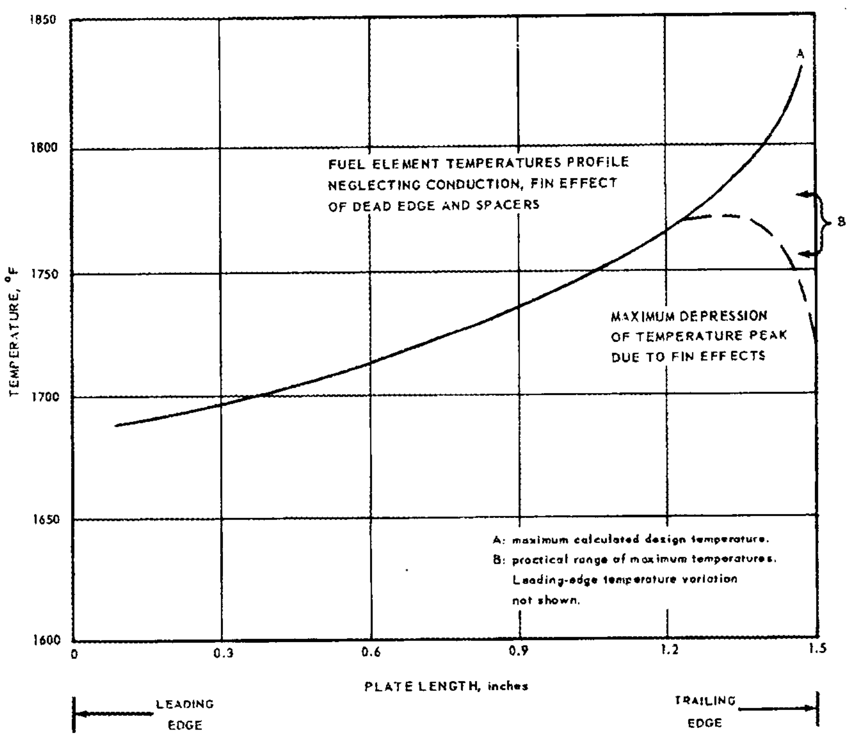

Fig. 2.34 – Eighteenth-stage axial temperature profile illustrating anticipated variation of temperature due to fin effects

2.3.3 FUEL ELEMENT DESIGN TEMPERATURES

Definition of maximum temperature depended on stress-oxidation-temperature relations, time at temperature, and location of temperature in the fuel element structure. Specifically, the maximum design temperature had to be one at which the fuel element had adequate strength to withstand aerodynamic loads and thermal stresses. At the same time, the fuel element had to maintain sufficient oxidation resistance to insure that the cladding would retain fission products and prevent oxygen penetration into the fuel material. These criteria were a function of time and of specific location in the fuel element structure; the location was significant since aerodynamic loads varied through the fuel cartridge.

Limitations assigned to maximum design temperature were somewhat arbitrary because of the interrelation of stress-oxidation-temperature effects and because fuel element stresses could not be defined or calculated. The following limitations, which will be discussed in subsequent paragraphs, were assumed:

1. Maximum average fuel element temperature for 100 hours operation = 1750°F
2. Maximum local temperature continuous = 1850°F
3. Maximum transient hot spot = 2100°F

Proof tests in the MTR and burner rig operations provided data that, in some degree, defined the limitations of allowable fuel element temperature.

Figure 2.35 shows an average-life-expectancy curve for D101A2 concentric-ring-type fuel elements based on MTR tests.

MTR tests of typical fuel element sections indicated no structural or cladding defects with local temperatures of 1850°F, aerodynamic loads approximately the same as the D101A2 reactor design maximum, and test times of more than 200 hours. In addition to confirming integrity of the clad, these tests offered further evidence of structural integrity since intra-element temperature variations, which promote thermal stresses, were considerably worse than anticipated in D101A2 reactor operation. No absolute limitations of fuel element temperatures were defined in MTR tests because of the limited number of tests.

The MTR tests confirmed the assumed temperature limitations and indicated possible conservatism. The values presented should be regarded as nominal figures. An initial operating range could probably be established without exceeding basic design temperatures in the apparently safe range of 1700° to 1750°F.

2.3.4 AFTERHEAT

Generation

Figure 2.36 presents basic afterheat data. These data are semi-empirical and apply to total afterheat level only.

The most common assumption was that afterheat was equally divided between gamma energy and beta energy. This assumption was used in arriving at the data given in the following paragraphs.

Accuracy claimed for the data was no better than ± 25 percent for a day or two after shutdown and up to ± 50 percent for shorter or longer times.

Only rough estimates of the distribution of fission-product-energy absorption were made Tables 2.17 and 2.18 show the results of these estimates, which were made for the core with and without moderator. The methods of calculation are given in reference 17. Energy-absorption estimates were limited mainly to the active core since it was assumed that heat-removal mechanisms designed for the active core would be more than adequate else-

UNCLASSIFIED

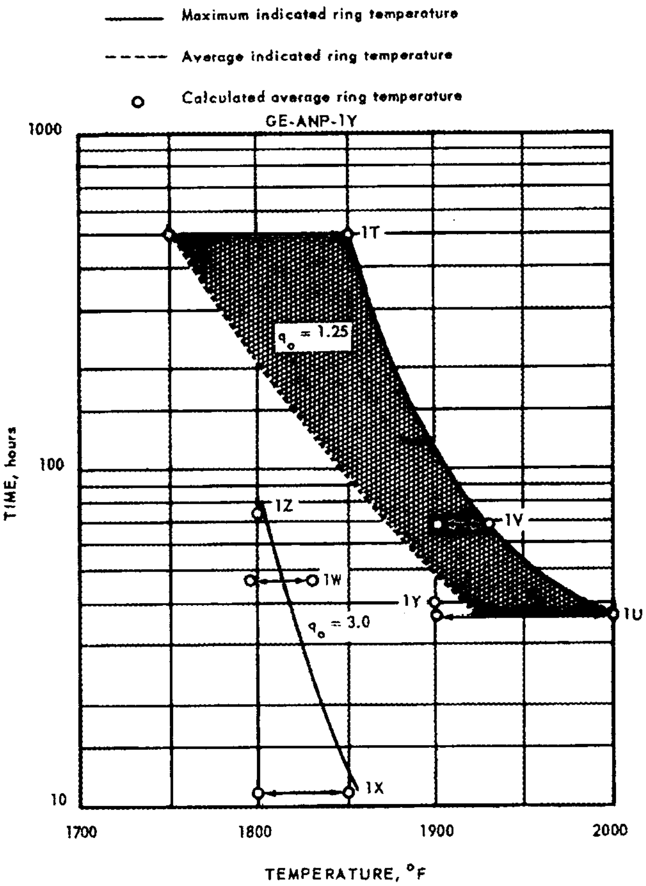

Fig. 2.35 – Average life-expectancy curve for concentric ring multistage-type fuel elements, MTR tests

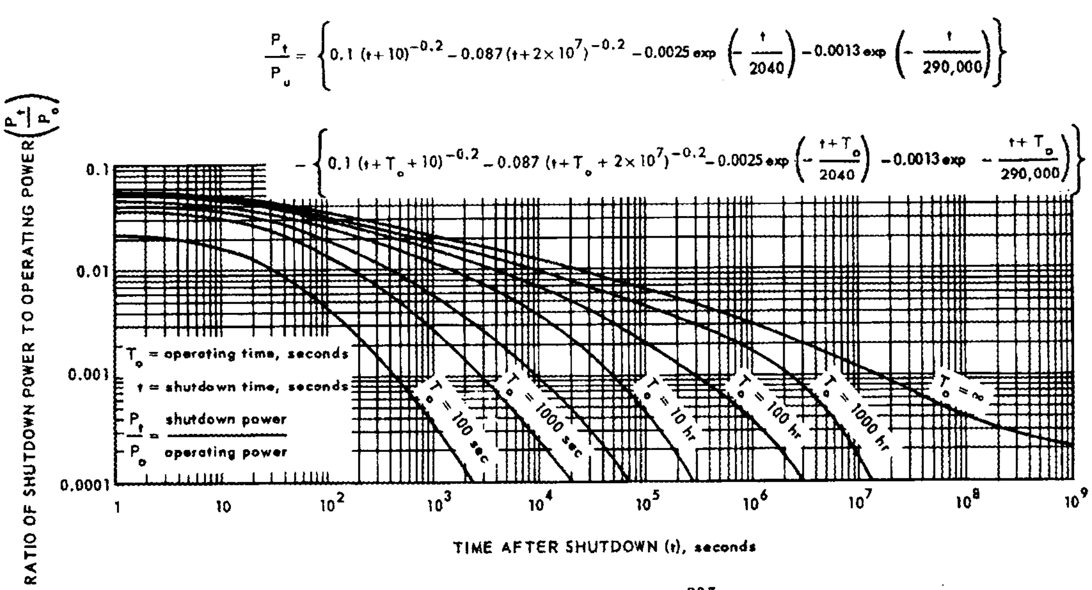

Fig. 2.36 – Total beta and gamma decay energy of U^{235} fission products as a fraction of total operating power versus time since shutdown

UNCLASSIFIED

TABLE 2.17

PARTITION OF AFTERHEAT POWER AMONG COMPONENTS OF CORE FILLED WITH WATER

Component		Percent Total Afterheat Power
Moderator[a]		29.4
Active core water	11.9	
Reflector water	17.5	
Fuel Elements		70.7
Beta power	50.0	
80 Ni - 20 Cr gamma power	8.5	
Uranium gamma power	12.2	

[a]Heat delivered from aluminum structure and beryllium reflector is included with heat delivered to water.

TABLE 2.18

PARTITION OF AFTERHEAT POWER AMONG COMPONENTS OF CORE DRAINED

Component		Percent Total Afterheat Power
Active core fuel tubes		3.20
Active core control rod guide tubes		0.7
Beryllium reflector		9.11
Fuel elements		76.4
Beta power	50.0	
80 Ni - 20 Cr gamma power	13.2	
Uranium gamma power	13.2	
Control Rod Heating Rates:		
Maximum rate per inch of control rod: 2.15×10^{-5} x total afterheat power		
Total rate per control rod: 5.38×10^{-4} x total afterheat power		

where. No attempt was made to account for all gamma energy; however, all energy not specifically accounted for could be assumed to be absorbed in the core assembly.

Aftercooling

The calculations of aftercooling heat generation were primarily concerned with determination of maximum temperatures of core and plug components after reactor shutdown and capacities and performance of afterheat-dissipation systems. The basic tenets, data, and limitations in aftercooling work were as follows:

1. Heat due to fission-product-decay energy was continually generated both in the fuel elements and moderator system after reactor shutdown. The predicted heat-generation rates are given in Figure 2.36.
2. Reactor shutdown implied at least temporary loss of primary air coolant. Therefore, some auxiliary coolant had to be introduced to prevent overtemperature due to afterheat generation.
3. If it were practical, the reactor system could be held at the test site until afterheat-generation rates were below those that would require auxiliary cooling in transit. However, the waiting times associated with this procedure were generally excessive, and auxiliary cooling was required in transit. As a result, capacity limits for the auxiliary coolant systems were introduced since there were both power and weight limitations imposed by the in-transit system.
4. The following afterheat-dissipation systems were available:
   a. Two two-speed blowers, each rated at 4 pounds per second, 45 inches water head at 3600 rpm; 2 pounds per second, 11 inches water head at 1800 rpm. Sufficient power was available at the test site to run both blowers at full speed. Blowers could be run at half speed with available in-transit power.
   b. The main moderator system could be run at full flow conditions after shutdown at the test site. The in-transit system consisted of two 60-gpm pumps and a forced-draft liquid-to-air heat exchanger cooled by a 3-horsepower fan, capable of dissipating approximately 75 Btu per second.

A reasonable time for considering transfer of the reactor from test site to hot shop was the time at which heat generation in the fuel elements was equal to 40 Btu per second (0.2 percent operating power).

Air cooling to prevent overtemperature in fuel elements due to afterheat generation was extremely critical in the first 10-20 seconds after shutdown and critical to a lesser degree until power levels of 0.2-0.3 percent were achieved. At this time, heat transfer from the fuel elements to moderator by radiation should have been sufficient to keep fuel element temperatures below 1700°F. The main purpose of air cooling below 0.2-0.3 percent operating power was to insure proper cooling of thermocouple and fuel tube disconnects, which were limited to temperatures of approximately 600°F and 900°F, respectively.

The thermal capacity of the wet-core tank system was approximately 4000 Btu per °F. The average thermal capacity of the fuel elements for the range 200° to 2000°F was approximately 85 Btu per °F.

The 2-pound-per-second in-transit blower could maintain maximum fuel element temperatures below 250°F for power levels in the range of 0.2-0.3 percent operating power.

Most of the problems of aftercooling were not concise conclusions because the problems were complex and assumptions had to be made for calculation purposes.

Maximum fuel element temperatures after the initial period following shutdown were determined by matching blower performance, system heating rate, and flow resistance to determine airflow mating points. The results of a typical calculation are shown in Figure 2.37.

Since the aftercooling flow rates were low and since the reactor core pressure loss was not a large portion of the total system loss, maldistribution of air through the core was anticipated. Data in Figure 2.37 show the range of fuel element temperatures for maldistributions of the order of 20-30 percent in airflow.

In-transit afterheat generation in the fuel elements could be removed either by the aftercooling blower operating at half speed or by heat leakage from fuel elements to the moderator system. In the range of powers considered for in-transit operation, 0-70 Btu per second or approximately 0.4 percent of 20-megawatt operating power, maximum fuel element temperatures with aftercooling blower were expected to be approximately 0° to $150^{\circ}F$ above maximum air temperature, expressed approximately by the relation:

$$T_{max} = 100 + 2.3\ P_F$$

where P_F = afterheat power in fuel elements (Btu/sec), and T_{max} = maximum fuel element temperature ($^{\circ}F$). The preceding relation assumes ambient temperature of $100^{\circ}F$ and aftercooling airflow of 2 pounds per second. These values were approximately correct for in-transit operation with $100^{\circ}F$ ambient temperature.

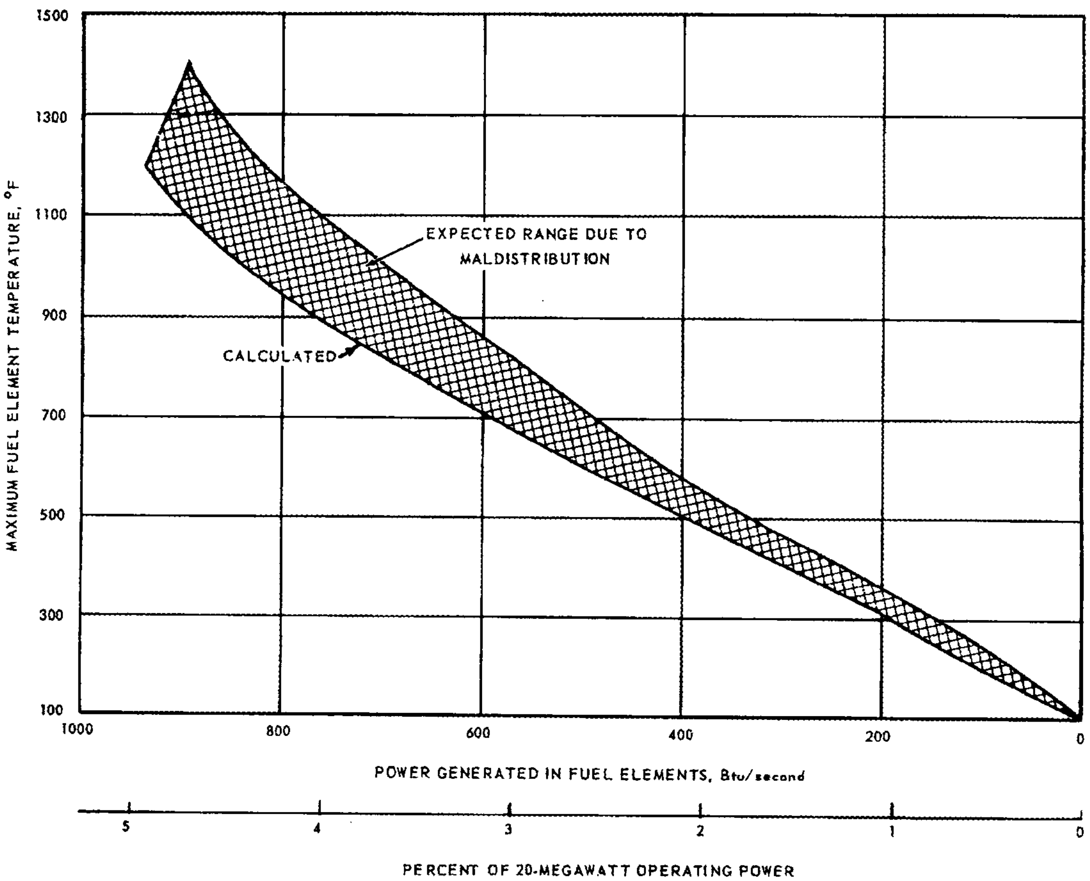

Fig. 2.37 – Maximum fuel element temperature versus afterheat rate with full-speed blower operation

Special problems that arose in connection with in-transit cooling of fuel elements mainly concerned temperatures of fuel tube components in the absence of airflow. Under these circumstances, cooling of the fuel elements occurred by free convection and by radiation and conduction through insulation liners to the moderator system. Since the flow of air through the reactor core by free convection currents could be limited by CTF ducting, system valves, and other auxiliary equipment, no cooling due to free convection was considered; the sole heat-leakage mechanism for the system was assumed to be radiation from fuel elements to insulation liners and conduction through the liners to the moderator system. The results of this analysis are shown in Figure 2.38. These calculations indicated that the fuel elements could be held to safe operating temperatures at in-transit power levels solely by radiant heat transfer. It should be pointed out, however, that radiant heat transfer calculations of this nature were sometimes inaccurate because of the sensitivity of temperature to surface emissivity, which had to be assumed. It appeared reasonable to assume that the fuel elements operated safely at power levels up to 30-40 Btu per second; higher levels were somewhat questionable.

Although it appeared that the fuel elements would be safe if air-supply failure occurred in transit, damage to the thermocouple and fuel tube disconnects, which had maximum temperature limits of 600°F and 900°F respectively, could be anticipated. Figure 2.39 indicates the time available following air-supply failure or cutoff before temperatures capable of damaging disconnects were attained in the fuel tube.

During operation at the test site, no problems were anticipated concerning moderator overtemperatures as long as the main moderator system was in operation. After shutdown,

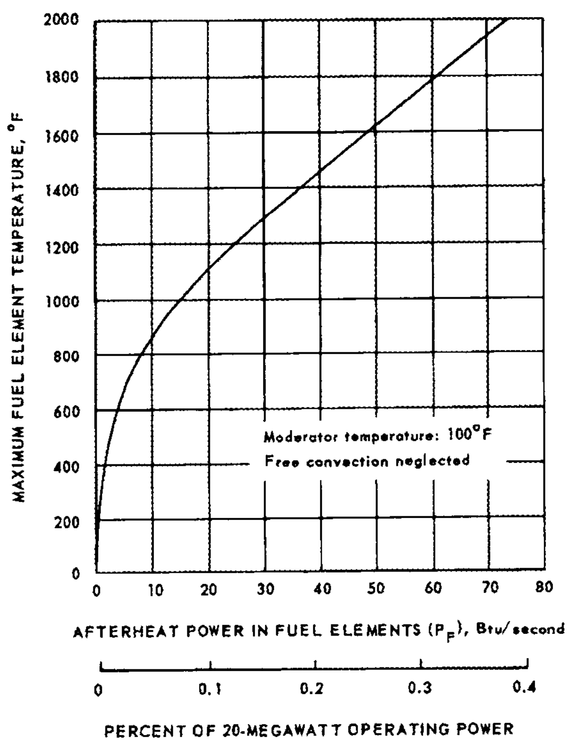

Fig. 2.38 – Maximum temperature of fuel elements versus reactor afterheat power for cooling by radiation of moderator system

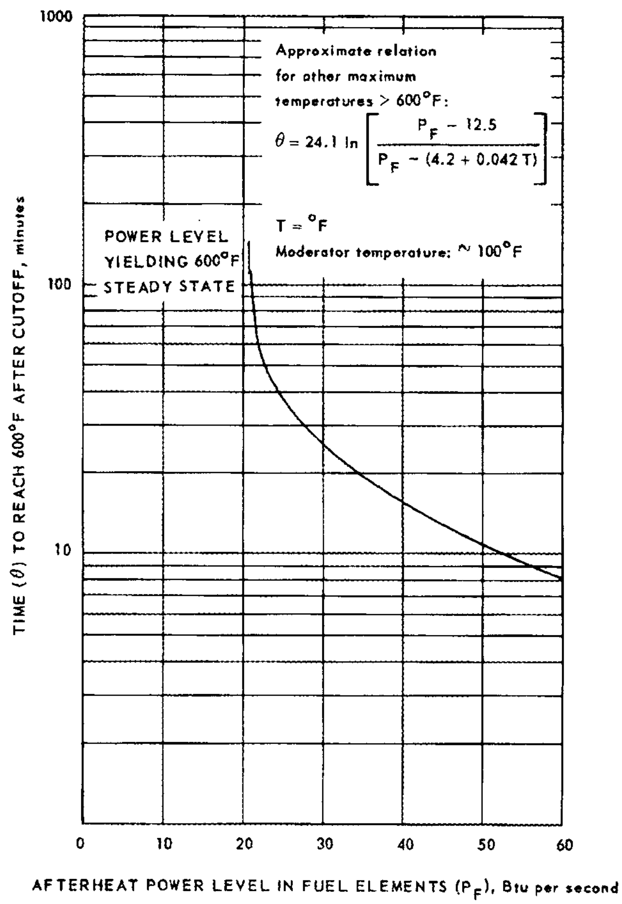

Fig. 2.39 – Time to reach 600°F in fuel tube after air cutoff versus power level during cutoff period

the moderator system temperature could be reduced essentially to ambient air temperature by short-time operation of the main moderator system at full cooling capacity. After cutoff of the main system, the auxiliary system could dissipate afterheat generation in the moderator so that the moderator system could again be run close to ambient air temperature if desired.

Special problems arose when moderator cooling systems were cut off either to permit replacement of control rod actuators or to provide additional power for in-transit air cooling. The time allowed for such operations was assumed to be the period before boiling of the moderator system could be expected. For removal of actuators, it was assumed that the moderator would be drained to approximately the level of the core tank. Since the thermal capacity of the core tank was approximately 4000 Btu per °F, the time before moderator boiling was:

$$\theta = \frac{4000}{3600\ P_M}(200 - T)$$

$$\theta = \frac{1.11}{P_M}(200 - T)$$

where

θ = time in hours before boiling

P_M = average power generation in moderator, Btu per second
T = initial moderator temperature

The equation could also be modified for the case of no air cooling of the fuel elements, with transfer of heat by radiation to the moderator by using total afterheat rates rather than afterheat generation in the moderator alone.

Two special heat-generation problems arose in the handling of the core and plug in the hot shop facilities. One problem concerned switching from aftercooling blower to the hot shop aftercooling system. At some period during this exchange, no cooling air was passing through the fuel tubes. How long this period could last without damage to disconnects can be determined from Figure 2.39.

A second problem concerned the possibility of draining moderator water from the core while it was in the hot shop handling fixture in order to insure fail-safe operation. This procedure was limited by maximum allowable temperatures of the aluminum structure and beryllium reflector, which were assumed to be $300^{\circ}F$ and $1000^{\circ}F$, respectively. Calculations indicated that the heat-loss capacity of the system (by radiation from core tank to hot shop surroundings) within limitations of these temperatures was approximately 1 Btu per second, generated outside the fuel tube. Therefore, auxiliary air cooling had to be supplied to the core tank to prevent overtemperaturing of materials. The required air supply, transient characteristics of the system, and expected maximum temperatures of components for dry-core operation are shown in Figure 2.40. These calculations assumed that heat generated in the fuel elements (approximately 75 percent of the total) is dissipated to the aftercooling system, and heat from the structure outside the fuel tubes is dissipated by free convection.

All of the previous calculations concerning aftercooling blower operation assumed ambient temperature of $100^{\circ}F$ as a reasonable "worst case." Since the blower capacity was reasonably sensitive to ambient temperature, and the transient heating times and temperatures were in turn sensitive to blower capacity, most transient calculations would have to be reworked for other ambient conditions if a questionable situation were to arise.

The only available relation between time and afterheat power generation is tabulated in Figure 2.36. These data may be in error by as much as ± 25 to 50 percent in the afterheat level for a given time. Therefore, considerable caution should be exercised in relating powers shown in various calculations to actual times after shutdown.

Transient Conditions

Figure 2.41 shows the transient behavior of afterheat generation in fuel elements during the time period in which the fissioning rate due to decaying neutron flux was important.

The most critical period for possible overheating of fuel elements occurred immediately after scram of the engine-reactor system operating solely on nuclear power. For approximately the first 20 seconds of this period, the afterheat rates were in the range of 10-20 percent of full operating power. The fuel elements were cooled by heat losses through the insulation liner and by convective heat transfer to air supplied by engine coastdown and aftercooling blowers. The heat losses through the liner were essentially negligible in this period. Since the afterheating rates in this period were high, fuel element temperatures were sensitive to airflow variations. Experimental evaluations of engine coastdown did not depict actual coastdown in the engine-reactor system because of lack of afterheat and pressure-loss simulation. Specifically, afterheat following scram supplied additional turbine power resulting in higher airflow than that shown in the chemical system. At the same time, however, since the pressure loss in the engine-reactor system was higher than in the chemical system, it tended to decrease airflow. Another complicating factor was that the aftercooling blower did not cut into the system until the pressure in the torus at the

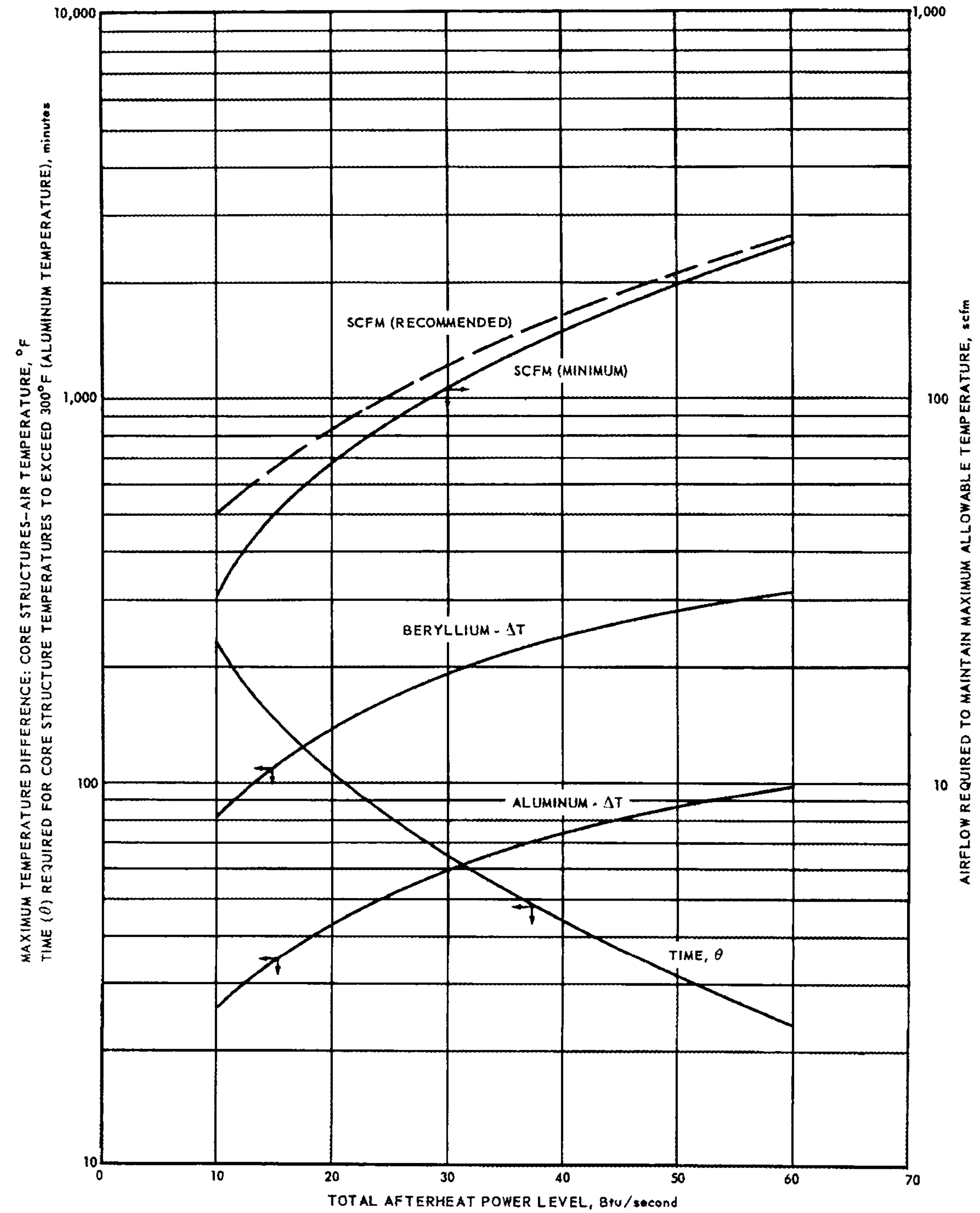

Fig. 2.40 – Time, temperature, and flow relations for dry-core operations as a function of afterheat power level

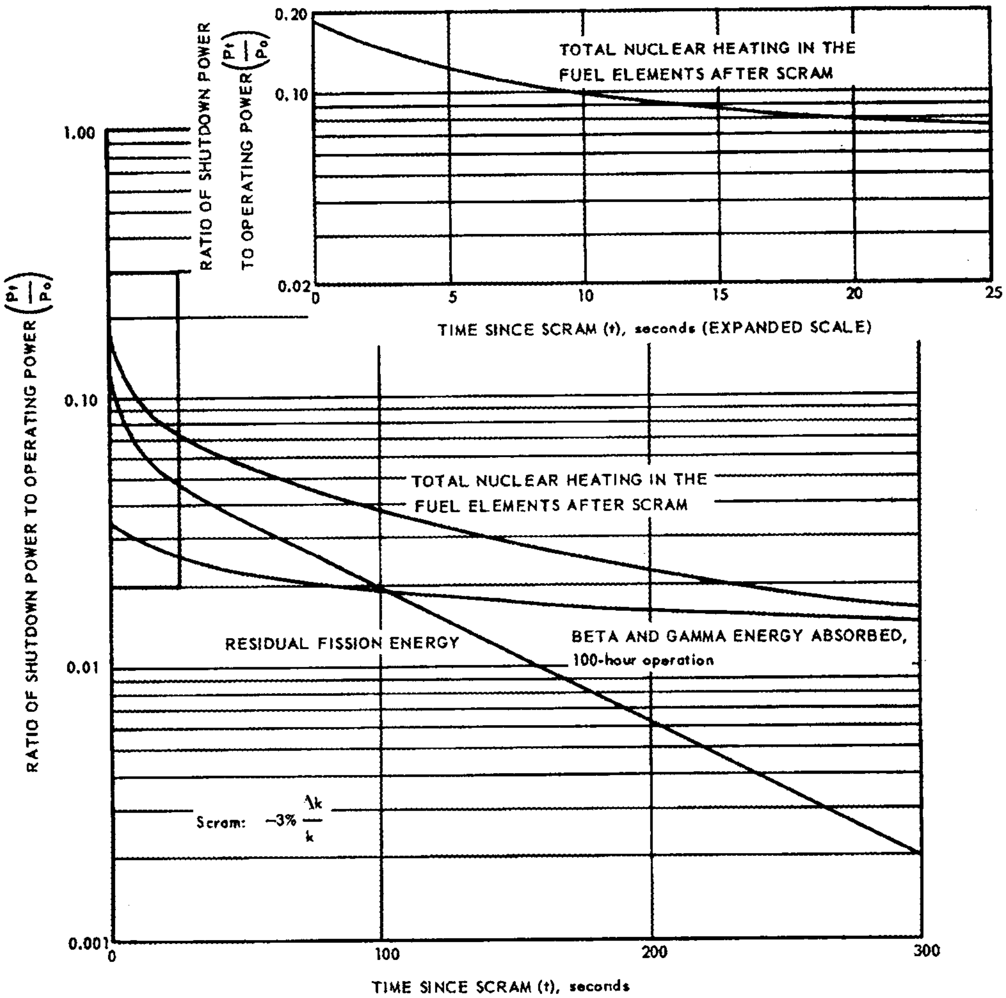

Fig. 2.41 – Fraction of operating power versus time for fuel elements

blower valve was less than the static no-delivery head of the blower. (This assumed that the blower was deadheaded at scram. An additional 8 seconds was required to bring the blower to full speed if it was inoperative at the time of scram.) Since torus pressure was also a function of engine coastdown, the time of aftercooling blower cut-in was also in doubt. Thus, an exact evaluation of fuel element temperatures immediately after scram could not be made since the variation of airflow could not be accurately depicted. Further, since these determinations were also extremely sensitive to such factors as the response time of control circuits and valves, it appeared that data for these calculations must be obtained during actual system tests.

Although a series of calculations was made by assuming various relations for coastdown time and blower cut-in, it was felt that the only reasonable limiting-case estimate was to assume that an airflow of approximately 4 pounds per second would be available continuously after scram. The resultant maximum fuel element temperatures, which generally occurred within 10-20 seconds after scram, are shown in Figure 2.42. Transient temperatures for some alternative conditions are also shown.

The curves presented in Figure 2.41 assume a step input of minus 3 percent Δk. Scram capacity of this magnitude could be absolutely guaranteed for the system; thus, these curves

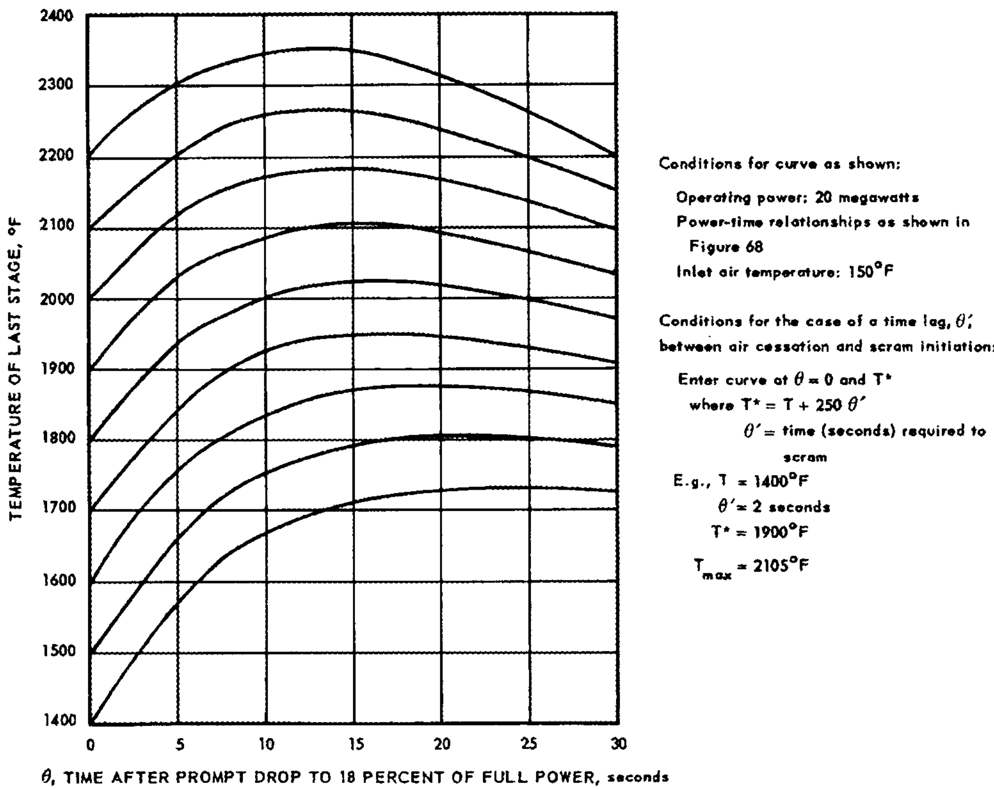

Fig. 2.42 – Maximum temperature of fuel elements for step reduction in airflow to 4 pounds per second as a parameter of fuel element temperature at time of prompt power drop

and the resulting heat-generation data are somewhat optimistic from the standpoint of power generation. Transient heat generation rates for scrams of other capacities may be estimated through the use of the following approximation.

1. Assume that the power dropped instantaneously to a value given by:

$$\frac{P_1}{P_0} = \frac{1}{1 - 1.11\,\Delta k}$$

where Δk is the change in reactivity expressed in percent (minus for scram).

2. Assume that the transient power after the instantaneous drop followed a curve parallel to that shown in Figure 2.41.

2.3.5 GENERAL OPERATIONAL PHILOSOPHY

The specified goal of work on the reactor was the operation of an X39-4 turbojet engine at an appreciable fraction of full rated speed on heat from a nuclear source. Although no specific values were implied by this goal, a nominal design point was set to insure adequate facilities and provide targets for development programs. The nominal design-point values and the anticipated operational ranges are shown in Table 2.19.

In addition to the basic goal, an effort was made to determine the potential of the D101A2 reactor system. Specifically, it was hoped that maximum fuel element temperatures and power densities during operation could be determined. To meet these aims the fuel element design was adjusted to meet the following conditions: (1) satisfactory system operation at

TABLE 2.19

SUMMARY OF NOMINAL DESIGN POINT AND PROBABLE OPERATING RANGE OF MAJOR SYSTEM VARIABLES

	Nominal	Operating Range
Reactor power, mw	20	13 - 20
Fuel element temperature, °F	1700	1600 - 1900
Reactor inlet air temperature, °F	380	300 - 450
Reactor exit air temperature, °F	1400	1200 - 1500
Airflow, lb/sec	60	45 - 60
Engine speed, rpm	7800	6000 - 7800
Core inlet pressure, psia	57	30 - 60

some point at which fuel element design temperatures were approximately 1700°F with considerable margin of safety for system perturbations, and (2) operation of fuel elements at or near maximum temperature and high power density within air temperature limitations imposed by the engine and the CTF, 1400°F-turbine and approximately 1500°F-reactor discharge temperatures. This adjustment necessitated the choice of a basic design point that is approximately 75 percent of the power level of the nominal figures, as depicted by the 7000-rpm mating point in Figure 2.27. Precise specification and evaluation of alternative mating points for evaluation of system potential depended on such factors as ambient conditions and characteristics defined during operation. No attempt was made to define these points other than in the typical mating-curve data of Figures 2.27 and 2.28.

2.4 CONTROL SYSTEM

2.4.1 NUCLEAR INSTRUMENTATION

Nuclear instrumentation for the D101A system consisted of three channels: the count rate, the log flux, and the linear channel, as indicated in Figure 2.43. All channels had three identical sensors and instruments so that operation did not depend on any single sensor or instrument.

Count-Rate Channel

The count-rate channel was the only means of determining the status of the reactor when the flux level was below 10^{-5} NF. Three fission chambers and their associated preamplifiers were situated on the fission-chamber actuators, which were mounted on the top plug. The fission chambers could be set in any one of three positions independently of each other.

Pulses from the preamplifiers supplied the linear amplifiers. Linear amplifiers selected pulses above a given energy level and shape, amplified them, and passed the resulting pulses to the log-count-rate and period amplifiers. The log-count-rate unit converted these pulses to a d-c voltage proportional to the logarithm of the number of pulses arriving per unit time. This logarithmic signal was also differentiated and yielded a period signal to control relays in the auctioned log-count-rate, period, and safety circuits. Each log-count-rate and period amplifier was monitored by meters.

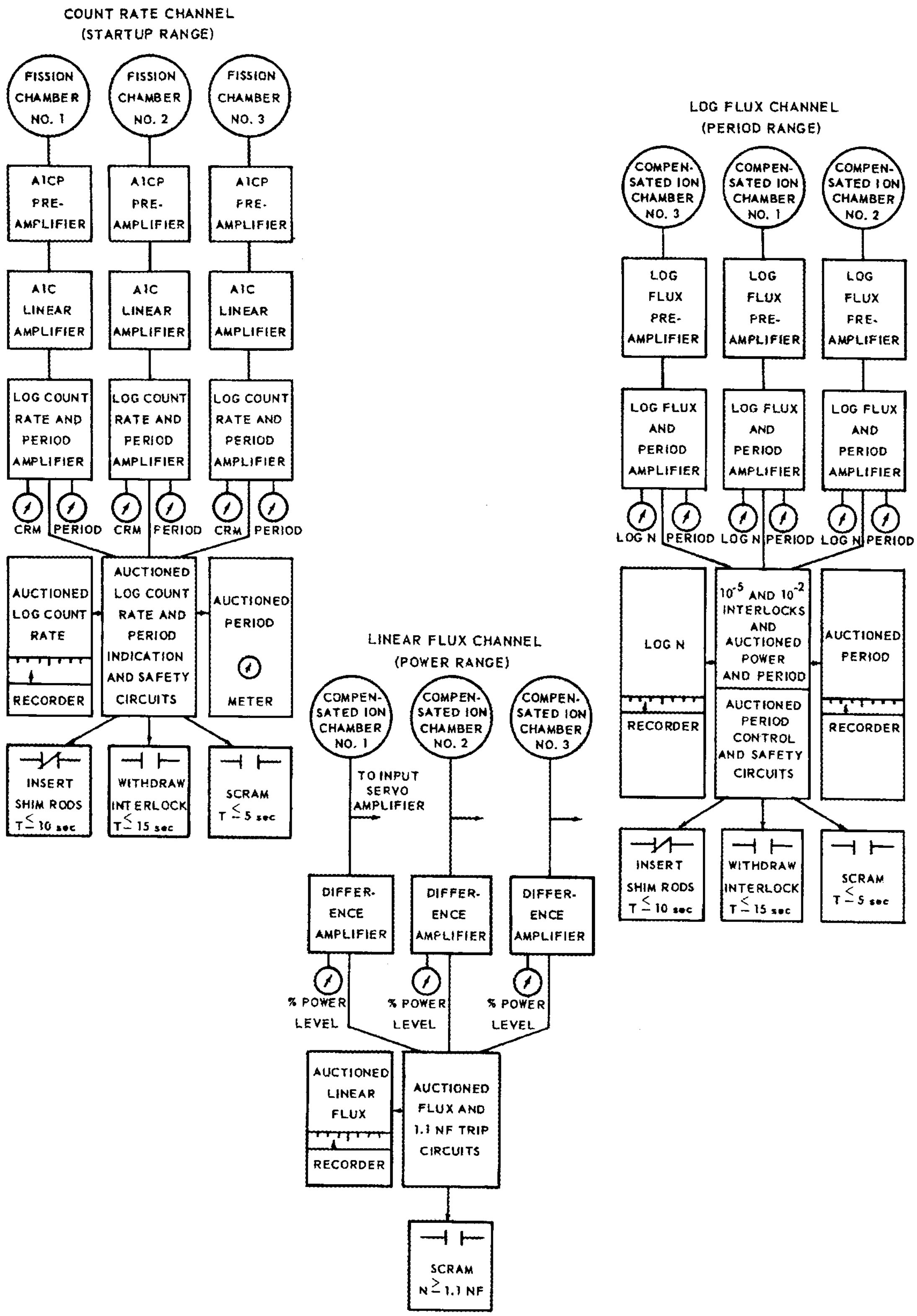

Fig. 2.43 – Schematic drawing of D101A nuclear instrumentation

The three signals from the log-count-rate circuit were auctioned and used to operate a log-count-rate recorder and a period meter. The auctioned signal also operated relays that restricted the operator's control of shim-rod position. If the period of any channel became less than 5 seconds, the reactor was scrammed. The period signal in the startup range was relatively slow because of the averaging time required to determine a reliable reading. However, this deficiency was not a particular drawback since the power level was six or more decades below full-power flux level.

Log-Flux Channel

The log-flux channel was supplied by compensated ion chambers situated in the side ports of the CTF. Each chamber supplied a d-c signal proportional to the flux level of the reactor in the range from 10^{-5} NF to full power. This current signal supplied the input to the log-flux preamplifier also located in the CTF. The log-flux preamplifier fed the log-flux and period amplifier. The log-N amplifier output was a voltage proportional to the logarithm of the input. This logarithmic signal was differentiated to obtain a period signal which was used to supervise the withdrawal of shim rods in the period range and scram the reactor if the period became less than 5 seconds. Each log-N and period amplifier was monitored by meters. All three log-N and period signals were auctioned, and the largest was used to operate the control relays and log-N recorder.

Linear-Flux Channel

Three compensated ion chambers situated in the top plug were used as the sensors in the power range. Each sensor supplied an input to the flux-regulation servo and a difference amplifier. Each difference amplifier was monitored by a flux meter. The three flux-level signals were auctioned, and the highest signal was recorded. The high signal also supplied the input to the 1.1 NF trip circuit. If the flux level exceeded 1.1 NF, the reactor was scrammed.

2.4.2 DYNAMIC CONTROL SYSTEM

The purpose of the flux-regulating servo was to maintain the reactor power level at the value selected by the operator. The proportional-plus-reset servo operated between 1 percent and 100 percent full power.

Figure 2.44 is a schematic diagram of the servo system. The output of two linear ion chambers, shown in the figure, was converted to voltage signals by cathode followers. These two voltage signals were auctioned, and the larger provided the input to a d-c amplifier whose gain was inversely proportional to the power-demand setting. An opposing reference current proportional to the power-demand setting was also fed into this amplifier. The difference quantity or error signal was amplified, and the output signal was fed to an integrating amplifier. The proportional-plus-integral error signal at the output of this second amplifier provided the input to a dynamic-rod position loop.

With zero voltage as the input to the position loop, the dynamic rods were held at the neutral position which was set at a withdraw displacement of 15 inches. By adjusting the control transformer in the feedback of the position loop, it was possible to set neutral at any designated rod displacement. A positive voltage at the output of the integrating amplifier inserted the dynamic rod, and a negative voltage withdrew the rod.

The minor position loop operated as follows. Dynamic-rod feedback voltage from a synchro transmitter was subtracted from the minor-loop-command voltage by unbalancing a 400-cycle carrier voltage applied to the plates of a balanced modulator. The difference, represented as a suppressed modulated carrier, was amplified and converted to sufficient power to drive a 2-phase servomotor. The servomotor positioned a four-way pilot valve.

Pressurized water applied at this pilot valve was admitted to an integrating piston-cylinder actuator when the valve was ported by the servomotor.

The voltage from the integrating amplifier also actuated a shim-rod-insert relay when the voltage exceeded a present positive value and actuated a shim-rod-withdraw relay when the voltage exceeded a corresponding negative level. When in motion the shim rods were driven at a constant speed to compensate for low-frequency changes and to maintain the dynamic rod near the neutral position.

A proportional-plus-reset temperature control provided a means of operating from fuel element or air discharge temperature. The flux loop remained intact, and the temperature control generated the power demand. A temperature signal was selected from retransmit slide wires of temperature recorders and matched against the temperature demand. The resulting error signal was fed into an integrating amplifier, which converted the error signal to the proper flux-demand voltage. A temperature-flux switch allowed the operator to transfer between the two modes of control when the null indicator read zero.

Supplementary and backup control equipment are described in reference 18.

2.4.3 SHIM-CONTROL SYSTEM

The following paragraphs describe the operation of the shim system when the shim-control selector switch was placed in the automatic position.

Figure 2.45 is a simplified schematic diagram representing typical essential elements of the shim-control system. The position-command bus was a part of the dynamic-rod servo system. When the current from the ion chamber that represents the reactor power level was larger than the reference level, a positive error voltage appeared on the position-command bus. Likewise, when the flux level was lower than the command level, a negative voltage appeared on the position-command bus.

The shim system began with a shim-rod magnetic preamplifier, which amplified the signal on the position-command bus and drove the insert- and withdraw-relay magnetic amplifiers. When the voltage at the position-command bus was sufficiently positive, a relay was energized and closed the insert circuit to the master motors. These motors positioned the shim frames in such a direction that the regulating dynamic rods were moved toward the neutral band. The magnitude of the voltages required to energize the shim-control relays determined the neutral-position band width of the dynamic rods. The band-width adjustments were located within the insert and withdraw magnetic amplifiers.

As indicated in Figure 2.45, a Scott T-connected transformer accepted 3-phase 400-cycle 115-volt power and delivered the 2-phase control power required by shim-rod-drive motors and their associated control components. There were two separate secondary windings: one supplied the control-phase voltage, and the other supplied the reference-phase voltage. The control-phase winding was center-trapped with 115 volts on each side of the common line so that it was ± 90 electrical degrees with respect to the reference phase. Standard 400-cycle, 2-phase servo motors were used as controlling elements.

Relays controlled the master-frame-drive motors. These motors, one of which is shown in Figure 2.45, drove synchro transmitters at a slow rate corresponding to a shim-rod-command movement of 1 foot per minute. The master-frame synchro transmitted its command position to each of its rod-control transformers, one of which is shown in Figure 2.45. This shim-rod-control transformer was the nulling element of a position servo consisting of a shim-rod electronic amplifier, and a shim-rod-drive motor and actuator geared back to the control-transformer rotor. Any signal from the master synchro created an error voltage until the shim-rod-drive motor repositioned the rotor of the control

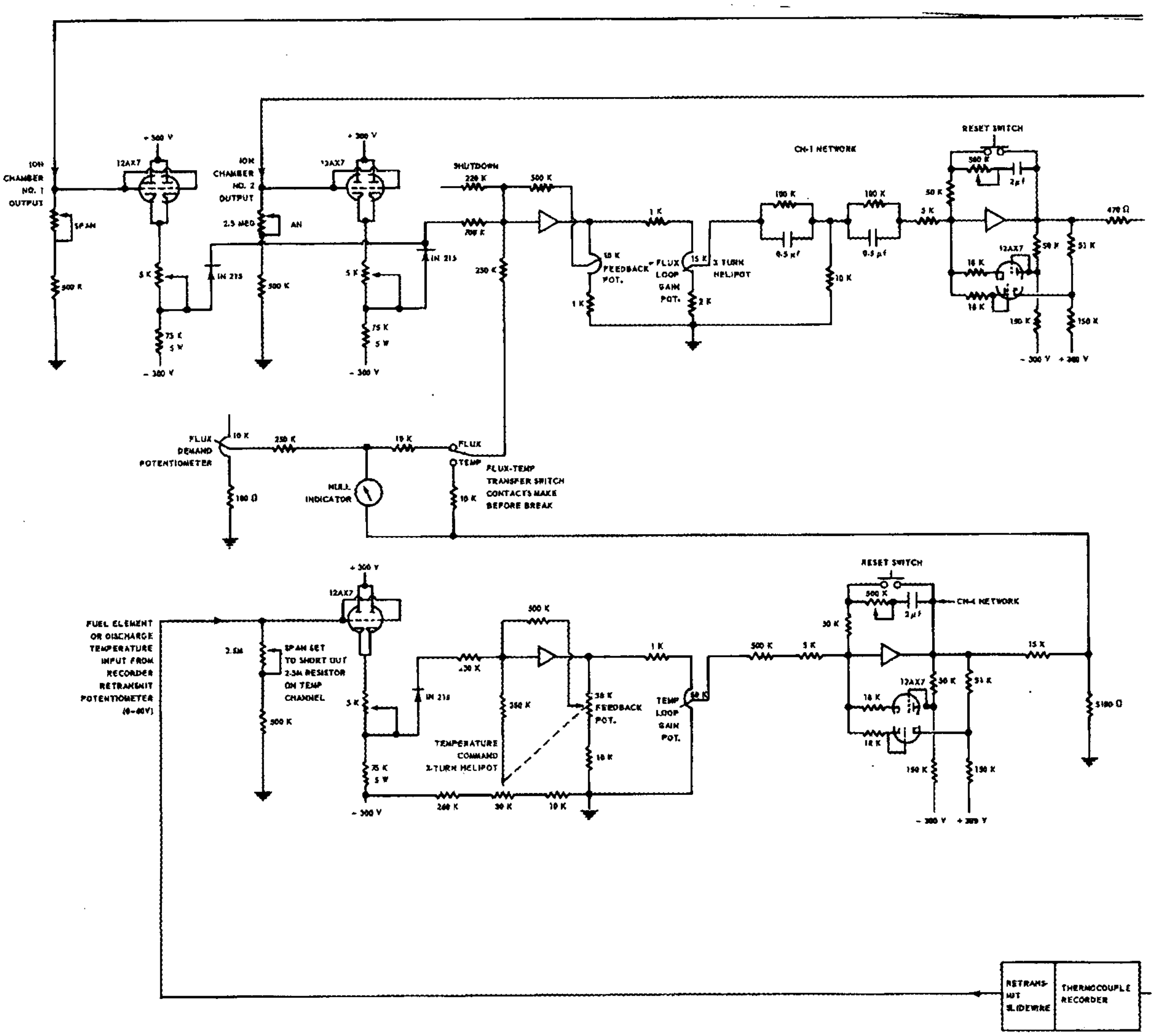

Fig. 2.44 – Schematic diagram of D101A servo system

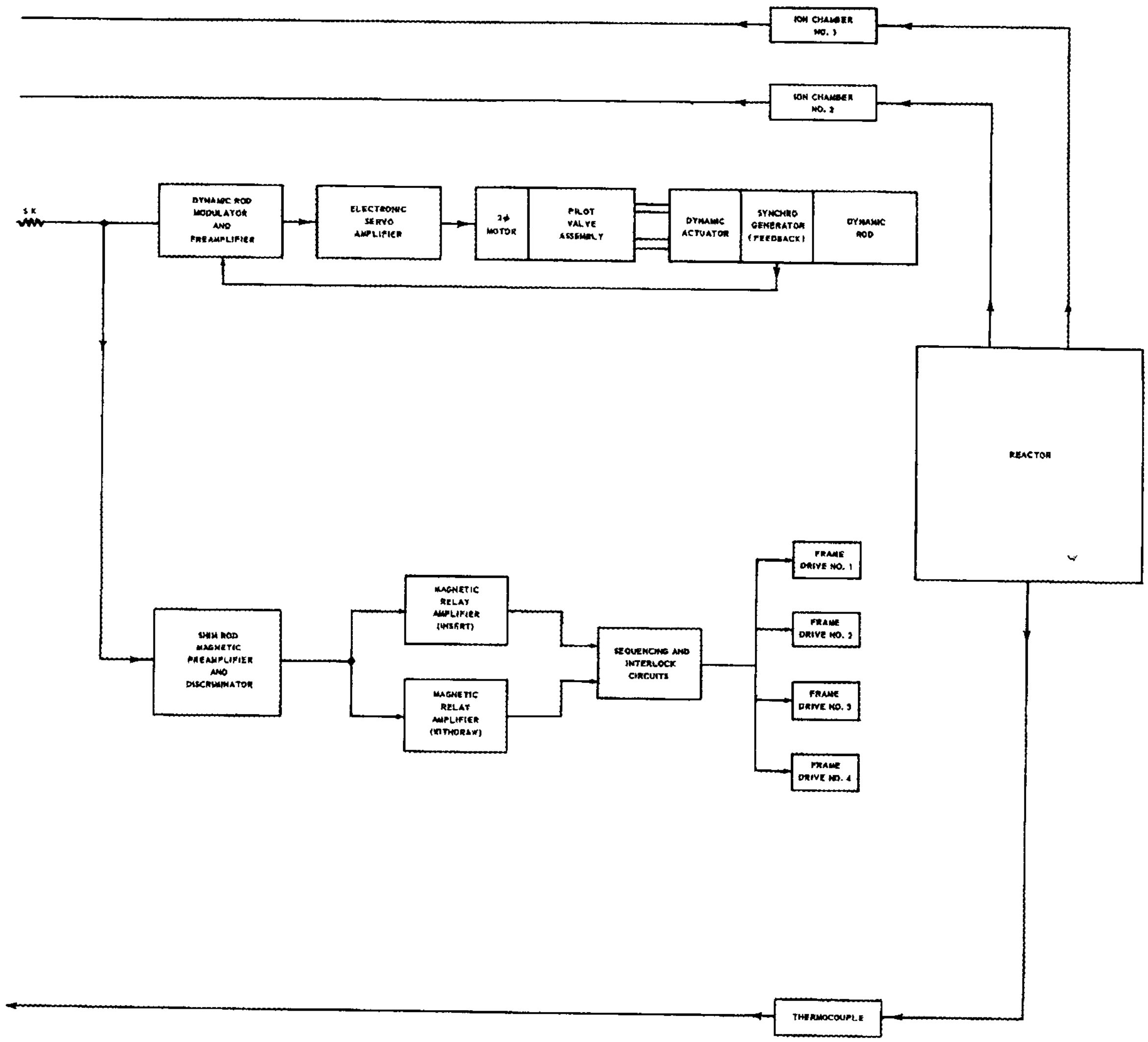

Fig. 2.44 – Schematic diagram of D101A servo system (Cont.)

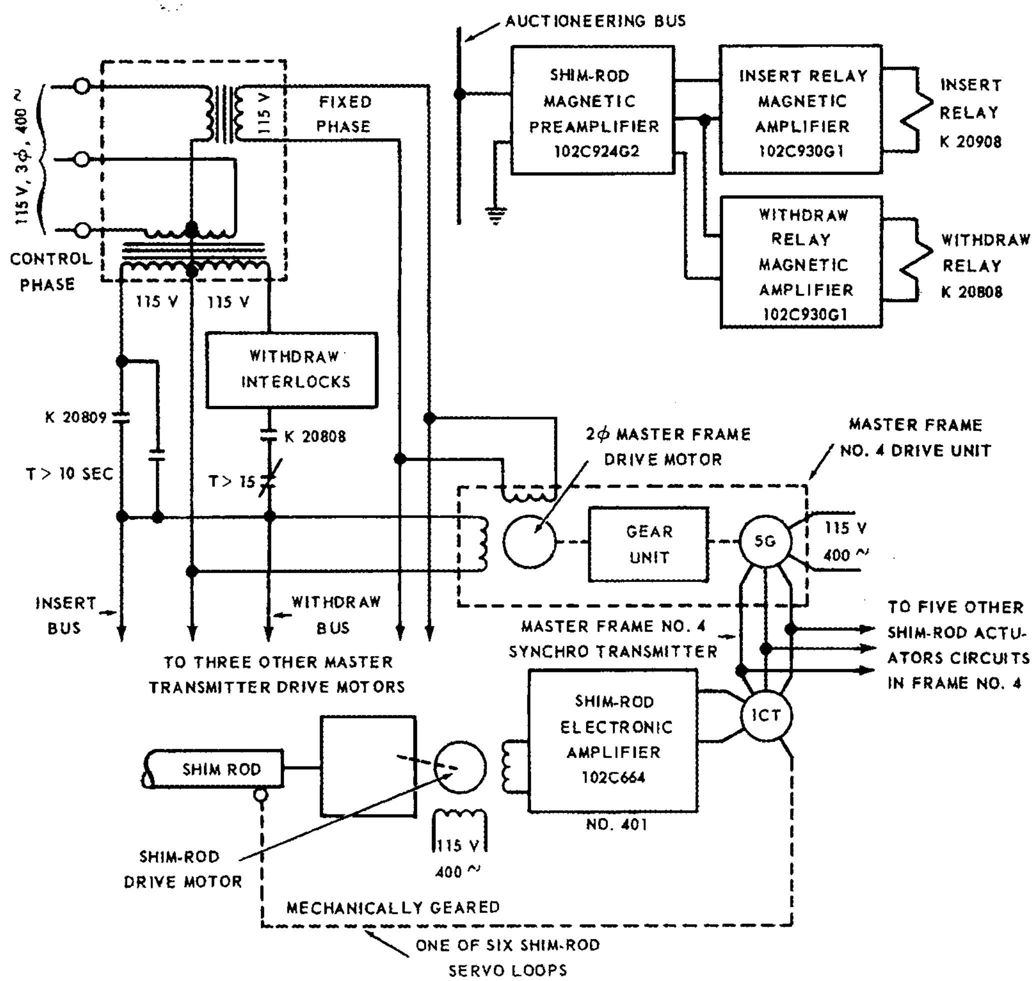

Fig. 2.45 – Schematic diagram of D101A shim-control system

transformer to match the transmitted signal. By this arrangement, all rods of a given frame followed their master synchro transmitter.

Figure 2.45 shows two other contacts in the insert and withdraw buses. These contacts were operated by period-control relays. There was a contact in the withdraw bus that was closed under normal operating conditions; that is, when the period, T, was greater than 15 seconds. This contact then opened the withdraw bus if T was less than 15 seconds, so that the shim rods could not be withdrawn further. If the flux rate continued to increase until the period became 10 seconds, another period relay took further corrective action by closing the insert bus. Shim rods were inserted until the period was sufficiently greater than 10 seconds. These relays were in operation between 10^{-5} NF and 1.0 NF, so that they were a controlling factor in both the period and power ranges.

The flux level was controlled in the startup range by withdrawing shim rods and observing the startup instruments. The shim-control selector switch, which had to be in the Manual position, was interlocked so that the operator could not withdraw shim rods until it was placed in the Manual position. The period was maintained above 50 seconds in this range.

At 10^{-5} NF, the log-N channel began to register, and the period control became effective. The operator could then raise the power level through the period range by manually positioning the frame-command switch and observing the log-N and period recorders, or by placing the shim-control selector switch on Automatic. The operator could, at his discretion, manually control the shim rods in the power range; however, the period circuits remained intact and overrode the operator when he was at fault.

The dynamic servo system controlled the power level from 10^{-2} NF to 1.0 NF. When the flux level was below this power range, the dynamic rods were fully withdrawn. The shim-control selector switch could be placed on automatic; when the flux level was greater than 10^{-5} NF, the period control assumed command until the flux level rose to 10^{-2} NF.

The shim rods were released during a scram. When the trouble cleared, the shim-rod motors automatically drove the rod clutches to their inserted position. These electromechanical clutches engaged and latched so that the reactor reset switch could be used to initiate a new startup in a minimum of time after a scram.

2.4.4 SAFETY SYSTEM AND INTERLOCKS

When the reactor was operating in unsafe or undesirable regions, the power level could be reduced in two ways: (1) shutdown and (2) scram.

1. Shutdown was employed for conditions that were not an immediate hazard, but that should be corrected before operation continued. In shutdown, the dynamic rods were driven into the reactor; this action initiated the insertion of all rods by sequence operation. After the trouble was discovered and corrected, a complete startup was necessary before operation could be continued.
2. Scram was employed when the engine or reactor operated in regions that were potentially unsafe. The shim-rod solenoid latches were released, and all spring-loaded shim rods were completely inserted within 200 milliseconds. The dynamic rods were also driven in at a rate of 750 milliseconds for 30-inch travel. Scram could be initiated manually or automatically. A reset was not possible until the scram trouble was corrected.

Scram Followup System

In the scram followup system, a solenoid-operated multideck stepping switch provided insert power to the shim actuators and all master-frame selsyns within 2 minutes after the scram condition was corrected.

Safety Circuits

The safety circuits are shown in Figure 2.46. The relays in each of the three circuits were connected in series; any one signal, upon reaching its limit, opened its associated contact, which de-energized the circuit relays. Many of the control circuits received signals from thermocouples operating limit switches on the temperature recorders.

Withdraw and Startup Interlocks

Withdraw and startup interlocks are shown in Figure 2.46. These interlocks opened the withdraw-power bus to prevent shim-rod withdrawal. Interlocks also open-circuited the withdraw-power bus as another contact closed the insert bus to prevent shorting the power supply.

2.4.5 TEMPERATURE SENSORS

Figure 2.47 shows the location of sensors of thermodynamic interest in the D101A system.

Figure 2.48 shows a schematic layout of the angular locations of fuel element thermocouples in the core as viewed from the top.

UNCLASSIFIED

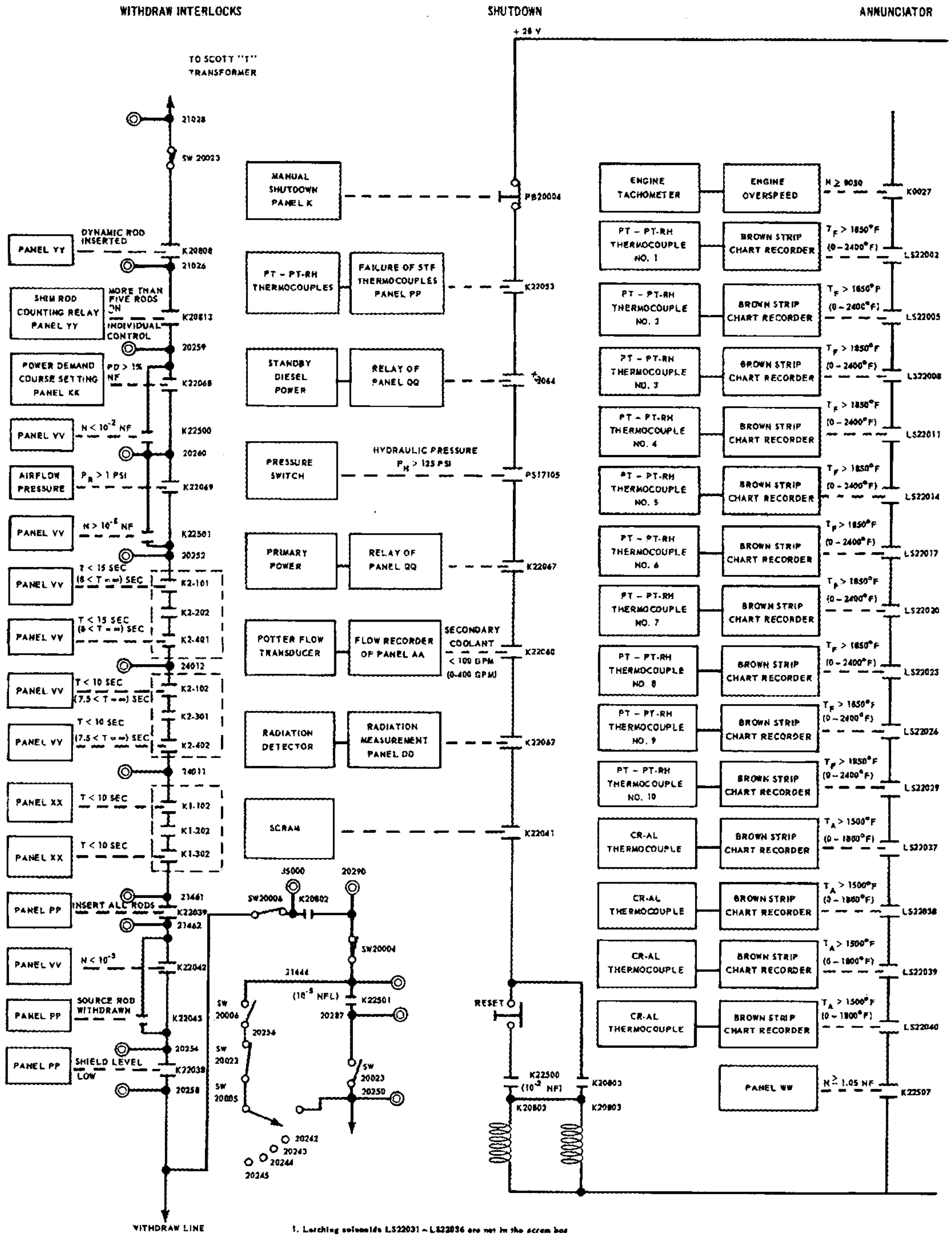

1. Latching solenoids LS22031 – LS22036 are not in the scram bus but operate relays in Brown recorders. These relays have contacts in the scram bus in place of the latching solenoids as labeled.
2. Log count rate and log-flux period scram contacts are coincidence circuits requiring two out of three channels to produce a scram condition.
3. designates jacks located on monitor board in panel YY.

Fig. 2.46 – Block diagram of D101A safety circuits

UNCLASSIFIED

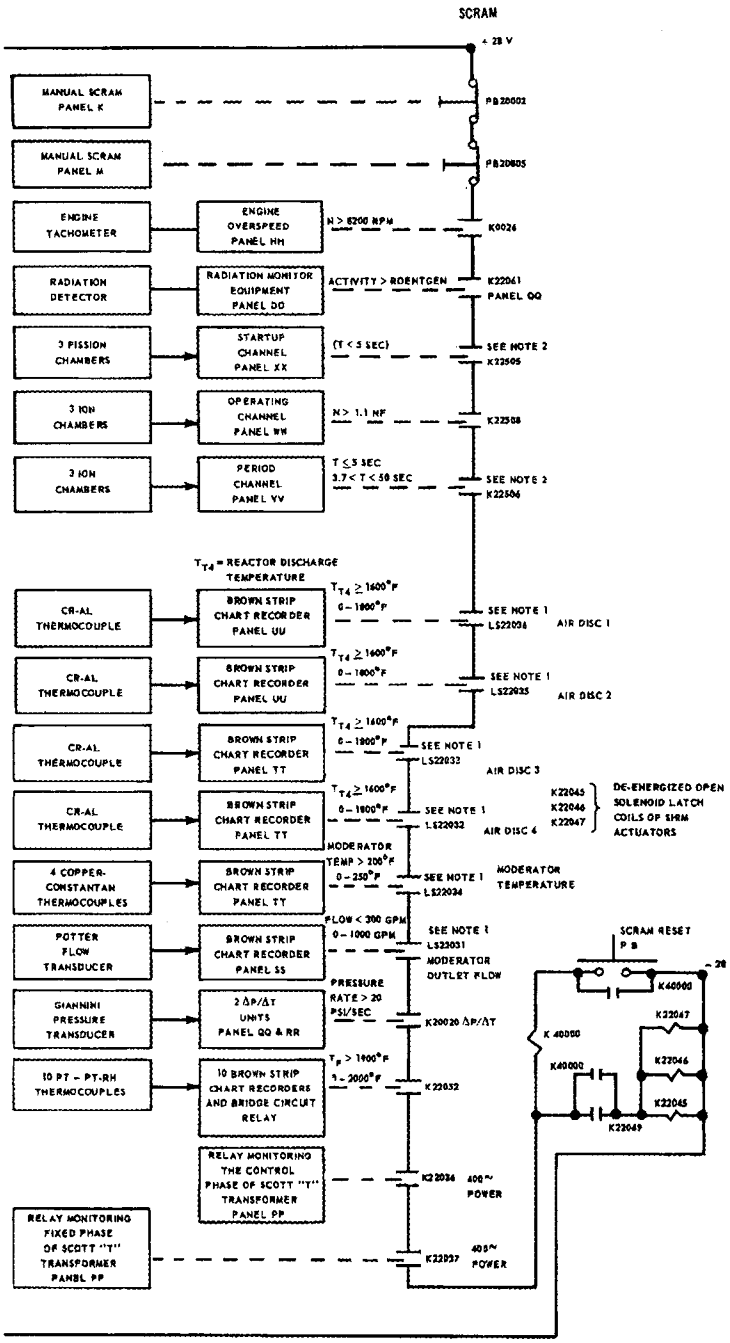

Fig. 2.46 – Block diagram of D101A safety circuits (Cont.)

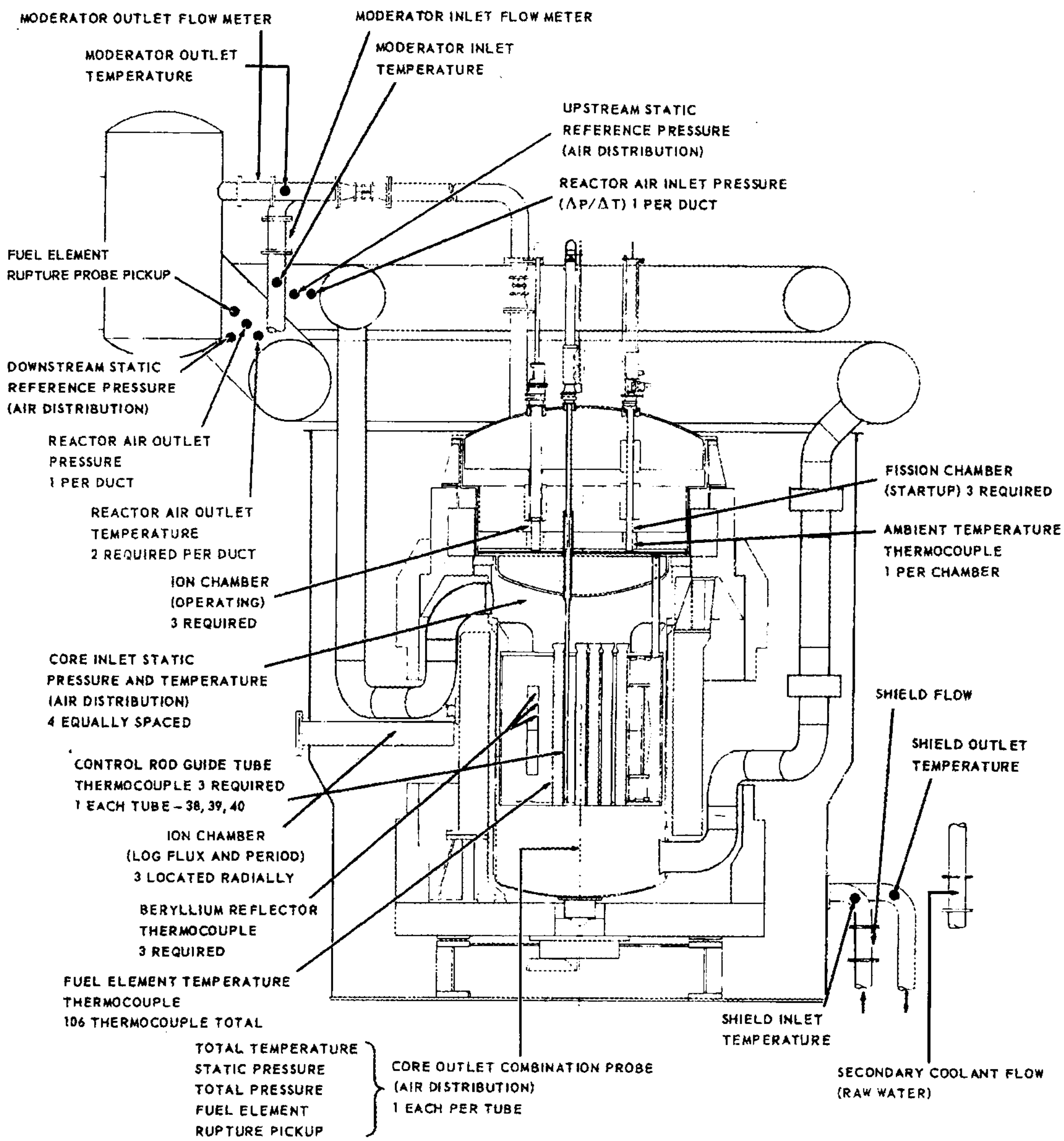

Fig. 2.47 – Schematic diagram of temperature-sensor locations in D101A test assembly

Fuel cartridges were divided into five types based on the number, stage, and plate location of the thermocouples. Cartridge types 1 and 2 had 18 thermocouples each and were located in tubes 15 and 18 respectively. The other three types had two thermocouples and were arranged as shown in Figure 2.48.

2.5 CORE TEST FACILITY

The D101A Core Test Facility (CTF) consisted of shielding, an air supply, and other necessary auxiliaries and services which were combined into test assemblies with a succession of direct cycle cores, fuel elements, controls, and other components. Design specifications and a description of the CTF are presented in APEX-903, "Reactor Core Test Facility," of this Summary Report.

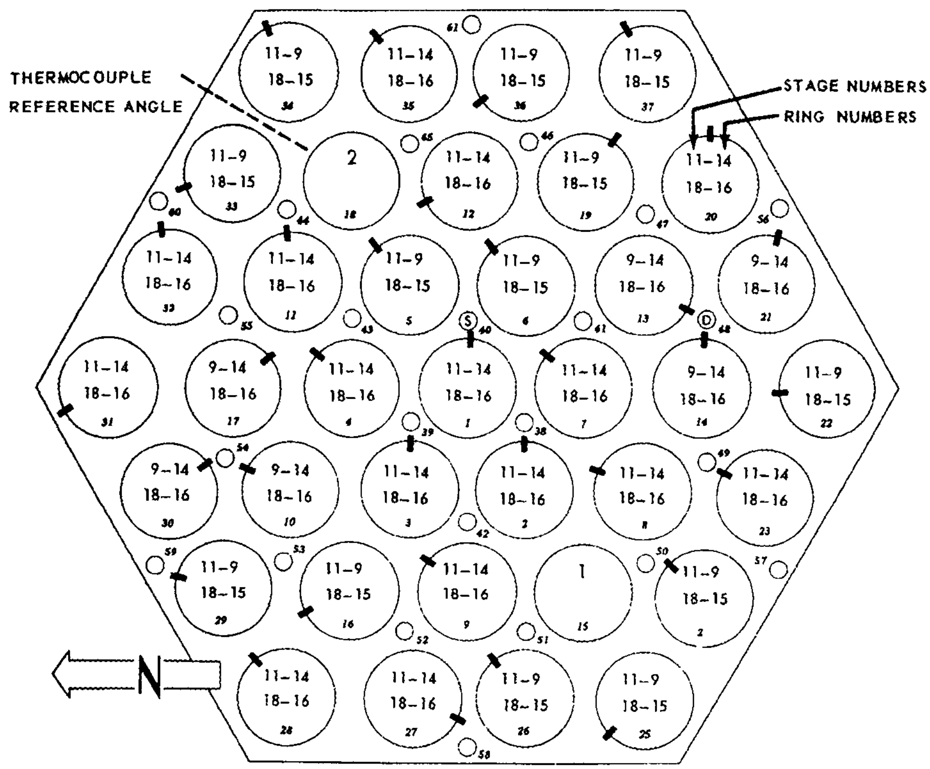

Fig. 2.48 – Stage and plate locations and angular orientation of thermocouples in D101A fuel elements

UNCLASSIFIED

2.6 REFERENCES

1. Crabbe, [redacted]RE-1 Guide to Documents and Drawings," GE-AN[redacted]D, DC 56-7-69, 1956.
2. Ross, A. L., et al, "Stress Analysis for Project 100," GE-ANPD, DC 55-5-130, 1955.
3. Minnich, S. H., "Detailed Nuclear Design of HTRE-2 A-2 Fuel Elements," GE-ANPD, DC 55-2-86, 1955.
4. Minnich, S. H., "HTRE Fuel Elements," GE-ANPD, DC 55-12-34, 1955.
5. Simpson, J. D., "Miscellaneous Reactivity Measurements on the TRA-2," GE-ANPD, DC 55-1-63, 1955.
6. Simpson, J. D., "Results of HTRE Loading Measurements," GE-ANPD, DC 55-2-42, 1955.
7. Selengut, D. S., "Pre-Analysis of TRA-3 Reflector Experiments," GE-ANPD, DC 55-8-86, 1955.
8. Selengut, D. S., "Pre-Analysis of TRA-3 Reflector Experiments," GE-ANPD, DC 55-8-87, 1955.
9. Minnich, S. H., "Design Fuel Inventory for HTRE Core A, A-2 Cartridges," GE-ANPD, DC 55-2-53, 1955.
10. Cohen, R. M., "Correlation of TRA-2 Power Mapping Data," GE-ANPD, DC 55-1-113, 1955.
11. Hilvety, N., "Gross Radial Power Distribution in the TRA-2," GE-ANPD, XDC 55-1-100, 1955.
12. Nemzek, T. A., "Critical Experiment Theory Calculation, TRA II," GE-ANPD, XDC 55-3-30, 1955.
13. Rosenthal, H. B., "TRA-III Gamma Survey," GE-ANPD, DC 55-8-26, 1955.
14. Jacoby, M. A., "Summary Fuel Element Thermocouple Temperature - Time History and Reactor Power - Time History," GE-ANPD, DC 56-6-704, 1956.
15. Lapides, M. E., "Summary Report of Thermodynamic Analysis for Project 100 Part II Fuel Elements," GE-ANPD, DC 55-7-28, 1955.
16. Lapides, M. E., "Cold Flow and Burner Rig Tests of A2 Cartridges," GE-ANPD, DC 55-3-38, 1955.
17. Hilvety, N., "Afterheat in Dry HTRE Core A," GE-ANPD, DC 54-8-72, 1954.
18. Gorker, G. E., "Instruction Operating Manual for XC Control Equipment," GE-ANPD, DC 56-2-65, 1956.
19. "HTRE No. 1 Design and Operational Study," GE-ANPD, APEX-398, August 15, 1958, Table 1, pp 43-48.

3. IET NO. 3

The first series of operational tests using the D101A test assembly was run at the Idaho Test Station during the period from December 27, 1955 to February 25, 1956. It was designated Initial Engine Test (IET) No. 3. The test operation, 44 runs in all, was generally successful in that the system operated without chemical assistance as intended; no inherent instabilities were observed. On February 11, 1956, during an attempted transfer to full nuclear power, a burst of stack activity was detected by the monitoring equipment. The presence of fission fragments was established during subsequent operation by the presence of I^{131} in the stack gas, an indication that damage to the fuel elements had occurred. The test series was terminated to assess the damage.

The technical results of the tests are reported in detail in reference 1. The results are summarized in the ensuing paragraphs.

Examination of reactor performance rather than complete system performance generally indicated good to excellent agreement between calculations and observed performance. The only major deviation observed was that both the scatter of fuel element temperatures around an average and the maximum value of selected fuel element temperatures were greater than anticipated. In many cases, data analysis was limited either by questionable instrumentation or by conflicting interpretation regarding types of instrumentation.

Some variation of performance continuity was observed during IET No. 3 operation. This variation was believed to be caused by fuel cartridge damage. For this reason, only the over-all system behavior was analyzed for operations in which damage was observed.

3.1 OPERATION

Following a series of cold-flow tests on the engines, the reactor was operated first without forced-air cooling to determine the heat dissipation of the core and next with various combinations of auxiliary afterheat blowers. The maximum operating levels are shown in Table 3.1.

The reactor was first operated at substantial power (above 200 kilowatts) on January 17, 1956, and was operated at powers above this level on 18 days for 40.21 total hours, 349 total megawatt-hours, 16.9 megawatts maximum, and 8.7 megawatts average. Table 3.2 summarizes all operation above 200 kilowatts. IET No. 3 operations showed that the test assembly was very stable. On partial chemical fuel, the engine speed was easily regulated by fuel control. All operation was performed with the jet nozzle open wide and with the secondary air augmentors clamped shut. The over-all transient response of the power plant was quite sluggish. There was a delay of approximately 2 seconds before the changes in reactor power were felt at the engine. The engine was frequently recovered, after reactor scram at 7000 rpm, from initial fuel flows as low as 400 pounds per hour and with less than 500-rpm loss of engine speed.

TABLE 3.1

OPERATING CONDITIONS FOR LOW-POWER TESTS

Operating Blowers	Remarks	Open Duct Valves	Maximum Reactor Power, kw	Maximum Fuel Element Temp., °F
None	No air cooling for 5 hours	All closed	5	500
None	Stack draft from 40-mph wind	1 Compressor	38	375
1 low-speed		1 Turbine	300	1200
2 high-speed		1 Turbine	1400	1600
2 high-speed		1 Compressor 1 Turbine	1200	1600

TABLE 3.2

REACTOR OPERATION, IET NO. 3

Date	Time Above 200 Kilowatts, hr	Maximum Power, mw	Total megawatt-hours	Time at 100 Percent Nuclear Power, hr: min
1/17/56	2.00	0.4	0.50	
1/18/56	2.00	1.5	1.13	
1/19/56	1.50	2.0	1.62	
1/26/56	1.00	3.0	3.30	
1/27/56	1.25	8.6	4.00	
1/28/56	2.50	12.0	25.35	
1/31/56	2.50	16.9	30.00	0:37
2/2/56	0.98	12.7	7.80	
2/6/56	1.25	16.9	17.67	Transfer unsuccessful
2/7/56	0.65	13.6	4.44	
2/8/56	6.40	13.2	68.25	
2/9/56	0.30	16.9	0.60	
2/11/56	1.78	15.2	8.81	Transfer unsuccessful
2/13/56	5.48	16.9	78.96	3:43
2/18/56	1.87	16.9	15.43	
2/21/56	2.03	14.3	17.61	Transfer unsuccessful
2/22/56	2.87	15.8	40.29	1:43
2/24/56	3.85	12.8	23.32	
	40.21		349.08	6:3

The reactor was easily controlled, even though it had a positive moderator temperature coefficient of reactivity. The reactor was found to be controllable manually as well as by servomechanism. Two of the transfers to all-nuclear power were on manual control while the servomechanism was not functioning. These manual transfers were made without serious temperature or power transients. While the system was on 100 percent nuclear power, fluctuations of about 50 rpm resulted from small reactor power fluctuations.

Although successful operation on all-nuclear power was carried out on three different occasions, all-nuclear operation was difficult to achieve without excessive fuel element temperature indications. Basically, all-nuclear operation was achieved by running the engine up to a fairly high speed on chemical fuel, then gradually bringing up reactor power and reducing chemical fuel until no chemical fuel was being used. If the reactor power at this point was sufficient to sustain operation of the system, the engine continued to run; if not, it slowed down and, unless resupplied with chemical fuel, stopped. For various reasons, the margin between the reactor power just sufficient to sustain operation and that sufficient to cause fuel element overheating in sustained operation was unexpectedly small.

The scram performance was partially explored during early operation. The reactor was "full" scrammed (all rods inserted) safely from 100 percent nuclear power, with engine coastdown from 6800 rpm to 2000 rpm in 30 seconds and with no excessive fuel element temperature during the transient. Both afterheat blowers were run continuously during all reactor operations, deadheaded against their check valves; they started blowing air through the reactor when the engine coasted down to 2000 rpm. The reactor was also successfully partially scrammed from 100 percent nuclear power. In this operation only rod frame 3 was used, and both dynamic control rods were permitted to fly out for a net $\Delta k/k$ decrease of 1.48 percent. The reactor power decrease was concomitant with engine coastdown so that no fuel element temperature exceeded 1800°F during the transient. The minimum safe reactivity change on scram was evidently less than 1.48 percent.

A study of exit-air temperature distribution and of fuel element temperature perturbations due to changes in the control rod pattern was carried out. The location of one of the damaged fuel cartridges was verified by a burst of stack activity when the proximate control rods were withdrawn. All fuel element thermocouples except one were good at the beginning of the reactor operations. During the test, 11 fuel element thermocouples failed by lead wires shorting and 13 failed by open circuit.

3.1.1 PERFORMANCE OF CONTROL ROD AND INSTRUMENT ACTUATORS

The chief difficulties in shim rod operations during IET No. 3 were failure to scram and failure to latch. Generally, latching could be accomplished by the application of additional voltage to the drive motor or by manipulation of the auxiliary scram switch.

During the last portion of the testing a certain amount of instability in cycling of the dynamic rods was observed. This condition was apparently caused by excessive play in the mechanical portion of the feedback system, possibly a result of excessive wear between the piston and spiral rod, which constitutes the primary drive for the control transformer.

3.1.2 INSTRUMENTATION PERFORMANCE

Thermocouples failed at about the rate of one air-discharge and two fuel element thermocouples per day. By the time the CTF was returned to the hot shop, 22 fuel element thermocouples had failed: 9 had shorted, and 13 were open; 12 air-discharge thermocouples had failed: 6 had shorted, and 6 were open. Shorted thermocouple leads were detected by resistance measurements to ground. Resistances were checked whenever a thermocouple reading appeared erratic or very high or low. Because of the limited accuracy of this method, it is possible that thermocouple leads may have shorted close to the thermocouple without detection.

The fission chambers worked very satisfactorily. After the first high-power operation, the photoneutron flux far exceeded the source flux. Therefore a movable source is not needed for any but the first of a series of high-power operations. A great deal of difficulty was experienced during low-power operation because of noise in the log-flux ion chambers. The linear flux channels had to be reworked since the three channel readings differed greatly and the highest reading was only half of what it should have been. Installation of cathode followers made possible adjusting all three channels to the same proper reading. Thereafter the channels worked satisfactorily.

The servo system presented the primary instrumentation difficulty during IET operations. Numerous scrams and delays were caused by instability in the servo system. Part of the difficulty was determined to be oscillations in one of the dynamic actuators, but the elimination of the faulty actuator did not appreciably help the situation. Without the rod oscillations, it appeared that the servo would control the reactor within ± 3 percent. Under these conditions, plate temperature oscillated through a range of ± 50°F.

3.1.3 ENGINE OPERATION

Cold-flow data and partial-reactor-power tests were performed on the average of 3 days per week. The engine and air turbine starter operating times are given in Table 3.3. The bypass-loop operating time was the total operating time less the common loop time.

The engine was normally operated either in manual control or semiautomatic control. The semiautomatic control consisted of manual speed control to maintain full-open jet nozzle and automatic temperature control. The augmenters were blocked shut at all times; this arrangement, with full-open jet nozzle, gave the coolest operating conditions. The

TABLE 3.3

OPERATING TIMES FOR ENGINE AND AIR TURBINE STARTER

	Time, hr:min		
	Total	Military	Over 1300°F T_4
Engine No. 5009 (No. 1 left)			
Total operating time	21:24	0:21	0:35
Common loop time	17:35	0:21	0:35
Engine No. 5010 (No. 2 right)			
Total operating time	56:53	1:04	1:09
Common loop time	51:09	0:56	1:09

Air Turbine Starter on No. 5009 (Hamilton Standard 1887)	Number of Operations	Motoring Time, sec
Motoring	0	--
Pre-starts	10	500
False starts	5	620
Starts	6	1117
Air Turbine Starter on No. 5010 (Hamilton Standard 1531)		
Motoring	4	690
Pre-starts	8	490
False starts	3	240
Starts	17	3065

engine was manually recovered with chemical-fuel flows as low as 400 pounds per hour. The maximum loss of engine speed was 500 rpm during recovery.

While in automatic control, the engine decelerated 300 rpm when the reactor scrammed from 50 percent nuclear power, and 350 rpm from 70 percent nuclear power. Automatic recovery from higher percentages of nuclear power was not attempted. The engine would normally accelerate 150 to 200 rpm when the reactor power was increased 2 megawatts.

The engine was successfully relit on chemical fuel. During the relight, the initial fuel flow was 500 pounds per hour, which accelerated the engine from 6900 rpm to 7500 rpm. The turbine inlet temperature increased from 1200° to 1380°F. The reactor power was then decreased slowly while chemical-fuel flow was increased to maintain engine speed.

3.2 GROSS THERMODYNAMIC PERFORMANCE

3.2.1 GROSS CYCLE PERFORMANCE

Figure 3.1 is a diagram of the significant airflow stations. Subscripts to parameters presented here refer to these station numbers. Figure 3.2 presents the average eighteenth-stage fuel element temperatures as a function of engine speed for the three runs in which transfer to full nuclear power was achieved. The predicted relationship is also presented. The comparison is not exactly on an equal basis since the predicted value is for a true average. The measured values are an arithmetic average of eighteenth-stage thermocouple readings that were available for each of the runs. These thermocouples were located in hotter-than-average positions; hence a true measured average temperature would fall somewhat lower. The significant point here was the increase in plate temperatures as oper-

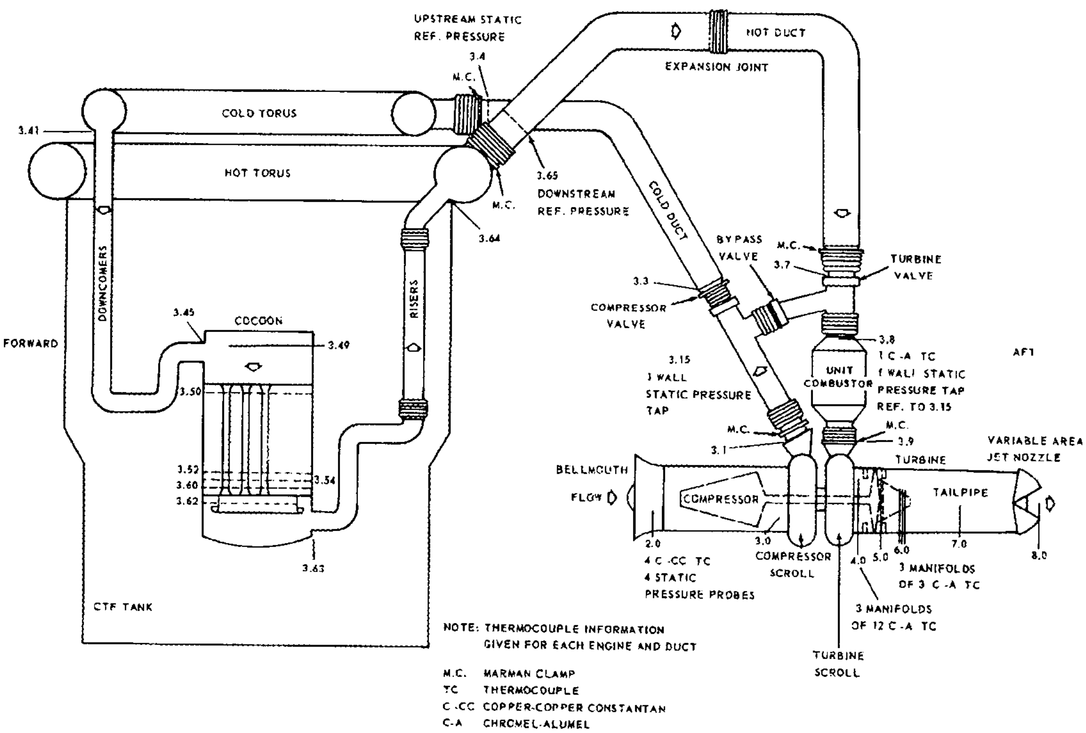

Fig. 3.1 – D101A instrumentation and station designations

ation progressed. Measurements (not shown here) at partial nuclear power indicate that plate temperature before run 21 would have been possibly 70°F lower. The fact that average temperatures in run 42 fell below those for run 34 is probably explained by the loss of several hotter-than-average plate thermocouples during the period between run 34 and run 42; hence readings from these thermocouples could not be included in the average for run 42.

Figure 3.3 presents the average reactor air-discharge temperature as a function of engine speed. Also shown on the curve is the predicted air temperature. The temperature is the arithmetic average of the individual thermocouple readings from each fuel tube exit. As in Figure 3.2, this curve also shows a trend toward increasing temperature as testing operations progressed. In this instance, however, temperatures for run 42 fall higher on the graph than those for run 34.

Figure 3.4 presents the airflow versus engine speed at both 0 percent and 100 percent nuclear power. There is no apparent reason why data from run 34 fell approximately 1-1/2 pounds per second higher than data from the other runs. Normal expectations were that the weight flow at constant speed would decrease in the presence of the higher system pressure drop associated with 100 percent nuclear power. Hence, it is reasonable to assume that the data from run 34 are not correct.

Figure 3.5 presents the pressure drop from the cold torus inlet to the hot torus outlet, i.e., the pressure drop through the reactor as a function of engine speed. The pressure drop was measured as a static difference and was corrected to a total pressure drop by the measured weight flow and the station areas and temperatures. An increase of approximately 3 percent in pressure loss during operation seemed reasonable and probable. This estimate was based on observation of the damage to the reactor after disassembly.

Figure 3.6 presents the pressure drop from the compressor scroll exit to the chemical combustor inlet as a function of engine speed for both 0 percent and 100 percent nuclear power. This curve shows an increased pressure drop of approximately 10 percent as oper-

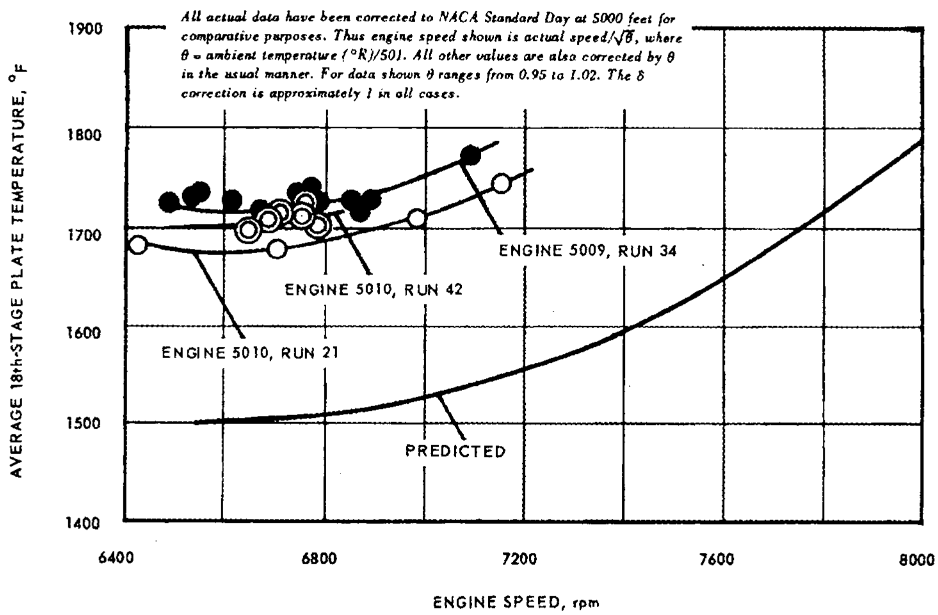

Fig. 3.2 – Average 18th-stage plate temperature versus engine speed

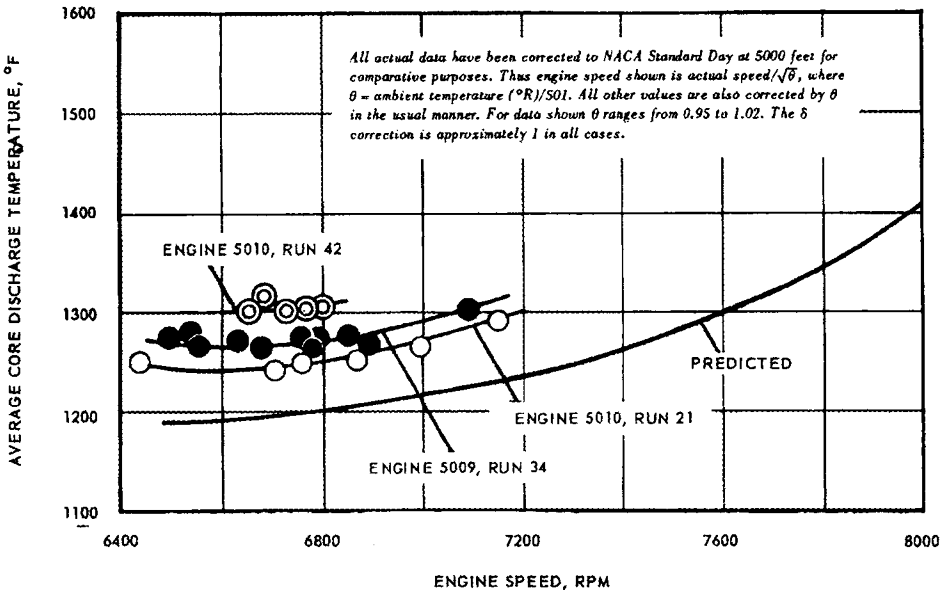

Fig. 3.3 – Average core-discharge temperature versus engine speed

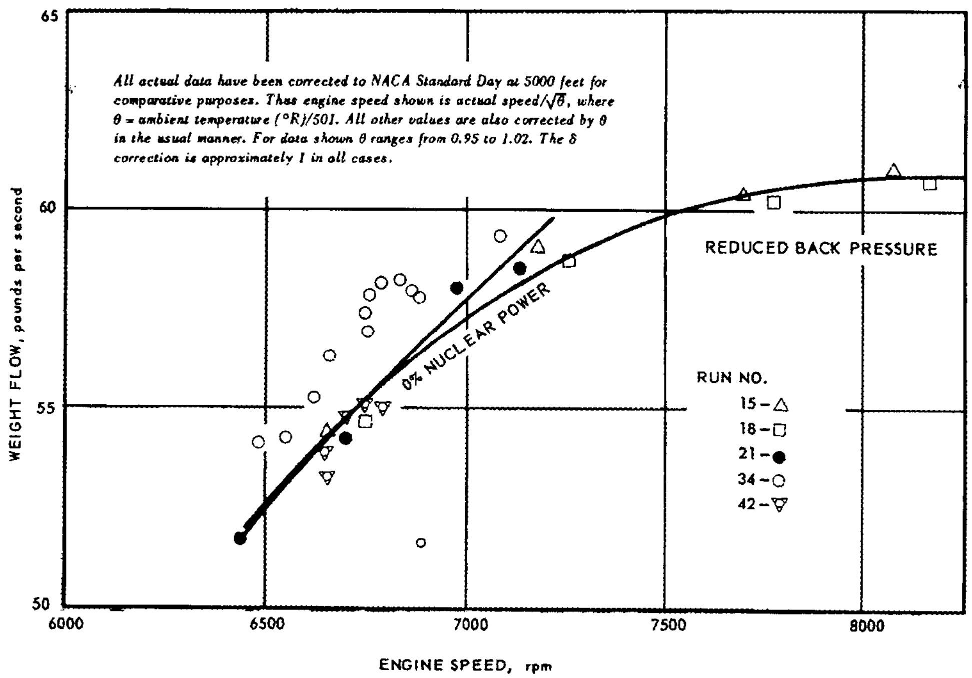

Fig. 3.4 – Weight flow versus engine speed

UNCLASSIFIED

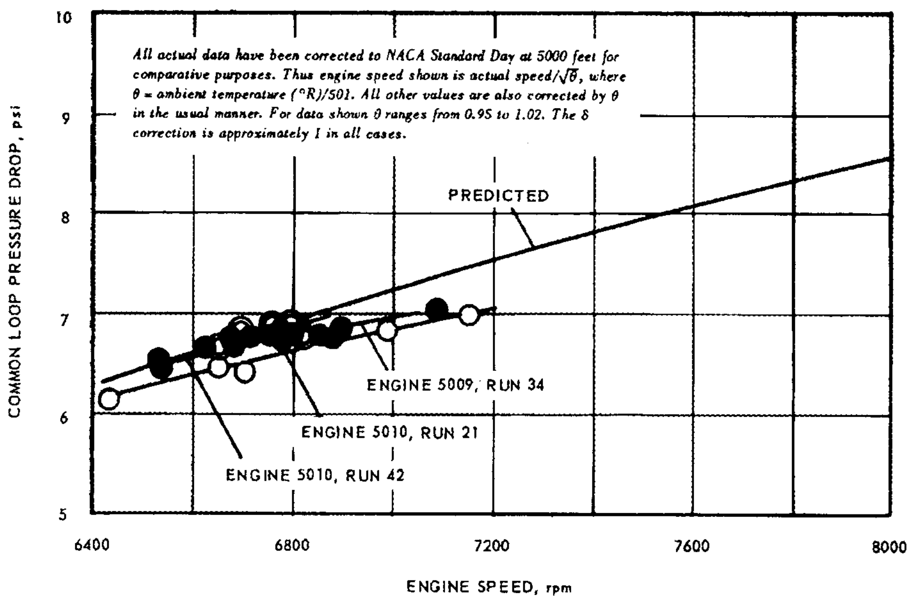

Fig. 3.5 – Common loop pressure drop (station 3.4 – 3.65) versus engine speed

ation progressed, whereas Figure 3.5 showed only a 3 percent increase. This difference is difficult to explain since there was no known damage to the ducting external to the tori.

Figure 3.7 presents the turbine inlet temperature as a function of engine speed for both 0 percent and 100 percent nuclear power. These temperatures are the arithmetic average of the measurements of 9 thermocouples placed at the inlet of the turbine nozzle. These temperatures also show an increase in turbine temperature required for the cycle to operate as reactor operation progressed. Scatter in the turbine temperatures at 100 percent nuclear power is unexplained. Many of these data were obtained when the inlet temperature to the engine compressor was varying because of wind eddies inside the test building. It is possible that the recorded turbine temperature did not correspond to the recorded inlet temperature.

Figures 3.8 and 3.9 are plots of system temperatures over the range of operation from no nuclear power up to and including initial full nuclear operation. For most of the data shown, θ ranged from 0.95 to 0.96. These power traverses were made by increasing reactor power while decreasing chemical fuel in order to hold a constant engine speed. In initial operation, chemical-fuel flow rate was not taken below 300 pounds per hour. Therefore, the transfer from partial chemical to full nuclear power involved a discontinuity in speed. Transfer was effected by operating at an engine speed higher than desired for full nuclear operation. When the final increment of chemical fuel was cut out the engine coasted down to the desired speed at full nuclear operation. Pretransfer tests consisted of traverses at constant speed to permit estimates of desired transfer points by extrapolation. In this work, traverses both at and below the designated speed after transfer were obtained. After transfer the engine was accelerated and decelerated over an 800-rpm range by variation of nuclear power using a single shim rod for reactor control.

Figure 3.10 shows the functional relationship between the required turbine inlet temperature and the system pressure drop from the compressor to the inlet of the chemical combustor, presented as lines of constant speed. The figure indicates the engine characteristics when the pressure drop in the system was artificially varied. The dotted constant-speed lines are the predicted relationships. The solid S-shaped curves are the measured engine characteristics at partial nuclear power. Superimposed on these two sets of curves are two

UNCLASSIFIED

mating lines, the actual measured line and the predicted line. The mating line is the functional relationship between the turbine temperature required to operate the cycle and the pressure drop of the reactor, when it was operating, to deliver the required temperature.

The preceding paragraphs have indicated significant deviations between predictions and observations. In cases of high deviation, the actual system performance was compared to over-all system performance predictions to illustrate both over-all system behavior and the apparent results of reactor damage. (For over-all system predictions it was necessary to specify only engine speed, nozzle position, and ambient conditions.) Such results may be subject to misinterpretation since a discrepancy in fuel element temperature could, for example, reflect excessive ducting pressure loss rather than inaccuracy in element temperature. Because of such ambiguities, the performance of individual system components were examined whenever possible. Table 3.4 illustrates a typical comparison of observed and predicted data for operation on full nuclear power.

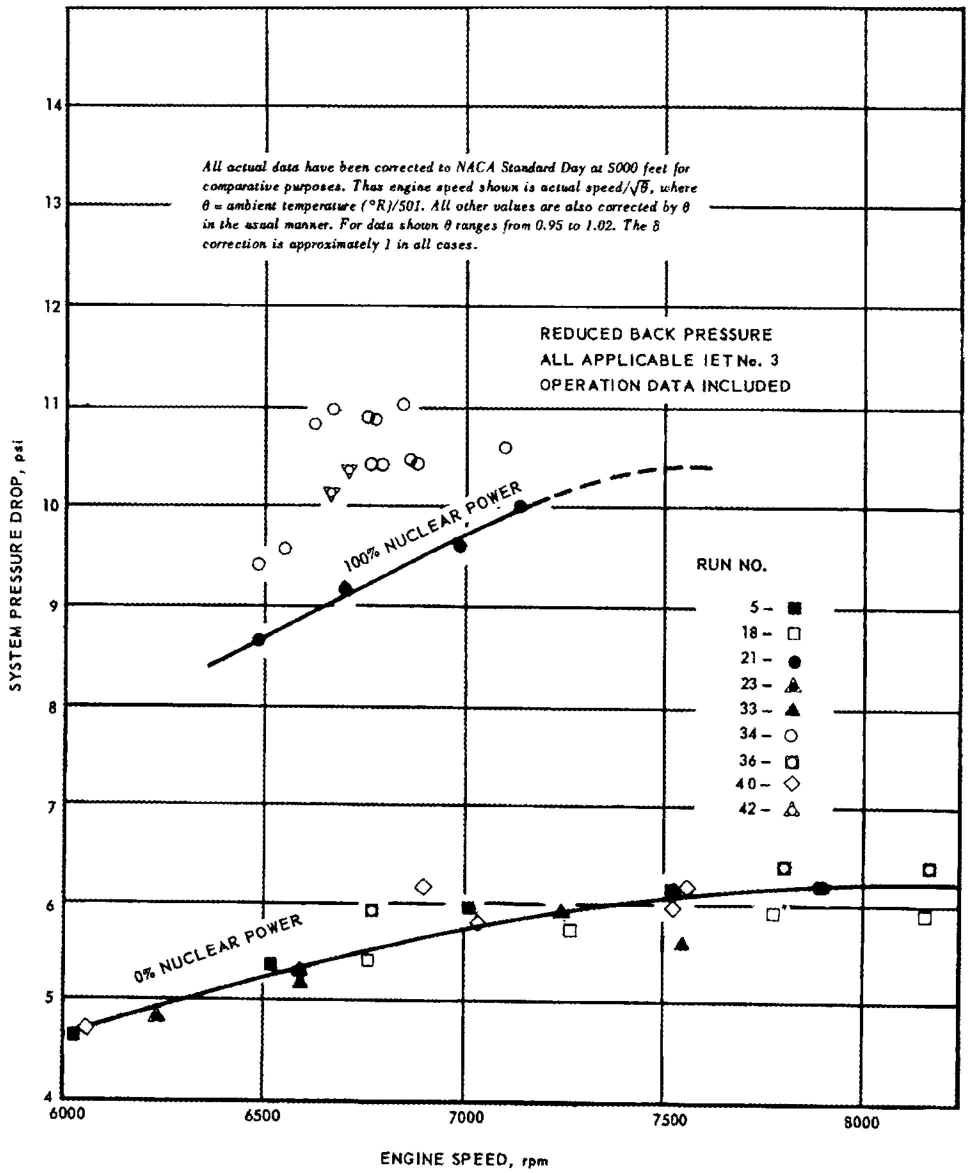

Fig. 3.6 – System pressure drop versus engine speed

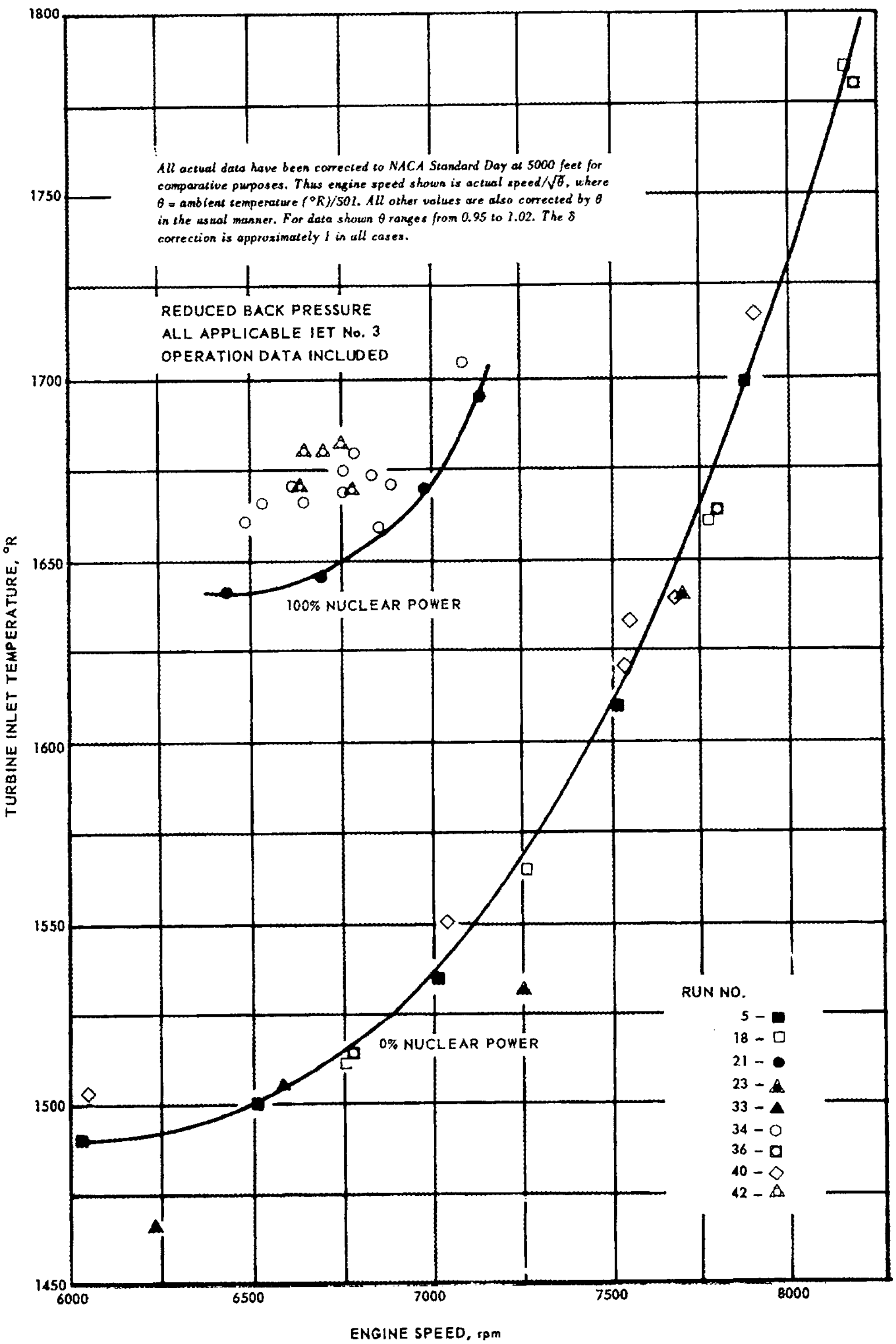

Fig. 3.7 – Turbine inlet temperature versus engine speed

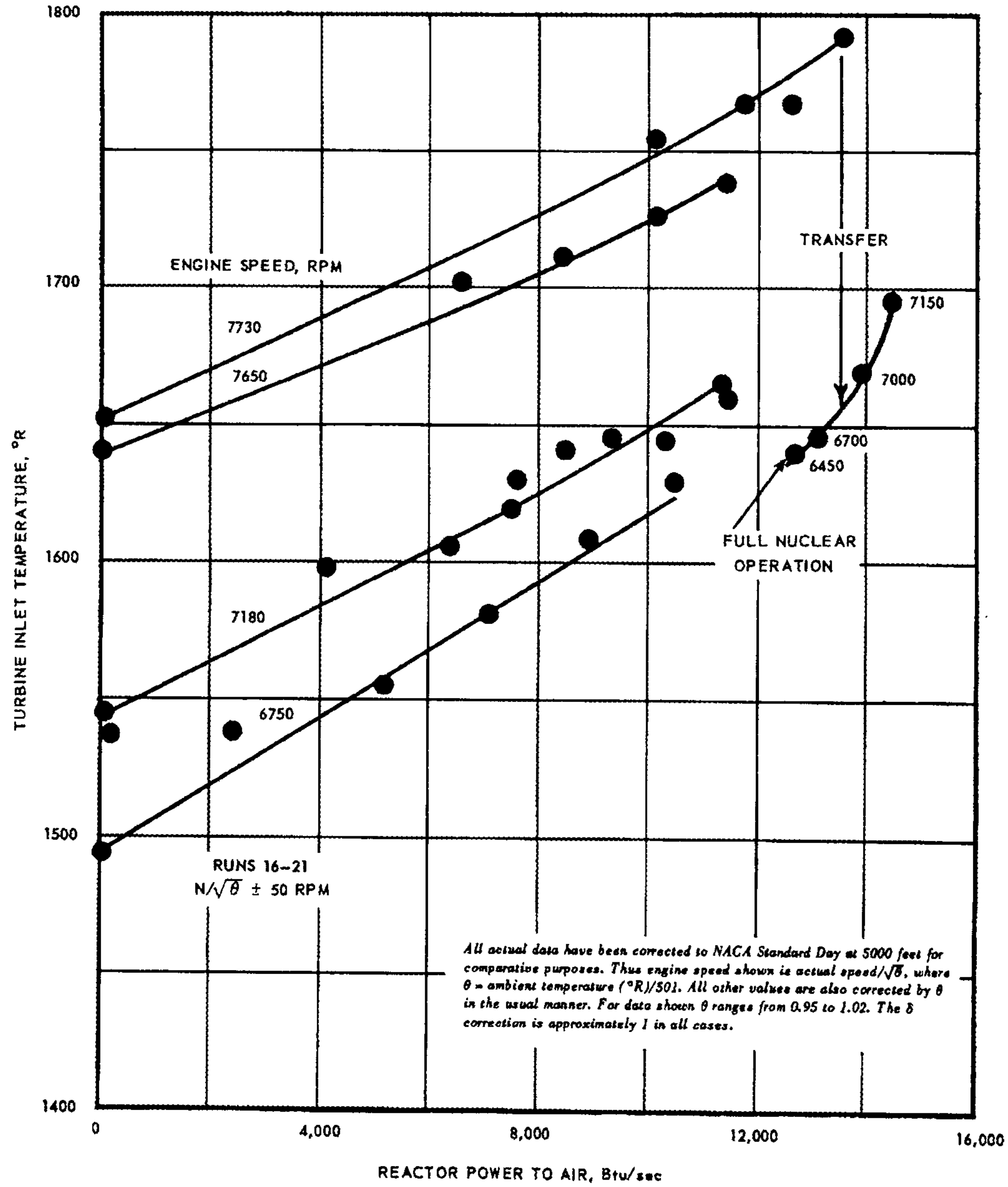

Fig. 3.8 – Summary of partial power runs leading to initial runs on full nuclear power

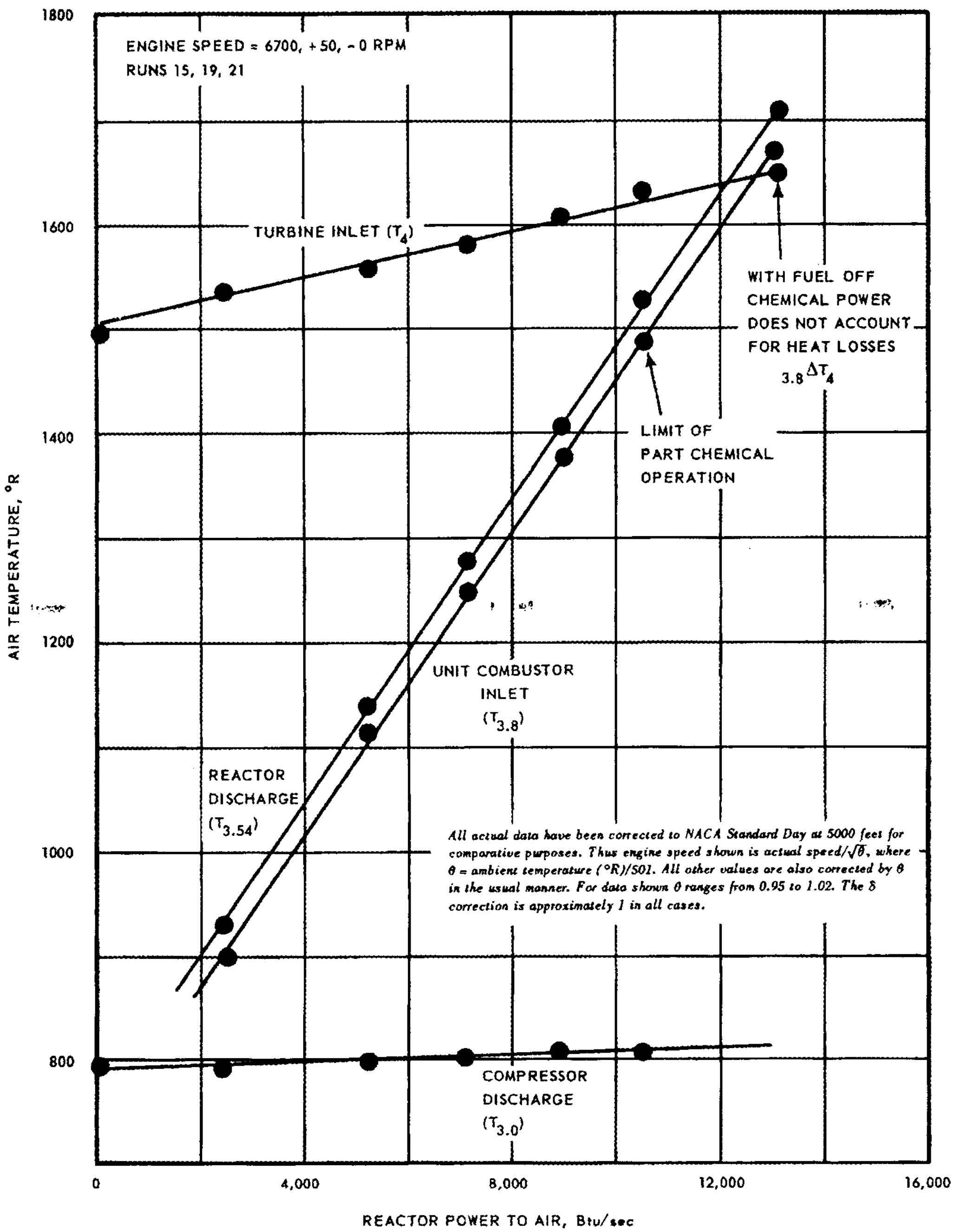

Fig. 3.9 – Typical plot of system air temperature at constant speed with varying reactor speed

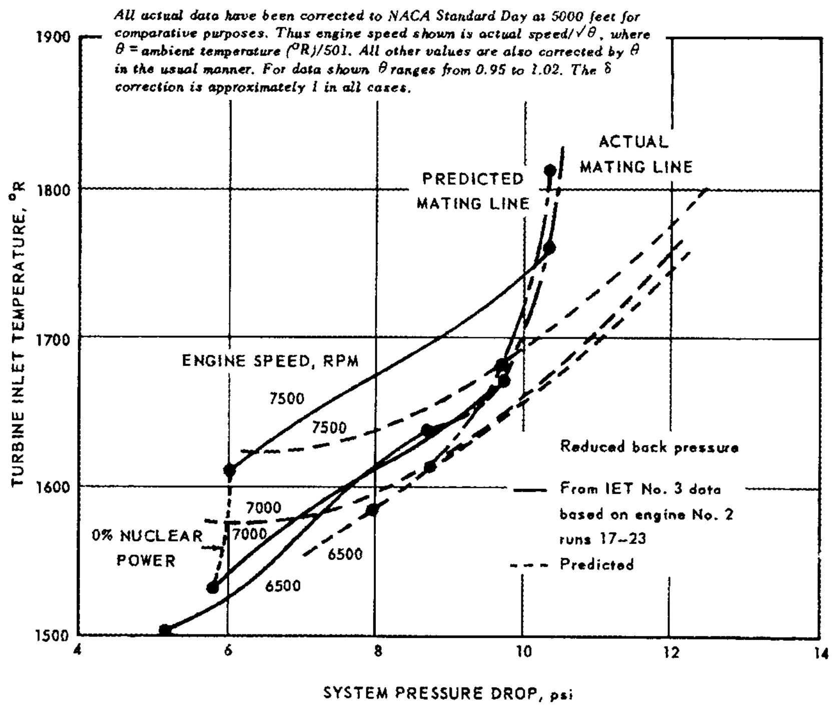

Fig. 3.10 – Turbine inlet temperature versus system pressure drop

TABLE 3.4

OBSERVED AND PREDICTED DATA FOR IET NO. 3 OPERATION ON FULL NUCLEAR POWER

Case No.	Data	Nozzle	Back Pressure	Speed, rpm	Power to Air, mw	$T_{3.54}$, °F	T_4, °F	T_{FE}, °F	$_{3.1}\Delta P_{3.8}$, psi	θ at 5000 ft
1	Predicted	Open	Reduced	7145	13.1	1231	1173	1535	9.1	1
2	Observed	Open	Reduced	7000	15.25	1226	1166	1655	10.15	0.96
3	Observed[a]	Open	Reduced	(7145)	(15.22)	(1297)	(1235)	(1735)	(9.97)	1
4	Predicted	Open	Ambient	7145	14.7	1320	1253	1665	9.3	1

[a]Figures in parentheses are observed data corrected to NACA Standard Day for comparison.

Significant inconsistencies between over-all predictions and observations may be seen in Table 3.4, for example in the fuel element temperatures (T_{FE}) for groups 1 and 3. However, the internal consistency of power and temperatures was considerably better than indicated by the comparison of temperatures alone. For example, although comparison of T_{FE} indicated a 200°F disparity, 110°F or more of this disparity was accounted for by the disparity in power and air temperatures.

Comparison group 4 is included to illustrate that the over-all system ran closer to performance predictions for ambient back pressure than for reduced back pressure. No data were available to substantiate the predicted engine performance at the IET under reduced back pressure for the nuclear operating range. Because of a difference in duct leakage, test pad operation with reduced back pressure may not have simulated reduced back pressure at the IET. Thus it is possible that the disparities noted in over-all predictions primarily reflected engine or ducting performance deviations. Because of this possibility and the general problem of instrument reliability, no further evaluation of the over-all D101A2 system was attempted. Instead, component performances were investigated in detail.

3.2.2 LOW-POWER TESTING

Tests With No Airflow

The reactor was made critical with system ducting valves closed, and the power was gradually increased to determine a reasonable power at which operation in the absence of air cooling could be maintained. Maximum reactor power reached was 5 kilowatts. At this point, transient fuel element temperatures and approximate steady-state element temperature profiles were recorded. Typical temperature profiles and transient data are shown in Figures 3.11 and 3.12. Throughout the tests, the moderator temperature was 95°F and the reactor air discharge thermocouples remained constant at or near 100°F.

Figure 3.11, a plot of a fuel ring temperature versus time, illustrates essentially expected behavior and confirms the calculated thermal capacity of the element system. For

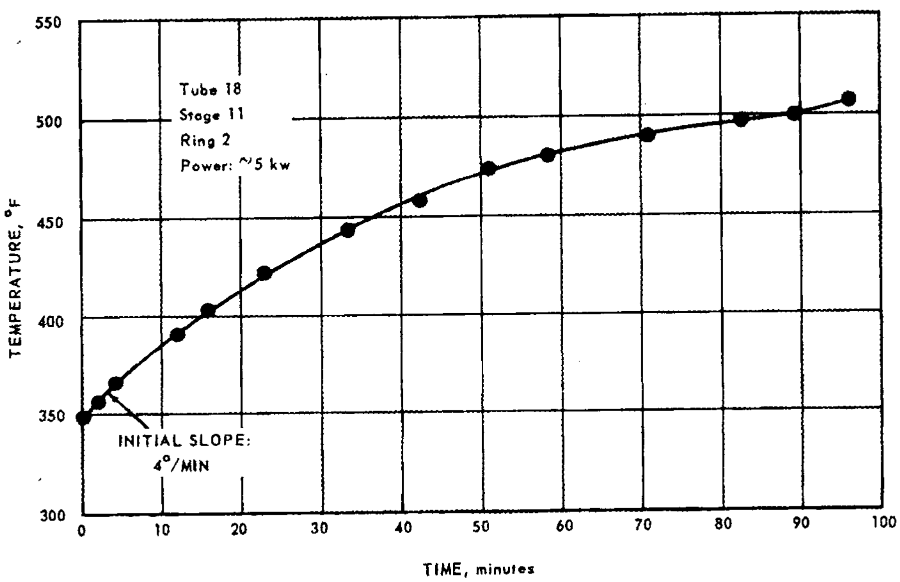

Fig. 3.11 – Fuel elements temperature versus time in the absence of air cooling

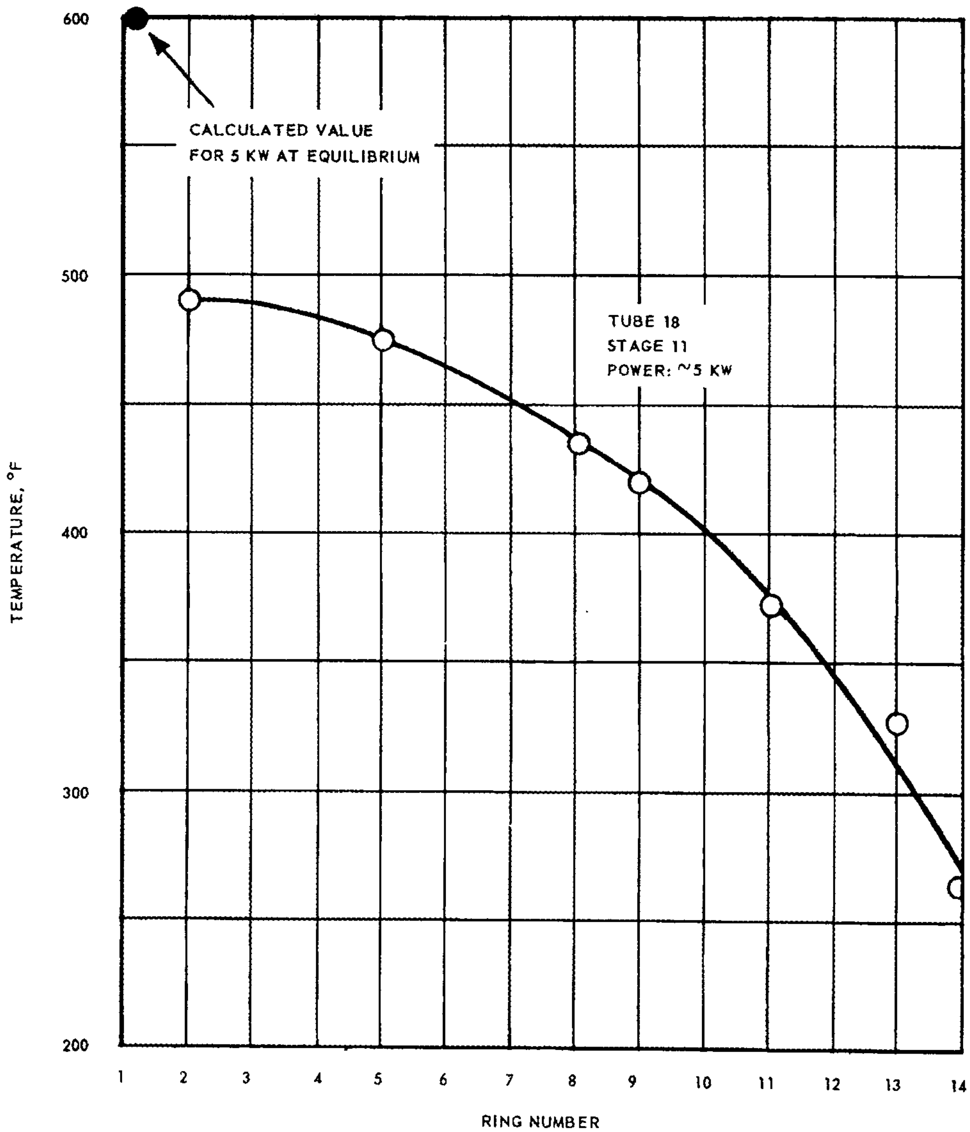

Fig. 3.12 – Plot of fuel element ring temperatures near equilibrium in the absence of air cooling

example, with the calculated thermal capacity of the fuel elements at 85 Btu per ^{o}F, the average rate of change of fuel element temperature was:

$$dT/d\theta = 2/3 \ P^{o}F/min$$

where P = power of fuel elements in kilowatts.

The relative power at stage 11 was 1.2 times the average, so that $dT/d\theta$ at stage 11 was:

$$(dT/d\theta)_{11} = 0.8 \ P^{o}F/min$$

The 4^{o}-per-minute slope observed in the beginning of the 5-kilowatt power run was thus in excellent agreement. As the fuel element heated, an increasing amount of the generated power was lost through the insulation liner. This was reflected as a decrease in $dT/d\theta$ with increase of element temperature until equilibrium was obtained.

Figure 3.12 illustrates the fuel-element-ring temperature profile near equilibrium, together with a predicted maximum temperature for 5-kilowatt power. It was assumed in the analysis that free convection currents were negligible and that heat transfer occurred by radiation from fuel element ring to ring and then by conduction through insulation to the moderator. Data from Figure 3.12 confirm this postulate since any free convection would have almost completely flattened the ring temperature profile.

Tests With Airflow Supplied By Blowers

The reactor was made critical with various combinations of high- and low-speed blowers operating. Power was gradually increased in order to determine a reasonable power limitation for a particular blower or combination of blowers.

Blower airflow rates were determined by monitoring blower motor power and comparing it to a previous calibration of blower power versus head and flow rate. Reactor-inlet-face air temperature was determined by observing fuel element and discharge air temperature while the reactor was operating at essentially zero power. Total power to air was calculated by heat balance. For low-speed blower operation, no measurement of airflow was available. In these cases, reactor power was determined from nuclear flux instrumentation calibrated in terms of heat balances obtained in tests with measured airflow, and therefore airflow rather than power was defined by heat balance.

A summary of averaged maximum fuel element and discharge-air temperatures, together with airflow rates and reactor powers obtained in operation, is shown in Figure 3.13.

Considerable credence was lent to the consistency of high-speed blower data since in one series of tests reactor power was held constant with both one and two blowers in operation. The heat balance in each case yielded the same reactor power.

One of the aims of this test series was to provide information regarding possible induced flow maldistributions at low flow rates. If the heat generation was not uniform in all tubes, a tube having a high ratio of power to flow tended to overheat. As this occurred, the particular tube tended to have a higher pressure loss than its neighbors. Since the overall system tended towards constant pressure loss in each tube, the overheated tube starved itself for flow to reduce its pressure loss. This in turn caused further overheating and required further flow starvation for balance. In single-phase systems in turbulent flow, a condition of equilibrium is achieved. However, in laminar flow systems the starvation effect may be continuous, leading to essentially complete loss of flow and burnout of a particular tube. In laminar flow, the starvation tendency is increased by increase of friction factor with both temperature increase and flow decrease. Maldistribution also increases with increase of temperature rise ratio of the coolant. The observed variation of individual fuel tubes indicated that net maldistribution effects accounted for mean variations of temperature rise of the order of ± 5 percent with extremes of 10 to 15 percent, with no indication of a continuous or nonequilibrium effect. Some tendency towards decrease of range of observed maldistribution with increase of flow rate was expected and noted. In design estimates, maximum maldistributions of the order of 20 percent were considered. It was not thought that maldistributions would be continuous since, among other reasons, the change of friction factor with Reynolds number for fuel elements is much more gradual than in simple pipe systems.

The amount of air delivered by the blowers was in good agreement with predictions at low heat-input rates. At higher temperature levels, the observed flow was higher than predicted. One possible reason for this is that, in calculations, a considerable portion of the system resistance was assumed to exist between the reactor discharge face and stack exhaust. In operation, reactor discharge air was cooled significantly by evapora-

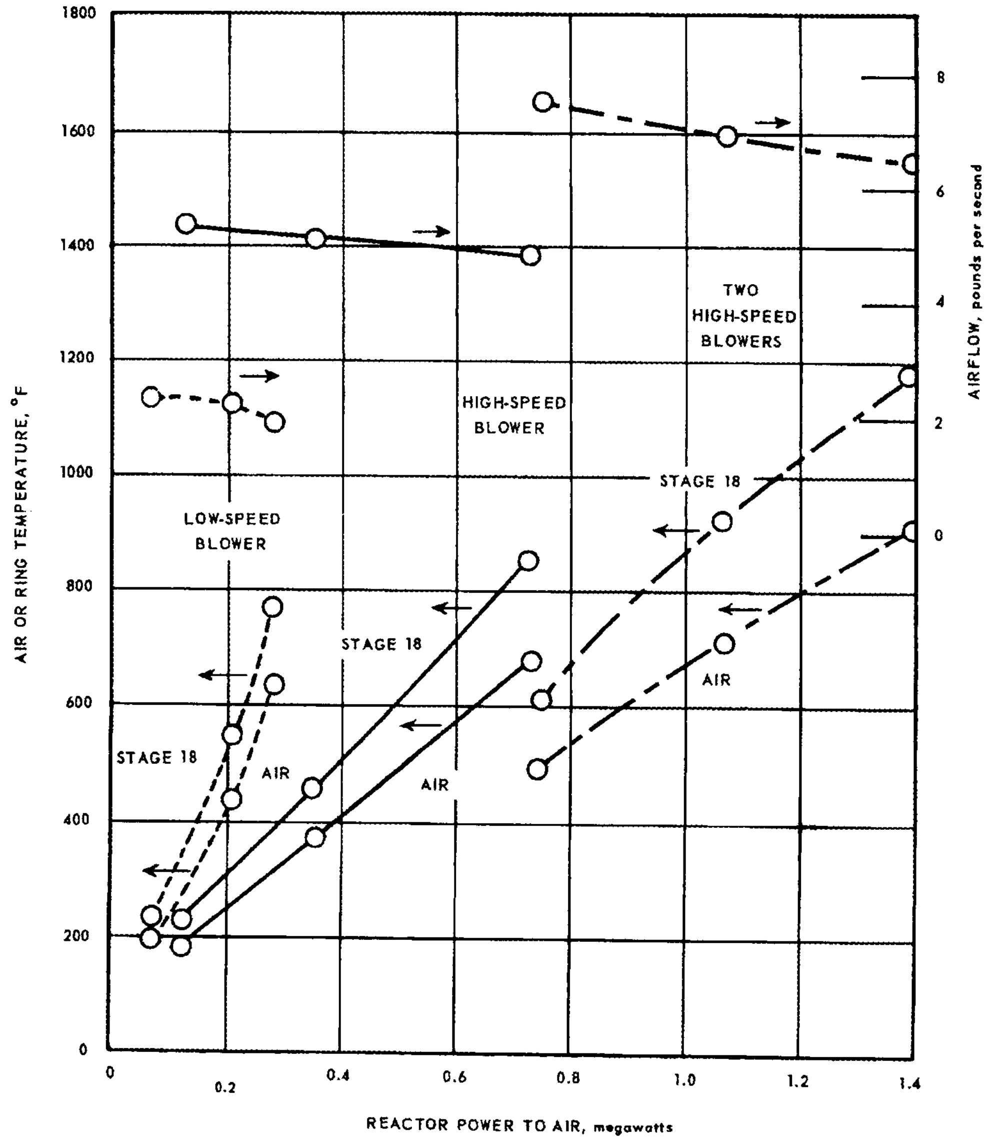

Fig. 3.13 – Summary of power operation of D101A2 core with blower air

tion of water leaking from the shield into the cocoon. This effect would cause a significant lowering of system resistance and result in increased blower flow.

Because of potential value to future systems, an attempt was made to correlate heat transfer data for the low-Reynolds-number range of tests. Heat transfer coefficients were calculated using average values for eighteenth-stage and discharge-air temperatures and for heat generation rates for the trailing edge of the eighteenth stage. The results of this work and a comparison with design estimates are shown in Figure 3.14.

Since these data are for low Reynolds numbers, it could be expected that the coefficient would vary with the length-to-diameter ratio, L/D. (The length is expressed in passage diameters between entrance and point of measurement.) If the heat transfer coefficient were independent of interelement gaps, the value of L/D for the data shown would be approximately 150; if each stage behaved as an individual section, the L/D would be approximately 10.

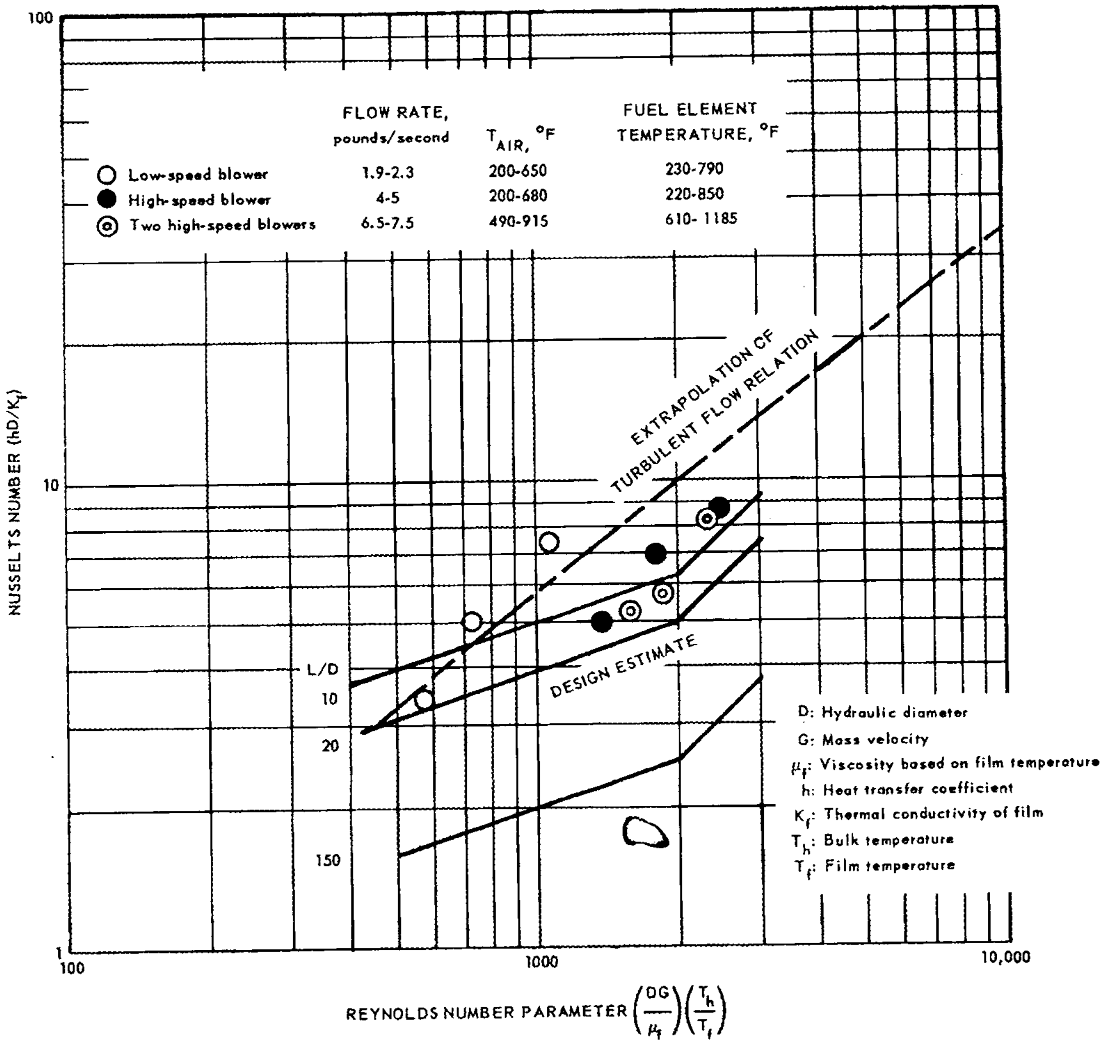

Fig. 3.14 – Low-Reynolds-number heat transfer data for stage 18

These ranges of variation are also included in Figure 3.14. Apparently the data follow the trend of prediction very well and lie close to the lower L/D approximation.

3.2.3 SYSTEM PRESSURE LOSSES

System pressure losses were recorded throughout all runs with airflow through the reactor core. In initial operation, essentially all pressure instrumentation in individual fuel tubes was found to be faulty. Hence the only available pressure measurements were from cold torus inlet to hot torus exit and from compressor discharge to unit combustor inlet. At flow rates corresponding to blower capacities, the range of instrumentation precluded data recording. As a result, only data at engine airflow rates are available. Typical data, obtained in various power runs, are shown in Figures 3.15 and 3.16. Since the pressure loss between stations 3.4 and 3.65 was predominately (90%) attributable to the reactor, Figure 3.15 illustrates that the methods of accounting for pressure loss variation with temperature level, heat input, and Reynolds number were reasonably correct. (Note that the calculated values are a constant percentage above observed values.) It is not certain whether the magnitude of deviation reflects instrument error, airflow bypassing or leaking ahead of the core, or anticipated deviation of element friction factors.

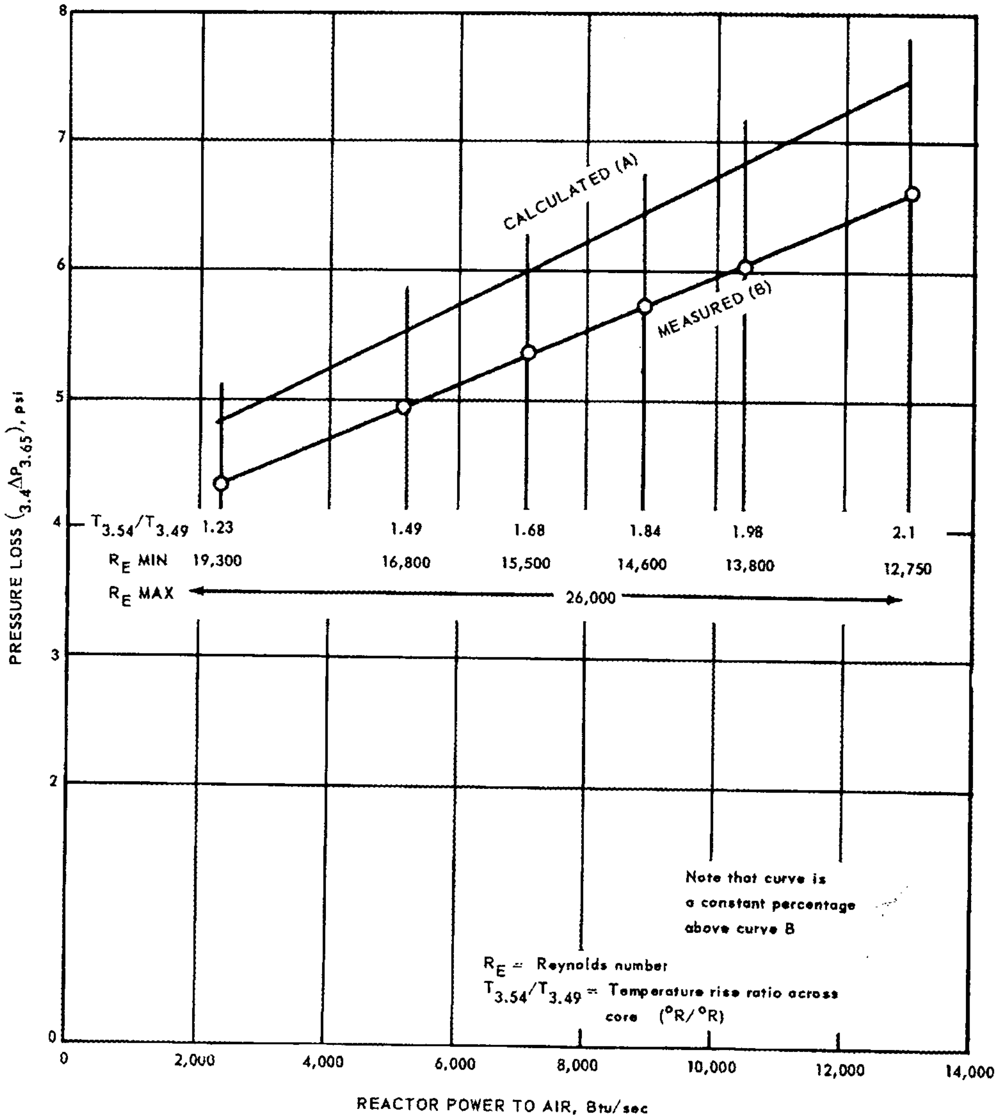

Fig. 3.15 – Typical plot of measured and observed pressure loss from cold to hot torus

Figure 3.16 also indicates good agreement between calculated and observed system pressure loss. However, a significant anomaly exists because of the change in relative position of measured and calculated data. The anomaly is identified in Figure 3.17. Specifically, the individual pressure losses were in reasonably good agreement among themselves. The difference between the two measurements reflects the pressure loss attributable to ducting between compressor and cold torus and between the hot torus and unit combustor. Since this ducting was essentially straight piping, it was unreasonable to expect any large deviation between calculated and observed data. However, the disparity indicated is of the order of 100 percent. Thus it can be assumed that either the magnitude of one or both of the measured pressure losses was in error in Figures 3.15 and 3.16, or that some structural variation existed in the engine ducting; in the latter case it is possible that the valves were not positioned precisely.

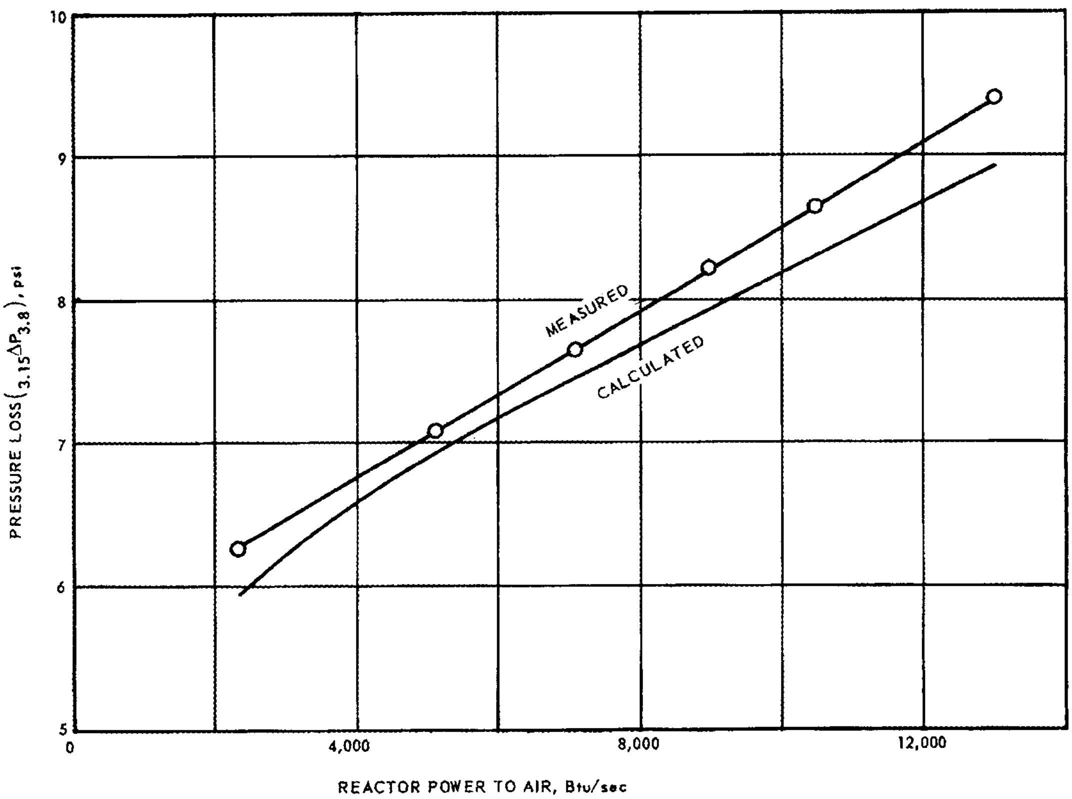

Fig. 3.16 – Typical plot of measured and calculated system pressure loss

3.2.4 SYSTEM HEAT BALANCES

In the course of power runs, various heat balances were made to establish reactor power to air, total reactor power, and system heat losses.

During initial criticality runs, uranium foils were exposed to obtain an absolute calibration of reactor power. At criticality power levels, an amplifier was required to obtain a usable instrument signal.

Measurement of amplifier current was possible up to about 2 megawatts. At powers above 2 megawatts, use of the amplifier was neither possible nor required. The power estimate extrapolated from foil and amplifier current measurements in blower runs was compared with that determined from air heat balances. The comparison showed that the absolute power indication was approximately 120 percent of that determined by heat balance. In engine flow tests the flux meters were set to power values determined by air heat balance.

The reactor power to air was defined by the relation:

$$P = W \int_{T_{3.49}}^{T_{3.54}} C_p \, dT$$

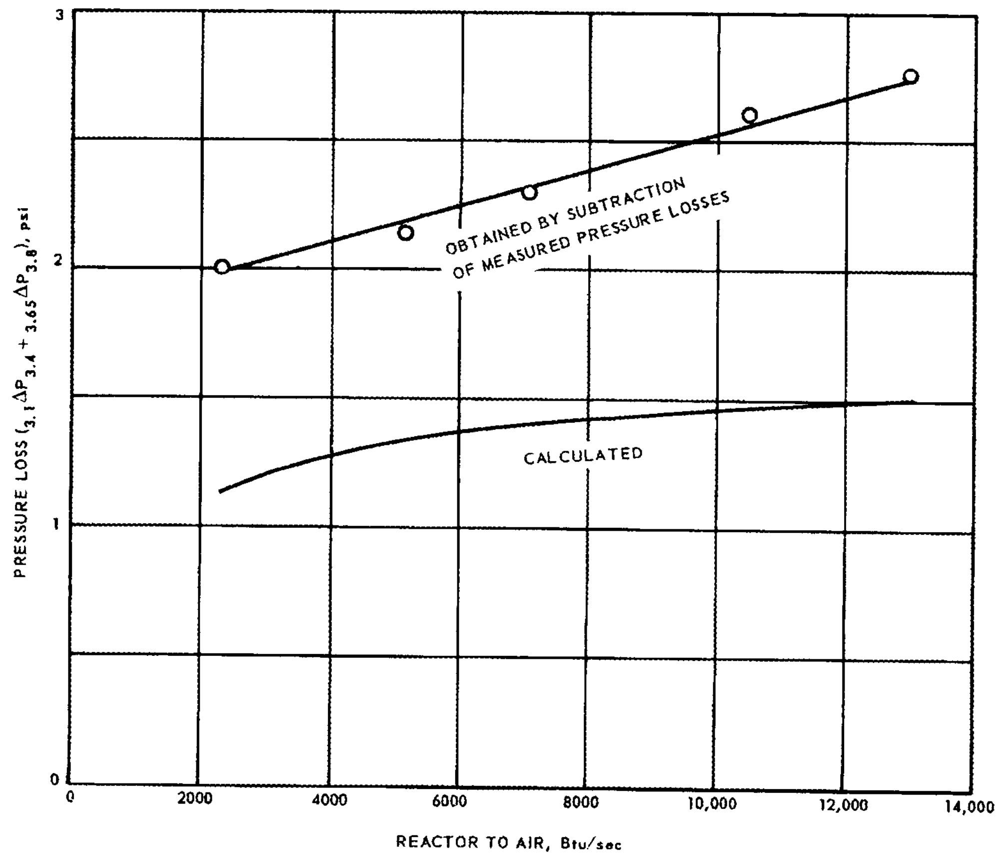

Fig. 3.17 – Comparison plot of engine ducting loss derived from measurements with calculated value illustrating observed disparity

where

C_p = specific heat of air
W = airflow determined from engine bellmouth instrumentation
$T_{3.54}$ = average value of reactor discharge air thermocouples
$T_{3.49}$ = calculated reactor inlet air temperature

Heat dissipation in the moderator system was determined from measurements of moderator flow rate and from temperature measurements at the plug inlet and outlet. The heat thus measured included all heat generated in the active core (except in fuel elements) and in the plug, together with heat loss from air to moderator water in upper plenum, fuel tube, lower plenum, and seal ring space between cocoon wall and core tank.

Shield system heat pickup was measured in a manner similar to that described for the moderator system. In this case, the heat measured reflected the heat generated in shield tank components; heat losses from air through cocoon walls, risers and downcomers; and line-of-sight radiation from tori to the surface of the shield tank water.

Precise measurements of heat loss ($T_{3.0}$ - $T_{3.49}$) could not be determined because of malfunctioning of upper plenum thermocouples. Some estimates were obtained from fuel element and fuel tube discharge air thermocouple readings while the reactor was running without nuclear power. In the absence of actual data, the calculated relation, $T_{3.49} = T_{3.1} - 35°$, was used for reactor power-to-air calculations.

Temperature losses ($T_{3.54}$ - T_4) from reactor discharge to torus exit, combustor inlet, and turbine inlet could be evaluated from the average of reactor discharge air thermocouples and other thermocouples situated on the discharge air ducting. Design calculations were mainly concerned with losses through the system to the turbine for full nuclear operation. Analyses were also limited to this type of loss, although consistency checks for other component losses were made.

Figure 3.18 illustrates the observed and predicted moderator heat load versus power to air for various reactor test points in runs 16 through 21.

The major source of heat in the moderator was generated within the moderator. Heat loss from air was a small, but not invariant, percentage of power to air. The results obtained were in good agreement with predicted values.

Figure 3.19 illustrates the observed shield-system heat load versus calculated components of heat input. For clarity, results are shown only for various powers at a fixed engine speed. The shield-system heat load depended more strongly on temperature level than it did on nuclear power to air. Figure 3.19 shows fair agreement between predicted and experimental results.

Measurements of heat loss from compressor exit to reactor inlet, determined in zero-power runs with reactor core thermocouples, yielded erratic results. About half of the data conformed to the predicted loss of 35°F, and the remainder grouped around a value

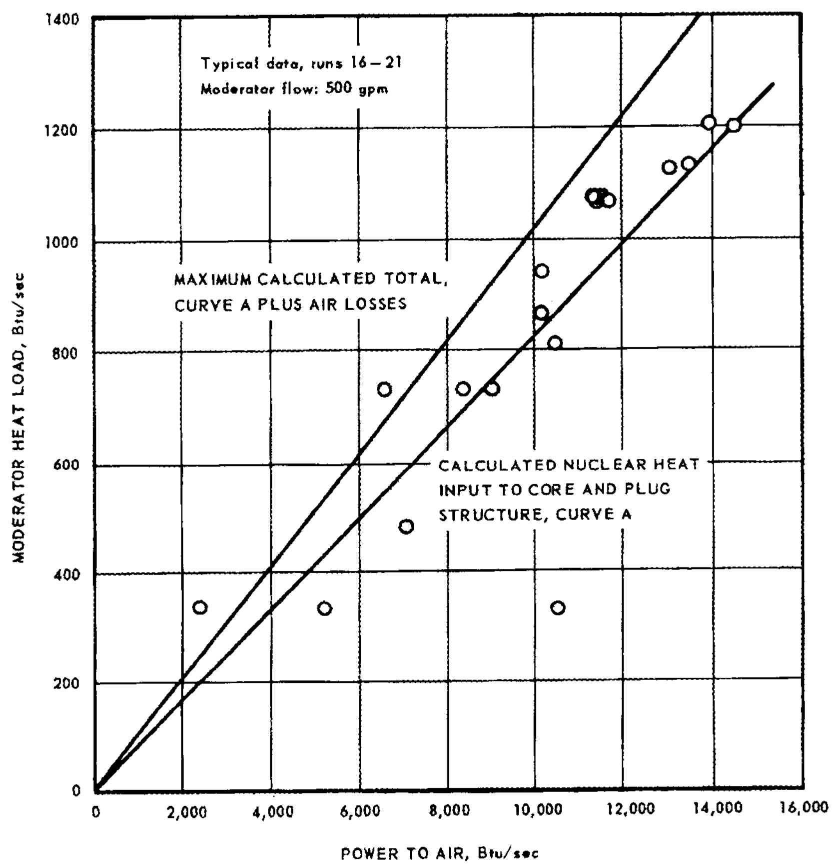

Fig. 3.18 – Comparison of predicted and observed moderator heat load versus reactor power to air

of 60°F. Since most data were obtained under identical conditions, the disparity appeared to lie with instrumentation and/or recorders. The disparity noted could account for significant errors in low-power runs (below 6 megawatts) and errors of 3 to 5 percent in power determinations for most other runs.

Figure 3.20 illustrates the calculated and observed heat losses for various full-nuclear-power runs. In general, the calculated heat losses somewhat overpredicted the actual heat losses, as was anticipated.

Power to Air

The measurements of power to air used throughout this work are based on the relation:

$$P = W \int_{T_{3.49}}^{T_{3.54}} C_p dT$$

Possible errors inherent in core inlet ($T_{3.49}$) and core exit ($T_{3.54}$) temperatures have already been considered. Several cross-check methods were tried in order to validate the averaged value of $T_{3.54}$. Hot-ducting heat losses between various measuring stations were evaluated to determine whether any illogical trend in $T_{3.54}$ was apparent. No such trend was noted; hence the averaged value of $T_{3.54}$ was used uncorrected in all calculations.

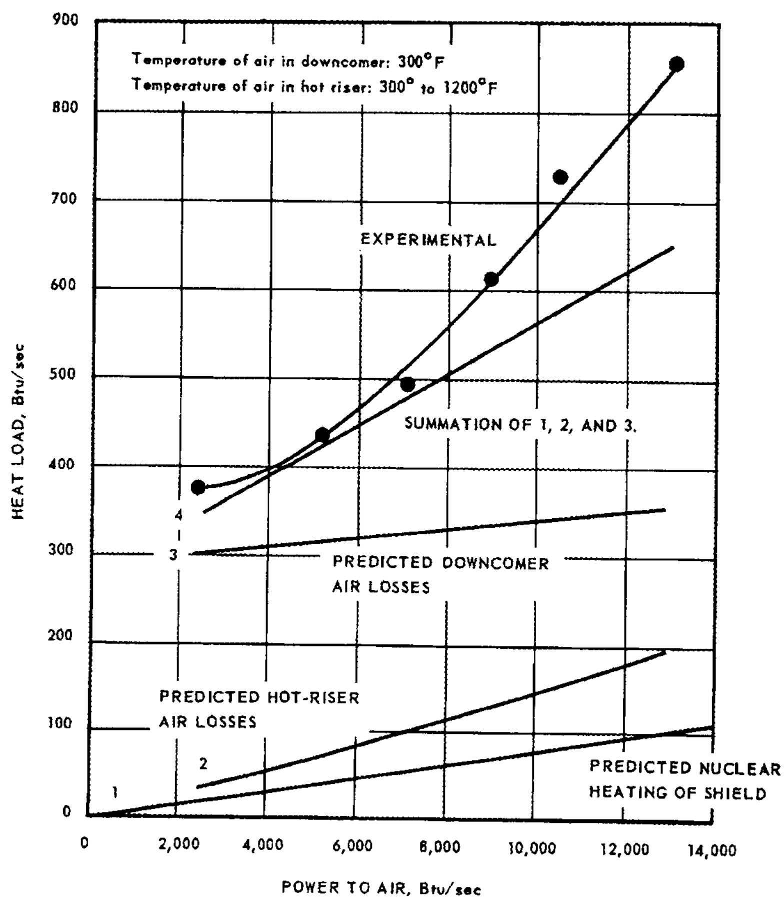

Fig. 3.19 – Typical shield circuit heat balance

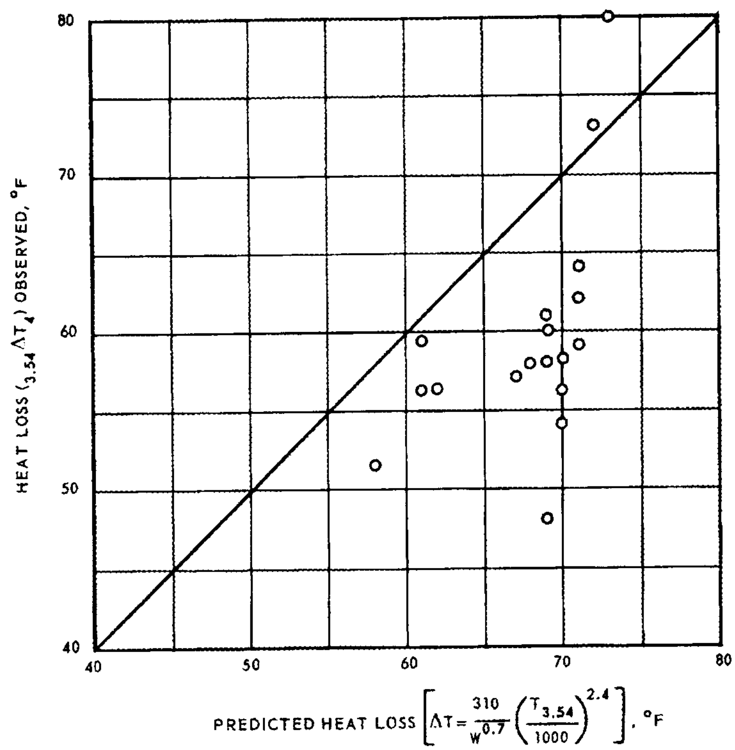

Fig. 3.20 – Comparison of observed and predicted temperature loss from reactor exit to turbine inlet

Similar cross-checks on airflow were made by comparing bellmouth weight flow to that predicted for the engine system and by heat balances across the unit combustor during partial-chemical-power runs. No gross disparity was noted, although weight flow predicted from engine speed was generally about 3 percent less than that calculated by bellmouth instrumentation.

The possibility of air leakage out of the system or bypassing the core was a significant problem. Continuous checks of system behavior through run 34 showed no variation that would indicate a change in either form of leakage. However, it was not possible to determine the extent, if any, of such leakage during initial operation of the system. Cold-flow tests indicated the possibility of approximately 3 percent leakage past the seal. This correction was not applied to power calculations.

Although the possible errors in flow rate and temperature could result in considerable uncertainty (±10%) in the stated power to air, it is not thought that any such deviation actually exited. This assumption appeared reasonable in terms of the aforementioned cross-checks and the data presented in Figures 3.8, 3.9, and 3.21. These data reflect a large range of flows, temperatures, ambient conditions, and core pressure losses, all of which could affect the power calculation. Since these data are generally without discontinuity, it appears that the actual power is closely represented by the calculated value. Accuracy of power calculations was further evidenced by the transfer operation. Because of the speed discontinuity, both airflow and temperature level changed during transfer. Power calculations before and after transfer showed a maximum variation of approximately 3 percent.

In addition to illustrating consistency of data, Figure 3.21 confirms the design postulate regarding variation of reactor power with ambient conditions. Specifically, design estimates indicated that the power required for nuclear operation was independent of ambient conditions and a function of actual speed only. This postulate is confirmed by data on Figure 3.21. It was recognized, however, that a combination of low engine speed and low ambient temperature required slightly decreased power.

3.2.5 TEMPERATURE DISTRIBUTION IN THE REACTOR

Run 21 of IET No. 3 was the first operation on 100 percent nuclear power. No fission product activity was noted during this run. Table 3.5 presents the temperature distribution obtained in the reactor during run 21. The actual temperatures are presented in the first and third columns for the eighteenth-stage plate temperatures and the air discharge temperatures, respectively. Also presented are the deviations of each air temperature from the average temperature expressed as a percentage of the average temperature rise across the reactor. This number is proportional to the relative power in the tube when equal airflow in all tubes is assumed. In all cases where values are missing from the table, the absence is due to instrumentation failure. As the table indicates, correlations between the plate temperatures and the air temperatures were not good in many cases. The scatter was apparently large and was possibly due to the locations of the thermocouples. Two possible conclusions may be drawn: (1) there was no apparent gross change from flat power across the reactor, and (2) the temperature spread (maximum to minimum) appeared to be larger than was anticipated in the design stages of the reactor.

Figure 3.22 is a diagram of the top view of the reactor and shows the detailed rod positions for run 21. The numbers in the small circles (rod locations) indicate the number of inches that the rod was withdrawn from the reactor. The completely withdrawn position is 30 inches. An x in some of the small circles denotes that the rod was fully inserted. Rod position 40 is the position of the source rod, which should be considered as completely withdrawn.

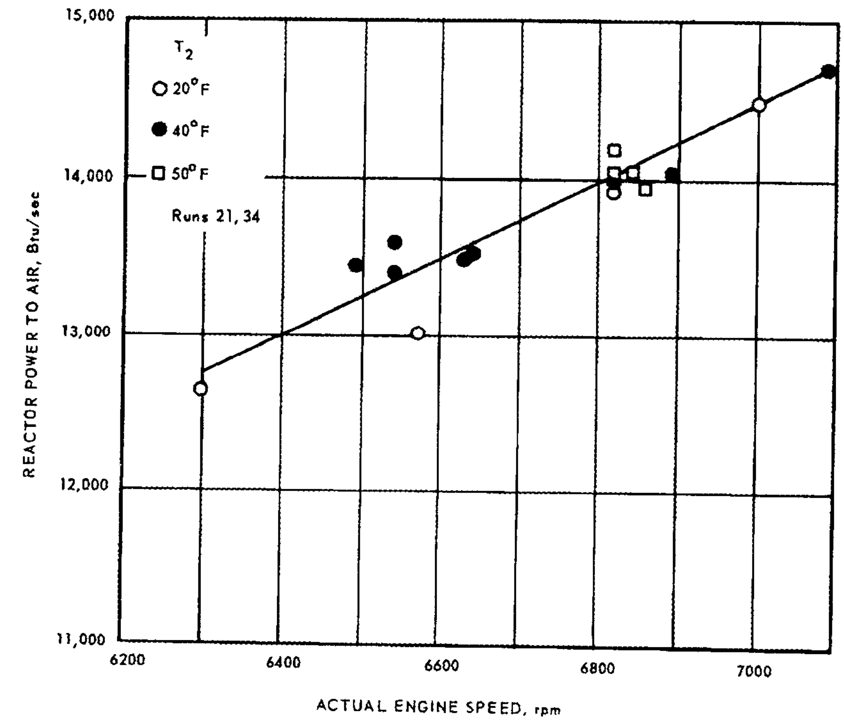

Fig. 3.21 – Reactor power to air versus engine speed for several bellmouth inlet temperatures

TABLE 3.5

TEMPERATURE DISTRIBUTION IN THE REACTOR DURING RUN 21, IET No. 3

Tube No.	18th-Stage Plate Temperature, °F	$T - T_{avg}$	Air Discharge Temperature, °F	$\frac{T_l - T_{avg}}{T_{avg} - T_{inlet}}$ (Air Discharge)
1	1623	10	1095	-10.73
2	1417	-196	1310	13.08
3	1558	- 55		
4	1621	8	943	-27.38
5			1233	4.59
6				
7	1628	15	1266	8.22
8	1750	137	1305	12.47
9	1603	- 10	1175	- 1.84
10	1678	65		
11	1607	- 6		
12	1564	- 49	1204	1.34
13	1662	49		
14	1567	- 46	1175	- 1.85
15	1708	+ 95	1234	4.54
16			1286	10.44
17	1571	- 42	1344	16.78
18				
19			1255	7.02
20	1623	10	1175	- 1.83
21	1714	+101	1294	11.32
22			1174	- 1.94
23	1597	- 16		
24			1110	- 8.95
25			1242	5.59
26			1206	1.63
27	1671	58	1156	- 3.93
28	1523	- 90	1166	- 2.82
29			1154	- 4.30
30	1786	173	1335	15.79
31	1652	39	1110	- 9.00
32	1637	24	1165	- 2.93
33			965	-24.98
34			1191	- 0.03
35	1518	- 95	1163	- 3.16
36				
37			1188	- 0.32

TUBE 18

STAGE	RING	ANGLE
9	8	322°
9	10	264°
10	8	102°
10	10	155°
11	2	338°
11	5	327°
11	8	322°
11	9	327°
11	11	222°
11	13	241°
11	14	111°
13	12	21°
15	15	21°
15	16	83°
18	9	322°
18	10	52°
18	13	111°
18	15	173°

ANGLE MEASUREMENT CLOCK-WISE FROM REFERENCE ANGLE

TUBE 15

STAGE	RING	ANGLE
9	12	350°
9	14	122°
10	12	327°
10	14	300°
11	6	332°
11	10	167°
11	12	237°
11	14	122°
12	12	55°
14	15	32°
14	16	147°
18	1	322°
18	4	322°
18	7	330°
18	12	147°
18	14	172°
18	15	234°
18	16	302°

ANGLE MEASUREMENT CLOCK-WISE FROM REFERENCE ANGLE

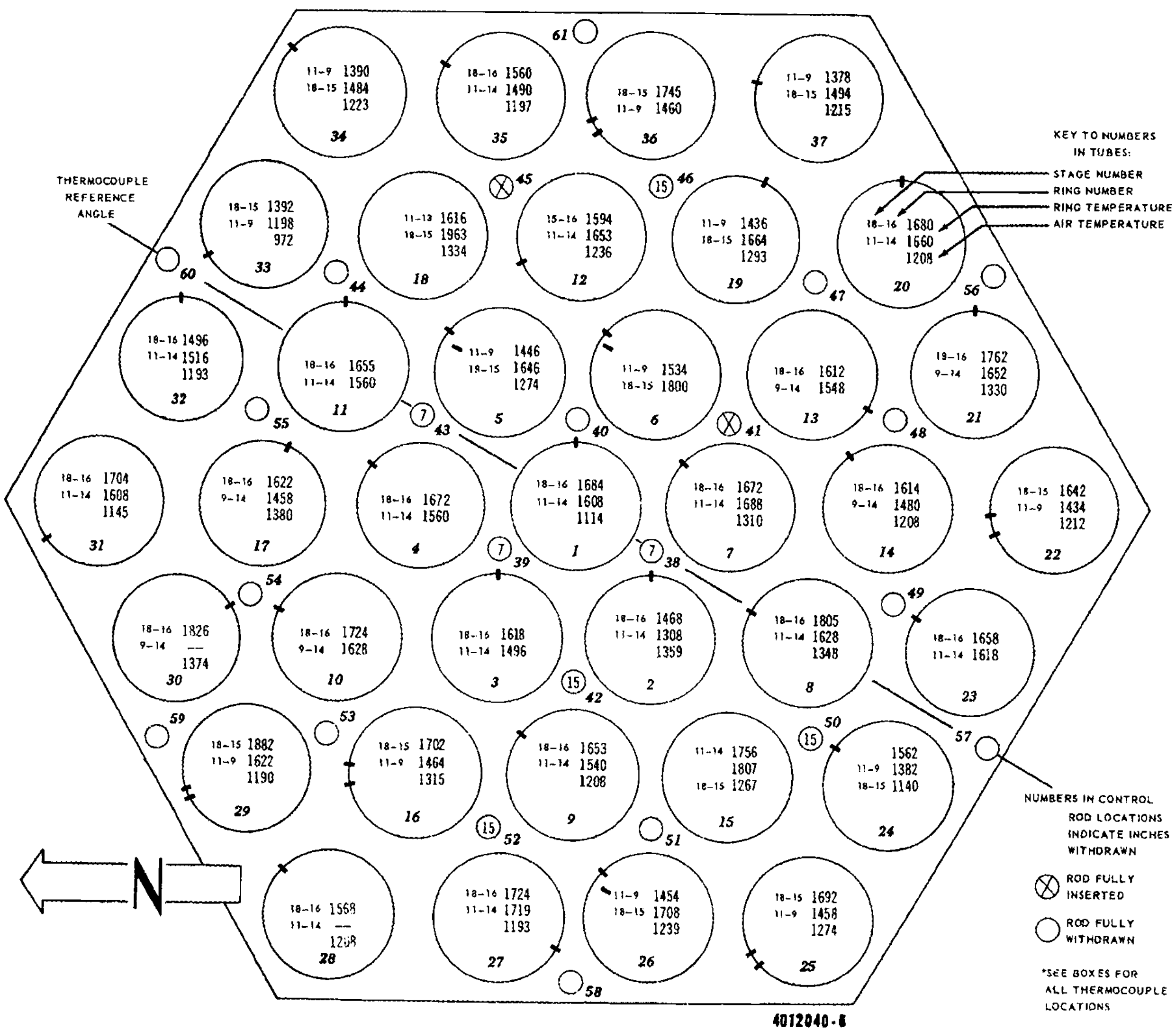

Fig. 3.22 – Plate temperatures, air temperatures, and control rod pattern for run 21-3, IET No. 3

Average plate temperatures for the ninth, eleventh, and eighteenth stages are shown in Table 3.6. On the average, the longitudinal profile compared very well with what was anticipated through calculations.

TABLE 3.6

AVERAGE PLATE TEMPERATURE IN THREE STAGES

Stage No.	Average Plate Temperature, °F	Difference From Stage 18, °F
18	1660	0
11	1570	90
9	1510	150

3.2.6 FUEL ELEMENT TEMPERATURES

The fuel element temperatures read at a particular position were basically defined by the convective heat transfer relation:

$$(T_{FE} - T_{AIR})_x = C\left(\frac{P}{A_H h}\right)_x$$

where

T_{FE} = fuel element temperature
T_{AIR} = local air temperature
P = reactor power to air
A_H = surface area at location x
C = power distribution constant for location x
h = heat transfer coefficient

The power distribution constant (C) is a function of relative power distribution among fuel tubes, fueled rings and fuel stages, and power distribution around fuel ring periphery. The latter two items were strongly affected by control rod position. In addition, variations of air temperature within a stage, which would affect stage temperature distribution, could also be anticipated. These variations were primarily the result of basic fuel element structure, although they could also be affected by control rod movement.

Considerable scatter of fuel element thermocouple readings about an average could be expected because the thermocouples were located differently in different tubes. For example, thermocouples were placed in various peripheral locations, in different rings of a fuel stage, in different positions with respect to control rods, etc.

Figure 3.23 is a summary plot of averaged temperature differences between fuel elements at stage 18 and exit air. A comparison with both minimum and maximum fuel element performance predictions indicates the range of variation of average conditions.

Figure 3.24 presents typical observed deviations of fuel element temperatures in individual tubes.

Figure 3.25 illustrates typical thermocouple readings on various rings of a fully instrumented stage, giving the fine radial temperature profile.

Because of the excellent correlation shown in Figure 3.23 and the range of variables considered, it was reasonable to assume the validity of the form of the design heat transfer coefficient relation in accounting for both temperature level and element-to-air temperature difference. It could also be assumed that there was no significant change of flow distribution with increase of heat input, which affected average temperature of fuel elements.

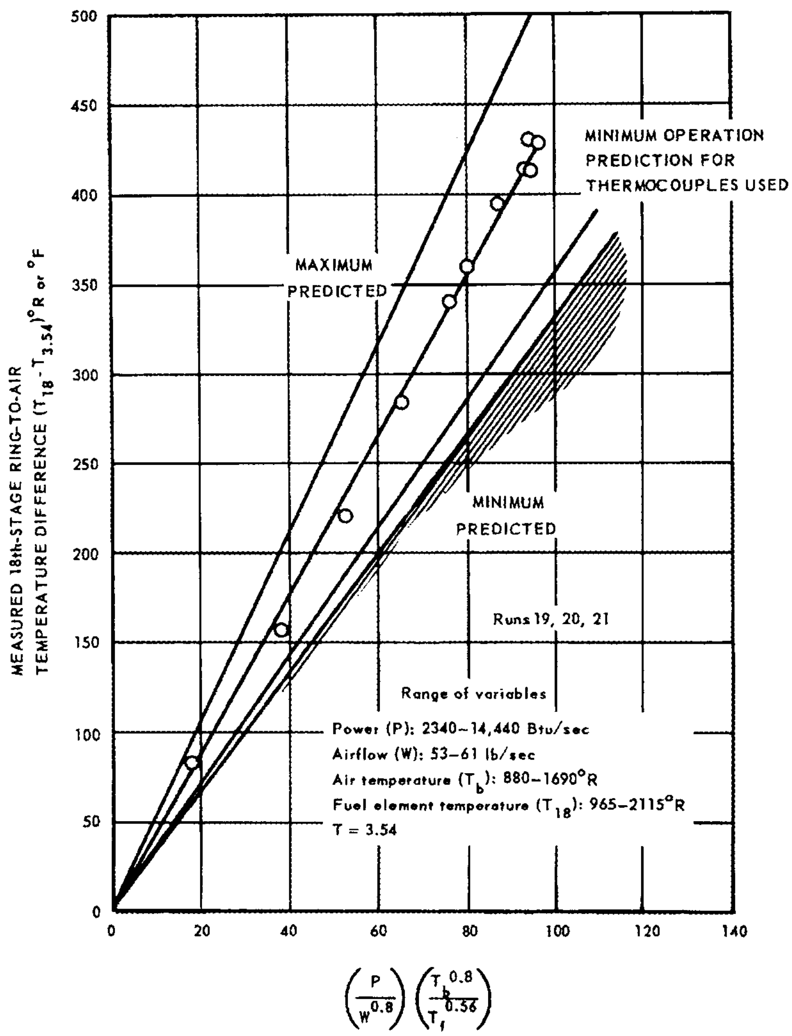

Fig. 3.23 – Summary of observed and predicted average stage-18 to exit air temperature difference

Before further analysis of observed temperature patterns is presented, it is necessary to explain some additional characteristics of Figure 3.23. First, two types of design predictions for fuel element temperatures were made for the core. The first, or minimum, prediction of average temperature assumed ideal behavior of all variables affecting temperature; e.g., airflow distribution, fine radial power flattening, heat transfer coefficient, and longitudinal power curve. (At the trailing edge of stage 18 there is a sharp upswing in flux. It was indicated in design, with some uncertainty, that items such as conduction and radiation would temper the effect of this peak to some degree, as indicated by the shadowed area in Figure 3.23.) The second prediction assumed maximum detrimental effects on average temperature. In the latter case, such items as observed imprecisions in power distributions, fuel element structure, and loading were considered. In addition, provision was made for certain operational variables, in particular the scalloping of flux about the ring periphery. The effect of location of thermocouples relative to flux scallops for the particular runs shown is also included in Figure 3.23. It was expected, therefore, that the observed temperatures would lie somewhere between the minimum and maximum predictions. It was not thought, however, that the observed data would lie as much above the minimum prediction as is indicated.

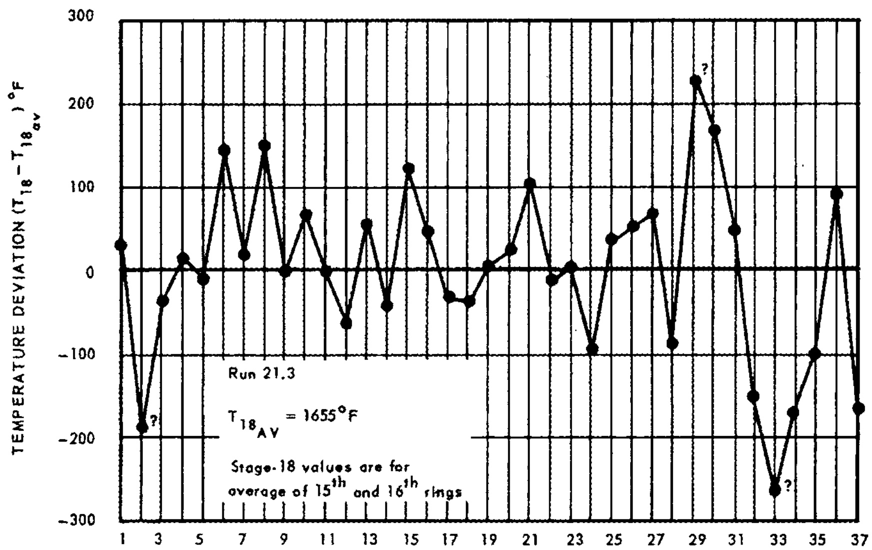

Fig. 3.24 – Deviation from the average of stage-18 plate temperatures

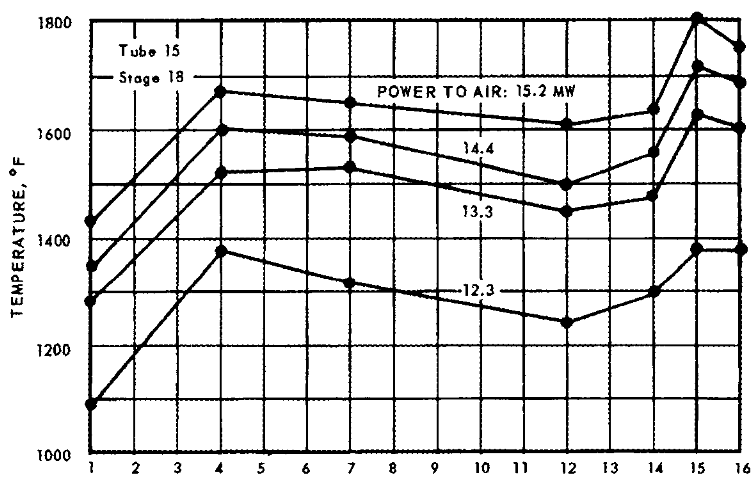

Fig. 3.25 – Fine radial temperature profile

A second problem concerns the type of thermocouples available for analysis. Basically, two types of instrumented fuel tubes were available. Two of the 37 cartridges were instrumented with 18 thermocouples to permit examination of fine radial temperature profiles. All other cartridges were instrumented with two thermocouples, usually on the outermost rings of stages 11 and 18. Thus, the average eighteenth-stage temperature depicted actually represents the average temperature of the outermost rings (rings 15 and 16). It was anticipated that ring 16 might show some deviation from the actual average temperature because of annulus design effects. However, it was hoped that examination of fine radial temperature traverses would permit correction if required.

Examination of fine radial traverses such as illustrated in Figure 3.25 indicated that rings 15 and 16 were running above average in temperature. It could not be determined, however, whether the indicated behavior was caused by erratic thermocouples or by a local peculiarity of the fuel element. Further examination of fuel element temperatures, such as presented in Figure 3.24, indicates that the data for rings 15 and 16 in Figure 3.25 might be erroneous or might reflect a local peculiarity. These thermocouples were among the hottest ones in the reactor.

It appears that average fuel element temperatures were somewhat higher, although not unreasonably so, than minimum predictions; however, the scatter of some of the data was in serious disagreement with predictions.

3.3 EFFECTS OF CONTROL ROD POSITION ON TEMPERATURES

Data from operation series 28 and 30 were analyzed to determine the effects of control rod movement on temperature distribution. The reactor was operated at a power of approximately 10 megawatts to air to deliver an exit air temperature of about 1000°F. Chemical power was added to maintain engine speed at 7000 rpm.

Series 28, runs 3-12, involved the complete interchange of rod frames 1 and 4 in increments of 3 to 5 inches. These runs were performed to determine the effect of the movement of a large number of rods on power distribution. Figure 3.26 shows the location of these frames in the initial positions, along with the number of rods in each frame.

Series 30, runs 1-8, involved the complete interchange of individual rods 44 and 45 with rods 50 and 51 in increments of 3 to 5 inches. These runs were performed to determine the effect of individual rod movement on tube power. Figure 3.27 shows the location of the rods and the initial position, along with the complete rod configuration for the reactor. The numbers in the fuel tube locations of Figure 3.27 indicate the relative change in exit air temperature associated with the insertion of rods 44 and 45 and the concurrent withdrawal of rods 50 and 51. The relative change in exit air temperature is expressed as a percentage of the average air-temperature rise across the reactor. Although there are minor inconsistencies, it is apparent that the change in position of these four rods warped or tilted the flux distribution of the reactor about the line of symmetry passing midway between the rods that were moved. The change in temperature does not imply the same change in flux because of possible flow change. The tests show that the power in a tube was affected by control rods remote from the tube.

Figures 3.28 and 3.29 plot the percent change in relative air-temperature rise as a function of control rod position for tubes 1, 2, 5, 9, 26, and 33. Figure 3.28 represents power changes for the interchange of large numbers of control rods by frames across the reactor in series 28. Figure 3.29 represents power changes for the exchange of four control rods in series 30. The power change for a given tube was caused by the movement of

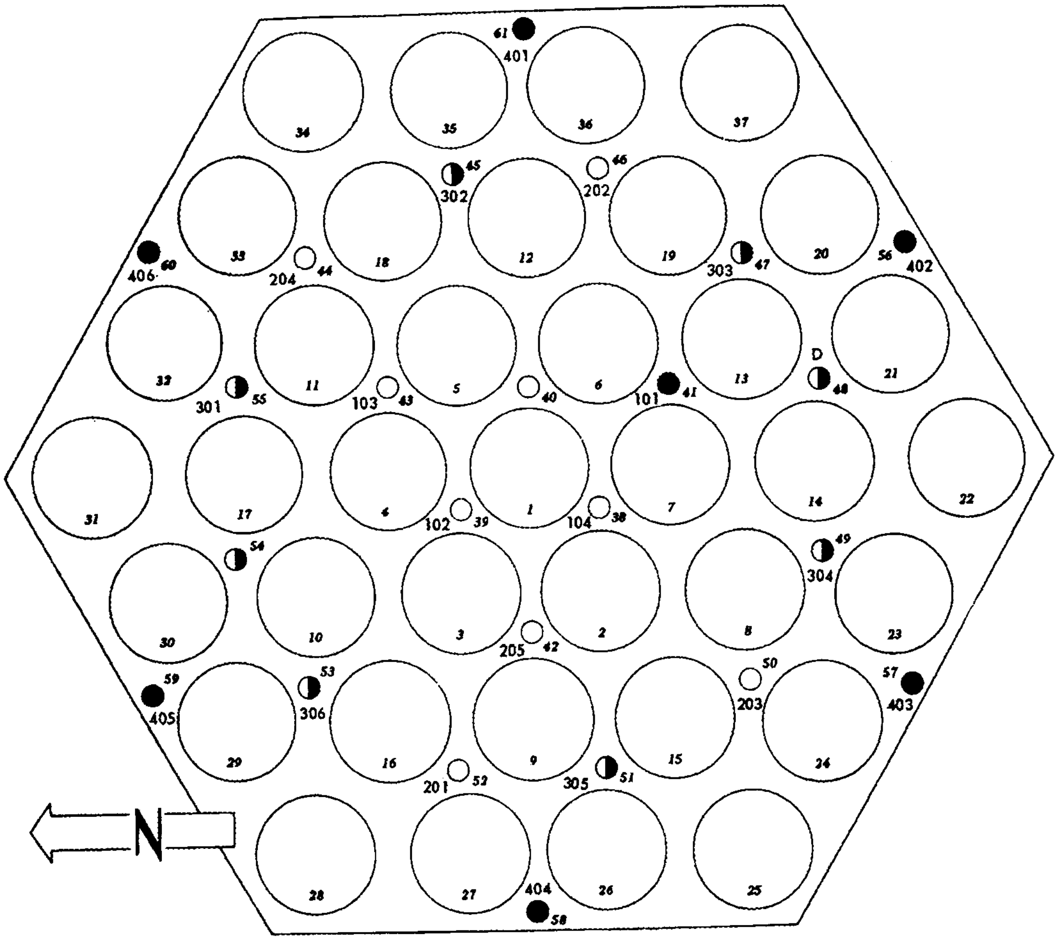

● Rod fully inserted

Frame 1, 4 rods
Numbers 102, 103, 104, 205

Frame 2, 4 rods
Numbers 201, 202, 203, 204

Frame 3, 6 rods
Numbers 301 to 306

Frame 4, 6 rods
Numbers 401 to 406

Fig. 3.26 – Rod pattern for series-28 runs, IET No. 3

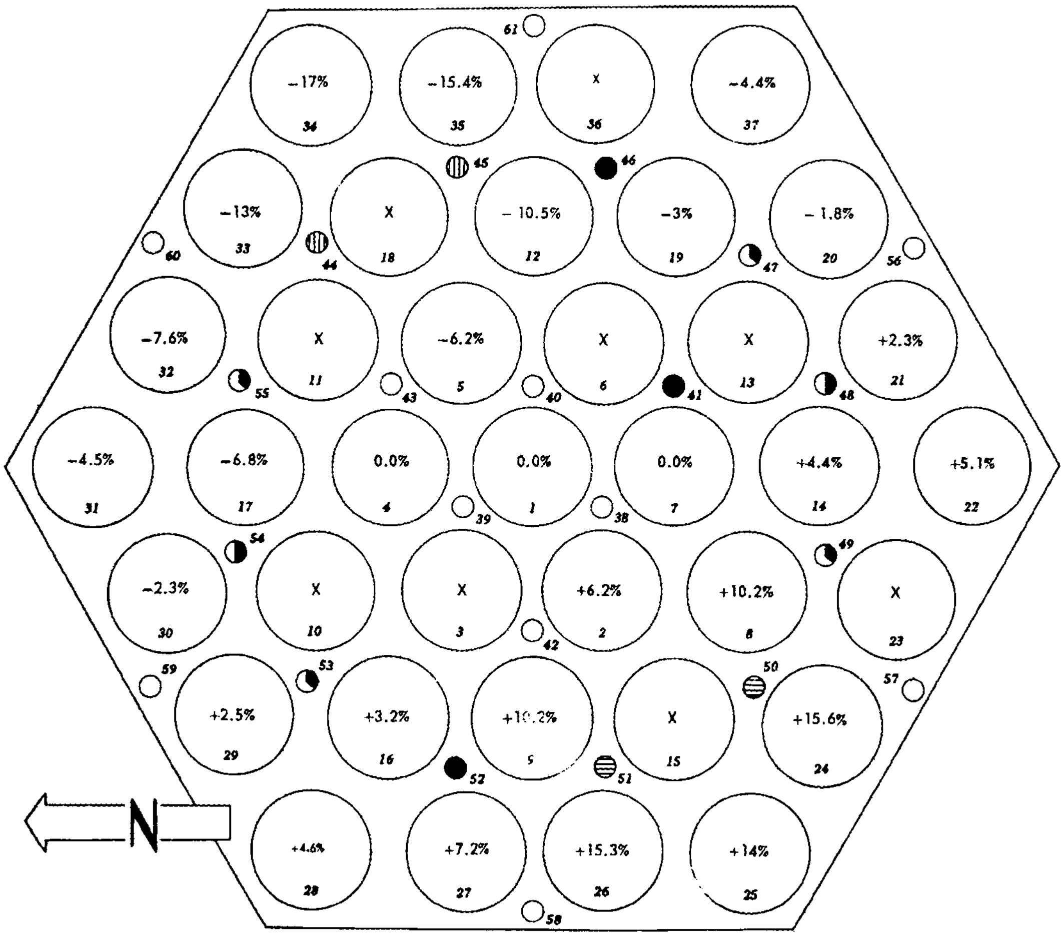

Rod fully inserted

Rod moved from out to in

Rod moved from in to out

Frame 1, 4 rods
Numbers 102, 103, 104, 205

Frame 2, 4 rods
Numbers 201, 202, 203, 204

Frame 3, 6 rods
Numbers 301 to 306

Frame 4, 6 rods
Numbers 401 to 406

X No thermocouple

Fig. 3.27 – Rod pattern for series-30 runs (IET No. 3) showing the relative change in exit air temperature associated with the insertion of rods 44 and 45 and the withdrawal of rods 50 and 51

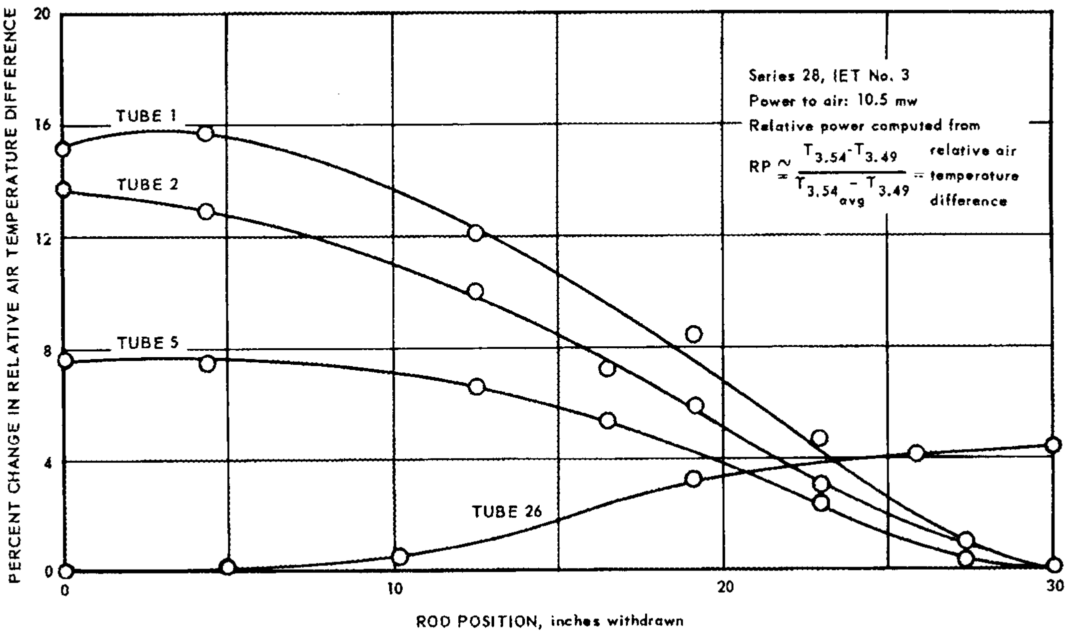

Fig. 3.28 – Percent change in relative air temperature differences versus control rod position, series 28, IET No. 3

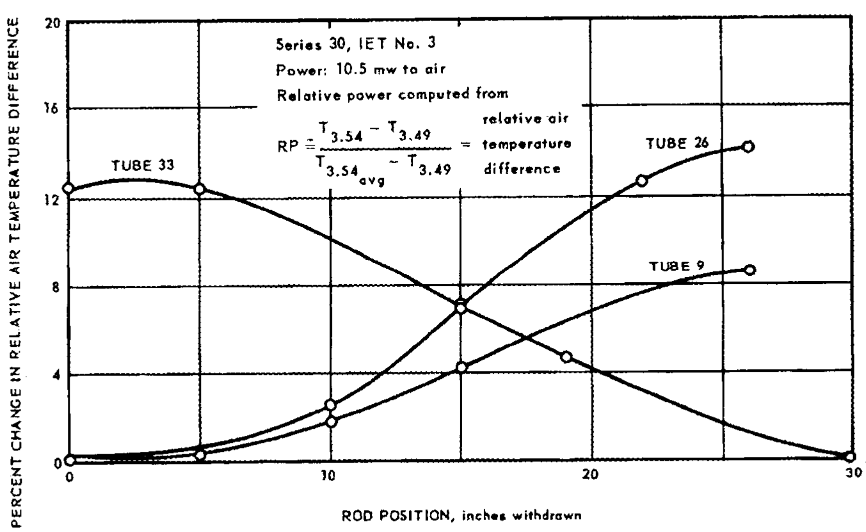

Fig. 3.29 – Percent change in relative air temperature difference versus rod position, series 30, IET No. 3

one or two rods adjacent to the tube. Comparison of Figures 3.28 and 3.29 shows that the total percent change of relative air temperature for the movement of a single rod was different for the same tube, tube 26, in the two runs.

Figure 3.30 shows a plot of percent change in relative air-temperature difference as a function of rod position for tubes remote from control rod movement. Here, a change in relative air-temperature difference of between 4 and 6 percent is noted for a complete rod removal, an indication of the degree of effectiveness of control rods on tubes across the reactor. It was observed that tubes that are remote from a single control rod movement by as much as half the distance across the core are affected to some extent. These changes may have been caused by an actual change in relative power, a change in air weight flow in the various tubes, or a combination of these causes. Figures 3.31 and 3.32 show a plot of fuel element plate temperatures as a function of rod position for movement of a single control rod next to a tube. These and similar curves were used to obtain correction factors for the thermocouples situated directly under, or shadowed by, a control rod. Figure 3.33 shows the location of thermocouples.

Analysis showed that although the general trend of reactor behavior was in accord with expectations, some effects were observed that required further investigation. One of these was the influence of control rods on temperature rise (or power) in the tubes remote from the rods. It was assumed in design work that a control rod would affect only the power in proximate tubes. Data indicate that power in remote tubes could also be affected, although changes in airflow may have been involved.

Since flow distribution varies simultaneously with power distribution, the air temperature variations could be expected to exceed the nuclear power variations in a particular cartridge; e.g., a tube showing 10 percent excess power would tend to show greater than 10 percent excess temperature rise. Because the experimental tube-to-tube power determinations were made exclusively on the basis of air temperature measurements, in the

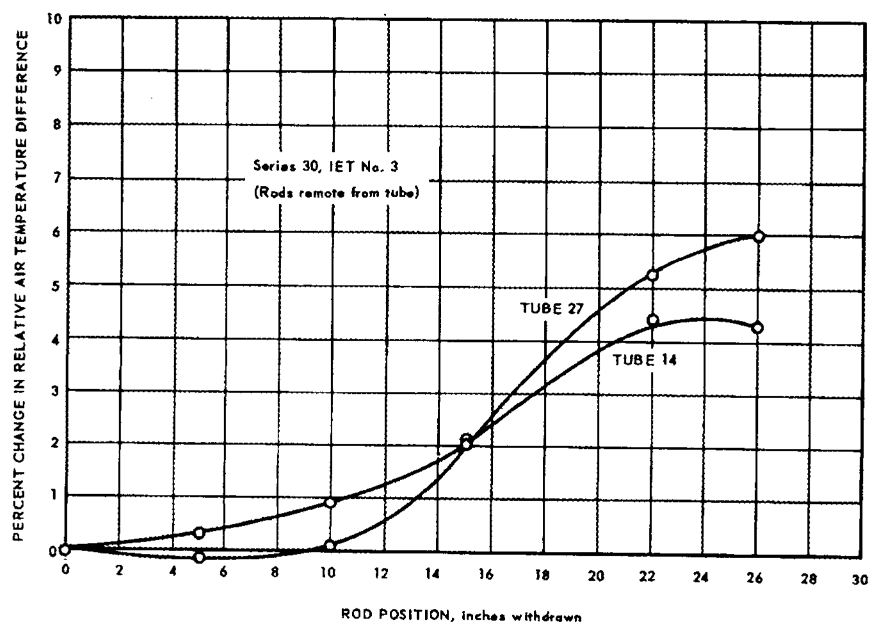

Fig. 3.30 – Percent change in relative air temperature difference versus position of rods remote from tube

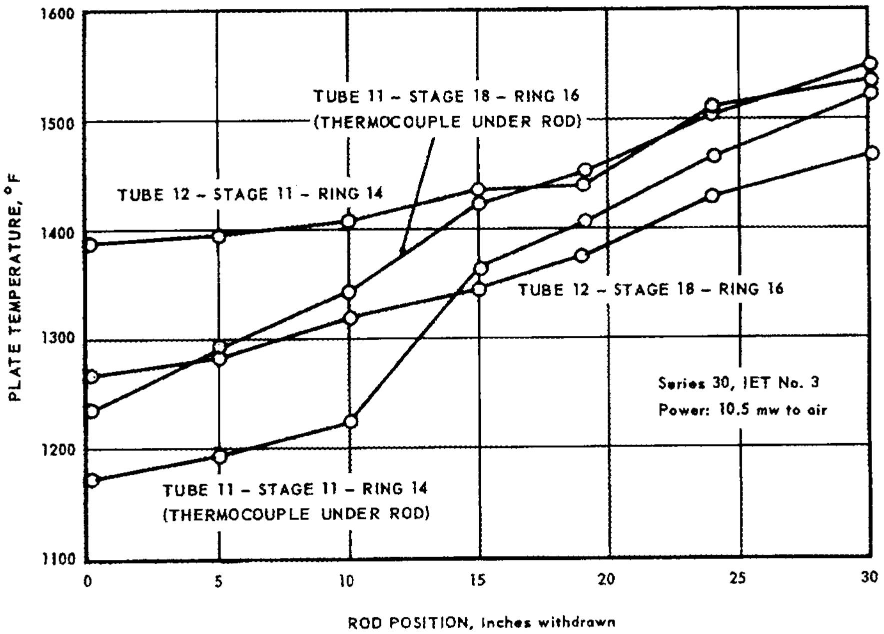

Fig. 3.31 – Plate temperature versus rod position, tubes 11 and 12

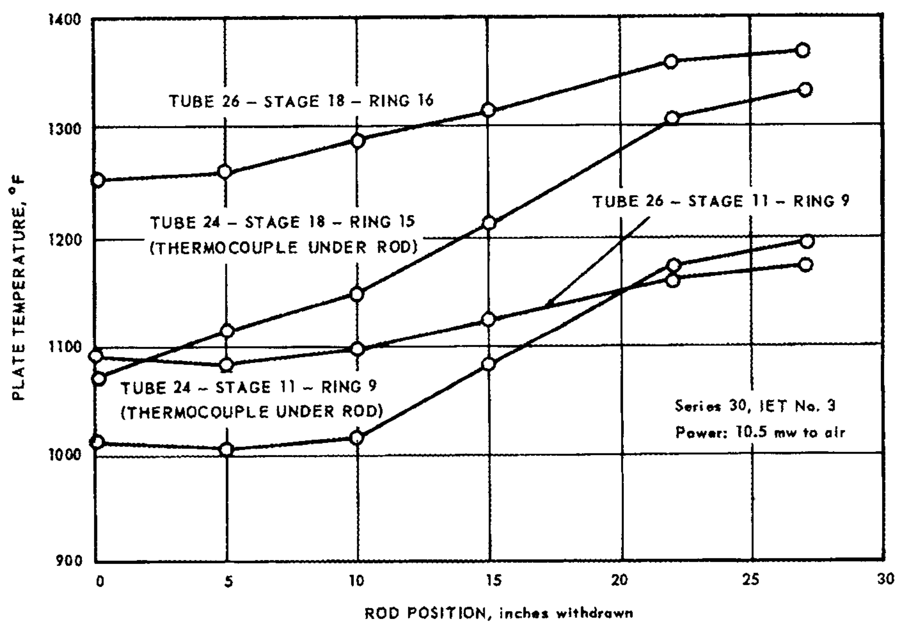

Fig. 3.32 – Plate temperature versus rod position, tubes 24 and 26

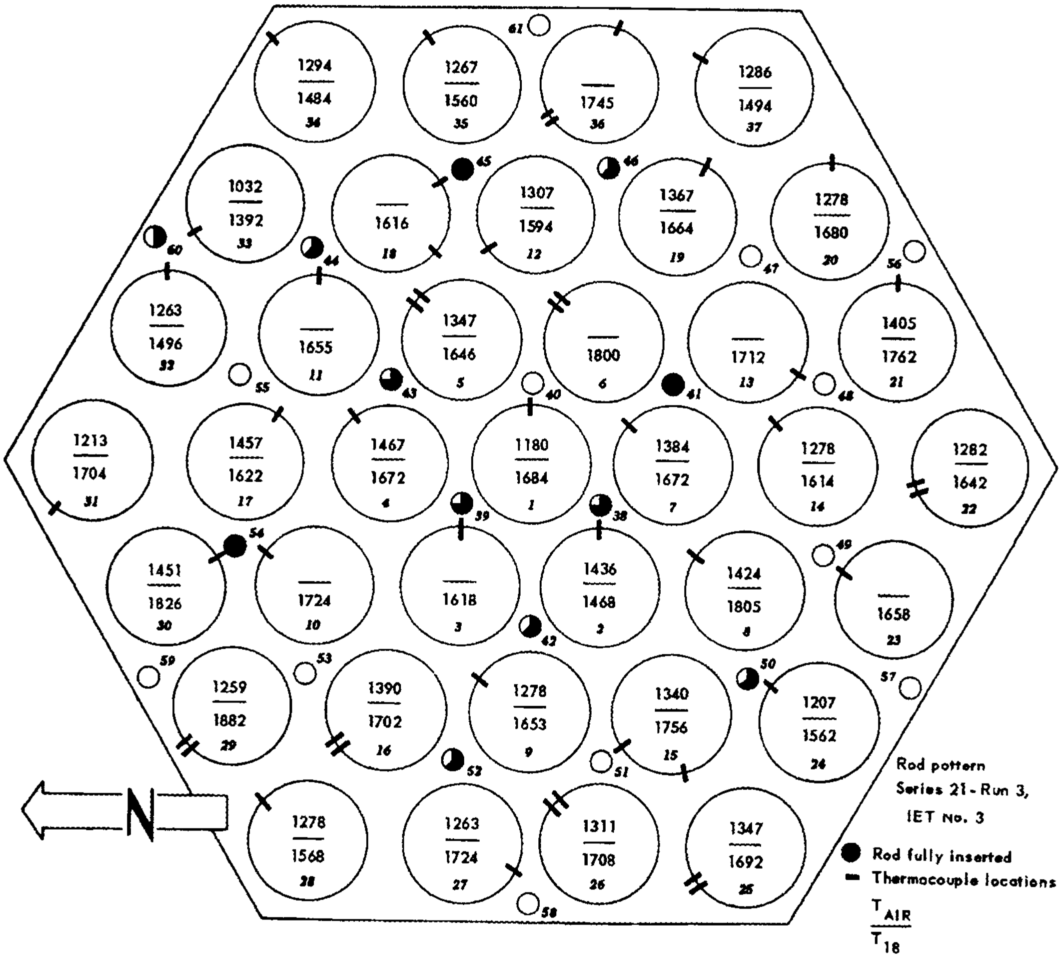

Fig. 3.33 – Air temperature and plate temperature distribution

absence of flow measurements, nuclear power distributions could not be defined exactly. Data indicated that disparities existed between predicted and actual control rod effects. In general, the temperature deviations were of greater magnitude than the predicted nuclear power variations; however, significant scatter appeared to exist.

3.4 RADIOACTIVE RELEASE

All operations at IET were under meteorological control. Operations were seriously limited by permissible wind direction. On many days, it was impossible to operate at all, and most of the time operation was possible only a few hours each day. On the other hand, the buildup of fission products was small, and operations were never limited by the maximum downstream dose regulations (lung dosage not to exceed 3.9 rem, with escape rate assumed as 1 percent of the total reactor fission products).

The release of radioactive material during IET No. 3 was first detected February 11, 1956, during an attempted transfer to full nuclear power. Fuel cartridge damage was suspected and later verified, during disassembly of the A2 core, as the cause.

The presence of fission products in the exhaust was definitely proved later in the test series when I^{131} was found in the particles carried out of the stack during the second 100 percent nuclear operation. The radioactive material released from the stack during this operation was estimated at 2000 curies over a 4-hour period. An AEC site-survey crew could find no trace of this radioactivity, even though they surveyed the area during and after the operation. This lack of evidence of radioactivity was probably caused by a head-on meeting of opposing winds, which caused an upward flow and dispersed the radioactivity to the mountains.

The measured radioactivity released from the stack during the third 100 percent nuclear power operation was about 1000 curies over a 2-hour period. There was some fallout from this operation at the IET area, the ANPD Administration area, and the A and M area, but not enough to seriously limit use of any of these areas. After the reactor was shut down, the AEC site-survey crew found some fallout at the ANPD main gate and along an AEC highway for 3 miles south of the ANPD main gate. None was found on any public highway.

Much smaller amounts of fission product radioactivity were released from the stack on succeeding days.

During early partial-nuclear-power operations, some low-level beta-emitting particles were measured by the stack monitor. This type of activity decreased as operation continued and was never identified with certainty. It may have been associated with leakage of the shield solution into the reactor.

During the last day of operation, an attempt was made to verify the location of the damaged fuel cartridges by observing the released radioactivity when control rods proximate to suspected tubes were withdrawn. The comparative activity levels of the rupture-detecting filters had indicated that tubes 26 and 30 were the most radioactive. A short run at about 60 percent nuclear power was made to locate the damaged fuel element. The wind was from the southwest at 30 miles per hour, and the Idaho site-survey crew was located downwind from the IET. The survey crew radioed that they were picking up a maximum air activity of about 1 mr per hour on the Salmon Highway and at Monteview but that most readings were near zero. At the request of the Idaho Operations Director of Health and Safety the operation was continued to allow the survey crew to get a better air sample. A short while later the control rods adjacent to tube 30 were pulled, and both the rupture detector and the stack monitor indicated a slight burst of activity. Twenty minutes later a portion of the monitoring crew located in Monteview, 10 miles away, detected some activity, apparently a result of this burst. At this point, with the concurrence of the Idaho Operations Director of Health and Safety, the reactor operation was terminated. About 100 curies was released during these tests. The power plant was still operating satisfactorily at this time.

3.5 POSTOPERATION EVALUATION OF FUEL CARTRIDGES

An investigation was conducted to determine how and why the fuel damage phenomenon occurred.

On February 25, 1956, the test assembly was moved to the A and M area for disassembly. Some difficulty was encountered in dismantling the reactor; minor damage to several of the cartridges resulted. A complete photographic record of the condition of core components on disassembly is given in references 2 through 6.

Noticeable damage was observed before the core was dismantled. Incrustations thought to be a residue from borated shield water were found in the core. Figure 3.34 shows this incrustation around several of the fuel cartridges. This solution could have come from leaks that developed ahead of the turbojet engine, at the tubes in the harness flange, or possibly at both flanges of the instrumentation rings located below the air ducts.

Heat oxidation accompanied by discoloration similar to that shown in Figure 3.35, appeared on a few of the insulation liners. Wrinkling, such as is shown in Figure 3.36, also occurred on a few liners. Damages of varying intensity caused by burning are shown in Figures 3.35 and 3.37. Figure 3.34 shows a damaged cartridge in the core prior to dismantling.

Damage to the cartridge rails appeared either in the form of dimpling or breaking, as shown in Figure 3.38. Broken rails occurred in only a very few instances.

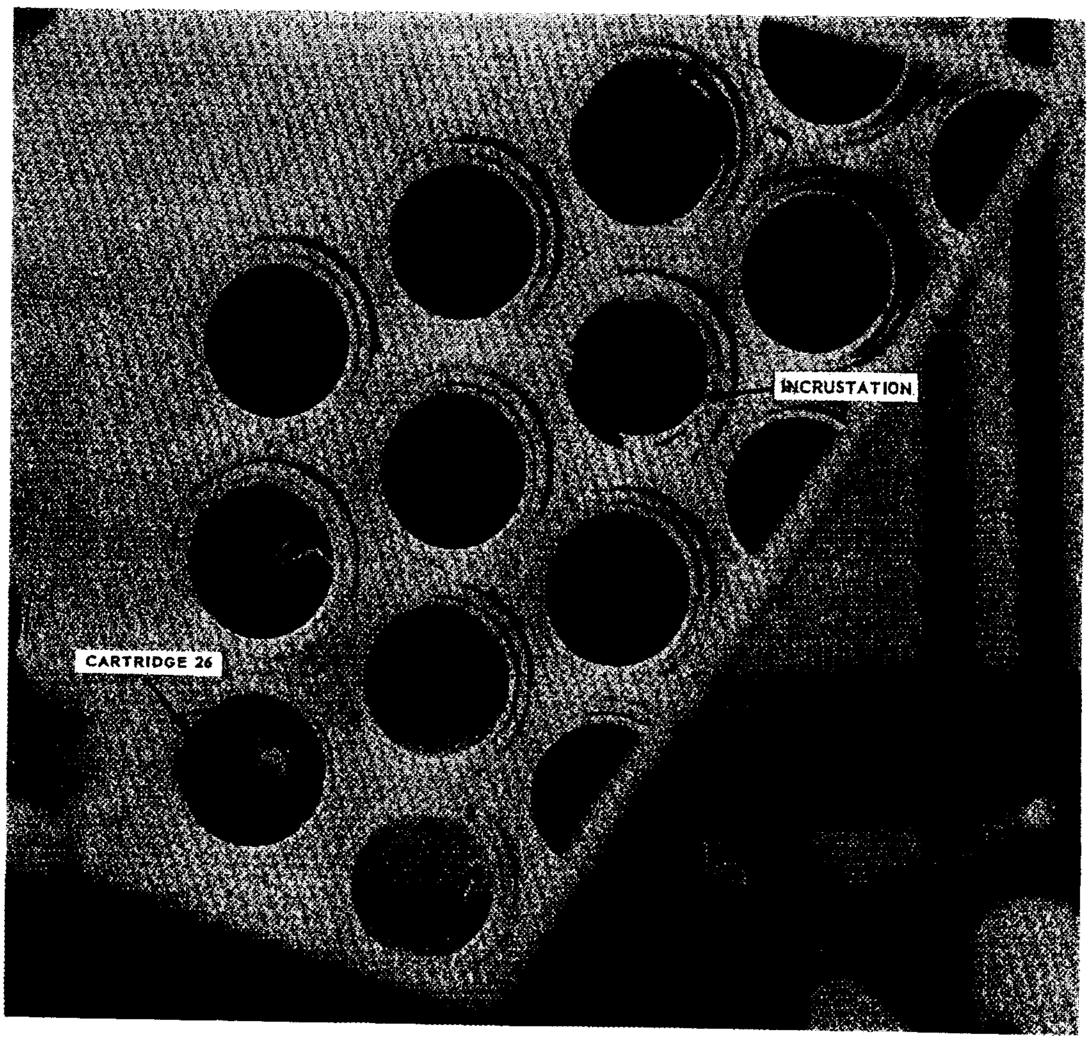

Fig. 3.34 – Reactor core showing boric acid leakage, burned cartridge, and several undamaged cartridges

Fig. 3.35 – Cartridge showing discoloration, burning, and melting

In the fuel elements, the damage ranged from ring buckling, shown in Figure 3.39, to burning and melting, shown in Figures 3.35, 3.38, and 3.40. Two cartridges were severely damaged, while only one other showed any melting or burning.

Twenty-four of the 37 cartridges used in IET No. 3 were in fair to good condition and were re-used in later tests, an indication that the heat damage was localized and did not extend over the complete system. This localization is seen even more clearly in Figure 3.34, which shows a burnt cartridge, a cartridge with incrustations, and several good cartridges, prior to removal from the core.

It was hypothesized that the failure of fuel elements during the initial operations of the D101A2 test assembly was caused by the collapse of the insulation sleeve against the latter stages of the fuel cartridge. An inspection of the fuel element cartridges after their removal from the core showed excessive damage due to severe oxidation and even melting of fuel elements in a number of cartridges. The severe damage was almost wholly limited to the latter stages where the oxidation had completely penetrated through the outer ribbons. The rails on most of the cartridges were bent, although this condition was not limited to those cartridges that had the severe oxidation.

The severe oxidation was believed to be the result of high plate temperatures due to maldistribution of cooling air caused by a blockage of the airflow path through the fuel element. Since the fuel cartridges that experienced the most severe oxidation also showed buckling failure of the insulation sleeve, study of the cause of fuel element failure was focused on the insulation sleeve.

Fig. 3.36 – Insulation liner showing wrinkling

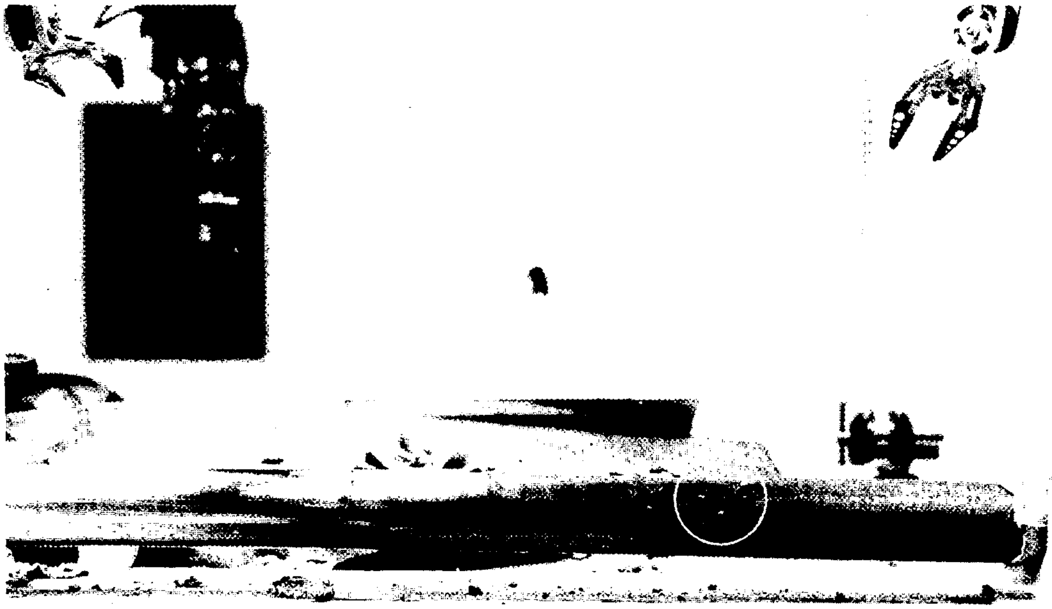

Fig. 3.37 – Insulation liner showing burning effects

The probability of collapse of the insulation sleeve against the outer ribbons of the fuel element was suggested by the similarity of the rail buckles observed in cold-flow tests to those observed in slightly damaged cartridges. The collapse of the insulation sleeve may have been the result of a large static pressure differential. Such a differential would develop at the downstream section of the sleeve if the outer air gap between the insulation and the fuel tube were partially or completely blocked. Blockage of the gap could occur because thermal growth of the insulation sleeve was more rapid in the higher temperature of the downstream section. It could also result from a gradual settling of the insulation material during an extended operation because of vibration and the contraction and expansion of the sleeve. In either case, a pressure buildup would occur if the sleeve had insufficient relief holes.

Fig. 3.38 – Fuel element melting effects, rail buckling, and breaking

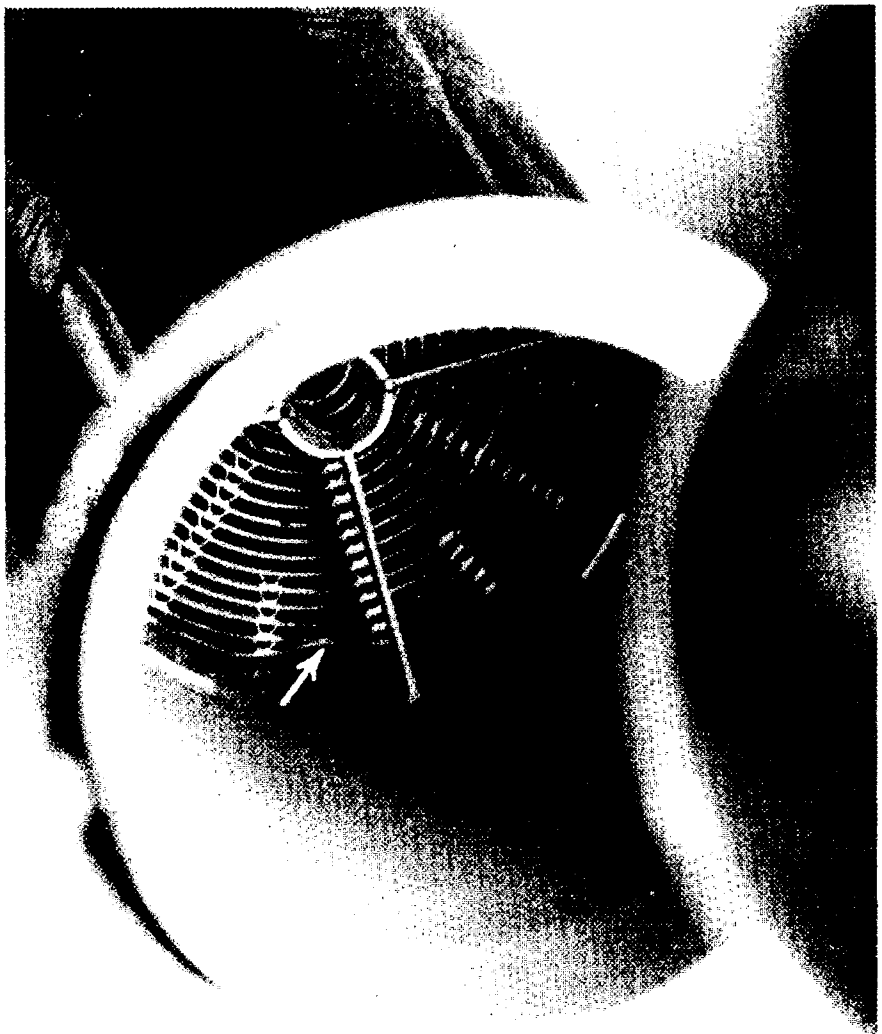

Fig. 3.39 – Fuel element ring buckling

Cold-flow tests[7] of the D101A2 insulation sleeve also indicated that:

1. The bleed holes in the sleeve were wholly inadequate to relieve the radial inward pressure across the insulation sleeve if the outer air gap was blocked at the exit end.
2. During normal reactor operations, a pressure buildup of a magnitude sufficient to buckle the rails and collapse the sleeve against the outer ribbon of the element could occur.
3. The collapse of the liner would occur at the latter stages of the cartridge.
4. The failure of the sleeve was more likely to occur when the slip joint of the liner was situated circumferentially between two rails of the cartridge.

Insulation tube replacements for the A2 core were redesigned and fabricated on the basis of data obtained from cold-flow tests previously described. Tests of insulation tubes of the

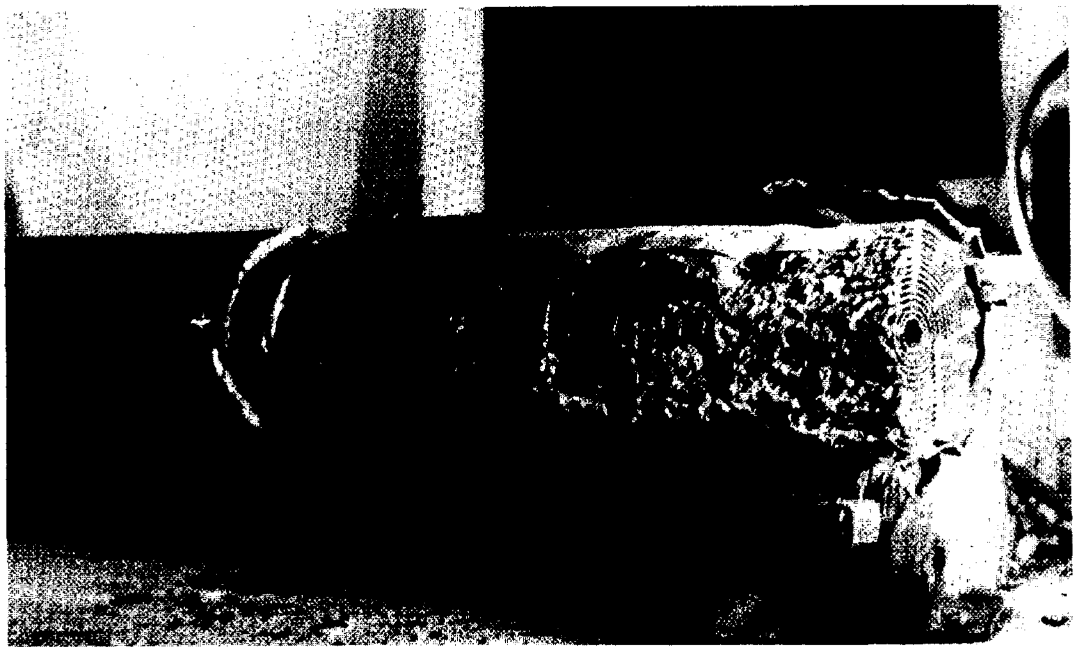

Fig. 3.40 – Fuel element melting effects

type used in the A2 operation indicated that deflection could occur at the slip joint at a cartridge pressure drop of 2.0 psi and a pressure drop of 2.3 psi across the sleeve. This pressure drop could occur only if an air seal existed between the rear of the insulation tube and the core fuel tube.

Airflow tests of the modified insulation sleeve showed that the differential pressure across the insulation sleeve was reduced by one-third by the addition of 25 holes 1/8 inch in diameter. An additional 25 1/8-inch holes gave little improvement.

Cold-flow tests on the modified insulation tube described in section 4 indicated a pressure drop of 1.9 psi at a cartridge pressure drop of 7 psi, a normal operating pressure drop. However, in this test a seal was made intentionally between the insulation liner and fuel tube and induced the pressure drop across the liner. Modification to the liners to prevent the occurrence of this seal indicated that all or part of the pressure drop across the liner could be eliminated.

According to ASME codes, the recommended external working pressure was 1 psi for a tube of this type operating at 1400°F. The collapsing pressure of the insulation liner operating at 1470°F was calculated to be 3.1 psi. This calculation indicated that the liner could develop a pressure drop greater than that recommended if a complete seal developed but that a factor of safety of about 1.5 existed over collapsing pressure.

3.6 REFERENCES

1. Minnich, S. H., "HTRE-1 Test Report," GE-ANPD, XDC 56-6-36, 1956.
2. Tuck, G. and Hoover, B. J., "Photographic Investigation of A-2 Fuel Elements, First Unloading," GE-ANPD, DC 56-6-706, 1956.
3. Tuck, G. and Hoover, B. J., "Photographic Investigation of A-2 Fuel Elements, First Unloading," GE-ANPD, DC 56-9-729, 1956.
4. Tuck, G. and Hoover, B. J., "Photographic Investigation of A-2 Fuel Elements, First Unloading," GE-ANPD, DC 56-9-730, 1956.
5. Tuck, G. and Hoover, B. J., "Photographic Investigation of A-2 Fuel Elements, First Unloading," GE-ANPD, DC 56-12-711, 1956.
6. Tuck, G. and Hoover, B. J., "Photographic Investigation of A-2 Fuel Elements, First Unloading," GE-ANPD, DC 57-3-725, 1957.
7. Holowach, J., "General Engineering Development Report No. 206, Investigation of the Failure of an Insulating Sleeve," GE-ANPD, DC 56-4-137, 1956.

4. IET NO.4

The second series of operational tests using the D101A test assembly was run at the Idaho Test Station during the period from April 17, 1956, through June 29, 1956, and was designated IET No. 4. The primary purpose of the tests was to determine whether the modifications based on the results of the first test series had significantly improved the capabilities of the reactor. Additional objectives were (1) to make complete measurements of the power-plant performance, (2) to measure xenon poisoning, and (3) to study and improve servo control of the reactor.

IET No. 4 utilized the A2 core in which several significant repairs and modifications were made as a result of IET No. 3 operation. Thirteen new fuel cartridges with extra rails were installed. Fifteen control rods were replaced.

A third major modification entailed redesign of the insulation sleeves to provide more assurance against liner collapse and subsequent fuel cartridge damage. The insulation sleeve was modified as follows:

1. Thinner liners were used, and Thermoflex insulating material was removed from the tail sections.
2. Thirty-six air bleed holes were incorporated through the insulation tube to prevent pressure buildup between the core tube and insulation sleeve.
3. A stiffening ring was added in the insulation tube at the rear of the eighteenth fuel stage to provide strength against collapse.
4. The diameter of the cartridge tail assembly was reduced to prevent the occurrence of an air seal at the rear of the insulation tube.
5. The insulation tube slip joint was removed to prevent collapse of the tube along this line.

The core was loaded with 24 cartridges used during IET No. 3 and 13 new cartridges. Table 4.1 gives the cartridge numbers and tube locations for the IET No. 4 operations. During this test series, the reactor was operated for a total energy release to the air of 1877 megawatt-hours at a maximum sustained power level of 16.0 megawatts to air. The maximum sustained plate temperature recorded was 1991°F, with a maximum sustained average of 1701°F. The maximum core discharge temperature was 1394°F. The total operating time at a power to air of 16 megawatts was 84 hours. Table 4.2 presents a summary of reactor operation during this period. The complete operating reports for the series are presented in references 1 through 6.

4.1 OPERATION

The D101A2 test assembly was returned to the IET on April 17, 1956, for IET No. 4 operations. The first 5 working days were devoted to checkout of the circuits and operating equipment. During this period, the core was cautiously filled and the fission chambers were watched for any unexpected increase in flux. On April 24, 1956, the reactor was made critical to measure the excess reactivity and to permit observation of any changes in this

TABLE 4.1

A2 CORE LOADING FOR IET NO. 4

Tube	Serial	Age	Tube Location for IET No. 3
1	206	New	
2	244	New	
3	214	Used	3
4	204	Used	4
5	243	New	
6	245	New	
7	201	Used	31
8	215	New	
9	202	Used	12
10	248	New	
11	235	Used	21
12	231	Used	24
13	233	Used	13
14	249	New	
15	238	Used	15
16	240	New	
17	242	New	
18	250	New	
19	246	New	
20	222	Used	6
21	221	Used	29
22	224	Used	22
23	213	Used	23
24	211	Used	11
25	219	Used	25
26	216	Used	28
27	212	Used	27
28	227	Used	33
29	207	Used	32
30	241	New	
31	217	Used	20
32	234	Used	14
33	239	Used	8
34	247	New	
35	208	Used	35
36	229	Used	37
37	228	Used	19

parameter during subsequent tests. Performance testing with an engine operating on the reactor loop was begun the following day. There was no change in reactivity with the air blowing through the core, such as would be expected if any of the fuel elements had been dislodged. Engine performance was comparable to that observed during the beginning of IET No. 3.

The first objective in the checkout of the D101A2 test assembly was to fill the core with moderator water. Before the last six fuel cartridges were inserted, the core was emptied during the operations in the hot shop as a precaution against the core becoming critical. The core was filled in a slow and controlled manner while the neutron flux was monitored. The reason for caution in this operation was that various changes in reactivity were possible because of the repairs and modifications to the A2 core.

To carry out the filling of the core, it was originally planned to have the source in the reactor, both dynamic rods withdrawn, and the fission chambers operating, as well as having the fill and evacuation mechanisms in operation. It proved to be impossible, how-

TABLE 4.2

REACTOR OPERATION, IET NO. 4

Date	Time Above 200 kilowatts, hours	Maximum Power of Total System, megawatts	Total System Power, megawatt-hours[a]
5/1/56	2.52	4.1	3.22
5/2/56	6.78	8.1	34.20
5/3/56	1.90	4.4	7.25
5/4/56	4.37	9.6	35.06
5/5/56	4.47	11.2	36.68
5/7/56	4.82	11.2	51.31
5/9/56	2.00	11.2	15.60
5/10/56	4.05	8.4	16.37
5/14/56	4.66	11.4	49.61
5/15/56	0.13	0.8	0.10
5/16/56	3.27	3.2	5.59
5/17/56	3.48	9.9	27.28
5/18/56	1.88	6.4	3.65
5/19/56	2.28	13.4	25.82
5/22/56	7.67	13.6	67.63
5/23/56	8.92	13.8	61.68
5/24/56	6.70	14.6	49.03
5/26/56	9.47	16.1	73.36
5/31/56	9.17	16.3	131.70
6/1/56	10.06	17.1	158.31
6/5/56	10.02	17.6	157.96
6/6/56	6.43	18.1	95.75
6/7/56	7.20	17.2	108.80
6/8/56	1.92	15.5	20.03
6/9/56	3.95	16.5	36.28
6/12/56	7.10	16.7	71.01
6/13/56	8.83	16.6	125.64
6/14/56	10.45	16.3	149.57
6/16/56	0.78	1.8	0.92
6/19/56	0.57	13.3	2.98
6/20/56	7.72	18.4[b]	53.51
6/21/56	7.85	17.8	109.08
6/23/56	4.87	17.1	72.57
6/26/56	6.92	17.7	87.67
6/29/56	8.73	16.8	119.76
Total, IET No. 4	193.94		2064.98
Total, IET No. 3 and IET No. 4	234.15		2414.06

63.2 hrs time-weighted avg. PL = 10.2 MW

128.74 hrs time-weighted avg. PL = 16.8 MW

when I add these up, I get 191.94

1272.35 MW-hrs in 41 days of operation

[a]Power to air = $\frac{\text{Total system power}}{1.1}$

[b]Maximum power

ever, to operate the dynamic pump without a positive inlet pressure, which was not easily obtained with the core drained. The procedure for filling the core was consequently modified to eliminate use of the dynamic and source rods.

Since photoneutrons from the beryllium reflector gave an adequate reading of the fission counters, the absence of the source was unimportant. Since the core was filled very slowly, at about 20 gallons per minute, the lack of any operating control rods was not important. The count rate of 10 counts per second on the fission chambers held constant for about an hour and then increased very rapidly to approximately double this rate. When the filling was completed, the count rate had decreased to less than one count per second. This behavior was attributed to the increase in multiplication as the core was filled with moderator water, followed by the shielding of the fission chambers as the top reflector and transition sections were filled. As soon as this filling operation was completed, the continuous circulation of the moderator was started. The dynamic pump was operated in the general checkout procedure.

A systematic check of the systems, components, and controls proceeded without incident. All electrical and fluid connectors were hooked up and checked out with little difficulty. Some difficulty was encountered with the dynamic circuit. An attempt to prime the dynamic pump to get it started was unsuccessful; the pump would operate only after the inlet had a continuous positive head. The moderator-system circuit was dirty, no doubt because of lack of circulation while it was in the hot shop. The resistivity on the first filling dropped, in a 48-hour period, from about 10^6 ohms to 2.5×10^5 ohms. After the fourth complete filling, accomplished in 6 days, the resistivity dropped from about 10^6 ohms to 8.5×10^5 ohms in a 24-hour period, with a change in pH factor from about 6.5 to 7.2.

The rest of the checkout of reactor controls proceeded smoothly. Difficulties were encountered with the position feedback circuit for both of the dynamic rods to the servo system, and it was necessary to install new wires on the CTF from the tank disconnect panels to the coupling station. During this period the dynamic rod servo system did not operate properly; the trouble apparently was in the electronic circuits.

The three preamplifiers for the log flux nuclear instrumentation were moved from the CTF to the coupling station. This was done to eliminate the aural and vibration noise problem that was experienced with these flux channels during the previous operation. This change produced excellent results. During operation with both the blowers and an engine running, the noise in the log flux channels was almost entirely eliminated.

The shim rod actuator performance was considerably better than during the previous operation; however, some minor difficulties were encountered. All actuators were successfully checked out; but just before the start of the nuclear testing, an open circuit developed in the servomotor power leads to actuator 101, making it inoperative. Although an attempt was made to repair this actuator, no consistent fix could be obtained, and the actuator was out of service during the entire period. Difficulty persisted in driving the shim actuators down to the fully inserted position for latching.

A mechanical operation of dynamic and source rods was satisfactory. Considerable difficulty was encountered with the servo feedback circuitry for the dynamic rods. Consequently these rods were never used in automatic controls.

After the CTF was coupled, a systematic functional check of all the engine circuits was made. The only difficulty encountered was a ground in an oil temperature lead in the engine No. 2 loop. This trouble was repaired by substitution of a spare lead in the circuit.

During the engine checkout running, the compressor-to-turbine static pressure-loss transducer on engine No. 1 was found to be faulty and was replaced.

Past experience had indicated that the capacitor-discharge ignition system was the most reliable. This type of ignition system was quite successful on engine No. 2 and was installed on engine No. 1.

4.2 GROSS THERMODYNAMIC PERFORMANCE

During IET No. 4, the system was operated under conditions that permitted extensive gross partial power mapping of the system characteristics. Data were obtained over the range from full chemical fuel operation to reactor powers requiring as little as 300 pounds per hour fuel flow. No data were obtained without any chemical fuel assist, i.e., no data were taken on full nuclear power.

The method chosen for obtaining thermodynamic data was to hold a constant indicated power on the linear flux meter and to vary engine speed by changing fuel flow, stabilizing and recording data at four to six engine speeds per flux setting. The data for each constant flux run were plotted against engine speed to obtain readings at even speed values. These values were then cross-plotted for lines of constant engine speed. In all, 27 separate constant flux runs at reactor powers to air above 3 megawatts gave 115 usable primary readings, 52 with engine 5009 and 63 with engine 5010. In addition, sufficient data were obtained with no reactor power to permit confident interpolation in the power range below that covered by the partial-power-characteristics mapping. No significant deterioration in system performance was observed during the tests, which included 84 hours of operation at the same conditions that caused fuel element damage in IET No. 3.

The general day-to-day and engine-to-engine consistency of data during IET No. 4 was much better than for IET No. 3. This was particularly true of pressure transducer data. The improvement was presumably due to more thorough calibration techniques.

Thermocouple readings also showed good consistency, but comparisons of mean plate and air temperatures at the core exit with similar data from IET No. 3 were clouded by the number of inoperative thermocouples. At the beginning of this series of tests, 17 fuel tubes had no usable fifteenth- or sixteenth-plate thermocouples at the eighteenth stage and 10 fuel tubes had defective outlet air thermocouples. At the completion of the partial power mapping these numbers rose to 24 and 25 respectively. Thus the arithmetic average of the eighteenth-stage thermocouples and of the core outlet air thermocouples involved fewer measurements than in IET No. 3. The fuel element temperature-time history for IET No. 4 is given in references 7 and 8.

Faired representations of IET No. 4 data are given on Figures 4.1 through 4.6. Parameters are shown plotted for lines of constant engine speed against percent nuclear power. (Percent nuclear power is the ratio of the enthalpy rise across the reactor to the total enthalpy rise across the reactor plus the chemical combustor.) The data were corrected to standard day conditions at 5000 feet by using the normal jet-engine correction factors for ambient air temperatures and pressure.

Figure 4.1 is a plot of the arithmetic average of the measured eighteenth-stage plate temperatures and the arithmetic average of the measured reactor outlet air temperatures. Individual data points from IET No. 4 are shown together with the faired curves from IET No. 3 data, all for a single engine speed of 7000 rpm. This plot shows the plate temperature values were lower and the air temperature values higher than comparable IET No. 3 data.

Figures 4.2 and 4.3 are faired representations of IET No. 4 plate and reactor-discharge-temperature data for the complete speed range.

Pressure-drop data obtained from IET No. 4 tests showed good consistency. The wide scatter in IET No. 3 data did not warrant statements concerning relative values obtained during the two tests. Figures 4.4 and 4.5 present faired plots of IET No. 4 data for total pressure drop from compressor discharge to combustor inlet and from cold torus inlet to hot torus outlet.

Figure 4.6 is a plot of the power to air, which was computed using engine weight flow and the enthalpy rise of the air through the reactor. Since the reactor outlet air temperature was higher than in the IET No. 3, the power to air was also higher by a proportionate amount.

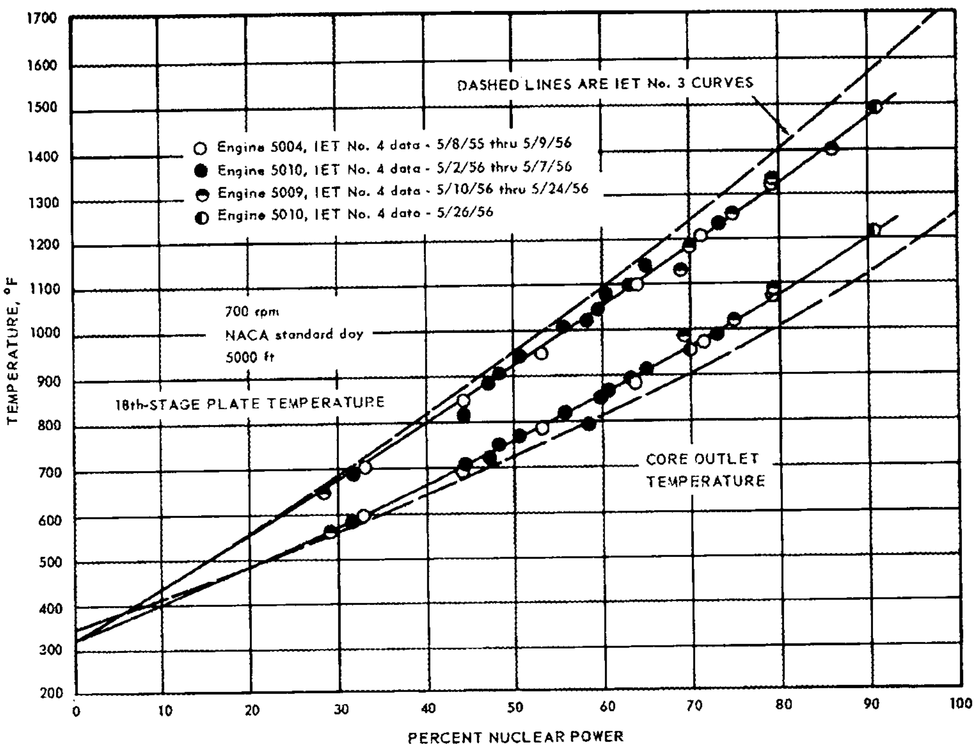

Fig. 4.1 -- Average 18th-stage and core-outlet temperatures

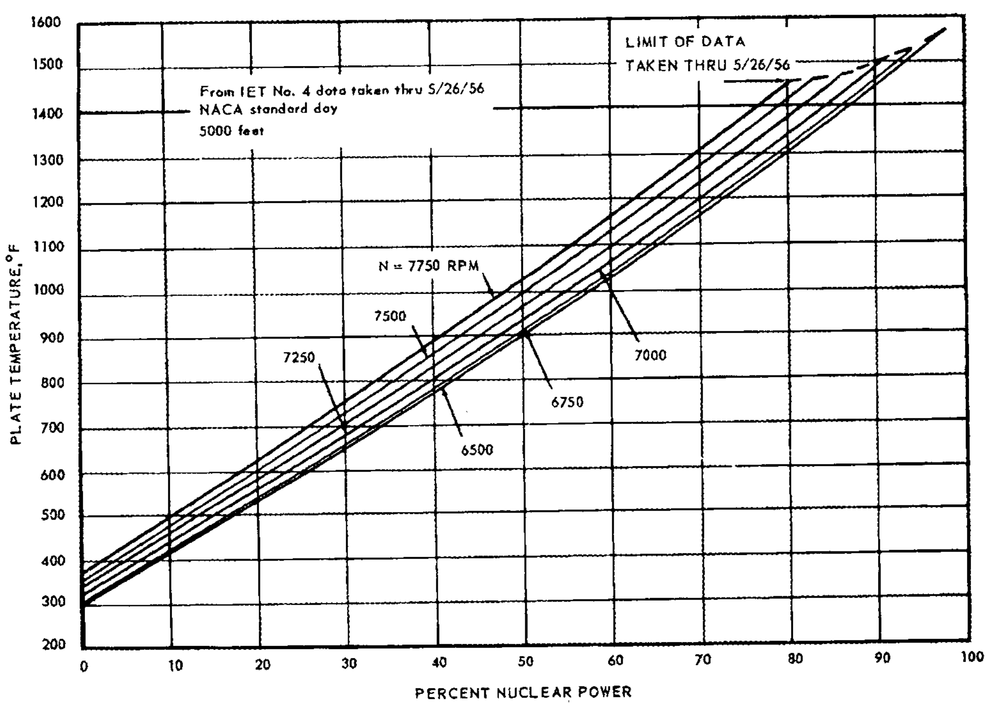

Fig. 4.2 -- Eighteenth-stage temperature versus percent nuclear power

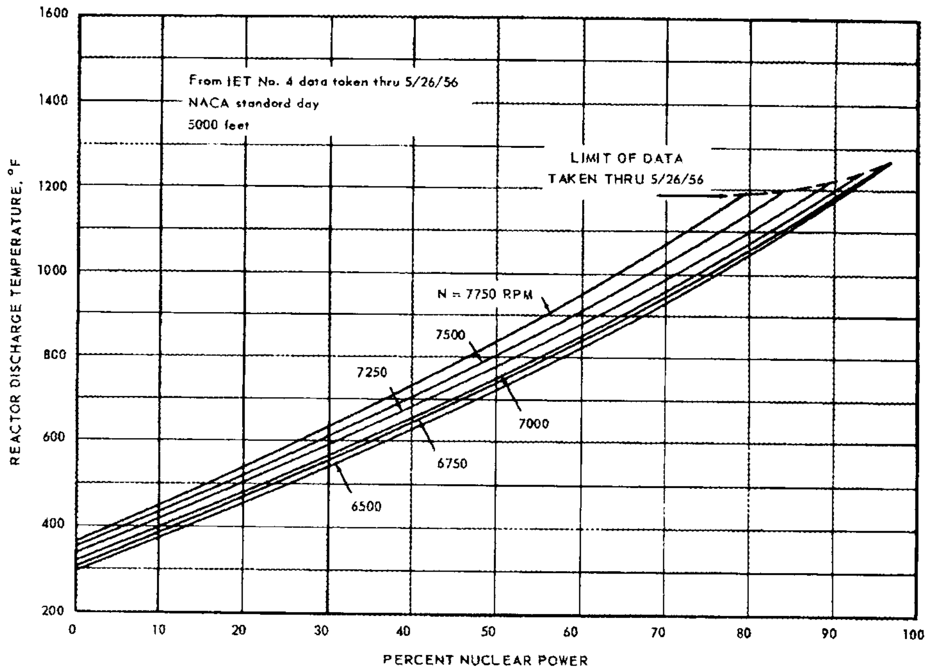

Fig. 4.3 – Reactor discharge temperature versus percent nuclear power

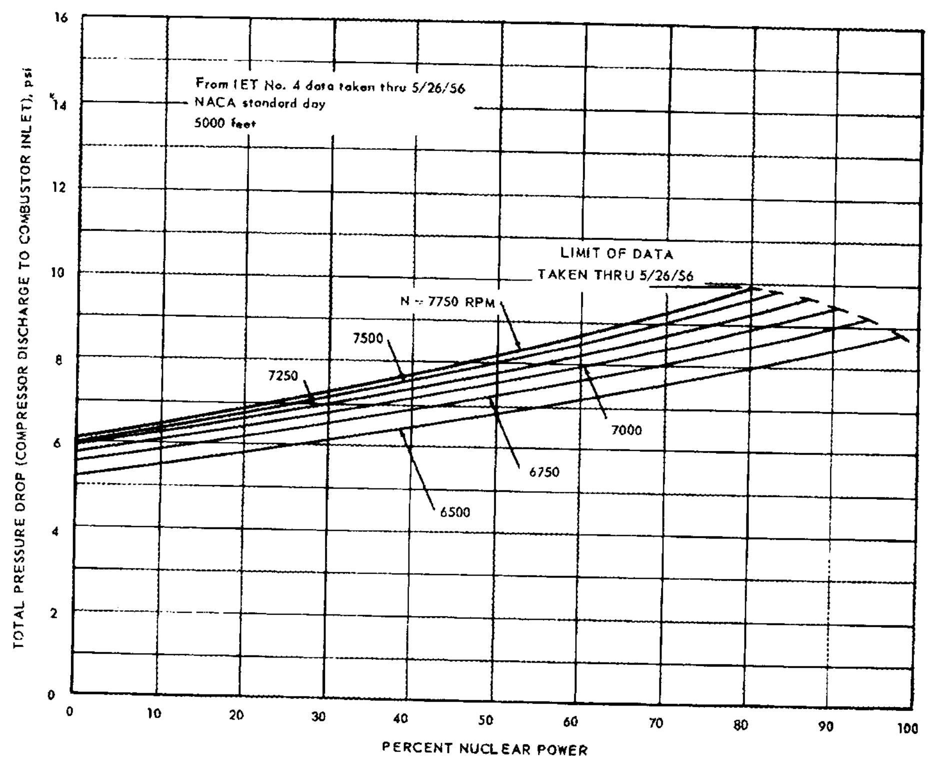

Fig. 4.4 – Total pressure drop versus percent nuclear power

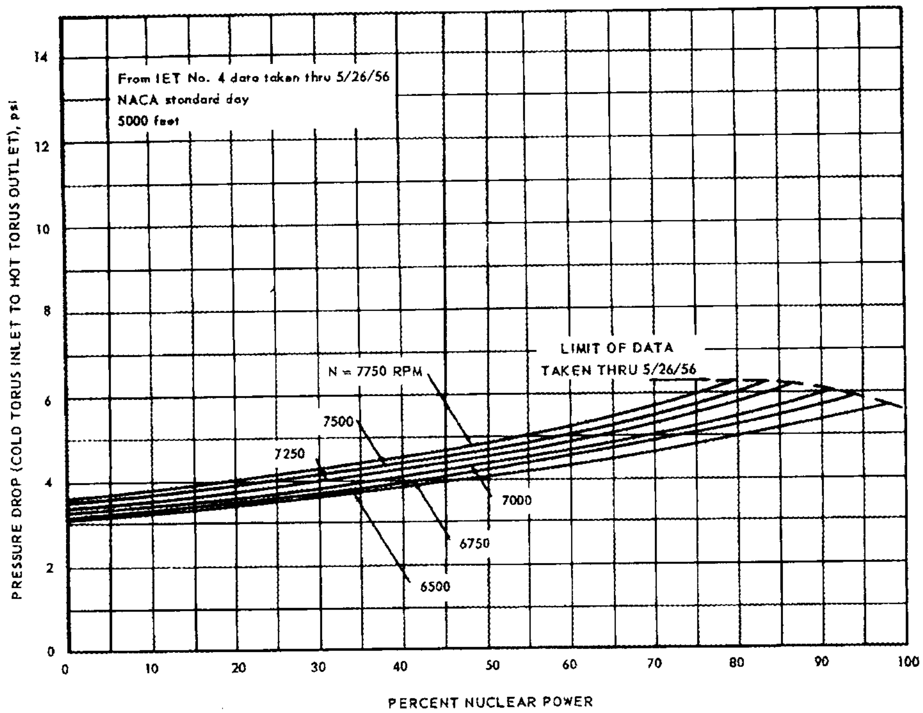

Fig. 4.5 – Pressure drop (cold torus inlet to hot torus outlet) versus percent nuclear power

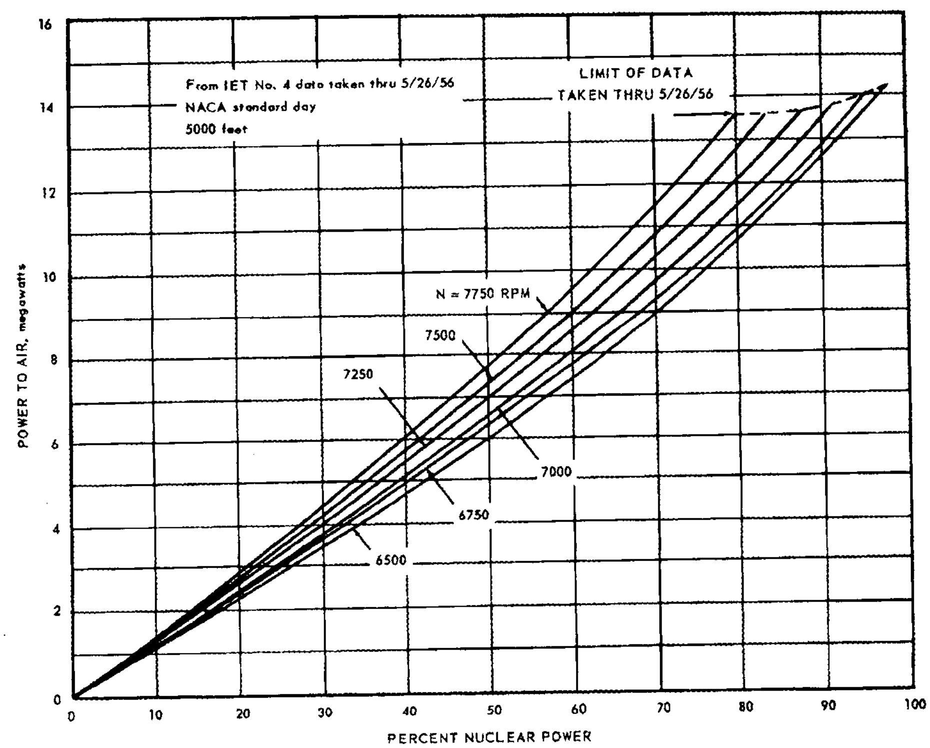

Fig. 4.6 – Power to air versus percent nuclear power

From the IET No. 3 data, analysis of the mean difference between the eighteenth-stage plate and the core exit air temperatures, T_{18}-$T_{3.54}$, showed that this difference was 100° to 150°F in excess of the expected value. However, the average T_{18} value was obtained from thermocouple readings taken from the fifteenth or sixteenth ring of the eighteenth-stage. Except for two fuel tubes, all plate thermocouples measuring the temperature of the eighteenth stage were located on these rings. A radial temperature traverse taken in a single tube is shown in Figure 4.7. These data show that the increase in temperature difference, T_{18}-$T_{3.54}$, above the expected value might have been due to a temperature perturbation in the outermost rings of the fuel element; that is, thermocouple readings did not measure the true average. This perturbation could have been caused by blocking of the airflow caused by the whole or partial collapse of insulation liners onto the outer plate. Thus, if insulation liner collapse were eliminated by modifications made in the liners for IET No. 4, the average indicated plate-to-air temperature differences should have been lower. As the following discussion shows, this appears to have been the case.

Table 4.3 shows typical data in IET No. 3 and IET No. 4. The IET No. 3 data contain the torus-exit temperature picked as a target temperature for the IET No. 4 endurance run. It is significant that the difference between core temperature discharge and torus-exit temperature was 75°F greater in IET No. 4 than in IET No. 3. This fact raised some question about the accuracy of the core-discharge reading and whether the indicated lowering in the plate-to-air temperature was caused by abnormally high core-discharge temperatures. This increased temperature difference could have been caused by leakage

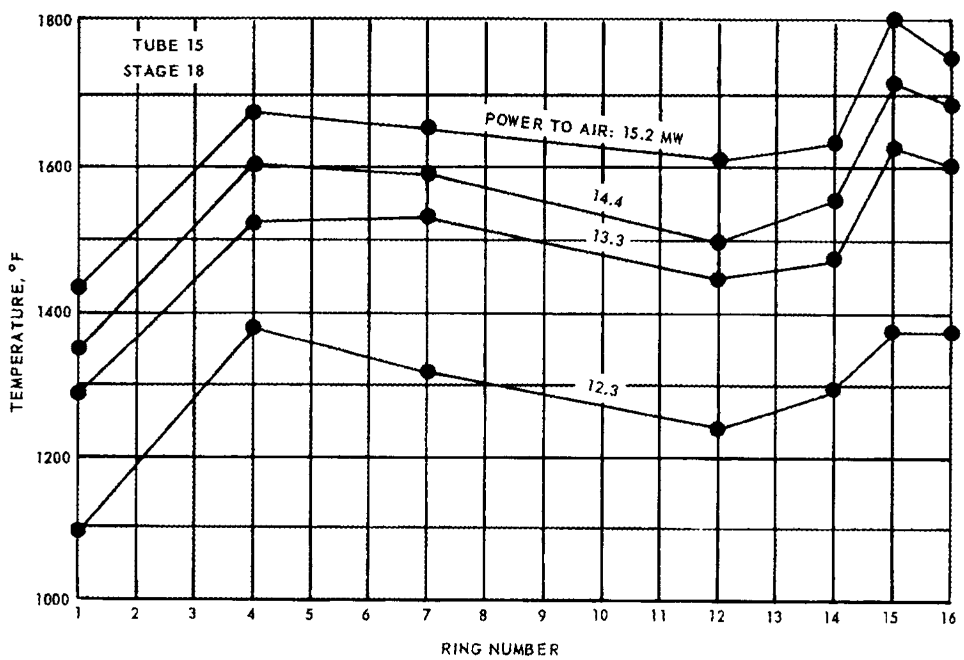

Fig. 4.7 – Fine radial temperature profile, IET No. 3

TABLE 4.3

HTRE NO. 1 DATA COMPARISON

	IET No. 3			IET No. 4		
	T	ΔT	ΔT	T	ΔT	ΔT
$T_{18, max}$	1975			1914		
		215			236	
$T_{18, avg}$	1760			1678		
		472			307	
$T_{3.54}$	1288		494	1371		404
		22			97	
$T_{3.65}$	1266			1274		
		31			20	
$T_{3.8}$	1235			1254		
					74	
$T_{4.0}$	1231			1328		
N		7096			7070	
Q		14,671			14,746	
%NP		100			92.76	

where:

$T_{18, max}$	Maximum 18th-stage plate temperature, °F
$T_{18, avg}$	Average 18th-stage plate temperature, °F
$T_{3.54}$	Core discharge temperature, °F
$T_{3.65}$	Hot torus exit temperature, °F
$T_{3.8}$	Unit combustor inlet temperature, °F
T_4	Turbine inlet temperature, °F
Q	Nuclear power to air, Btu/sec
%NP	(Nuclear Power) ÷ (Total Power) x 100
N	Engine speed, rpm

past the core in the CTF since such leakage would lower the temperature at the torus exit as a result of air at the compressor-discharge temperature mixing with the heated core air.

Table 4.3 shows, however, that the difference in temperature between the fuel-plate average and the torus exit was 90°F less than it was in IET No. 3; thus it appears that some gain was realized.

The table also indicates that during IET No. 4 operation ambient temperatures were sufficiently high that even though the temperature produced at the torus exit was the same as in IET No. 3, the engine operation was not self-sustaining (some chemical power was used). It should be noted, however, that 92 percent of the power delivered to the engine was produced by the reactor and that the unit combustor furnished only a 75°F-temperature rise to the system.

The thermodynamic performance data for the IET No. 4 runs are presented in Figures 4.8 through 4.11. Figure 4.8 presents a comparison of gross thermodynamic performance of fuel cartridges for IET No. 3 and IET No. 4. For convenience in comparison, the IET No. 3 data points have been duplicated in this figure. The mean straight line through the IET No. 4 data predicted plate-to-air temperature differences for all runs to be within ± 25°F. Figure 4.8 also indicates that for a given abscissa value the temperature difference (T_{18}-$T_{3.54}$) in IET No. 4 was approximately 73 percent of the IET No. 3 value.

The IET No. 4 data fall almost precisely on the minimum predicted fuel-element-temperature line. This prediction line was based on an assumption of ideal behavior of all variables affecting temperature, e.g., airflow distribution, fine-radial-power flatten-

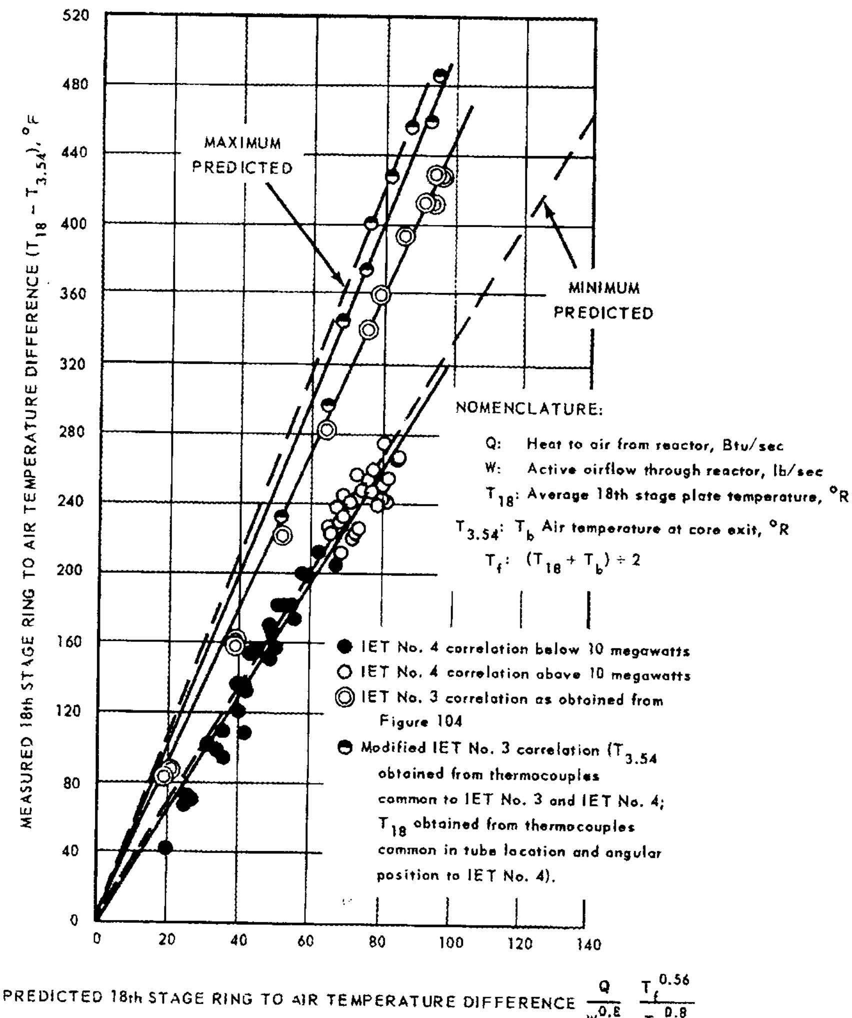

Fig. 4.8 – Comparison of gross thermodynamic performance of fuel cartridges for IET No. 3 and IET No. 4 using plate thermocouples common in tube location and angular position

ing, heat transfer coefficient, longitudinal power curve, etc. The maximum temperature predicted was based on the assumption of detrimental effects such as observed inaccuracies in power distributions and fuel element structure and loading.

It is possible that the lower IET No. 4 value of T_{18}-$T_{3.54}$ could be an incorrect interpretation, because the temperature averages used in IET No. 4 were different from those used in IET No. 3 and because 13 of the 37 fuel cartridges were replaced. To justify this interpretation, a recalculation of the IET No. 3 data was plotted in which $T_{3.54}$ was obtained from an average of just those thermocouples that were used in IET No. 4 and T_{18} was obtained from those plate temperatures common in tube location and in angular position in the tube to those of IET No. 4. The results of such a calculation indicated still higher values of the temperature difference, T_{18}-$T_{3.54}$, in the IET No. 3 runs.

In Figure 4.9, for both IET No. 3 and IET No. 4 runs, $T_{3.54}$ was again obtained from an average of just those thermocouples that were used in IET No. 4 and T_{18} was obtained from an average of eight eighteenth-stage plate temperature readings and fuel cartridges

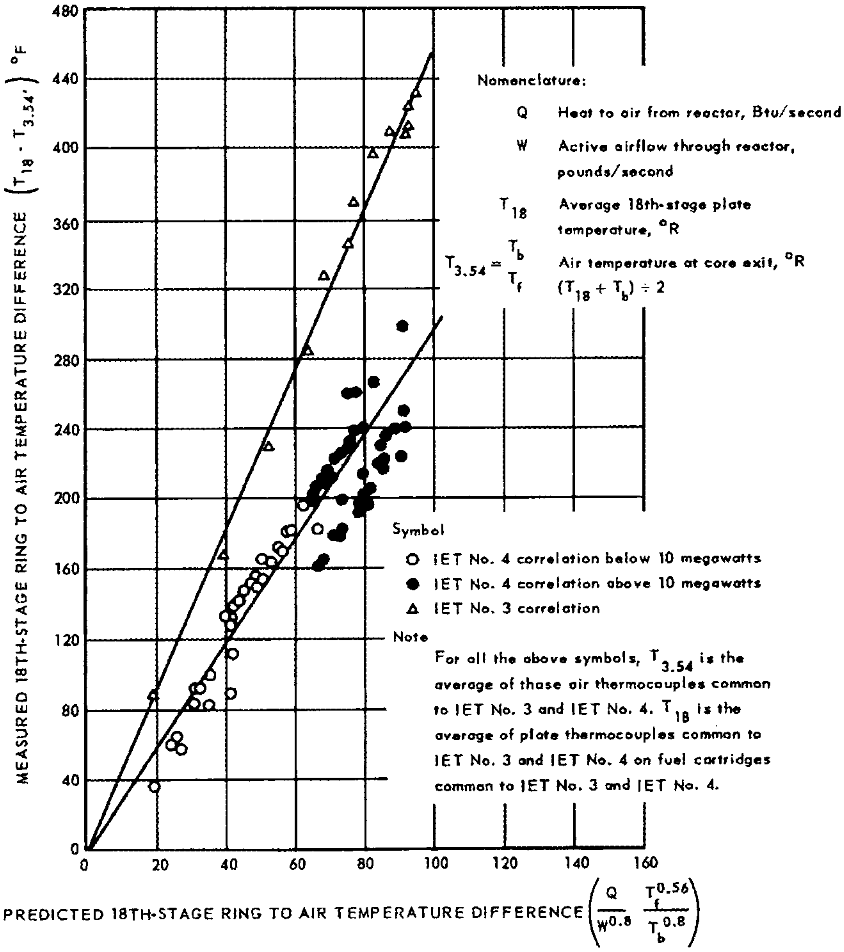

Fig. 4.9 – Comparison of gross thermodynamic performance of fuel cartridges in IET No. 3 and IET No. 4 using plate thermocouples on fuel cartridges used in both test series

common to both IET No. 3 and IET No. 4. Although there was more scatter, essentially the same results were obtained. (The temperature difference in IET No. 4 was approximately 70 percent of the IET No. 3 value for the abscissa coordinate position.) These results indicated that the substitution of 13 new fuel cartridges in IET No. 4 had little or no effect on T_{18} or $T_{3.54}$.

In a similar manner of averaging temperatures, Figures 4.10 and 4.11 show the temperature difference, T_{18}-$T_{3.49}$, as a function of $T_{3.54}$-$T_{3.49}$, where $T_{3.49}$ is the core inlet temperature. In Figures 4.10 and 4.11, the method of averaging temperatures is the same as in Figures 4.8 and 4.9. Figures 4.10 and 4.11 indicate that for a given value of plate-to-inlet-air temperature difference, T_{18}-$T_{3.49}$, approximately 15 percent more heat was added to the air in IET No. 4 runs than in IET No. 3.

In order to ascertain differences in operating temperature between fuel cartridges of the A2 core, an average eighteenth-stage plate temperature was obtained for each of 20 fuel cartridges from IET No. 4 data.

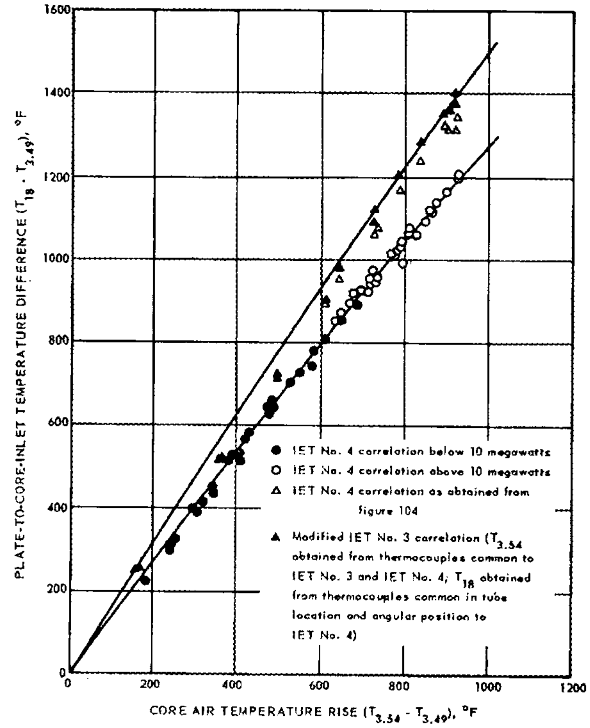

Fig. 4.10 – Comparison of actual to available core temperature rise in IET No. 3 and IET No. 4 using plate thermocouples common in tube location and angular position

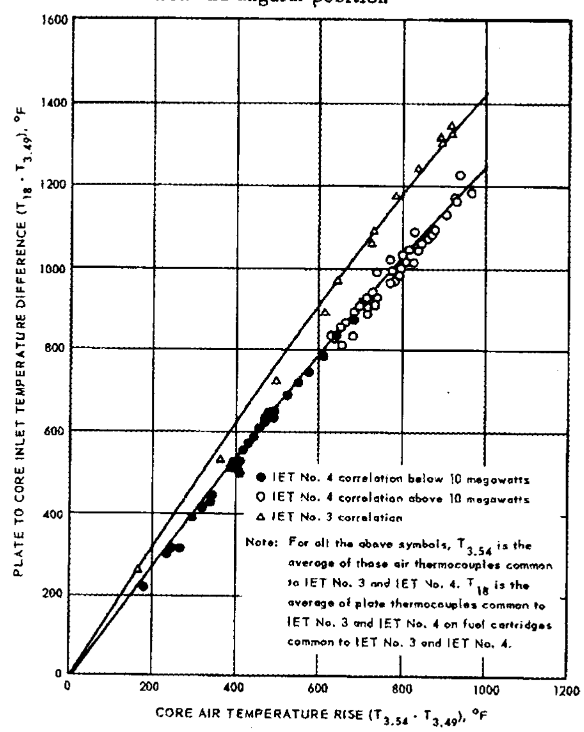

Fig. 4.11 – Comparison of actual to available core temperature rise in IET No. 3 and IET No. 4 using plate thermocouples on fuel cartridges used in both test series

At the start of IET No. 4 operation, only 20 operable thermocouples (one for each fuel tube) were measuring the trailing-edge temperature on either the fifteenth or sixteenth fuel plate in the eighteenth stage. After 75 runs, the plate thermocouple in tube 26 failed. By the completion of IET No. 4 tests, only six thermocouples were in operation. Consequently, to get indications of the operating temperature level of the greatest number of fuel cartridges, only the first 75 runs of IET No. 4 were used for obtaining averages. These are shown in Figure 4.12 by the hollow circles.

Among the 75 runs was a set of 38 runs for which all 20 thermocouples were nominally reading above 1000°F. An average was made of these 38 runs for each of the 20 fuel cartridge thermocouples. These are shown by the solid circles in Figure 4.12.

It can be seen that both curves are similar and that differences between fuel tube plate temperatures were greater during higher temperature operations. The largest difference between solid point readings was (for tube 6 minus tube 35) 1303° - 911° = 392°F. Since the remainder of the IET No. 4 tests were predominantly above the power level indicated by the black points, it was concluded that temperature differences between tube 6 and tube 35 were in excess of 400°F.

No readings were available for 17 fuel tubes. As a consequence, it is possible that some temperature differences were in excess of the maximum indicated in Figure 4.12. An over-all compilation of the temperature differences and further discussion are given in reference 8.

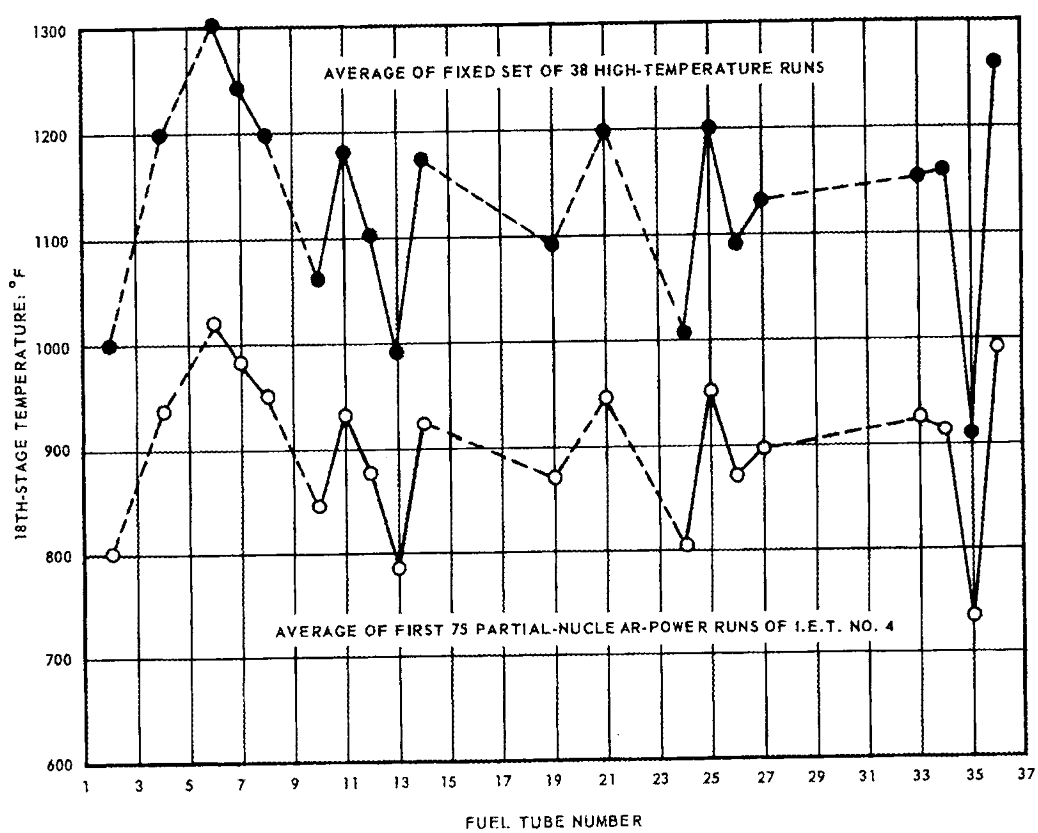

Fig. 4.12—Comparison of average 18th-stage plate temperatures

Figure 4.13 shows data from both IET No. 3 and IET No. 4 for heat loss to the moderator. Although both sets of data indicated scatter, the data trend indicates that the heat loss to the moderator in IET No. 4, about 9 percent, increased approximately 25 percent over that in IET No. 3. This increase in heat loss resulted from the removal of insulation from the 13-inch tail assembly at the beginning of IET No. 4. The insulation was removed to insure that the sleeve would not expand against the core tube and create a rear seal with resulting pressure-differential buildup.

Because of the large amount of scatter in the data shown in Figure 4.14, little interpretation can be obtained from this plot. The scatter was probably caused by thermal-lag effects in the large water capacity of the shield system. The figure does indicate, however, that the heat loss to the shield was of the order of 5 percent of the heat release to the engine airflow.

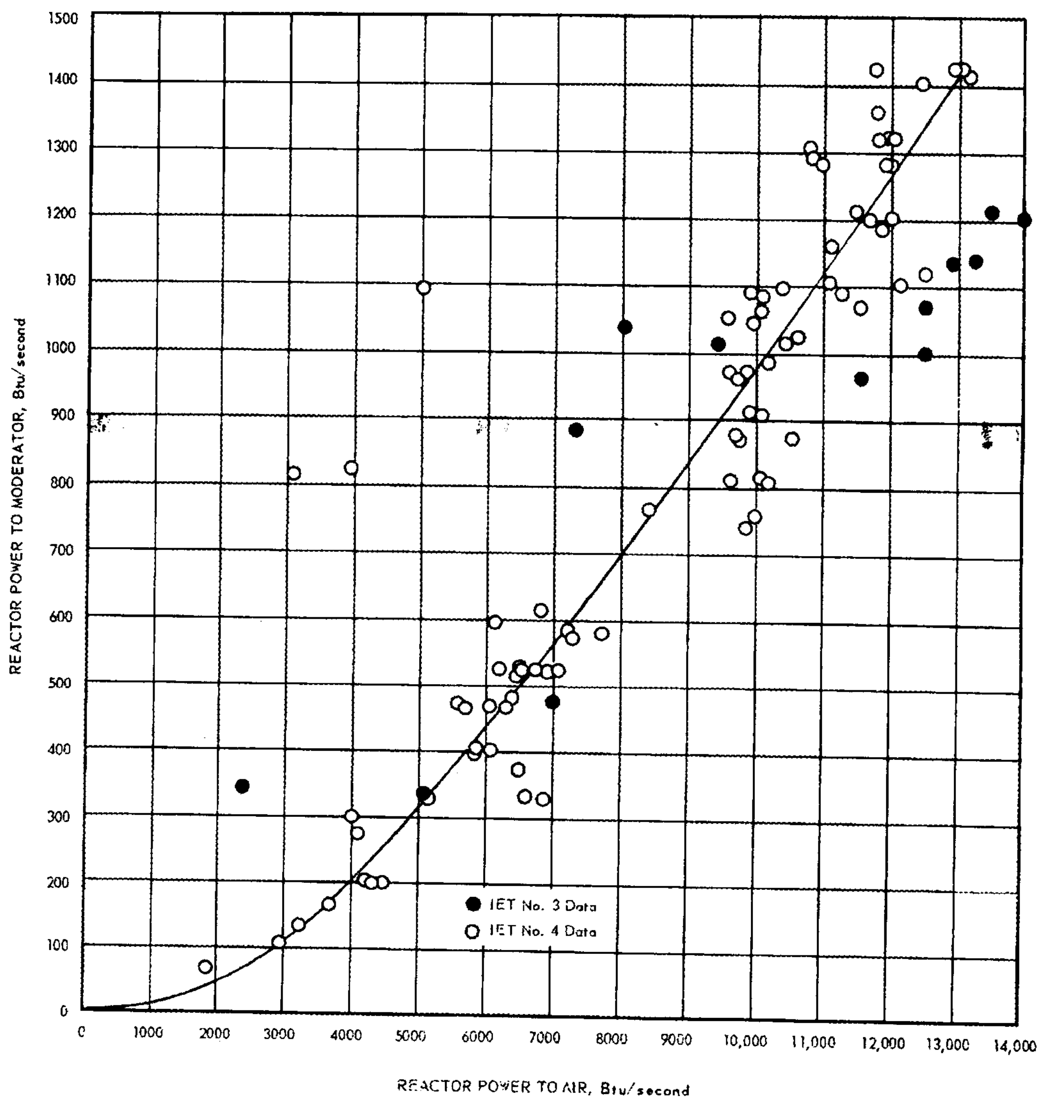

Fig. 4.13 – Core heat loss to moderator

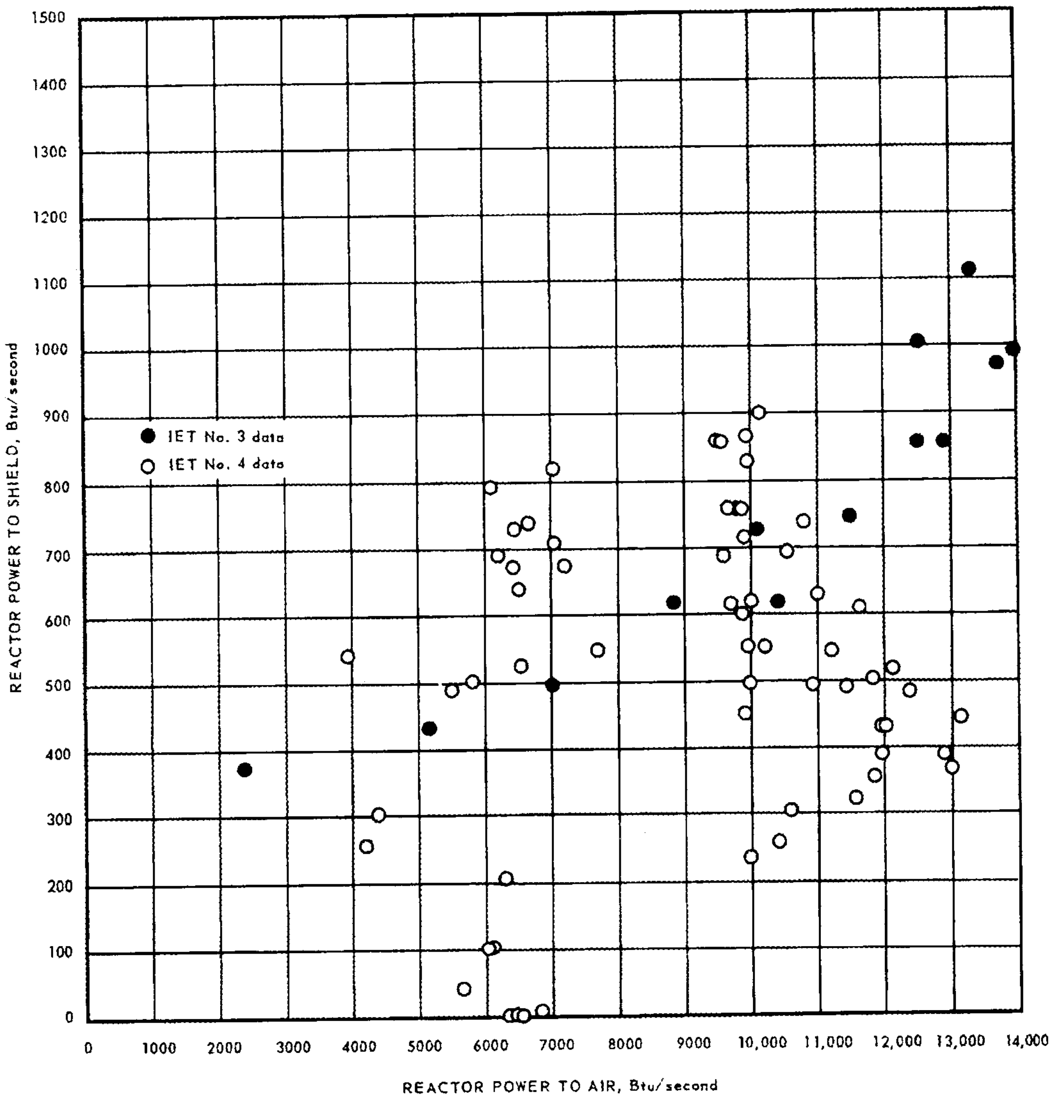

Fig. 4.14 – Core heat loss to shield

The plate-temperature patterns shown in Figure 4.15 were compiled for all fuel cartridges that had operable thermocouples at the start of IET No. 4 operation on both the outermost fuel plate of stage 11 and the outermost fuel plate of stage 18. Most of these temperature patterns showed sharp discontinuities in behavior. It is unlikely that these discontinuities were caused by a change in control rod position. For example, tube 27, which showed the greatest discontinuity, was next to a rod that was situated in the outermost frame and was withdrawn throughout the entire IET No. 4 test series. It also seemed unlikely that these discontinuities could have been caused by insulation-liner collapse, since in the case of tube 27 there were two distinct discontinuities and the second one fell just a little below the original data trend. One possible explanation for this temperature behavior is malfunctioning of plate thermocouples.

The correlation of the air temperature loss from the core exit to the hot torus exit, as shown in Figure 4.16, was strictly empirical. However, the correlation was such that most of the data, before apparent insulation failure, fell within 10°F of the mean correlation line. In compilation of the ordinate and abscissa values used in this figure, an average value for $T_{3.54}$ was obtained from only those thermocouples that remained operative throughout the duration of the IET No. 4 runs. Thus a consistent $T_{3.54}$ average was obtained. A calculation indicated that the 50 percent increase in heat losses during the last 3 weeks of operation could be accounted for by a 15 percent loss of insulation of the inside of the vertical risers leading to the hot torus.

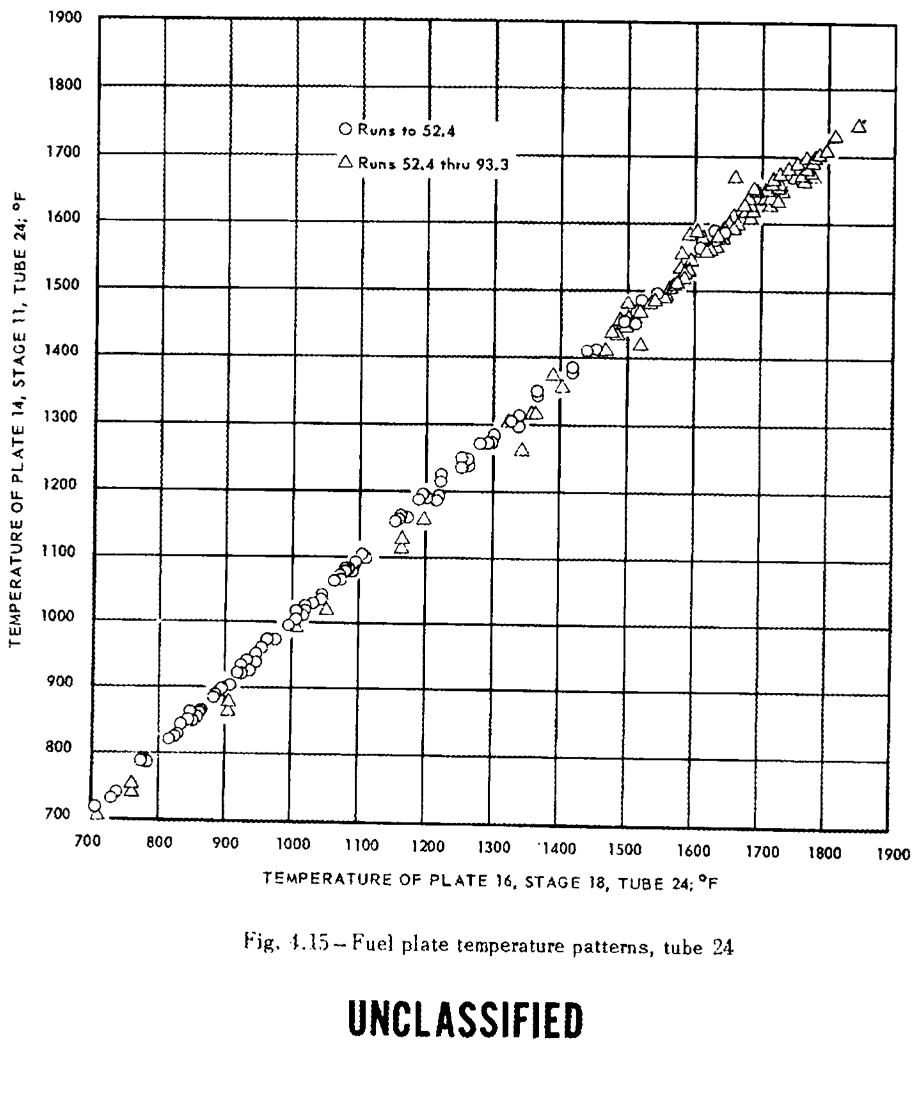

Fig. 4.15 – Fuel plate temperature patterns, tube 24

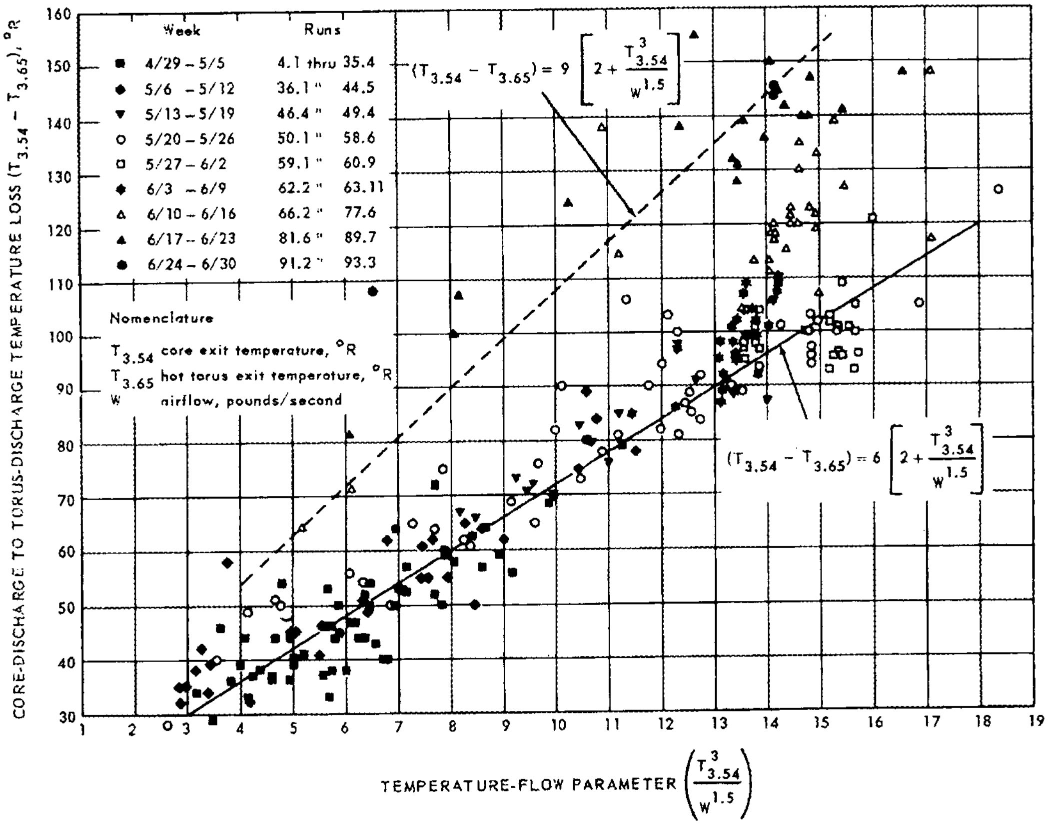

Fig. 4.16 – Exit ducting heat losses

4.3 XENON EXPERIMENTS

During IET No. 4 tests, frequent checks of the excess reactivity of the A2 reactor were made. Initially there was some uncertainty as to whether some of the cartridges had securely latched, and these checks were intended primarily to note any gross shifting of fuel within the core.

The initial check indicated an excess reactivity of 4.16 percent. This check was made with no airflow in the core and with the reactor just critical. As with all such measurements, the value had been corrected to a base moderator outlet temperature of 95°F. A subsequent check indicated an excess of 4.10 percent with engine No. 2 operating at 6565 rpm, approximately 27 psi air pressure on the core. No operating time for the reactor was logged during the time between these checks. These values compare favorably with the 3.65 percent excess measured for the IET No. 3 series tests, with the thick insulation liners in the reactor.

After the first extended operation at high power, 34.3 megawatt-hours, it was noted that the excess reactivity had decreased to 3.46 percent at 20.5 hours after shutdown. Careful checking of the rods indicated that all were latched and operating. After an additional 19.5 hours shutdown, the excess reactivity had again increased to 4 percent.

The only logical explanation of this effect lay in xenon poisoning. However, the magnitude of the decrease in excess reactivity was at least twice the best value obtainable from extrapolation of data presented in section 2.2. Consequently, experiments were planned and conducted for the purpose of determining the xenon concentration during operation and after shutdown.

For the first test, the reactor was allowed to remain idle for a period of 90.5 hours. This procedure was followed to assure adequate time for decay of residual xenon from any previous operation.

The reactor was again brought to criticality with one blower on high speed. The excess reactivity was found to be 3.90 percent. A second check taken with no airflow gave a value of 3.93 percent, and a third check with engine No. 1 operating at 6060 rpm showed a value of 3.88 percent.

When weather conditions were favorable, the reactor was taken to power. The reactor was maintained at a power of 8.4 megawatts for 20 minutes while the erratic behavior of some electronic equipment was checked. After it was determined that sufficient equipment was operating properly, the reactor was taken to a nominal power of 11.3 megawatts. Operation was steady at this power until unfavorable winds necessitated a shutdown. The reactor was maintained at a power of 10^{-3} NF and critical rod positions recorded for approximately 17 hours after reactor shutdown.

Erratic operation of the ion and fission chamber circuits caused two scrams after the reactor shutdown. With the exception of these two scrams, operation was without incident. Resulting data for the first tests are shown in Figure 4.17. The dotted curve on Figure 4.17 indicates the calculated xenon poisoning (see references 9, 10, and 11). It is of interest to note that the theoretical value was only about 38 percent of the measured value at the peak of the curve.

During the second xenon poisoning experiment, considerable instrumentation difficulties were encountered in bringing the reactor to power. The reactor scrammed very shortly after the power level steadied out at 15.9 megawatts. This period of operation accumulated 7.35 megawatt-hours of operation. The reactor was again started up and reached full power. Engine No. 2 was run at 7070 rpm throughout this operation.

Operation continued steady at 15.9 megawatts until a reactor scram terminated the power operation. The reactor was subsequently maintained at a power of 0.5 percent NF to assure that the reactor was well above the photoneutron level. This operation continued until the reactor was taken to a power of 16.4 megawatts and again scrammed. After two successive power operations, a final scram ended the xenon experiments.

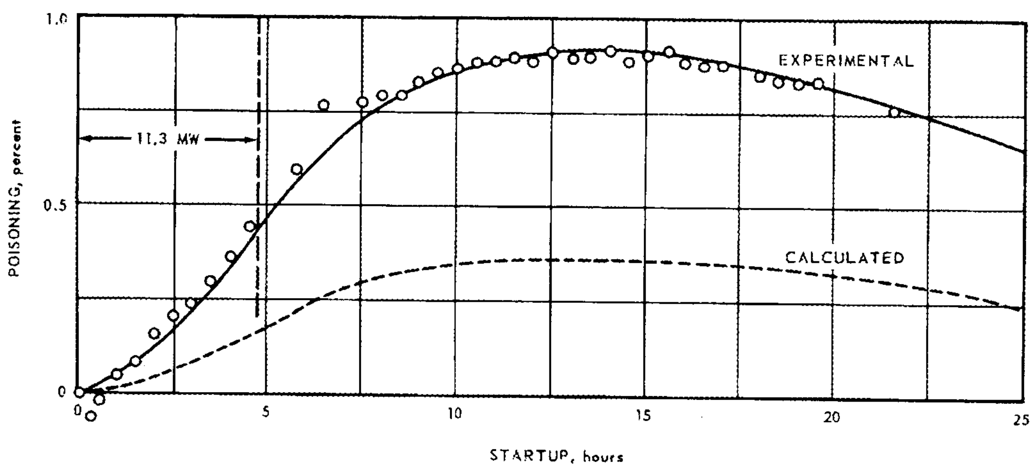

Fig. 4.17 – Observed xenon poisoning versus time for 4.75 hours operation at 11.3 megawatts

The results of these tests are shown in Figure 4.18. Because of the instrumentation difficulties and the inadvertent scram that occurred during the first part of the experiment, a weighted zero time was chosen and probably entails some error. The decrease in the reactivity at 21 hours after startup was caused by pressurization of the core when the engine was started. The increased reactivity following the scram at 27 hours after startup was unexplained. It was tentatively assumed that a rod was unlatched during a portion of the experiment from 8 hours to 28 hours after startup. This would have lowered that portion of the curve by the amount of rod drop, which was probably 0.40 percent. The dotted curve on Figure 4.15 accounts for these corrections.

The observed xenon poisoning at the conclusion of testing was 2.6 and 2.3 times larger than the calculated values for tests 1 and 2 respectively. Since the uncertainty in flux levels should not be greater than 20 percent, it appeared that the method of calculation was in error. Another method, utilizing IET No. 4 data, was later developed for predicting xenon poisoning. These calculations indicated that correction factors would be applied to the standard calculating procedure. These correction factors were determined from the ratio of experimental data to calculated data at a particular time for the two xenon tests performed during IET No. 4. These ratios are plotted as a function of time, and the mean value of the two resulting curves gives a pseudo correction factor. Figure 4.19 shows curves of the ratios of the experimental value to the calculated values as a function of time measured from startup. The dotted curve represents the mean value between the two solid curves and is the curve used to obtain the correction factors. The

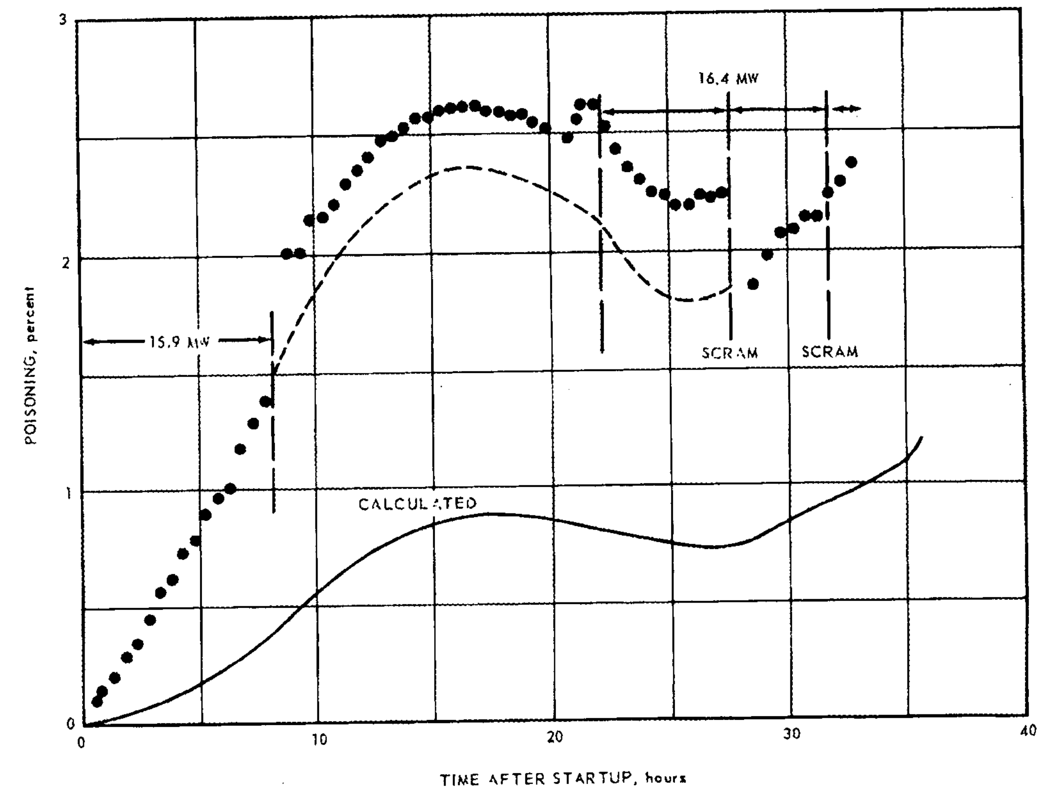

Fig. 4.18 – Observed xenon poisoning versus time for 8.2 hours operation at 15.9 megawatts followed by 14 hours shutdown and 10.75 hours operation at 16.4 megawatts

analytical significance of the difference between the two solid curves is not known, although it seems to be partially a function of the total power and operating time.

Figure 4.20 shows the xenon poisoning history for runs performed June 20 through 23 as a function of time measured from startup on June 20. These data have been corrected to an excess reactivity of 1.974. The corrected curve fits the experimental data quite well.

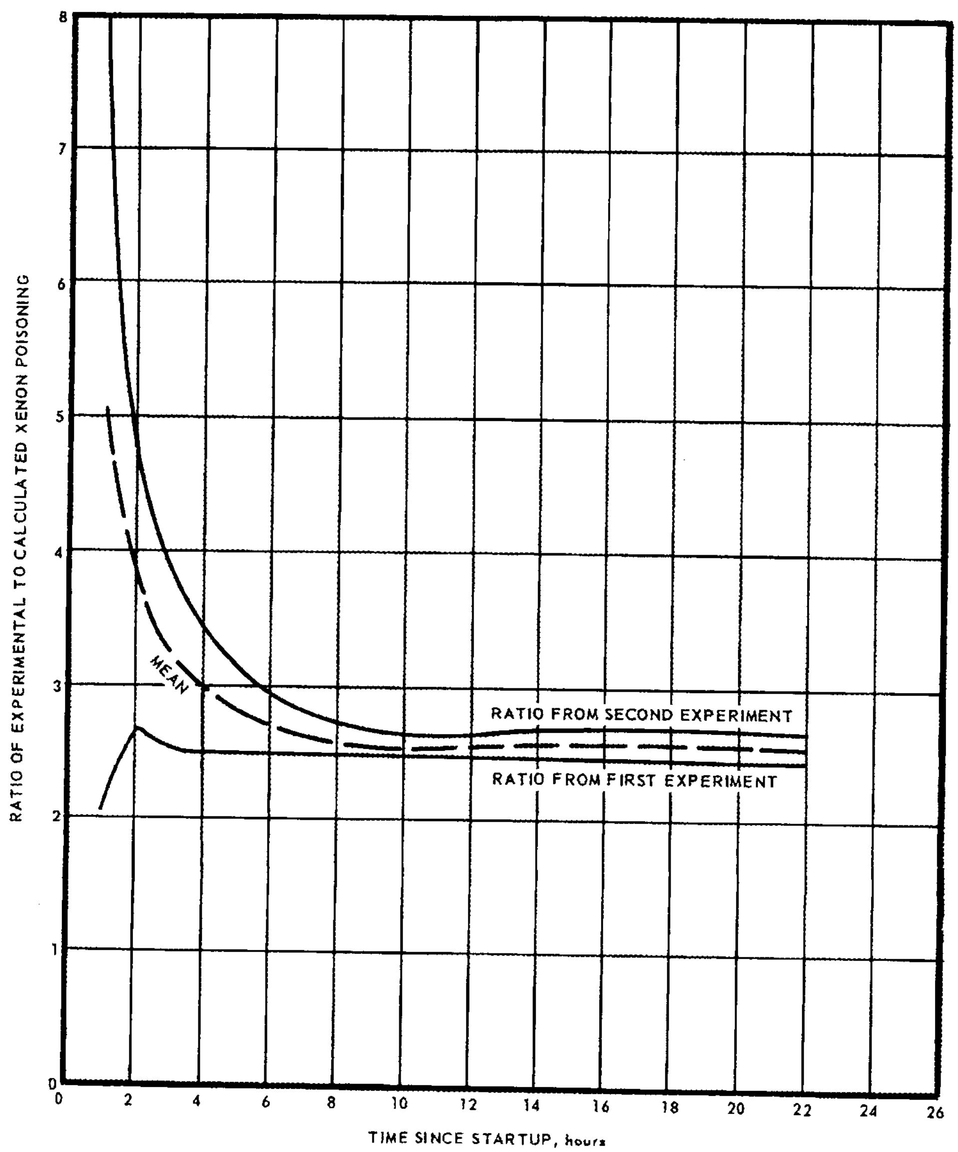

Fig. 4.19 – Ratio of experimental xenon poisoning to calculated xenon poisoning versus time

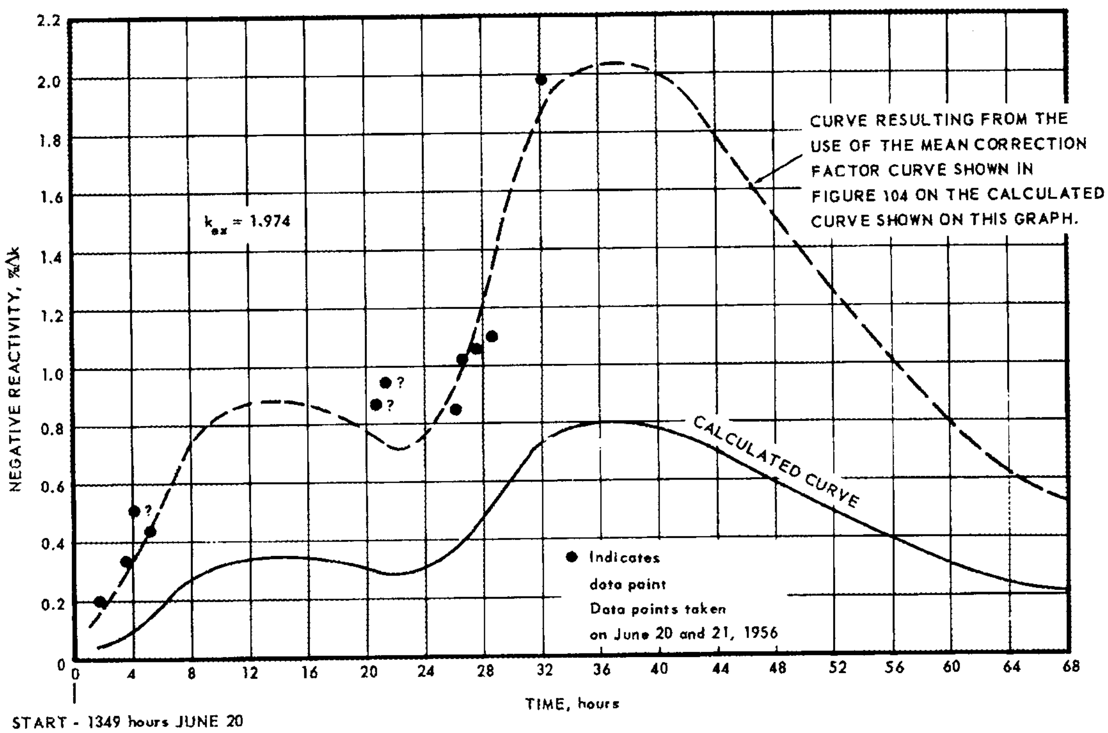

Fig. 4.20 – Plots of xenon buildup and decay versus time from initial startup

4.4 EXHAUST-GAS ACTIVITY

A probe was inserted in the exhaust-gas duct at the IET, and samples of gas were passed through filters to collect particles. The following particle characteristics were determined:

1. The mean diameter of carbon particles was 0.9 micron.
2. The mean mass diameter of carbon particles was 3 microns.
3. A mean diameter of 0.7 micron was found for a mixture of particles when the engines were operating and the reactor was at high nuclear power. A mass mean diameter of 7 microns was found for this distribution, with the assumption that all particles are of the same density. A radioautograph of the filter showed approximately 20 radioactive particles per square inch out of approximately 10^8 total particles per square inch.

Air samples were drawn through a portable filter at various distances from the stack. Fallout from the exhaust-gas plume tended to increase with distance from the stack. Samples of I^{131} collected from the stack gas with an iodine scrubber indicated that no appreciable hazard was created by this isotope although detectable amounts of gaseous I^{131} were present in stack gases under those operating conditions. The I^{131} output in the gaseous state could be increased by a factor of 10^3 without the downwind dose approaching maximum permissible concentration values if reasonable mixing occurred. Most of the iodine in the stack appeared to be in the gaseous state except when some absorbing agent such as carbon from the chemical fuel or zinc chloride and carbon from smoke bombs was added. Then iodine in particulate form became predominant. The iodine absorption phenomenon was localized for any part of the exhaust-gas system. Cooling of the gases appeared to be important in the design of a particulate removal system.

During the high-power operation of the A2 reactor in IET No. 4, tests were conducted to correlate IET exhaust-gas activity to fuel flow, reactor power, and reactor plate temperature. The tests were conducted by setting constant chemical-fuel flow and constant reactor flux while varying the reactor plate temperature by changing the position of the jet engine nozzle. For each setting of these parameters, stack activity was determined by measuring the count rate of filters to which a portion of the stack gas flowed. The total particulate activity was computed by proportioning the filter-sample flow reading to the total volumetric flow of gases up the stack. The sample filter flow was regulated to provide isokinetic sampling. In this manner, measurements were taken to separate the effects of such parameters as power, fuel flow, and temperature. Results of the tests are presented in the following paragraphs.

An increase in reactor power from 11.7 to 13.5 megawatts, with a fuel flow of 1080 pounds per hour at mean plate temperatures of 1326° and 1335°F and maximum plate temperatures of 1620° and 1603°F, showed no measurable increase in activity. The total activity was computed as 24 curies per hour for each condition. A similar increase of reactor power from 13.5 to 15.5 megawatts, with a fuel flow of 930 pounds per hour at mean plate temperatures of 1408° and 1474°F and maximum plate temperatures of 1676° and 1773°F, showed a slight increase in activity from 25 to 33 curies per hour. Since plate temperature was also inadvertently increased, this activity increase may not have been entirely due to power effects.

Reduction of fuel flow from 1080 to 930 pounds per hour at a reactor power of 13.5 megawatts, mean plate temperatures of 1335° and 1332°F, and maximum plate temperatures of 1603° and 1600°F, gave a slight decrease in activity from 24 to 16 curies per hour. A similar change from 930 to 730 pounds per hour at a reactor power of 15.5 megawatts, mean plate temperatures of 1474° and 1496°F, and maximum plate temperatures of 1773° and 1805°F, showed a decrease in activity from 33 to 27 curies per hour. Detailed results of these tests are given in reference 12.

The Effect of Plate Temperature

At a reactor power of 11.7 megawatts and a fuel flow of 1080 pounds per hour, with an increase of mean plate temperature from 1207° to 1326°F and a corresponding increase in maximum plate temperature from 1395° to 1620°F, values of activity ranged from 23 to 26 curies per hour. At a power of 13.5 megawatts and a fuel flow of 930 pounds per hour, with an increase of mean plate temperature from 1332° to 1408°F and a corresponding increase in maximum plate temperature from 1600° to 1676°F, values of activity ranged from 16 to 25 curies per hour.

At a power of 15.5 megawatts, a fuel flow of 730 pounds per hour, an increase in mean plate temperature from 1496° to 1538°F, and a corresponding increase in maximum plate temperature from 1805° to 1893°F, activity increased from 27 to 70 curies per hour. At this same fuel flow and reactor power, further increase in mean plate temperature to 1605°F with a corresponding maximum plate temperature of 1942°F gave an increase to 186 curies per hour. Table 4.4 summarizes the results of these tests.

The particulate activity showed no significant dependency on plate temperature at low temperature levels but increased sharply at high temperatures. The activity showed a moderate dependency on fuel flow, decreasing with reduction of fuel flow. The effect of power on activity was not detectable at low powers but showed minor increase at the maximum power tests. Therefore it is concluded that the temperature level is by far the most critical parameter.

TABLE 4.4

STACK ACTIVITY TEST DATA

Sample No.	Mean Plate Temperature, °F	Highest Plate Temperature, °F	Particulate Activity, curies/hr	Stack Gas Temperature, °F	Fuel Flow, lb/hr	Total Reactor Power, mw
70	1207	1395	26	520	1080	11.7
71	1223	1476	23	525	1080	11.7
72	1326	1620	24	540	1080	11.7
73	1335	1603	24	530	1080	13.5
74	1332	1600	16	525	930	13.5
75	1361	1600	22	540	930	13.5
76	1408	1676	25	550	930	13.5
77	1474	1773	33	550	930	15.5
78	1496	1805	27	560	730	15.5
80	1538	1893	70	585	730	15.5
81	1605	1942	186	600	730	15.5

4.5 POSTOPERATION EVALUATION OF FUEL CARTRIDGES

At the conclusion of the IET No. 4 test series, the CTF was returned to the hot shop and the A2 core was removed. Inspection revealed that cartridges 4, 9, and 20 had become unlatched and had dropped several inches. Cartridge 33 fell completely out of the core and remained in the cocoon during the core removal operation. In addition, the tail assembly was missing from cartridge 9 and was not found until later.

Complete unloading of the fuel cartridges required 6 two-shift working days. It was not possible to strip cartridges 4, 9, and 20 on the tube-loading machine because the tail assembly had been pulled off the first two and was missing from the third. These three cartridges and cartridge 33, which was wedged tight in the liner, had to be stripped in the Radioactive Materials Laboratory.

Damage to the cartridges consisted mainly of rail dents with some quadrant dents and some broken rails. Cartridges 5, 20, and 24 were the three most severely damaged. Of these, cartridge 5 suffered the most damage; portions of rings were missing from eight stages, 11 through 18. Figure 4.21 shows the entire cartridge; Figure 4.22 shows a closeup of stage 18. Photos of other typical cartridges are shown in references 13 and 14. It was significant that the burnout appeared to result from high-temperature oxida-

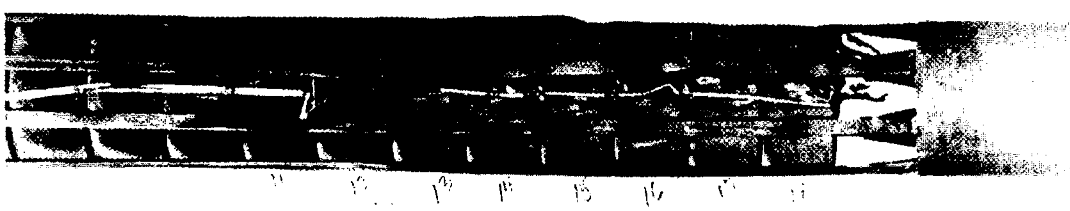

Fig. 4.21 – Fuel cartridge 223, tube 5

Fig. 4.22 – Damage to stage 18, cartridge 223, tube 5

tion rather than from fusion as noted after IET No. 3 operation. Cartridge 24 displayed a heavily oxidized area on stage 15, as shown in Figure 4.23. Circumferential striations corresponding to the corrugations on the insulation sleeve were plainly visible. This indicated that insulation-sleeve collapse was still occurring. Cartridge 20 was heavily oxidized on stages 10 and 11, and small portions of the heavily oxidized area were gone. Figure 4.24 illustrates the damage to this cartridge. A number of cracks extended from the holes, indicating the brittleness of the heavily oxidized area.

While it was not conclusively proved that insulation-sleeve collapse was the cause of the fuel cartridge damage, this hypothesis was strengthened by the fact that redesigned insulation sleeves completely eliminated this type of damage during IET No. 6.

4.6 POSTIRRADIATION LEVELS

Postirradiation readings of radiation levels at various points in the D101A2 system were taken in periods when the reactor was not operating. Sample readings from the Core Test Facility, the control rods, and the A2 core are discussed in pages 219 through 227 of reference 15.

UNCLASSIFIED

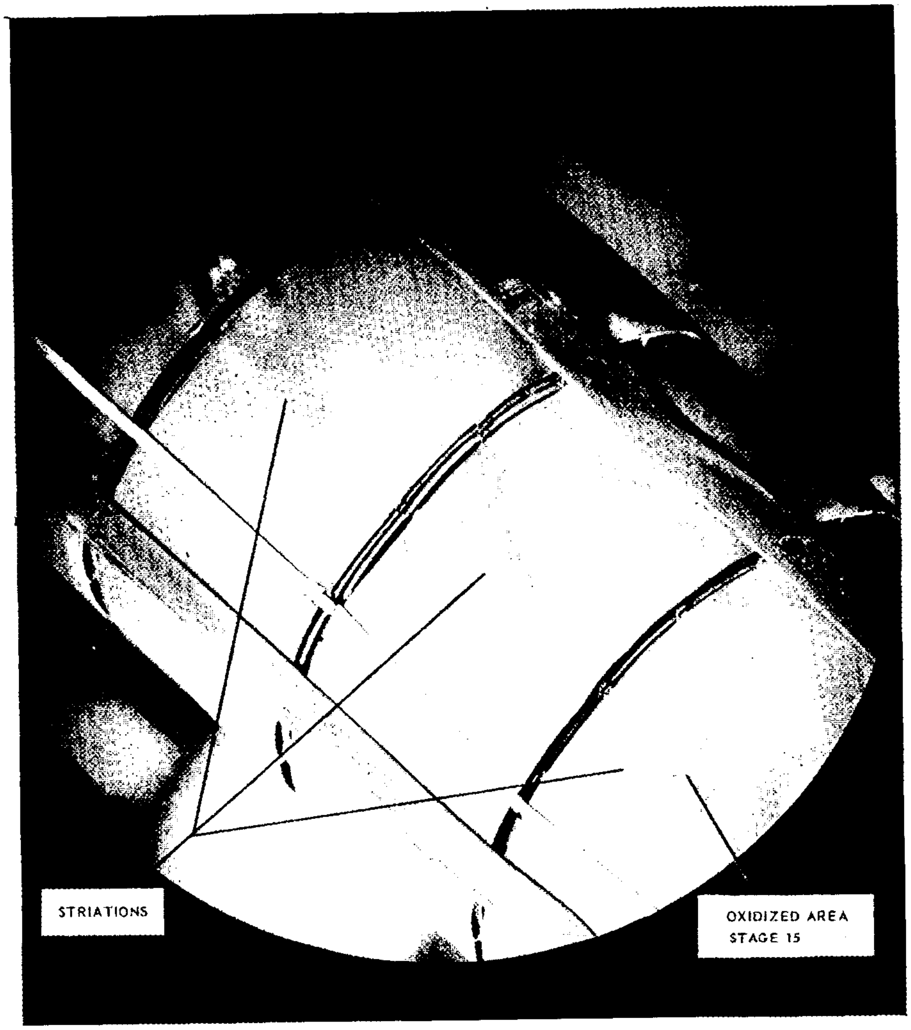

Fig. 4.23 – Damage to fuel cartridge 231, tube 24

UNCLASSIFIED

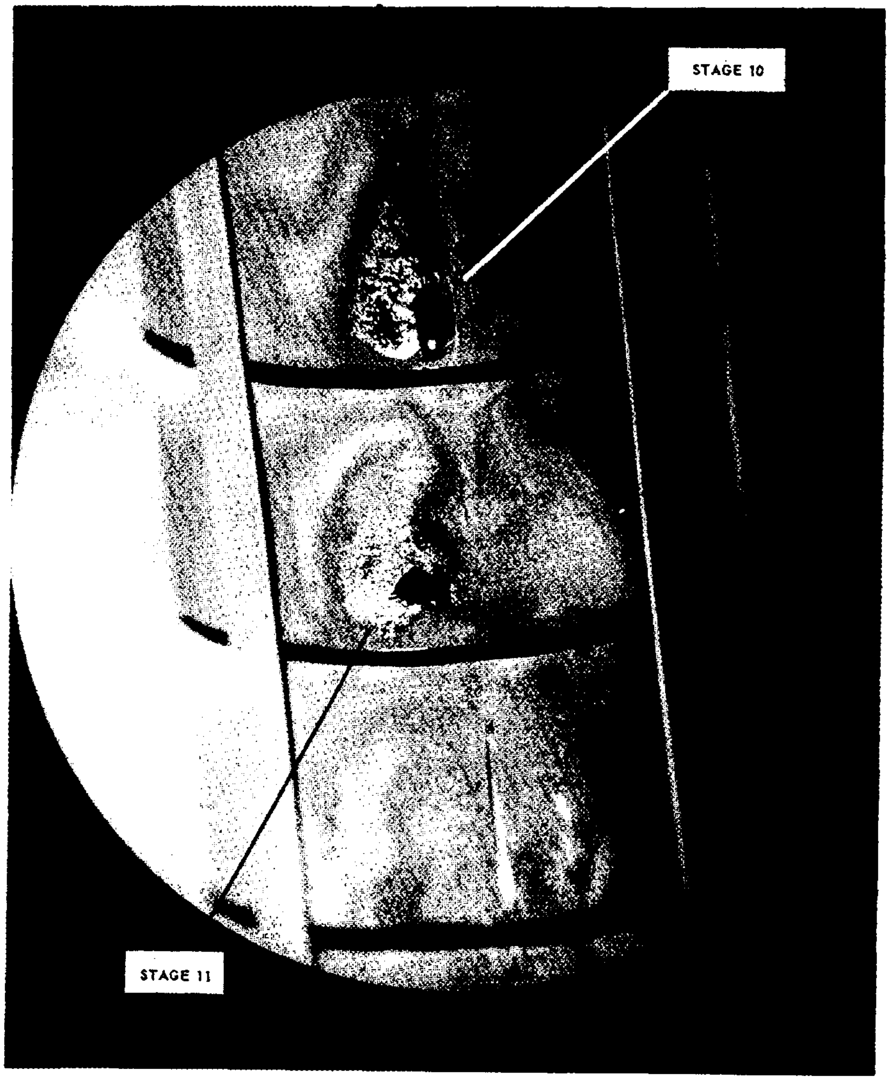

Fig. 4.24 – Damage to fuel cartridge 217, tube 20

4.7 REFERENCES

1. Hansjergen, J. F., "IET Operating Report 6-24-56 to 7-2-56 Completion of IET #4 Series of Tests Summary of A-2 Reactor Operation," GE-ANPD, DC 56-9-723, 1956.
2. Masson, L., "IET Operating Report 5-11-56 to 5-26-56," GE-ANPD, DC 56-8-729, 1956.
3. McClure, J. S., "IET Operating Report 5-28-56 to 6-9-56," GE-ANPD, DC 56-9-701, 1956.
4. Noakes, J. C., "IET Operating Report 4-30-56 to 5-11-56," GE-ANPD, DC 56-8-728, 1956.
5. Orillion, A. G., "IET Operating Report 4-7-56 to 4-28-56," GE-ANPD, DC 56-6-712, 1956.
6. Scarborough, W. T., "IET Operating Report 6-11-56 to 6-24-56," GE-ANPD, DC 56-7-708, 1956.
7. Jacoby, M. A., "IET #4 Summary Fuel Element Thermocouple Temperature - Time History and Reactor Power - Time History," GE-ANPD, DC 56-7-709, 1956.
8. Noyes, R. N., "Gross Radial Fuel Element Temperature Perturbations in the A-2 Reactor," GE-ANPD, DC 56-8-8, 1956.
9. Baker, J. K., "Analog Computer Simulation of Xenon Poison Transients in the HTRE Core A-2 Reactor," GE-ANPD, DC 56-9-160, September 1956.
10. Evans, R. C., "Xenon Calculations and History of HTRE-1," GE-ANPD, DC 56-11-78, 1956.
11. Feinauer, E. and Wood, R. E., "HTRE-1 Xenon Poisoning Experiments," GE-ANPD, DC 56-7-707, 1956.
12. Holtslag, D. J., "Stack Gas Activity Correlation," GE-ANPD, DC 56-8-720, 1956.
13. Hoover, B. J. and Brekken, T., "Photographic Investigation of A-2 Fuel Elements Second Unloading," GE-ANPD, DC 56-8-723, 1956.
14. Hoover, B. J. and Brekken, T., "Photographic Investigation of A-2 Fuel Elements Second Unloading," GE-ANPD, DC 56-8-715, 1956.
15. "HTRE No. 1 Design and Operational Summary," GE-ANPD, APEX-398, 1958.

5. IET NO. 6

Test series IET No. 6, which utilized the A3 reactor core, was conducted during the period from September 24, 1956, through January 3, 1957. The A3 reactor consisted of a new core assembly and new fuel elements and differed from the A2 in a new insulation sleeve design. The new sleeve employed a helical winding technique and stiffening rings that enhanced the structural integrity of the sleeve against pressure collapse (see Figure 5.1). This design resulted from an intensive development effort performed to determine the cause of fuel cartridge damage and to prepare for operation of the A3 reactor.

The new insulation liner incorporated several new features:

1. The sleeve was designed to resist substantial pressure differences without collapse. Fifteen-mil metal was used in the liner for extra strength. In addition nine stiffening rings of 0.050-inch stock were laced around the liner coincident with the center of the last eight fuel stages. These stiffening rings were intended to provide sufficient strength to resist any pressure differences encountered in reactor operation. A liner having only four stiffening rings of a less elegant design had previously withstood pressure differences (cold) up to 15 psi in the air laboratory. A wire probe spaced within 0.050 inch of the outer ring of the fuel cartridge indicated no deformation.
2. An attempt was made to seal the inlet end of the liner by applying additional layers of insulation. Compression of this insulation by the tube wall was intended to provide a partial, but adequate, seal. A special tool was used to insert the liner to avoid subjecting it to deleterious forces generated by friction between the outer foil and the tube wall on insertion. This liner design was thought to be failure-proof against differential air pressures. The pressure-relief holes incorporated for IET No. 4 were retained.
3. The liner was fabricated by a spiral wrapping process. Experience in the shop had indicated that the tolerances on concentricity, straightness, and diameter could be approached within much closer limits by this method. Sample liners of the kind previously operated in the reactor had been checked and found to deviate substantially from the prescribed tolerances. The stiffening rings were also intended to aid in maintaining dimensions. The liners were subjected to rigid inspection so that those that were out of tolerance could be rejected.

   Strict maintenance of tolerances was intended to solve two problems. First, the gap or annulus between the liner and the fuel cartridge could be maintained in much better fashion than previously. The local hot spots, created by flow restrictions caused by inadequate gap, could have initiated further deformations, which then avalanched to produce either collapse or severe deformation in the fuel cartridge. Second, inspection reports on the A2 and A3 fuel cartridges indicated that almost all of them were longitudinally bowed to a substantial degree. Similar bows had been observed in previous insulation sleeves. Therefore, it was thought that maintaining straightness, concentricity, and diameter tolerance should do much to alleviate any interference and subsequent buckling due to thermal stresses that might arise in either the cartridge or the liner. No adequate theory was generated that

UNCLASSIFIED

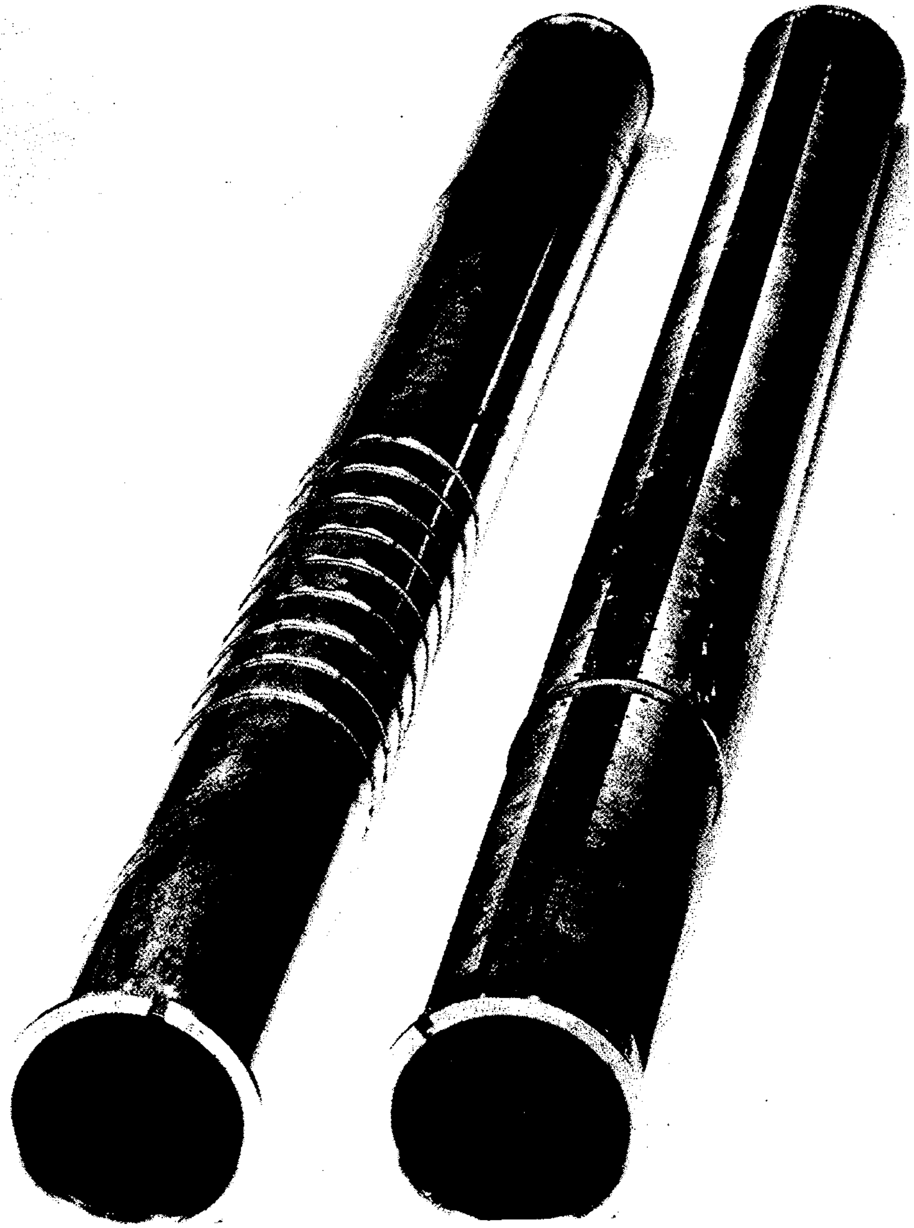

Fig. 5.1 – Insulation liners, corrugated and spiral wound

attributed the rail buckling to a single factor or a small combination of factors. It was not certain that railbuckling and burnout were attributable to the same or to similar causes. As indicated in item 4, the design dimensions eliminated binding between cartridges and liners.

4. Insulation felt of approximately half the density previously used was used in the A3 liners. The dimensions were such that calculated expansions, both of the cartridge and insulation liner, would cause no interference between the cartridge and the liner or between the sleeve and the tube wall. The tail assembly of the A3 cartridge was 0.060 inch smaller in diameter than the A2 tail assemblies, an aid in relieving interferences.

It was therefore thought that a substantial improvement was made over the sleeves previously used. These improvements enabled the sleeves to resist collapse due to air pressure and, by maintenance of a uniform gap, to induce a more uniform temperature distribution in the reactor.

IET No. 6 operations required the following modifications to the CTF:

1. A new instrumentation harness was installed to make possible more reliable pressure and temperature data.
2. The engine nozzles were cut off to improve engine performance.
3. Compressor scrolls with slightly lower pressure drop and a bypass combustor with 1 psi lower pressure drop were installed.

The immediate objectives of IET No. 6 test series were to:

1. Evaluate the performance of the redesigned insulation liners (see Figure 5.1).
2. Extend and supplement IET No. 3 low-flow, no-flow, and nuclear characteristics.
3. Verify the xenon characteristics determined during IET No. 4.
4. Continue basic controls investigations.
5. Conduct endurance testing with the engine on full nuclear power.

The reactor was first made critical on October 3, 1956, and exceeded 200 kilowatts or 1 percent power on October 12, 1956. During IET No. 6, the reactor was transferred to full nuclear power 40 times and operated for a total energy release to air of 2811 megawatt-hours and a maximum sustained power level of 18.4 megawatts to air. The day-by-day summary of operations above 200 kilowatts is found in Table 5.1. Table 5.2 presents a comparison of the IET No. 3, IET No. 4, and IET No. 6 endurance tests.

The initial transfer to full nuclear power occurred on November 7, 1956. The conditions immediately after transfer are shown in Table 5.3, together with comparable data from the previous tests. IET No. 3 and IET No. 6 data are directly comparable since they both represent 100 percent nuclear power and were run at close to the same ambient temperature. Although 100 percent nuclear power operation was not achieved during IET No. 4 and the ambient temperature level was 40 to 50 degrees higher, these data are included for comparative purposes.

The salient points of this comparison are:

1. For essentially the same engine speed and heat addition in the reactor core, the turbine inlet temperature for IET No. 6 was 100°F cooler than during IET No. 3.
2. The loss in air temperature between core exit and combustor inlet was 3 times as great during IET No. 6 as in IET No. 3. However, this temperature loss was similar to that observed in the latter part of IET No. 4 operation.
3. The maximum and average recorded temperatures for the eighteenth fuel element were 234°F and 176°F lower respectively than during IET No. 3.

TABLE 5.1

REACTOR OPERATION, IET NO. 6

Date	No. of Transfers	Time Above 200 Kilowatts, hr	Max. Power, mw	Total Megawatt-Hours	Time at 100 Percent Nuclear Power, hr $T_{3.54}$[a] = 1280°F	Time at 100 Percent Nuclear Power, hr $T_{3.54}$ = 1380°F
10/12/56		7.92	2.4	9.45		
10/16/56		0.50	0.9	0.44		
10/17/56		1.08	1.6	1.62		
10/19/56		6.53	0.2	1.37		
11/1/56		6.35	9.5	38.83		
11/2/56		5.42	10.8	29.15		
11/3/56		4.57	14.2	43.35		
11/6/56		5.03	14.0	55.04		
11/7/56	1	6.92	16.8	97.32	1.52	
11/8/56		3.67	8.9	5.97		
11/13/56		0.40	0.9	0.30		
11/15/56	1	6.70	18.2	112.79	5.87	
11/16/56	1	8.95	18.2	141.94	7.60	
11/17/56	3	8.38	17.9	107.42	5.88	
11/20/56		1.03	11.8	4.84		
11/21/56	2	8.08	18.2	93.88	4.42	
11/26/56	3	5.53	18.5	38.03	0.98	
11/27/56		1.62	16.4	12.41		
11/28/56	2	9.35	17.1	139.17	8.15	
11/29/56	1	6.88	17.7	86.51	4.30	
11/30/56	1	8.27	17.8	133.78	7.80	
12/1/56	1	8.40	17.1	137.76	8.03	
12/4/56	3	12.05	16.9	173.18	9.60	
12/5/56		16.37	18.6	290.66	16.30	
12/6/56	3	9.17	18.3	151.16	7.95	
12/7/56	1	13.13	19.5	169.78	8.63	
12/10/56		0.95	6.6	2.02		
12/11/56	2	9.07	18.3	76.13	3.23	
12/12/56	3	6.83	19.2	79.32	1.83	1.88
12/13/56	4	7.80	18.7	70.24	0.05	3.03
12/14/56	3	9.02	19.8	114.14	0.62	4.71
12/17/56	1	5.97	19.2	104.67	0.07	5.40
12/18/56	3	23.80	20.2	352.70	1.92	15.67
12/19/56		7.82	19.4	148.29		7.63
12/20/56	1	5.87	18.7	11.26	0.37	
12/21/56		2.10	18.9	24.78	0.70	0.63
12/26/56		0.65	1.1	0.7		
12/28/56		0.43	0.2	0.09		
12/29/56		1.03	5.6	5.06		
Total IET No. 6	40	257.61		3092.20	105.82	38.95
Total IET No. 4	0	193.94		2060.03	0	0
Total IET No. 3	3	40.2		349.08	0	6.06

[a]$T_{3.54}$ = Reactor exit air temperature

TABLE 5.2

COMPARISON OF ENDURANCE TESTING

	IET No. 3	IET No. 4	IET No. 6
Days operated above 200 kw	18.0	35.0	38.0
Total hours of operation above 200 kw	40.2	187.78	257.61
Total energy release to system, mwh	349.08	2064.98	3092.20
Total energy release to air, mwh	317.0	1876.0	2811.0
Maximum power, mw	16.9	18.4	20.2
Total number of transfers	3.0	0	40.0
Total hours at 100% nuclear power	6.02	0	105.82[a] 38.95[b]
Initial k_{ex}	3.52	4.16	3.45

[a]Reactor exit air temperature = 1280°F.
[b]Reactor exit air temperature = 1380°F.

TABLE 5.3

D101A2 DATA COMPARISON

	IET No. 3			IET No. 4			IET No. 6		
	T	ΔT	ΔT	T	ΔT	ΔT	T	ΔT	ΔT
T_{18}, max	1975			1914			1741		
		215			236			157	
T_{18}, avg	1760			1678			1584		
		472			307			287	
$T_{3.54}$	1288		494	1371		404	1297		426
		22			97			139	
$T_{3.65}$	1266			1274			1158		
		31			20			19	
$T_{3.8}$	1235			1254			1139		
					74				
$T_{4.0}$	1231			1328			1131		
N		7,096			7,070			7,070	
Q		14,671			14,746			14,230	
% NP		100			92.76			100	

T_{18}, max	Maximum 18th-stage plate temperature, °F
T_{18}, avg	Average 18th-stage plate temperature, °F
$T_{3.54}$	Core discharge temperature, °F
$T_{3.65}$	Hot torus exit temperature, °F
$T_{3.8}$	Unit combustor inlet temperature, °F
T_4	Turbine inlet temperature, °F
N	Engine speed, rpm
Q	Nuclear power to air, Btu/sec
% NP	(Nuclear Power) + (Total Power) x 100

The testing of the A3 reactor core brought to a successful conclusion the HTRE No. 1 testing program with full realization of test objectives. The successful operation of the reactor in this test confirmed the hypothesis that fuel cartridge damage during previous tests was caused by mechanical difficulties with insulation liners and that basic characteristics of the reactor were as predicted. Thus the gross, or average, thermodynamic performance of the reactor was the same as that observed during IET No. 4. The significant improvement was accomplished through the elimination of mechanically induced hot spots. The net result of the testing was that, although some minor difficulties remained to be resolved, no basic unforeseen difficulties were encountered, and the HTRE No. 1 system operated successfully as predicted in almost every respect.

A detailed review of the technical data obtained during IET No. 6 is presented in reference 1. Some of these data are summarized in the following paragraphs. The gross thermodynamic performance and the control rod calibration are described in detail in reference 2, pages 236 through 269.

5.1 XENON EXPERIMENTS

In the Fall of 1956, tests were made to determine the xenon poisoning characteristics of the D101A3 core. Prior to these tests, the reactor had had an idle time of approximately 66 hours to permit any residual xenon poisoning to decay to less than 0.10 percent. When the reactor was made critical, the excess reactivity was computed to be approximately 3.0 percent. This computation used a moderator temperature coefficient of 0.02 percent per ^{o}F, corrected to 95 degrees. The reactor was started up on a positive period to bring it to power. The power was increased at a linear rate rather than on a constant period. When a power level of 14 megawatts was reached, a set of data was taken. For the remainder of the run, power was held constant at 14 megawatts. Data were taken every half hour or less for the remainder of the power part of the run. A set of data was taken before and after each occurrence that was considered abnormal, including the shutdown of the reactor and the engine. Shutdown became necessary prematurely because of a windshift into the standby sector. Immediately following the shutdown, data were taken at approximately 1 percent full power to avoid the possibility that the reactor might not be exactly critical but only multiplying photoneutrons. The data point was taken immediately after engine shutdown and gave an approximate value of 0.05 percent for the coefficient of reactivity caused by the pressure as presented by the engine. The data were later corrected to a pressure condition using blowers as a reference. Because of the occurrence of a scram, there was a delay of more than an hour between data points. While the buildup and decay of poison were followed, period calibrations of representative rods from each ring were made. During these period calibrations, the motions of the rod 202 actuator did not affect the reactivity. It was found that the actuator had lost a poison tip, and this was corrected on the following maintenance day. Since the data show no discontinuities that would account for the loss of rod 202 during the operation, it appears that rod 202 was never operative during this test.

A curve of the xenon poisoning data is presented in Figure 5.2. The data are corrected for the apparent loss of the poison tip on rod 202, the experimentally determined moderator temperature coefficient, and pressure coefficient of reactivity. The value of the pressure coefficient of reactivity was 0.05 percent negative with respect to increasing pressure, i.e., the difference in pressure between engine operation and blower operation.

The corrected curve of poisoning versus time appears smooth and without gross error with the exception of the first point taken at power. The value of poisoning at the end of the power run was 0.4 percent as compared with a calculated value of 0.20 percent.

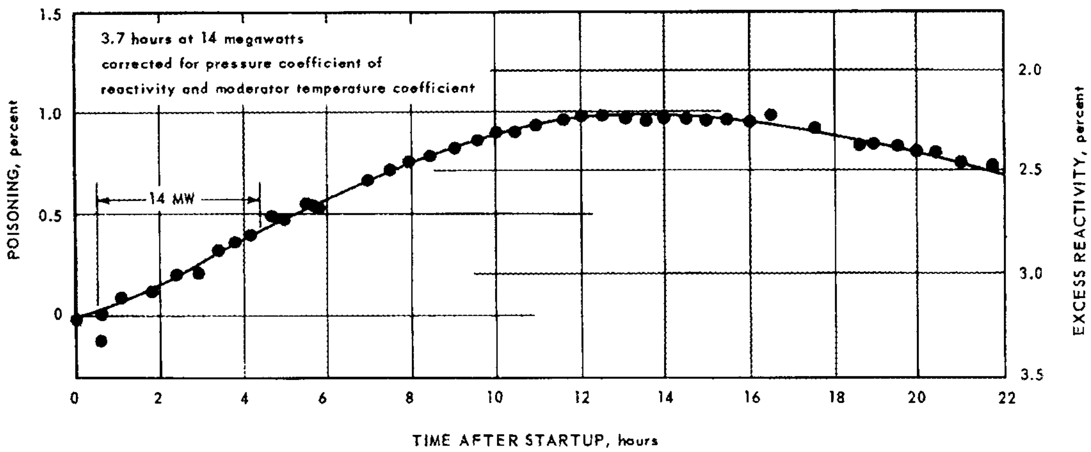

Fig. 5.2 – Xenon poisoning versus time for A3 core

Figure 5.3 presents the xenon history determined from the power history of IET No. 6. An equation for reactivity that accounts for the change in the thermal utilization factor due to xenon was used in computing this history. The experimental data points are included for comparison.

Analog analysis of the xenon poisoning indicated that an adjustment of the xenon burnout term in the elementary xenon-concentration equation and adjustment of the xenon-poisoning equation makes the computed value of poisoning agree more closely with the observed values. By use of the adjusted parameters and the known power history of the reactor, the xenon poisoning for operations from December 18, 1956, to December 22, 1956, was calculated to within 10 percent of measured values. These results are shown in Figure 5.4. Computation of the samarium poisoning with the adjusted parameters indicates that the operation was carried on sufficiently long to cause reactivity loss on the order of 1 percent excess reactivity which agrees quite closely with the observed value.

5.2 MODERATOR TEMPERATURE COEFFICIENT OF REACTIVITY

During this test series, the moderator temperature coefficient of reactivity measurements were repeated using the A3 core in the hope that the measurements would confirm the values taken during IET No. 2. The experiment performed during IET No. 2 was in some respects different from the experiment performed with the A3 core.

During IET No. 2, the reactor was mounted on the Initial Criticality Experiment dolly. By circulating the moderator water to the facility system, the moderator water was heated at a uniform rate from a relatively low point to approximately 160°F. With the A3 core however, the moderator temperature coefficient of reactivity could not be checked until after the reactor had been placed in the CTF. This precluded any possibility of heating the moderator water by use of the facility heater, since the moderator water could not be circulated adequately through the core by use of the facility pumps. The moderator water, therefore, was heated by using the engine as a heat source.

The moderator water was cooled to approximately 56°F by using the dolly heat exchanger. The moderator temperature was then increased in steps by running engine No. 1 until the temperature increased approximately 10°F. The engine was then shut off and the moderator temperature allowed to stabilize. It was observed that the moderator tem-

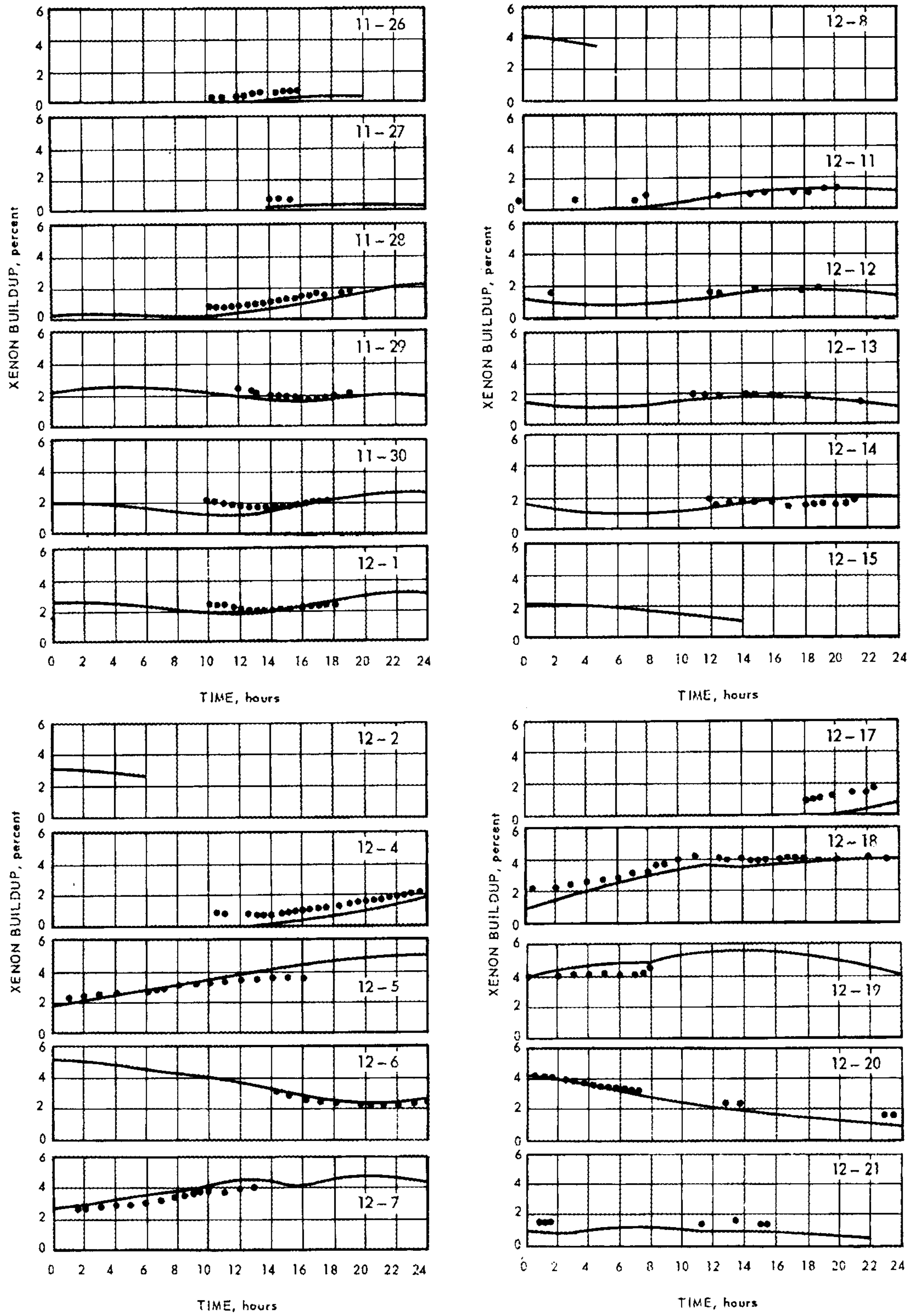

Fig. 5.3 – Summary of xenon poisoning data, A3 core

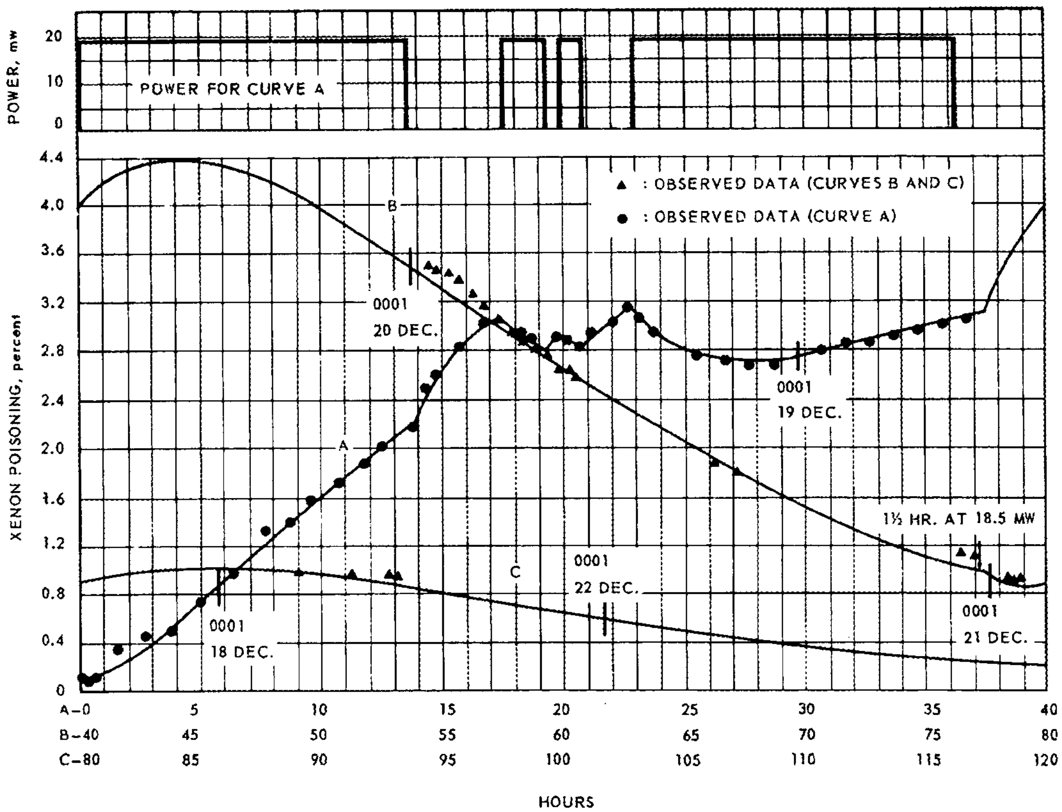

Fig. 5.4 – Observed and computed xenon poisoning for extended run (using adjusted parameters)

perature remained stable for periods of 5 minutes or longer. Rod positions were recorded for each stabilized moderator temperature, and the data were recorded on the control rod logs and on the IET data sheets.

Control rod 38 was selected as the standard rod for measuring change in reactivity due to a change in moderator temperature; this rod had been calibrated at least twice by the period method during IET No. 6 and was considered to be the most accurate standard against which to measure. The total worth used for the rod was 0.532 percent. Rod 38 was inserted in order to maintain the reactor critical as the moderator temperature was increased. At intervals it was necessary to insert portions of frame 2 and frame 3 and pull rod 38 to the Out position to have continued control with rod 38. After this change was made, the moderator temperature was again increased and the standard control rod 38 was re-inserted as required for control. This process was repeated until the moderator temperature had reached approximately 162°F, at which time the test was terminated because of unfavorable effects occurring in the rod mechanism at temperatures in excess of 160°F.

As the experiment proceeded, the standard rod progressed from a partially shadowed condition to a more shadowed condition. However, the maximum error introduced by this procedure should not have exceeded 10 percent since the value obtained for rod 38 on the basis of a clean geometry as compared with the maximum shadowing changed only by 10 percent. This estimate was based on the results from the partial calibration of rod 38 with a rod pattern in which rod 39 and rod 43 were withdrawn 8 inches. If applicable, these results would decrease the value for the moderator temperature coefficient from 0.022 to 0.020.

The results of these tests are presented in Table 5.4 and in Figure 5.5. The data indicated that for a temperature change of 106°F (from 56° to 162°F) the corresponding change in reactivity was 2.351 percent. The average moderator temperature coefficient of reactivity, over the entire range of 106°F, was 0.022 percent per °F. Figure 5.5 indicates that the data were not linear, but that the rate of change of reactivity with temperature decreased somewhat as the temperature increased. The figure presents the data as an average of the control-room moderator outlet thermocouple and the data-room moderator inlet and outlet thermocouples. It is believed that using the average temperature minimized the effect of any error inherent in the reading of a single thermocouple.

These data indicate that the moderator temperature coefficient of reactivity as measured in IET No. 2 did not agree with measurements from IET No. 6. In addition, the value used for the worth of rod 38 was 0.532 percent as compared to 0.597 percent from IET No. 2.

TABLE 5.4

VARIATION OF REACTIVITY WITH MODERATOR TEMPERATURE

Reactivity Change, percent	Moderator Temperature Change, °F	Cumulative Reactivity Change, percent
0.246	56-66	0.246
0.085	66-68	0.331
0.235	68-78	0.566
0.177	78-86	0.743
0.229	86-98	0.972
0.226	98-104	1.198
0.218	104-115	1.416
0.211	115-125	1.627
0.277	125-137	1.904
0.210	137-148	2.114
0.237	148-162	2.351

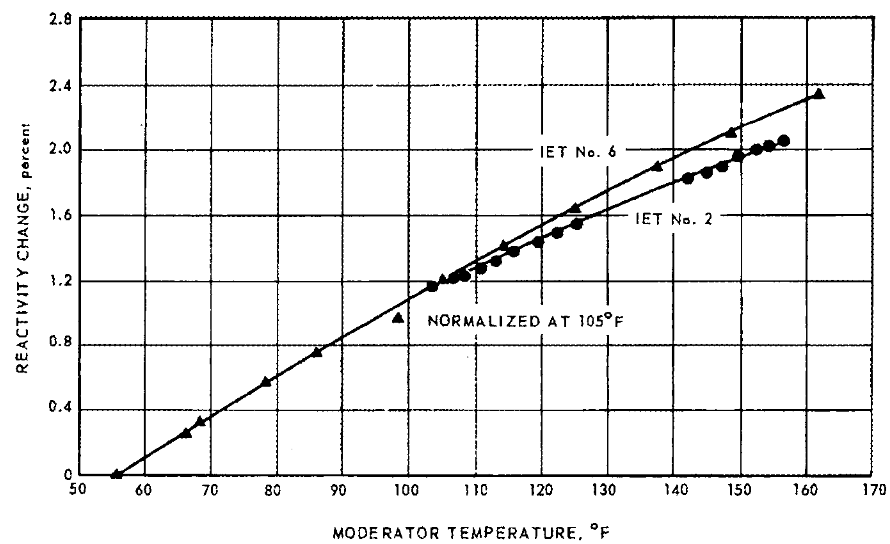

Fig. 5.5 – Moderator temperature coefficient of reactivity

Whether this difference in the magnitude of moderator temperature coefficient of reactivity was due to differences in the construction of the core or to the environment of the CTF is not known.

5.3 EXHAUST-GAS ACTIVITY

In order to duplicate sampling tests performed during IET No. 4, an improved system and procedure was obtained during IET No. 6. The purpose of these tests was to determine the constituents in the exhaust gases. The following techniques were used:

1. Determination of decay curves.
2. Determination of total iodine activity as soon as possible after collection.
3. Spectrographic analysis to determine constituents.
4. Chemical analysis for specific constituents.
5. Determination of total activity as soon as possible after collection.
6. Identification of the isotopes of iodine and determination of percentages present.
7. Determination of specific activity of particulates.

Figure 5.6 indicates the schematic arrangement of the sampling system. The velocity in the main duct was checked with Pitot static tubes, and a sampling nozzle was selected to give equal flow velocity. The isokinetic sample passed through a water heat exchanger and then through a 4-inch-diameter millipore-filter holder. The millipore filter was capable of filtering out most of the radioactive and the particulate matter.

Although particulate activity was detected on the stack filter during the initial transfer to full nuclear power, it was not positively identified as fission products. Spot samples indicated that the particulate activity before transfer was about 5 curies per hour and upon transfer to full nuclear power the particulate stack activity dropped to about 0.1 curie

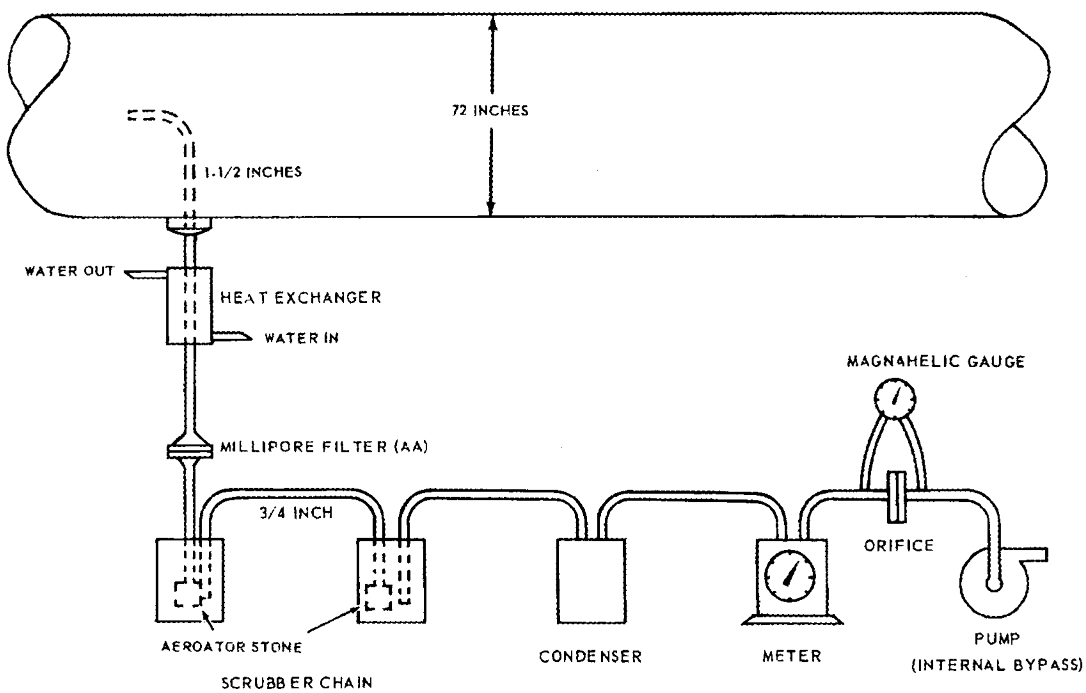

Fig. 5.6 – Test system for evaluating gas constituents

per hour. It was conjectured that the higher value before transfer was caused by absorption of gaseous particles in the chemical combustion products, which were then trapped by the stack filter. Since the carrier and the combustion products may have been a function of combustion efficiency and fuel flow rate, subsequent checks of stack activity were obtained at various percentages of full nuclear power. These data are shown in Figure 5.7. The abrupt drop near 90 percent was caused by cutting off the chemical fuel. Radiation measurements on the turbine scrolls of the engines after operation indicated a maximum reading of 20 milliroentgens per hour compared to readings of several roentgens per hour during operation in IET No. 4. Figure 5.8 presents a summary of particulate activity for all three tests series.

The first indication that detrimental changes were occurring within the A3 core was detected on the night of December 18, 1956. During the third transfer to full nuclear power on this date, the activity at 75 to 80 percent full nuclear power was observed to be 17 curies per hour, as shown in Figure 5.9. As the reactor power was increased to 90 percent, the activity as determined by the stack monitor increased to 25 curies per hour and then rapidly decreased to about 0.4 curie per hour after transfer to full nuclear power. To verify the high activity observed prior to transfer, smoke was introduced into the stack for a short time. At a nominal (recorded) plate maximum of 1750°F and a core discharge temperature of 1280°F (point A on Figure 5.9) with the smoke, the stack activity was 9.5 curies per hour. When the reactor was brought to a nominal plate maximum of 1850°F and a core discharge temperature of 1380°F (point B on the figure), the activity increased to 12 curies per hour decayed according to the line shown in the figure as the smoke was dissipated. Some 12 hours later, the activity level was down to about 3.5 curies per hour. When the jet engine was relit, the activity rate increased to about 20 curies per hour. The dotted portion on the right of the curve in Figure 5.9 indicates a normal transfer. At the conclusion of this operation, several of the individual tube filters were taken from the reactor and examined. These indicated strong iodine peaks and other possible fission fragments.

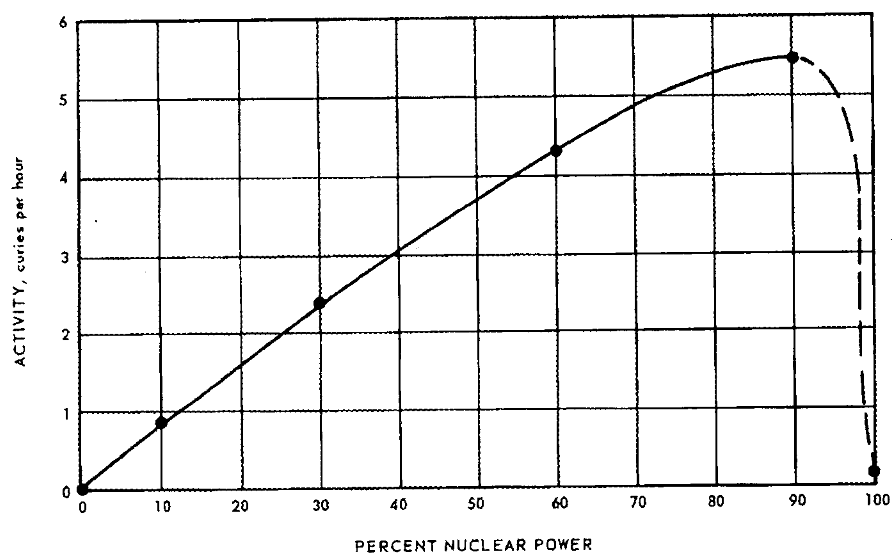

Fig. 5.7 – Particulate stack activity as a function of percent nuclear power

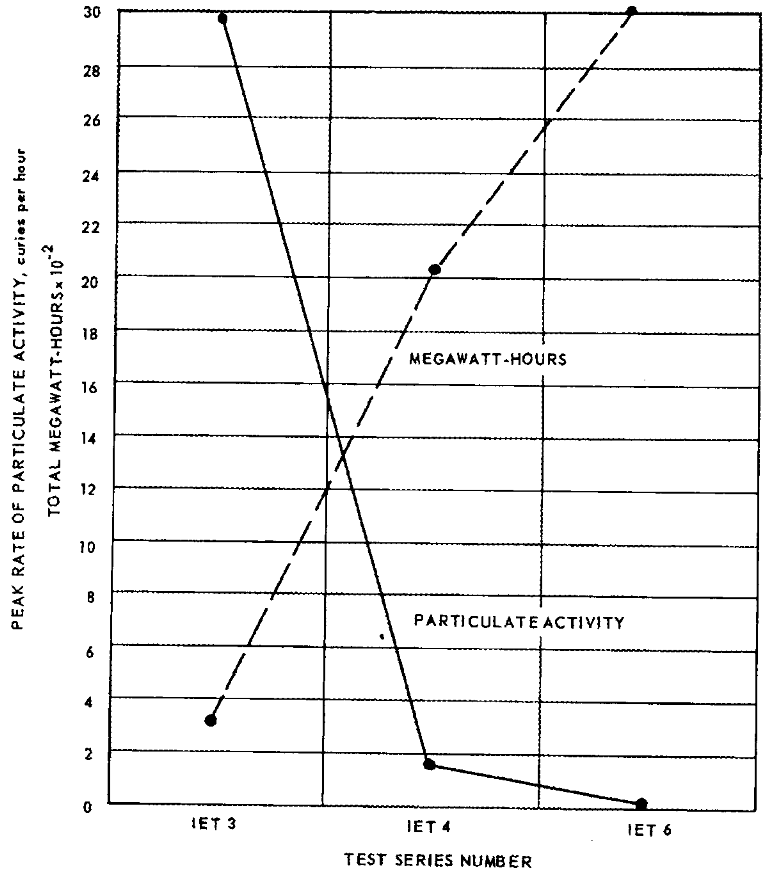

Fig. 5.8 – Summary of particulate activity for IET No. 3, IET No. 4, IET No. 6

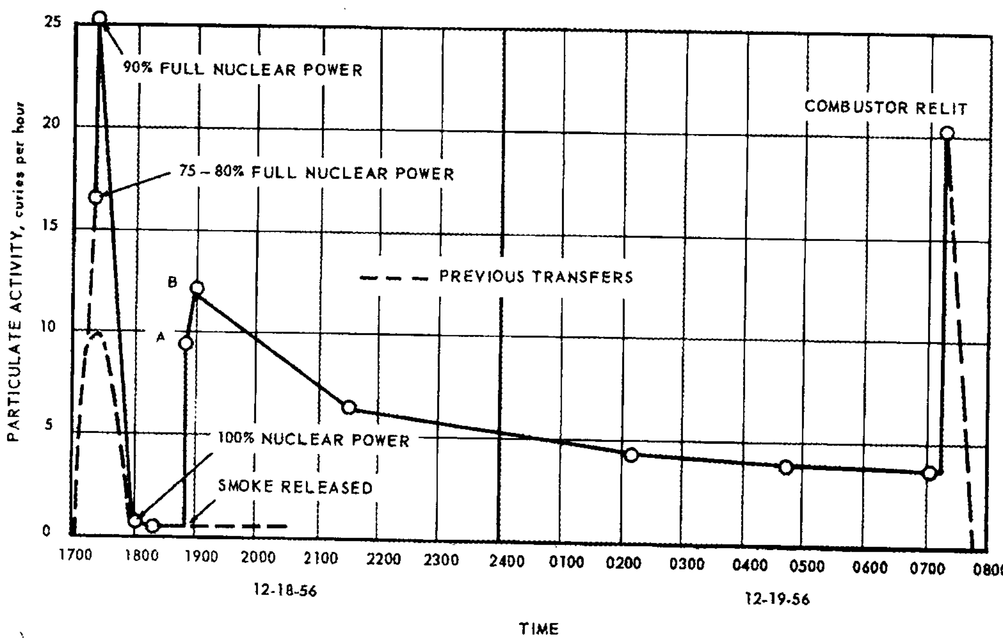

Fig. 5.9 – Particulate activity as a function of time

Figure 5.10 shows the size distribution of particulate matter observed. This test was performed with the engine on full nuclear power at 7070 rpm and the reactor on 89 percent of full power. The total nuclear operating time on the core was approximately 7.39 hours. The particle-size distribution is very similar to that for normal atmospheric dust.

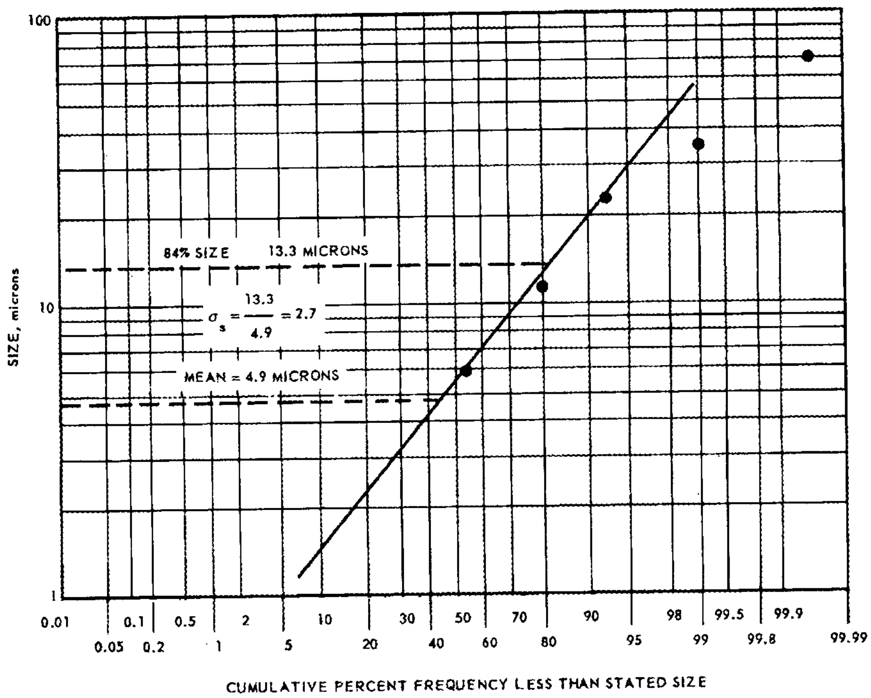

Fig. 5.10 – Size distribution of particulate matter in exhaust gases

5.4 CONTROLS TEST

An attempt was made during this test series to demonstrate the feasibility of automatic reactor startup. For these tests the reactor control circuitry was modified as follows:

1. The period interlock on the output from the fission chambers was modified to actuate at a period of 25 seconds instead of the original 10 seconds.
2. The interlock was modified to stop rod withdrawal. The original operation of the interlock was to insert rods and open up the withdrawal bus.

Operational modification was also made; two fission chambers were inserted all the way with one in midposition. This was done to determine the difference in period output between inserted chambers and midposition chambers, and to determine period output from the chambers when the instrumentation was reading full scale. It was found that the initial photoneutron background as indicated by the inserted fission chamber was approximately two counts per second; consequently, it was not necessary to actuate the source mechanism. After a preliminary check of the reactor instrumentation, the insert withdrawal switch for the shim frame command was held in the withdraw position so that the shim rods were withdrawn by frame in reverse order. At the beginning of frame 3 withdrawal, a noise signal actuated the period interlock and stopped rod withdrawal temporarily. As the log count rate increased to 20 counts per second, the period circuit generated a reasonably steady signal; however, it was necessary to shut down to wire out the low airflow interlock since only the blowers were operating. After the temporary delay, rod withdrawal started again; this time it was noted that when the withdrawal commands shifted from frame 4 to frame 3 there was not a spurious signal to give a period to temporarily stop rod withdrawal. As withdrawal continued, the count rate increased on the most fully inserted fission chambers while the fission chambers in midposition were not indicating. When withdrawal command was shifted to frame 2 from frame 3, there was a spurious signal to stop rod withdrawal temporarily again. When the count rate, as produced by the most fully inserted fission chambers, reached approximately 25,000 counts per second, the fission chamber in the midposition started to come on to scale. Also, it was noted that the log flux instrument started to read above background when the most fully inserted fission chambers were reading approximately 2000 counts per second.

When the designated power level had almost been reached, a period signal from one of the log-flux ion chambers gave a false indication of a short period and caused a scram. After the scram had been cleared and the rod relatched, the experiment was started again. This time fission chamber 1 was put in the midposition and the others in the inserted position. As rod withdrawal proceeded, the transfer from frame 4 to frame 3 was smooth; however, there was a false indication again on the transfer from frame 3 to temporarily stop rod withdrawal. The transfer from frame 2 to frame 1 was smooth. Apparently some rods were not latched after the scram because, for the reactor to become critical, rods in frame 1 had to be withdrawn, whereas in the second attempt the reactor was apparently critical when frame 2 was withdrawn. One ion chamber apparently was noisy and was putting out an erratic period signal. To prevent a recurrence of the scram, this ion chamber was disconnected from the circuit.

Although the most fully inserted fission chambers were reading full scale, the fission chambers and the electronic components were not saturated since a period signal was being generated by the electronic components connected to each fission chamber. This signal was noted on the individual period meters.

At approximately 10 minutes from the start of rod withdrawal, the reactor was apparently supercritical and on a true positive period and rod withdrawal was halted. The period, as indicated by the period meter, was approximately 30 to 40 seconds. The reason that rod withdrawal did not occur at 30 to 40 seconds was that the hysteresis in the withdrawal interlock relay would not reset until a period greater than 50 seconds was obtained. When indicated power had reached 5×10^{-3} percent of full power, shim rods were inserted to obtain an infinite period. At this power level, it was certain that the reactor was critical and not just multiplying photoneutrons. Having reached and stabilized at this level of 5×10^{-3} percent of full power, the reactor was shut down in an orderly manner.

Automatic startup of this type of reactor appears feasible; it requires the use of the regular period instrumentation and relatively simple relay mechanisms. The reactor could be brought to any power in the power range by the method described above and control transferred to the dynamic servo system. This would require making appropriate interconnections in the shim withdrawal bus.

Sinusoidal inputs and step inputs were also impressed on the servoamplifier that compares the demand level and actual flux level. Instrumentation difficulties rendered the sinusoidal data of little value; however, the step input data were analyzed extensively. These data were obtained at relatively low reactor powers (5 megawatts) because of operating limitations on temperature that were in effect late in IET No. 6 operation. Response traces of flux (ϕ), fuel plate temperature (T_{18}), and exit air temperature ($T_{3.54}$) were recorded on the oscillograph.

The step-input-response traces were analyzed to some degree by complex plane integration techniques to determine the sinusoidal frequency response and the reactor-temperature transfer function. The results are shown in Figure 5.11.

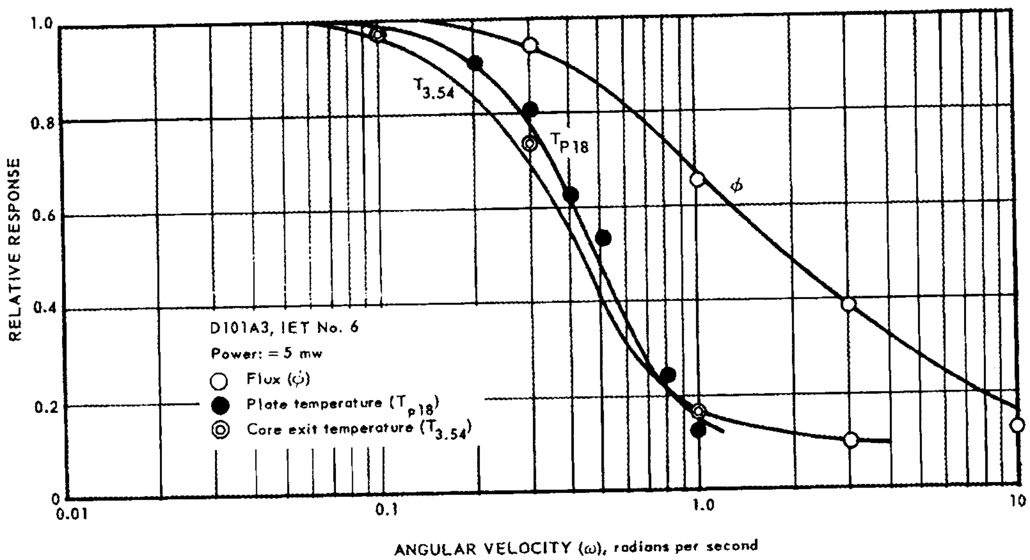

Fig. 5.11 – Frequency response of flux, plate temperature, and core exit temperature from numerical integration of the step input response

5.5 POSTOPERATION EVALUATION OF FUEL CARTRIDGES

During the latter stages of IET No. 6, when it was suspected that deterioration was occurring within the core, a concerted effort was made to ascertain, by the use of filters, the location, extent, and nature of fuel element deterioration. Predictions for the tests were based on the results of the radiochemical analysis of the filtrate deposited on stainless steel and paper filters located on the air-sampling tubes at the exit of each fuel cartridge. In an attempt to correlate fuel element and air temperatures and control rod positions with radiochemical analysis, a history of the air and fuel thermocouple readings during IET No. 6 was compiled along with the history of the control rod positions.

During the period from December 10, 1956, to December 20, 1956, a number of stainless steel filters were removed from the reactor assembly for examination. Radiochemical analysis of these filters indicated that significant amounts of iodine were present in almost every case. The fission products Ba^{140}, La^{140}, Ru^{103}, Ce^{144}, as well as U and Cr^{51}, were tentatively identified on some of the filters.

Since there was evidence that the stainless steel filters were possibly contaminated from previous use during fuel element failure, a low-power run at a fuel element temperature of about 800°F was made with the stainless steel filters replaced by No. 41 Whatman filter paper. Each of the 37 filter papers was placed in a scintillation crystal gamma-ray counter and the relative gamma activities determined. Gamma-ray spectral analysis proved a definite presence of fission products on some filter papers, a possibility of fission products on others, and the probable absence of fission products on the remaining papers. Since a 0.32-Mev line, proved to be caused by Cr^{51} during the stainless steel work, appeared consistently in the paper spectra, it was tentatively assumed that Cr^{51} was present on the filter papers.

With the information obtained from both the stainless steel and the paper filters, predictions of the relative fuel element fission-fragment release were made in three classes: definite, uncertain, and no release. These predictions are presented in Figure 5.12 along with the following information:

1. The gross gamma-ray count rate in arbitrary units from each of the 37 filter papers from a low-power run on January 2, 1957.
2. The gross rate in milliroentgens per hour, measured by placing a survey meter in contact with each of the 37 stainless steel filters from a high-power run on December 20, 1956.
3. Intensities in arbitrary units of the I^{131} component of the filter-paper spectra.
4. Intensities in arbitrary units of the supposed Cr^{51} component of the filter-paper spectra.

During IET No. 6, the temperature readings as a function of time were recorded for thermocouples on the fuel elements and at station 3.54 (core exit air temperature). Duration of thermocouple readings in chosen temperature brackets was compiled and is shown in Figure 5.12. Because of failures of the thermocouples on the fuel elements, some fuel element data were extrapolated by the assumption that a thermocouple that had operated in a given temperature bracket before failure would have continued to read in that bracket for the remainder of the test. This extrapolation was not necessary for the air temperatures since only four thermocouples failed at station 3.54 during the entire 150 hours operation. Correlation between high temperatures and the radiochemical analysis for each fuel element was much better than would be expected by chance.

The control rod positions were determined as a function of time from the operation log sheets and were compiled into three groups: In (0 to 10 inches withdrawn), Mid (10 to 20 inches), and Out (20 to 30 inches). The percentage of total running time which each rod remained in each position was computed and is shown graphically on Figure 5.12. No consistent correlation between the control rod position and the result of the radiochemical analysis was found.

The A3 core was removed from the CTF cocoon for inspection and unloading on January 7, 1957. Preliminary inspection[3] of the core and plug indicated excellent condition except that there were large and thick deposits of boric acid on the lower section of the core shell as a result of shield-water leakage into the cocoon during operation. The core was successfully unloaded without apparent damage to fuel cartridges. The tube-28 web assembly was pulled through the tube along with the cartridge because the tube-loading machine failed to unlatch the cartridge from the web assembly. The protruding webs of the tube-28 assembly caught the insulation sheet of the core bottom face and tore approximately one-third of the area loose from the core bottom face. The upper limit switch of the tube-loading machine failed to function during unloading, and it was difficult to determine the exact location of the table in relation to the position required for unlatching.

At the conclusion of the fuel-unloading operations, the core was flushed and cleaned of boric acid and other contaminants. The core was then inspected in detail and monitored. Radiation levels varied from 8 to 25 roentgens per hour in the transition section and 7 to 14 roentgens at the bottom face. Eight web assemblies were found to be bent and distorted to such an extent that replacement was required; further inspection indicated that five additional web assemblies were also damaged. It is believed that these web assemblies were damaged when the upper limit switch of the tube-loading machine failed to function and the table was allowed to travel too far.

On January 23, 1957, radiation measurements were taken on fuel elements 323 and 306. The fuel elements were suspended 17 feet in the air at the doorway of the hot shop. Mea-

LEFT SIDE OF CIRCLE:

1. Relative gross gamma count from filter papers exposed in low-power run.
2. Relative dose rate from stainless steel filters exposed in high-power run.
3. Relative height of iodine peak in filter-paper spectra.
4. Relative height of supposed Cr^{51} peak in filter-paper spectra.

Center strip of large circles indicates relative time that exit air thermocouples indicated over 1500°F and plate thermocouples indicated over 1800°F.

RIGHT SIDE OF CIRCLE:

1. Number of hours and minutes exit air thermocouple read over 1400°F.
2. Number of hours and minutes exit air thermocouple read over 1500°F.
3. Number of hours and minutes fuel thermocouple read over 1700°F (extrapolated)
4. Number of hours and minutes fuel thermocouple read over 1800°F (extrapolated)

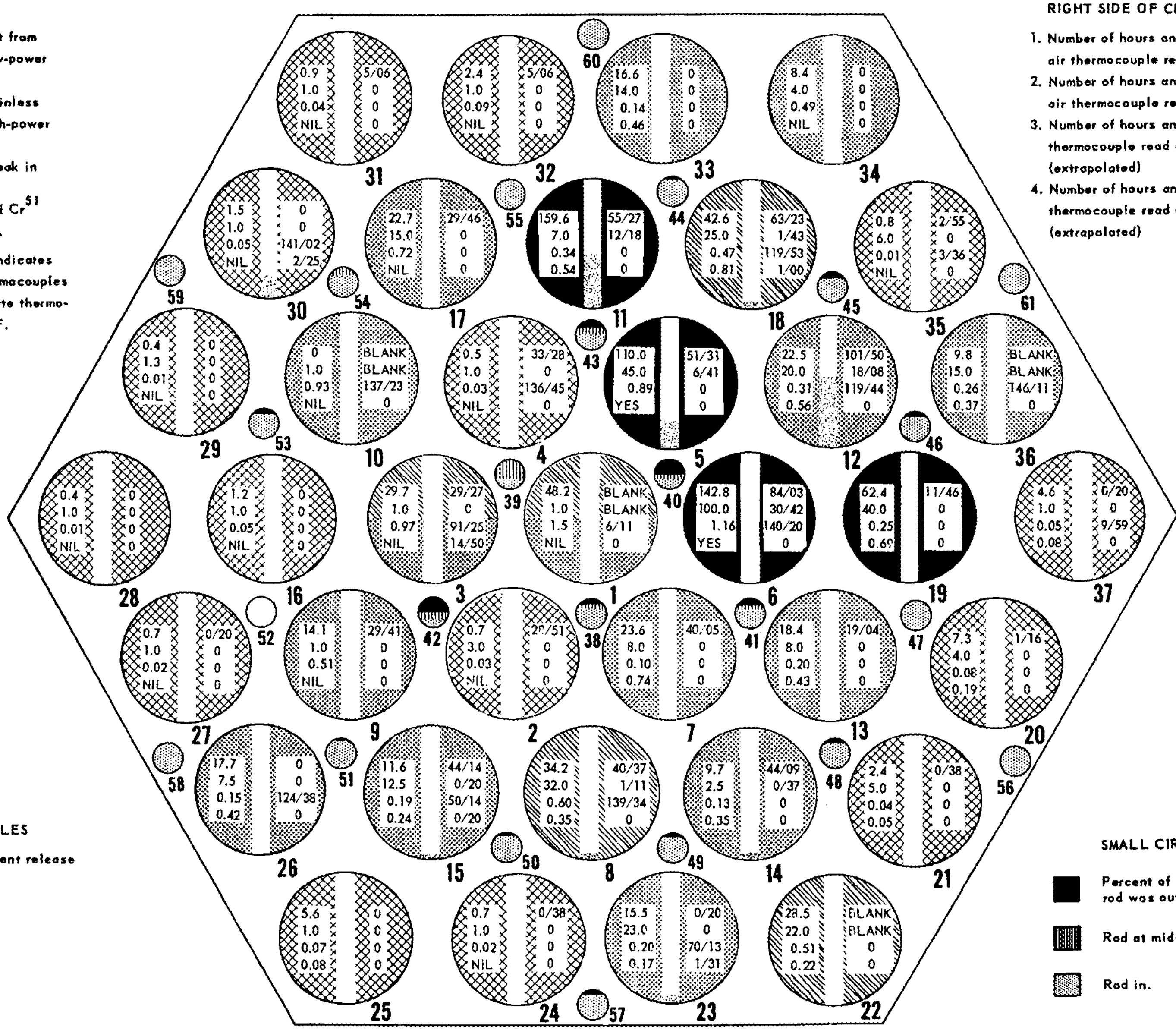

LARGE CIRCLES

Relative fission fragment release

- Probable
- Possible
- Uncertain
- Improbable

SMALL CIRCLES

- Percent of 150 hours that rod was out.
- Rod at mid-position.
- Rod in.

Fig. 5.12 – Predictions of probable release of fission fragments by individual fuel tubes

UNCLASSIFIED

surements were made with a Jordan Radector portable ion chamber instrument and a Technical Associated C. P. ion chamber instrument. Both instruments agreed within 10 percent at each point at which measurements were taken. Some cave effect could be expected, since the CTF was located about 30 feet behind the elements at the time the measurements were taken. Additional details on post-test investigation of core activation and metallurgical evaluations are given in references 4 and 5. In general, the fuel cartridges removed from the core appeared to be in excellent condition. Figure 5.13 indicates the condition of the outer foil on tube 6, which is typical. Figure 5.14 shows an end view of the tube 6 cartridge with an eighteenth-stage blister visible on ring 7. Photographs of other typical cartridges are shown in references 6, 7, and 8.

The six cartridges in which damage was suspected were examined superfically without destruction. These were cartridges 335, 325, 326, 306, 322, and 323. As a result of these examinations, stage 18 from cartridge 323 and stages 16, 17, and 18 from cartridge 325 were removed and shipped to Evendale for more detailed examination in the Radioactive Materials Laboratory.

Cartridge 335 was completely disassembled, and stages 16, 17, and 18 of cartridge 333 were removed and separated into individual rings. Each ring of each stage was examined in detail for defects. Defects were found in various rings from stage 9 through stage 18 of cartridge 335. All of the defects or blisters found on the outside of the rings were open (fissured) with the possible exception of two that were of doubtful status. In most cases of a blister on the outside of a ring, a corresponding defect on the inside of the ring was also observed. Such coexistence was not universal, but no defects were found on the inside surface except in coexistence with outside blisters. It appeared that internal defects were predominantly still closed, within the viewing limits of the periscope and lighting in the Radioactive Materials Laboratory.

Examination of stages from tubes 3, 4, 6, and 19 revealed blisters distributed as indicated in Table 5.5. The frequency of occurrence is portrayed graphically in Figure 5.15. Figure 5.16 summarizes the distribution of blisters longitudinally on the cartridge as a function of fuel element stage location for the three fuel cartridges that were examined in detail. The blisters vary in size from 1/8 inch to 1/2 inch in diameter. Occasionally, two or more adjacent blisters coalesced into one large blister as shown in Figure 5.17. Their locations were not associated with hardware, with leading or trailing edge, or with any particular quadrant. All blisters examined contained fissures

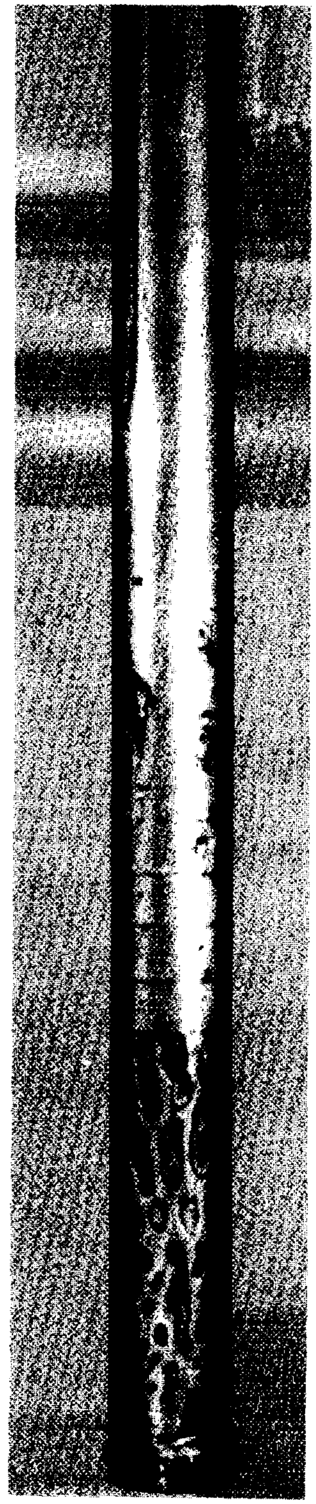

Fig. 5.13 – Typical postoperation condition of insulation liner foil (cartridge 335, tube 6)

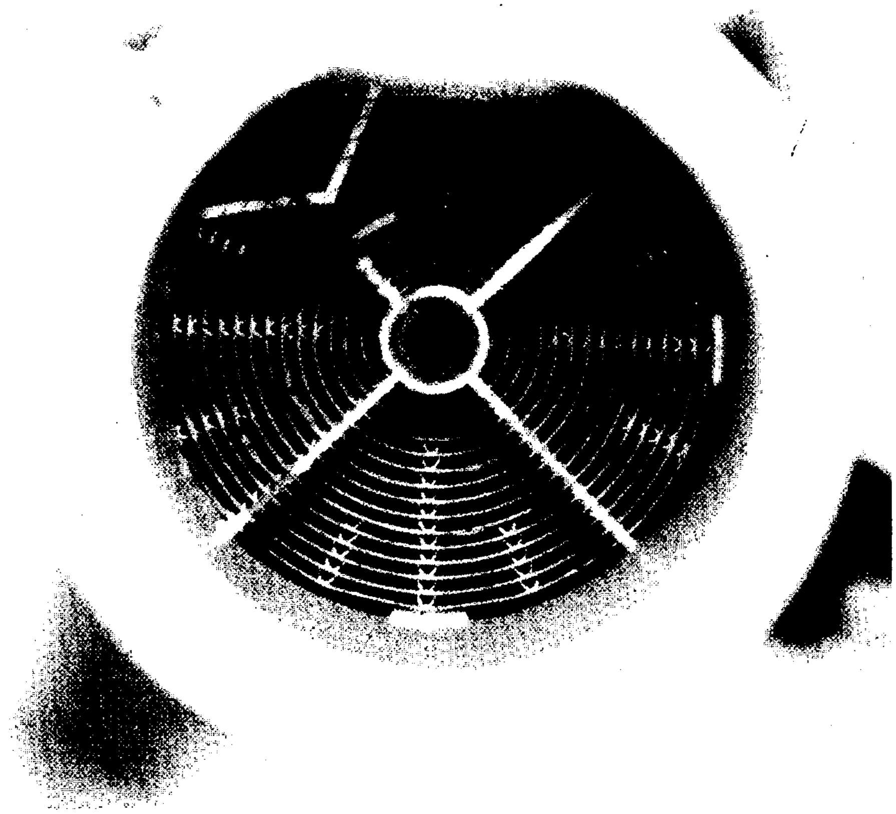

Fig. 5.14 – End view of cartridge 335, tube 6, showing blister on ring 7

on the outside surface of the rings. Metallographic examination showed that the clad surface in the blistered area as well as in the areas removed from blisters was only slightly oxidized, with oxide penetration less than 2 mils. The surface oxidation of all rings was quite uniform with no evidence of local overheating at blisters.

Perusal of inspection data back to the fuel batch from ORNL and in-process fabrication data showed no correlation between blisters and fuel ribbon quality. Likewise, no thermodynamic or metallurgical evidence was uncovered that indicated severe local overheating. On the contrary, most of the blisters observed occurred in the relatively cool portion of each stage.

Some rails of the cartridges were buckled into the outermost rings of the 11 through 18 stages, with one rail cracked in the buckled area. Ring 8 of stage 18 from core tube 19 was exfoliated, as shown in Figure 5.18. The X-ray examination of this segment showed that the dead edge had been trimmed to 1-mil width in one area, which accounted for exfoliation of the edge during operation.

Investigations were made to establish the cause of the blisters. A review of reactor operating history, assembly operations, and results of blister formation investigations indicated that surface contamination of the fuel ribbon may have caused the blisters. Although analyses showed the presence of zinc, lead, and copper contaminants on the fuel ribbon surfaces, subsequent laboratory tests were inconclusive in establishing the influence of these contaminants on blister formation.

TABLE 5.5

LOCATION OF BLISTERS ON FUEL RINGS REMOVED FROM THE D101A3 CORE

Tube Number	Stage Number	Ring Number 1	2	3	4	5	6	7	8	9	10	11	12	13	14	15	16
2[a]	18			1				1									
3	18								2								
	16								2					1			
	15			1		1		2			1	2					
	14							1			1	2					
	13								3		1	2					
	12							1			2						
	9			1													
4	18					2	1	6	3								
	17			1		5		1	5	6		1					
	16		2			1											
5[a]	18							1									
6	18							1	4		1						
	17					1						1					
	16				1	1		1									
	15							3		1	1	2	1				
	14						1		3	1		1					
	13			2	3			1	1		2		1				
	12							1									
	11			1	1			1									
	10					1	1	2									
	9						3										
	8							3									
7[a]	18				1	4	4	4			1						
8[a]	18								1				1				
9[a]	18					1			1		1	1					
10[a]	18						1										
11[a]	18					1											
15[a]	18											1					
16[a]	18					1		1									
18[a]	18						1	1	1								
19[a]	18			1		3	1				2	1					
21[a]	18					1											
23[a]	18					1											
25	18			1													
	17			2					5								
30[a]	18					1											
32[a]	18					2		1									
36[a]	18					2											
Total by rings		0	2	11	6	29	13	33	31	8	13	14	3	1	0	0	0

[a]Only the 18th stage examined

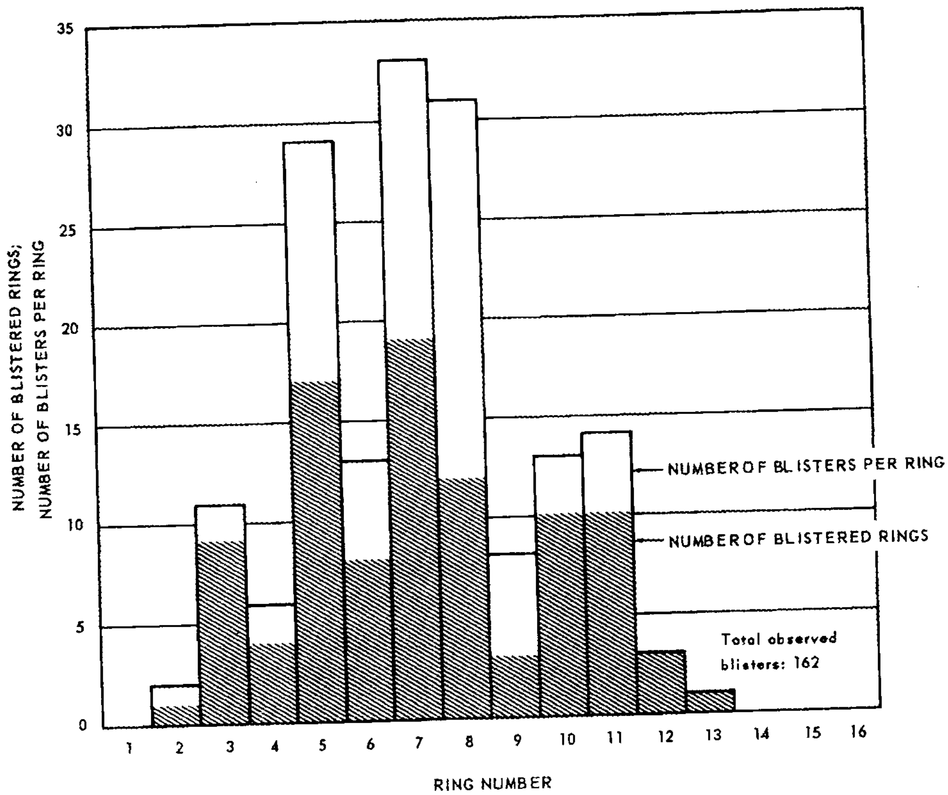

Fig. 5.15 – Summary of ring blister damage

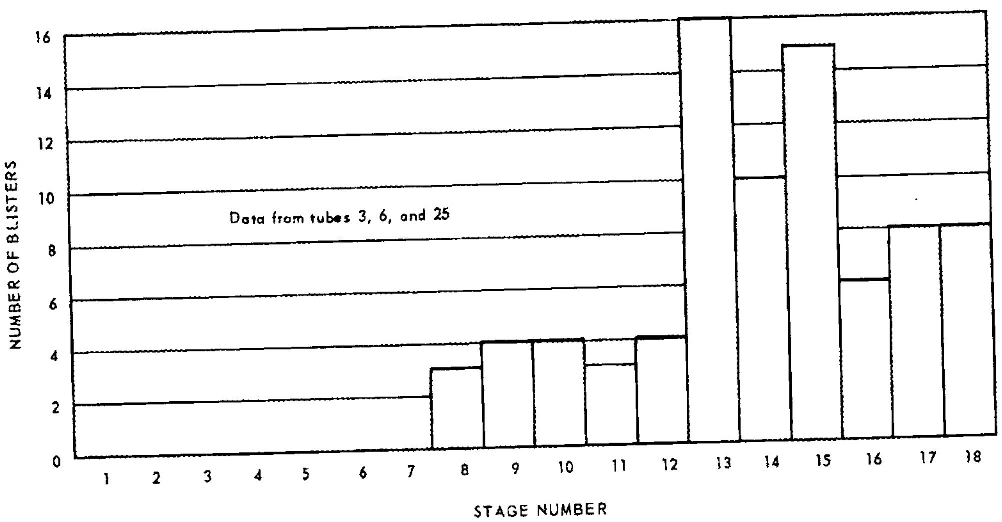

Fig. 5.16 – Longitudinal blister summary, tubes 3, 6, and 25

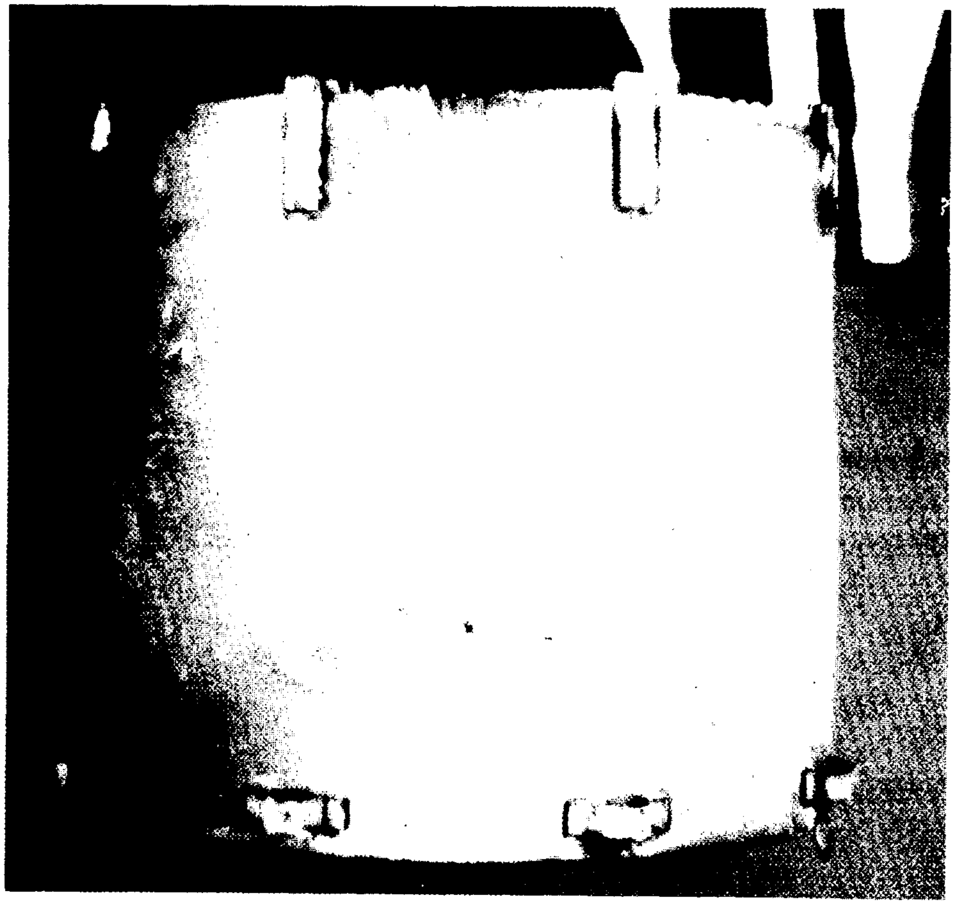

Fig. 5.17 – Blisters and blister fissures; ring 7, stage 18, cartridge 325

The cause of blister formation became apparent when fuel cartridges for the D102A reactor were re-inspected following a criticality experiment. These cartridges, which had been at 700°F for over 50 hours, were found to contain blisters around the tack-welded thermocouple hold-down straps, around the joint strap, in weld-burn areas remote from hardware, and at the edge seal. It was postulated that random arcing from the fuel sheet to ground during the tack-welding process had damaged the clad in such a way that the affected area was permeable by air. It is known that UO_2 is oxidized to the higher oxide U_3O_8 at temperatures as low as 500°F with a significant volume change.

A series of experiments was conducted using fuel sheet samples with a small hole drilled through one side of the cladding. On exposing these samples to air at various temperatures, it was found that blisters formed at the point where the fueled matrix was exposed. These tests showed that blister growth was most pronounced in the temperature range from 600° to 800°F with a rapid increase in blister size with time at temperature. Blister growth was found to be negligible at 500°F for exposure periods of less than 50 hours. In the 1000° to 1500°F range, there was no blister formation, probably due to the rapid reduction of U_3O_8 by chromium. At temperatures of 1750°F and higher, the rate of blister growth was found to be fairly linear with time and increased with increasing temperature.

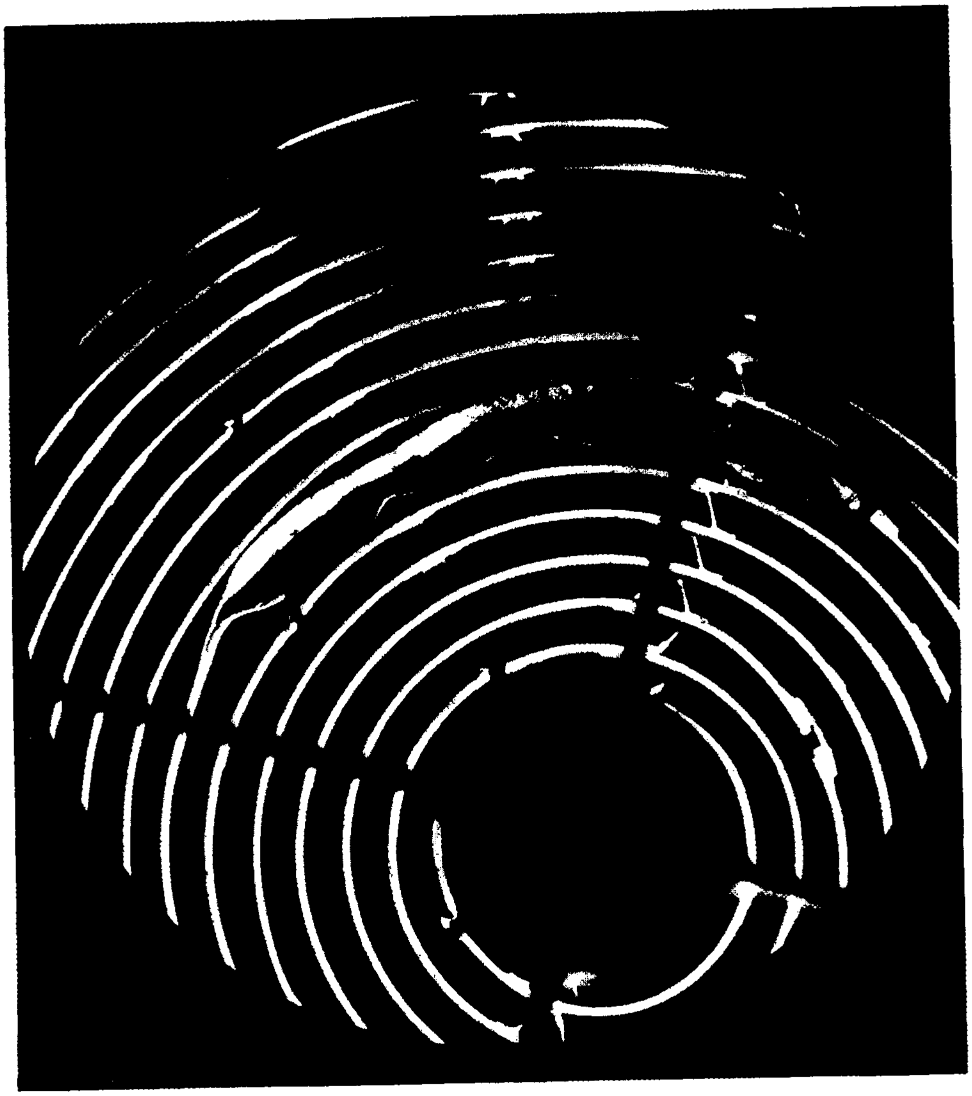

Fig. 5.18 – Trailing-edge exfoliation due to insufficient dead edge; ring 8, stage 18, cartridge 323

The results of the experiments described above were conclusive in regard to the mechanism of blister formation. To further investigate the quality of the fuel cartridges used in IET No. 6, a spare cartridge (No. 315) was returned from ITS for proof testing. Cartridge 315 was disassembled into individual stages. Nine stages were tested in air at 800°F and the other nine stages were tested at 1850°F.

The results of the 800°F proof test for 24 hours are shown in Table 5.6. A total of 63 blisters was found on post-test inspection, three blisters being associated with edge-seal leakage and the remainder with weld burns. Additional testing for a period of over 100 hours did not result in additional blistering but there was a general increase in the size of the initial blisters.

The results of the 1850°F proof test for 24 hours are given in Table 5.7. A total of 15 blisters was formed, all of which were attributed to weld burns. Continued testing at 1850°F for longer periods (85 hours) did not result in additional blister formation.

The number, distribution, and appearance of the weld-burn blisters formed during the 800°F proof test were essentially the same as noted on the fuel cartridges after IET No. 6 operation. A comparison of the blisters on the cartridge from core tube 6 after IET No. 6, and the blisters noted on the nine stages of cartridge No. 315 after 24 hours at 800°F, is given in Table 5.8.

The investigation described above definitely showed that A3-type fuel cartridges were susceptible to blistering caused by edge-seal leaks and weld burns. The weld burns resulted from improper grounding connections during cartridge fabrication.

Additional details on the experimental investigation are reported in reference 9.

TABLE 5.6

BLISTER DISTRIBUTION ON NINE STAGES OF
FUEL CARTRIDGE NO. 315 PROOF-TESTED AT 800°F FOR 24 HOURS

	Number Of Blisters At Ring Number:															
Stage No.	1	2	3	4	5	6	7	8	9	10	11	12	13	14	15	16
2			4	1[a]										1		
4			1	1									1[a]			
6							1				1					
8						1	3	4								
10																
12					5	1		2		2	4	3	1[a]			
14					2			1		1	4	1				
16									1		1	1				
18			5	1	2	1	3		1		1					

[a]Blister at edge seal.

TABLE 5.7

BLISTER DISTRIBUTION ON NINE STAGES OF
FUEL CARTRIDGE NO. 315 PROOF-TESTED AT 1850°F FOR 24 HOURS

	Number Of Blisters At Ring Number:															
Stage No.	1	2	3	4	5	6	7	8	9	10	11	12	13	14	15	16
1																
3																
5																
7				1			1									
9													1			
11														2		
13				3	2											
15				2	3											
17																

TABLE 5.8

COMPARISON OF BLISTERS ON IET NO. 6 FUEL CARTRIDGE NO. 6
AND SIMILAR NONIRRADIATED CARTRIDGE NO. 315 PROOF-TESTED AT 800°F FOR 24 HOURS

Cartridge No.	Stage No.	Number Of Blisters At Ring Number: 1	2	3	4	5	6	7	8	9	10	11	12	13	14	15	16
6	18							1	4		1						
315										1		1	1				
6	17					1						1					
6	16				1	1		1									
6	15							3		1	1	2	1				
315						2			1		1	4	1				
6	14						1		3	1		1					
315						5	1		2		2	4	3				
6	13			2	3			1	1		2		1				
315				5	1	2	1	3		1		1					
6	12							1									
6	11			1	1			1									
6	10					1	1	2									
315							1	3	4								
6	9						3										
315								1		1		1					
6	8							3									
315				4	1												
6	7 to 1							No blisters									
315				1	1									1			

NOTE: The stages of cartridge No. 315 are arranged to show similarity between number and location of blisters only. They do not correspond with the stages specified for cartridge No. 6 from IET No. 6. There were no blisters on one stage of cartridge No. 315.

5.5 REFERENCES

1. Heddleson, C. F., "A Summary Report of the Technical Data Obtained in the Third Series of Operational Tests of the ANPD HTRE-1-A3," GE-ANPD, XDC 57-5-113, 1957.
2. "HTRE No. 1 Design and Operational Summary," GE-ANPD, APEX-398, 1958.
3. Spofford, N. P., "Special Excerpts of Damages to the A-3 Reactor," GE-ANPD, XDCL 57-8-705, 1957.
4. Brekken, T. and Hoover, B. J., "A-3 Disassembly and Investigation Report," GE-ANPD, DC 58-9-725, September 1958.
5. Faupell, L. C. and Hoover, B. J., "Damage Survey A-3 Core," GE-ANPD, DC 57-8-702, 1957.
6. Brekken, T. and Hoover, B. J., "A-3 Unloading," GE-ANPD, DC 57-1-717, 1957.
7. Spofford, N. P., and Hoover, B. J., "A-3 Unloading," GE-ANPD, DC 57-2-705, 1957.
8. Spofford, N. P., and Layman, R. E., "A-3 Unloading," GE-ANPD, DC 57-3-712, 1957.
9. Muehlenkamp, G. T., "Blister Susceptability of Fuel Cartridges Prior to D102A," GE-ANPD, DC 58-12-202, 1958.